

**Gold Molecular Clusters to Nanoparticles : A Bottom-up  
Approach to Supported Nanoparticles for Heterogeneous  
Catalysis**

**Rozie Sarip**

**2013**

Department of Chemistry  
University College London  
London  
United Kingdom



**Gold Molecular Clusters to Nanoparticles : A Bottom-up Approach to  
Supported Nanoparticles for Heterogeneous Catalysis**

A thesis presented to the University College London in partial fulfilment of the  
requirements for the degree of Doctor of Philosophy

**Rozie Sarip**

2013

University College London

*Declaration*

I hereby declare that the work described within this thesis is entirely my own except where specifically acknowledged in the text.

*Rozie Sarip*

November 2012

## Abstract

This thesis covers a number of different aspects of chemistry including molecular inorganic chemistry, nanochemistry and heterogeneous catalysis. The key aspect of our research is a bottom-up approach towards generating gold nanoparticulate heterogeneous catalysts. Two phosphine-stabilised gold clusters containing **Au<sub>9</sub>** and **Au<sub>13</sub>** cores were prepared and used as molecular precursors to tailor specific size of gold nanoparticles. A number of techniques were employed to characterise the clusters as well as the catalysts in order to follow the nanoparticulate creation. The conventional incipient wetness impregnation (WI) method was used to deposit clusters onto SiO<sub>2</sub> nanosphere and Al<sub>2</sub>O<sub>3</sub> supports followed by high temperature calcination (300 °C and 500 °C) for catalyst activation. A highlight of this thesis is the development of the *tert*-butyl hydroperoxide (TBHP) assisted deposition-precipitation method towards producing smaller size of gold nanoparticulate catalysts. Catalyst activation at relatively low temperatures (95 °C) *via* the TBHP method minimised gold agglomeration, gold nanoparticles obtained by this method being < 10 nm in diameter. The relationship between catalytic activity and the size of clusters used as well as the catalyst preparation method (WI *vs* TBHP) was studied by liquid phase oxidation of benzyl alcohol. Higher turnover frequencies (TOF) were observed employing catalysts prepared *via* the TBHP method and proved to be recyclable up to at least six times with only minimal decrease in catalytic performance. Attempts had also been made to synthesise heterobimetallic gold-metal catalysts containing palladium and tin. The synthesis, characterisation and catalytic activity of both heterobimetallic catalysts are also reported.

---

## Table of Contents

<b>Abstract</b>	<b>i</b>
<b>Abbreviations</b>	<b>viii</b>
<b>List of Equations</b>	<b>x</b>
<b>List of Figures</b>	<b>xi</b>
<b>List of Schemes</b>	<b>xix</b>
<b>List of Tables</b>	<b>xx</b>
<b>Acknowledgement</b>	<b>xxiii</b>
<b>Dedication</b>	<b>xxiv</b>
<b>Chapter 1    General Introduction</b>	<b>1</b>
<b>1.0    Overview</b>	<b>1</b>
<b>1.1    Catalysts and Catalysis : Concepts</b>	<b>4</b>
<b>1.2    Homogeneous vs. Heterogeneous Catalysis</b>	<b>6</b>
<b>1.3    Gold in Catalysis</b>	<b>8</b>
<i>1.3.1    Relativistic Effects and Auophilicity</i>	<i>11</i>
<i>1.3.2    Molecular Gold Cluster</i>	<i>13</i>
<i>1.3.3    Phosphine-stabilised Molecular Gold Clusters</i>	<i>15</i>
<i>1.3.4    Molecular Gold Clusters as Catalyst Precursors</i>	<i>18</i>
<b>1.4    Heterobimetallic Gold-Metal Cluster as Catalyst</b>	<b>21</b>
<b>1.5    Research Aim</b>	<b>22</b>
<b>1.6    References</b>	<b>23</b>

---

<b>Chapter 2</b>	<b>Synthesis and Characterization of Gold Molecular Clusters and Gold Nanoparticulate Catalysts</b>	<b>32</b>
<b>2.0</b>	<b>Abstract</b>	<b>32</b>
<b>2.1</b>	<b>Introduction</b>	<b>32</b>
<b>2.2</b>	<b>Synthesis of Gold Molecular Clusters</b>	<b>34</b>
2.2.1	<i>Synthesis of Au<sub>9</sub> Clusters</i>	35
2.2.2	<i>Synthesis of Au<sub>13</sub> Clusters</i>	37
<b>2.3</b>	<b>Synthesis of Gold Nanoparticle Catalysts</b>	<b>38</b>
2.3.1	<i>Wet Impregnation (WI) Method</i>	39
2.3.2	<i>tert-butylhydroperoxide Deposition-Precipitation (TBHP) Method</i>	40
<b>2.4</b>	<b>Characterization Techniques</b>	<b>40</b>
2.4.1	<i>Carbon, Hydrogen, Nitrogen (CHN) Elemental Analysis</i>	41
2.4.2	<i>Ultraviolet-Visible (UV-Vis) Spectroscopy</i>	42
2.4.3	<i><sup>1</sup>H and <sup>31</sup>P Nuclear Magnetic Resonance (NMR) Spectroscopy</i>	43
2.4.4	<i>Thermogravimetric Analysis-Differential Scanning Calorimetry (TGA-DSC)</i>	45
2.4.5	<i>Electrospray Ionization-Mass Spectrometry (ESI-MS)</i>	47
2.4.6	<i>X-ray Diffraction (XRD) Spectroscopy</i>	49
2.4.7	<i>Transmission Electron Microscopy (TEM)</i>	50
2.4.8	<i>X-ray Absorption Near Edge Structure (XANES)</i>	51
2.4.9	<i>Extended X-ray Absorption Fine Structure (EXAFS)</i>	54
<b>2.5</b>	<b>Conclusion</b>	<b>57</b>
<b>2.6</b>	<b>References</b>	<b>57</b>

---

<b>Chapter 3</b>	<b>Gold Molecular Clusters – Structure, Stability and Size Effects on Nanoparticle Catalyst Generation by the Wet Impregnation Method</b>	<b>62</b>
<b>3.0</b>	<b>Abstract</b>	<b>62</b>
<b>3.1</b>	<b>Introduction</b>	<b>63</b>
<b>3.2</b>	<b>Characterizations of Gold Molecular Clusters</b>	<b>64</b>
3.2.1	<i>Elemental Analysis</i>	64
3.2.2	<i><sup>1</sup>H and <sup>31</sup>P{<sup>1</sup>H} nuclear magnetic resonance</i>	65
3.2.3	<i>Electrospray Ionisation-Mass Spectroscopy (ESI-MS) analysis</i>	68
<b>3.3</b>	<b>Catalyst Activation</b>	<b>69</b>
<b>3.4</b>	<b>Stability of Clusters</b>	<b>70</b>
3.4.1	<i>Structural Rearrangements Study by Thermogravimetric Analysis-Differential Scanning Calorimetry (TGA-DSC)</i>	70
3.4.2	<i>Gold Nanoparticles Formation Monitored by X-ray Diffraction (XRD) Spectroscopy</i>	72
3.4.3	<i>X-ray Absorption Spectroscopy; XANES and EXAFS</i>	76
<b>3.5</b>	<b>Size Effect</b>	<b>86</b>
<b>3.6</b>	<b>Conclusions</b>	<b>88</b>
<b>3.7</b>	<b>References</b>	<b>89</b>
<b>Chapter 4</b>	<b><i>tert</i>-Butyl Hydroperoxide (TBHP) Assisted Deposition-Precipitation – A New Low Temperature Method for Generating Gold Nanoparticulate Catalysts</b>	<b>92</b>
<b>4.0</b>	<b>Abstract</b>	<b>92</b>
<b>4.1</b>	<b>Introduction</b>	<b>92</b>

<b>4.2</b>	<b>Experimental</b>	<b>94</b>
4.2.1	<i>Generating Au nanoparticles with tert-butyl hydroperoxide (TBHP)</i>	95
<b>4.3</b>	<b>Results and Discussion</b>	<b>96</b>
4.3.1	<i>Study of formation of gold nano particles</i>	96
4.3.2	<i>X-ray Diffraction (XRD)</i>	98
4.3.3	<i>X-ray Absorption Spectroscopy; XANES and EXAFS</i>	100
4.3.4	<i>In-situ Studies of Au<sub>9</sub> Deposited on Alumina</i>	103
4.3.5	<i>Transmission Electron Microscopy (TEM) Analysis</i>	104
<b>4.4</b>	<b>Conclusion</b>	<b>111</b>
<b>4.5</b>	<b>References</b>	<b>111</b>
<b>Chapter 5</b>	<b>Catalysis – Oxidation of Benzyl Alcohol: Clusters Effect and Comparison of TBHP Deposition Precipitation vs. Wet Impregnation Method</b>	<b>114</b>
<b>5.0</b>	<b>Abstract</b>	<b>114</b>
<b>5.1</b>	<b>Introduction</b>	<b>115</b>
<b>5.2</b>	<b>Experimental</b>	<b>118</b>
5.2.1	<i>Oxidation of Benzyl Alcohol</i>	118
5.2.2	<i>Instrumentation and Data Analysis</i>	119
<b>5.3</b>	<b>Results and Discussions</b>	<b>122</b>
5.3.1	<i>Gold Loading Optimization</i>	122
5.3.2	<i>Catalyst Activation and Particle Size Effect</i>	125
5.3.3	<i>Catalytic Performances : % Conversion of Benzyl Alcohol</i>	127
5.3.4	<i>Turnover Number (TON) and Turnover Frequency (TOF)</i>	132
5.3.5	<i>Support and Selectivity Effect</i>	134

5.3.6	<i>Leaching and Recyclability</i>	136
<b>5.4</b>	<b>Conclusion</b>	<b>140</b>
<b>5.5</b>	<b>References</b>	<b>140</b>
<b>Chapter 6</b>	<b>Heterobimetallic Gold-Metal Clusters and Nanoparticles - Synthesis, Characterization and Catalysis</b>	<b>146</b>
<b>6.0</b>	<b>Abstract</b>	<b>146</b>
<b>6.1</b>	<b>Introduction</b>	<b>147</b>
<b>6.2</b>	<b>Experimental</b>	<b>148</b>
6.2.1	<i>Synthesis of Heterobimetallic Gold-Metal Clusters</i>	149
6.2.1.1	<i>Synthesis of Au<sub>6</sub>Pd Clusters</i>	149
6.2.1.2	<i>Synthesis of Au<sub>8</sub>Sn Clusters</i>	150
6.2.2	<i>Synthesis of Heterobimetallic Gold-Metal Nanoparticle Catalysts</i>	152
<b>6.3</b>	<b>Results and Discussions</b>	<b>152</b>
6.3.1	<i>Carbon, Hydrogen, Nitrogen (CHN) Elemental Analysis</i>	152
6.3.2	<i>Ultraviolet-Visible (UV-Vis) Spectroscopy</i>	153
6.3.3	<i><sup>1</sup>H and <sup>31</sup>P Nuclear Magnetic Resonance (NMR) Spectroscopy</i>	154
6.3.4	<i>Thermogravimetric Analysis-Differential Scanning Calorimetry (TGA-DSC)</i>	156
6.3.5	<i>Electrospray Ionization-Mass Spectrometry (ESI-MS)</i>	157
6.3.6	<i>X-ray Diffraction (XRD)</i>	159
6.3.7	<i>X-ray Absorption Near Edge Structure (XANES) and Extended X-ray Absorption Fine Structure (EXAFS)</i>	161
<b>6.4</b>	<b>Catalysis: Oxidation of Benzyl Alcohol</b>	<b>166</b>

---

<b>6.5</b>	<b>Conclusion</b>	<b>170</b>
<b>6.6</b>	<b>References</b>	<b>171</b>
<b>Chapter 7</b>	<b>Conclusions and Future Works</b>	<b>175</b>
<b>7.0</b>	<b>Conclusions</b>	<b>175</b>
<b>7.1</b>	<b>Future Works</b>	<b>183</b>
	<b>Publication</b>	<b>184</b>
	<b>Appendix</b>	<b>185</b>

---

## Abbreviations

$E_a$	activation energy
$\Delta H$	change in enthalpy
NaOH	sodium hydroxide
RT	room temperature
SiO <sub>2</sub>	silica
Al <sub>2</sub> O <sub>3</sub>	alumina
<i>fcc</i>	face centred cubic
NaBH <sub>4</sub>	sodium borohydride
<b>Au<sub>9</sub></b>	[Au <sub>9</sub> (PPh <sub>3</sub> ) <sub>8</sub> ](NO <sub>3</sub> ) <sub>3</sub> clusters
<b>Au<sub>13</sub></b>	[Au <sub>13</sub> (dppm) <sub>6</sub> ](NO <sub>3</sub> ) <sub>4</sub>
<b>Au<sub>6</sub>Pd</b>	[(PPh <sub>3</sub> )Pd(AuPh <sub>2</sub> P( <i>p</i> -tol)) <sub>6</sub> ](NO <sub>3</sub> ) <sub>2</sub>
<b>Au<sub>8</sub>Pd</b>	[Pd(AuPPh <sub>3</sub> ) <sub>8</sub> ](NO <sub>3</sub> ) <sub>2</sub>
<b>Au<sub>8</sub>Sn</b>	[Au <sub>8</sub> (PPh <sub>3</sub> ) <sub>7</sub> (SnCl <sub>3</sub> ) <sub>2</sub> ][SnCl <sub>6</sub> ]
B <sub>2</sub> H <sub>6</sub>	diborane
dppm	1,1-bis(diphenylphosphino)methane
<i>p</i> -tol	diphenyl( <i>p</i> -tolyl)phosphine
WI	wet impregnation
TBHP	<i>tert</i> -butyl hydroperoxide
HAuCl <sub>4</sub>	chloroauric acid
NMR	nuclear magnetic resonance
ESI-MS	electrospray ionization-mass spectroscopy
TGA-DSC	thermogravimetric analysis-differential scanning calorimetry

---

TEM	transmission electron microscopy
XRD	x-ray diffraction
XAFS	x-ray absorption fine structure
XANES	x-ray absorption near edge structure
EXAFS	extended x-ray absorption fine structure analysis
UV-Vis	ultraviolet-visible
QEXAFS	quick extended x-ray absorption fine structure analysis
FT	Fourier transforms
AAS	atomic absorption spectroscopy
GC	gas chromatography
DFT	density functional theory
FWHM	full width at half maximum
$\sigma^2$	mean square deviation in distance for EXAFS
N	coordination number
R	bond distance, Å
$r_t$	retention time
$r_f$	retention factor
TON	turnover number
TOF	turnover frequency

---

## List of Equations

### Chapter 2    Synthesis and Characterization of Gold Molecular Clusters and Gold Nanoparticulate Catalysts

<b>Equation 2.1</b> Bragg's Law	49
<b>Equation 2.2</b> EXAFS Equation	56

---

## List of Figures

### Chapter 1 General Introduction

- Figure 1.1:** Grafting or anchoring process of supported catalyst<sup>6</sup> 2
- Figure 1.2:** Development of cluster-based catalysts<sup>33</sup> 4
- Figure 1.3:** The relationship between activation energy ( $E_a$ ) and enthalpy of formation ( $\Delta H$ ) with and without a catalyst<sup>6</sup> 5
- Figure 1.4:** Gold nanoparticles capped with alkanethiol supported on SiO<sub>2</sub> structure. Alkanethiols shown as thick lines (right), provides the organic links between the metal particles and the inorganic mesoporous silica<sup>51</sup> 8
- Figure 1.5:** Different size gold nanoparticles appear different colours in solution<sup>56</sup> 9
- Figure 1.6:** X-ray crystal structure for [Au<sub>102</sub>(*p*-mba)<sub>44</sub>]<sup>91</sup> 14
- Figure 1.7:** The ligand cone angle 16
- Figure 1.8:** Solid state structures of Pt(AuP)<sub>x</sub> cores of the clusters (1) [Pt(AuPPh<sub>3</sub>)<sub>8</sub>](NO<sub>3</sub>)<sub>2</sub>, (2) [(PPh<sub>3</sub>)Pt(AuPPh<sub>3</sub>)<sub>6</sub>](NO<sub>3</sub>)<sub>2</sub><sup>15</sup> 21

### Chapter 2 Synthesis and Characterization of Gold Molecular Clusters and Gold Nanoparticulate Catalysts

- Figure 2.1:** Crystal structure of [Au<sub>9</sub>(PPh<sub>3</sub>)<sub>8</sub>](NO<sub>3</sub>)<sub>3</sub> clusters referenced from literature. Hydrogen and carbon atoms omitted for clarity<sup>29</sup> 36
- Figure 2.2:** Crystal structure of [Au<sub>13</sub>(dppm)<sub>6</sub>](NO<sub>3</sub>)<sub>4</sub> clusters referenced from literature. Hydrogen and carbon atoms omitted for clarity<sup>31</sup> 38

<b>Figure 2.3:</b>	Proton Chemical Shift Ranges <sup>40</sup>	43
<b>Figure 2.4:</b>	Example of TGA-DSC curve that measured simultaneously	46
<b>Figure 2.5:</b>	Example of TEM images (a) high resolution bright field TEM up to $1 \times 10^6$ times magnification (b) conventional negative film dark field TEM up to $1 \times 10^3$ times magnification	51
<b>Figure 2.6:</b>	Experimental L <sub>III</sub> -edge XAS spectrum of Au foil showing the regions observed for characterising a material	53
<b>Figure 2.7:</b>	Outgoing photoelectron waves (solid lines) propagate to neighbouring atoms represented by open circles. The back-scattered waves (dashed lines) modify the wave function at the central atom <sup>38</sup> .	54
<b>Figure 2.8:</b>	Plot of (a) raw data showing mass absorption obtained from EXAFS experiment (b) normalised fitting for analysis	55
<b>Figure 2.9:</b>	Plot of (a) XANES and (b) Fourier Transform of model compound (standard); HAuCl <sub>4</sub> and Au foil	56
<b>Chapter 3</b>	<b>Gold Molecular Clusters – Structure, Stability and Size Effects on Nanoparticle Catalyst Generation by the Wet Impregnation Method</b>	
<b>Figure 3.1:</b>	ESI-MS spectrum of Au <sub>9</sub> cluster; [Au <sub>9</sub> (Ph <sub>2</sub> P( <i>p</i> -tol)) <sub>8</sub> ] <sup>3+</sup> .	68
<b>Figure 3.2:</b>	ESI-MS spectrum of Au <sub>13</sub> cluster; [Au <sub>13</sub> (dppm) <sub>6</sub> ] <sup>4+</sup> .	69
<b>Figure 3.3:</b>	TGA-DSC curve of Au <sub>9</sub> (left) and Au <sub>13</sub> clusters (right) ramping at 2 °C/min rate to 600 °C	72
<b>Figure 3.4:</b>	XRD patterns of Au <sub>9</sub> precursor (Ph <sub>2</sub> P( <i>p</i> -tol)AuNO <sub>3</sub> complex) prepared by the wet impregnation on Al <sub>2</sub> O <sub>3</sub> in-situ heating up to 450 °C.	73

- 
- Figure 3.5:** XRD patterns of **Au<sub>13</sub>** precursor physically mixed with Al<sub>2</sub>O<sub>3</sub> in-situ heating up to 450 °C 74
- Figure 3.6:** XRD patterns of **Au<sub>9</sub>** clusters physically mixed with Al<sub>2</sub>O<sub>3</sub> in-situ heating up to 450 °C (left) and **Au<sub>13</sub>** clusters physically mixed with Al<sub>2</sub>O<sub>3</sub> in-situ heating up to 450 °C (right). 75
- Figure 3.7:** Au L<sub>III</sub> XANES plot for both precursor complexes recorded at room temperature and after heating along with the Au foil standard 77
- Figure 3.8:** Best fit corresponding Au L<sub>III</sub> edge EXAFS; Fourier transforms of the experimental and calculated data are shown for Ph<sub>2</sub>P(*p*-tol)AuNO<sub>3</sub> prepared by wet impregnation on Al<sub>2</sub>O<sub>3</sub> in-situ heating up to 450 °C; at 45 °C (top left), 295 °C (top right) and after cooling down (bottom). 78
- Figure 3.9:** Best fit between experimental Au L<sub>III</sub> edge EXAFS and theory/calculated data for dppmAu<sub>2</sub>(NO<sub>3</sub>)<sub>2</sub> physically mixed with Al<sub>2</sub>O<sub>3</sub> in-situ heating up to 450 °C; at 35 °C (top), 240 °C (middle) and after cooled down 62 °C (bottom). On the right corresponding Fourier transforms of the experimental and calculated data are shown. 80
- Figure 3.10:** XANES plot of **Au<sub>9</sub>** clusters physically mixed with Al<sub>2</sub>O<sub>3</sub> in-situ heating up to 450 °C (left) and **Au<sub>13</sub>** clusters physically mixed with Al<sub>2</sub>O<sub>3</sub> in-situ heating up to 450 °C (right). 81
- Figure 3.11:** Best fit corresponding Au L<sub>III</sub> edge EXAFS; Fourier transforms of the experimental and calculated data are shown for **Au<sub>9</sub>** clusters physically mixed with Al<sub>2</sub>O<sub>3</sub> in-situ heating up to 450 °C 83
- Figure 3.12:** Plot of the change in coordination number (top left), bond distances (top right) of Au-P and Au-Au atom pair and corresponding Fourier transforms (bottom left) of the experimental data according to

---

different temperatures collected for **Au<sub>13</sub>** clusters physically mixed with Al<sub>2</sub>O<sub>3</sub> in-situ heating up to 450 °C. N = coordination number; R = bond distance (Å);  $\sigma^2$  = standard deviation 85

**Figure 3.13:** TEM images of (a) **Au<sub>9</sub>** clusters on SiO<sub>2</sub> nanospheres calcined at 300 °C; (b) **Au<sub>13</sub>** clusters on SiO<sub>2</sub> nanospheres calcined at 300 °C; (c) **Au<sub>9</sub>** clusters on Al<sub>2</sub>O<sub>3</sub> calcined at 300 °C; (b) **Au<sub>13</sub>** clusters on Al<sub>2</sub>O<sub>3</sub> calcined at 300 °C 87

#### **Chapter 4 *tert*-Butyl Hydroperoxide (TBHP) Assisted Deposition-Precipitation – A New Low Temperature Method for Generating Gold Nanoparticulate Catalysts**

**Figure 4.1:** XANES spectra of **Au<sub>13</sub>** clusters dissolved in TBHP *ex-situ* heating up to 95 °C for 6 hours 96

**Figure 4.2:** Best fit between experimental Au L<sub>III</sub> edge EXAFS and theory/calculated data for **Au<sub>13</sub>** deposited on SiO<sub>2</sub> (top) and Al<sub>2</sub>O<sub>3</sub> (bottom) reacted with TBHP at 95 °C after 3 hours (catalyst was filtered and dried before analysis). On the right corresponding Fourier transform of the experimental and calculated data are shown. 97

**Figure 4.3:** (a) comparison of **Au<sub>9</sub>** clusters on SiO<sub>2</sub> nanospheres support and alumina support; (b) **Au<sub>9</sub>** and **Au<sub>13</sub>** clusters on SiO<sub>2</sub> nanospheres uncalcined and calcined at 300 °C 98

**Figure 4.4:** Best fit between experimental Au L<sub>III</sub> edge EXAFS and theory/calculated data for **Au<sub>9</sub>** deposited on SiO<sub>2</sub> calcined at 300 °C (top), Al<sub>2</sub>O<sub>3</sub> uncalcined (middle) and Al<sub>2</sub>O<sub>3</sub> calcined at 300 °C

	(bottom) by TBHP method. On the right corresponding Fourier transform of the experimental and calculated data are shown.	101
<b>Figure 4.5:</b>	Best fit between experimental Au $L_{III}$ edge EXAFS and theory/calculated data for <b>Au<sub>13</sub></b> deposited on SiO <sub>2</sub> (a) uncalcined and (b) calcined at 300°C, Al <sub>2</sub> O <sub>3</sub> (c) uncalcined and (d) calcined at 300°C by TBHP method. On the bottom corresponding Fourier transform of the experimental and calculated data are shown.	102
<b>Figure 4.6:</b>	XRD patterns of <b>Au<sub>9</sub></b> clusters catalyst deposited on Al <sub>2</sub> O <sub>3</sub> by TBHP method in-situ heating to 500°C	103
<b>Figure 4.7:</b>	Plot of the changes in coordination number (left) and bond distances (right) of Au-P and Au-Au atom pair collected at different temperature in-situ heating <b>Au<sub>9</sub></b> clusters deposited on Al <sub>2</sub> O <sub>3</sub> by TBHP method	104
<b>Figure 4.8:</b>	Film negative TEM images of <b>Au<sub>9</sub></b> and <b>Au<sub>13</sub></b> deposited onto SiO <sub>2</sub> nanospheres and Al <sub>2</sub> O <sub>3</sub> support <i>via</i> TBHP method; uncalcined and calcined at 300°C	106
<b>Figure 4.9:</b>	High resolution TEM images of <b>Au<sub>13</sub></b> clusters catalyst deposited on SiO <sub>2</sub> nanospheres <i>via</i> TBHP method uncalcined and histogram of particles size distribution	108
<b>Figure 4.10:</b>	High resolution TEM images of <b>Au<sub>13</sub></b> clusters catalyst deposited on SiO <sub>2</sub> nanospheres <i>via</i> TBHP method calcined at 300°C and histogram of particles size distribution	110
<b>Chapter 5</b>	<b>Catalysis – Oxidation of Benzyl Alcohol: Clusters Effect and Comparison of TBHP Deposition Precipitation <i>vs.</i> Wet Impregnation Method</b>	

- 
- Figure 5.1:** Perkin Elmer Clarus 500 GC with WCOT fused silica 60m × 0.25mm internal diameter (CP7818) column. Temperature program: starting at 80°C for 5 minutes then ramping at 10°C/min to 250°C for 8 minutes.
- Figure 5.2:** Calibration curves of substrate, internal standard and expected products in oxidation of benzyl alcohol 121
- Figure 5.3:** Comparison of % conversion of benzyl alcohol using **Au<sub>9</sub>** catalysts on SiO<sub>2</sub> prepared by wet impregnation method with different gold loading calcined at different temperature 124
- Figure 5.4:** Kinetic comparison between uncalcined catalysts prepared using wet impregnation (WI) method and TBHP method over 4 hours of catalysis reaction 129
- Figure 5.5:** Kinetic comparison between calcined at 300°C catalysts prepared using wet impregnation (WI) method and TBHP method over 4 hours of catalysis reaction 132
- Figure 5.6:** Product selectivity from oxidation of benzyl alcohol after 4 hours 135
- Figure 5.7:** Leaching test, oxidation of benzyl alcohol for **Au<sub>9</sub>** on SiO<sub>2</sub> calcined at 300°C prepared by TBHP method 139

## **Chapter 6 Heterobimetallic Gold-Metal Clusters and Nanoparticles - Synthesis, Characterization and Catalysis**

- Figure 6.1:** (a) Au<sub>6</sub>Pd<sup>31</sup> and (b) Au<sub>8</sub>Pd<sup>16</sup> crystal structure from literature. Carbons and hydrogens were omitted for clarity. 150

<b>Figure 6.2:</b>	Crystal structure of <b>Au<sub>8</sub>Sn</b> from literature <sup>24</sup> . Carbons and hydrogens were omitted for clarity.	151
<b>Figure 6.3:</b>	UV-Vis spectrum of <b>Au<sub>6</sub>Pd</b> and <b>Au<sub>6</sub></b> in methanol solution	153
<b>Figure 6.4:</b>	<sup>31</sup> P{ <sup>1</sup> H} NMR spectrum of <b>Au<sub>6</sub>Pd</b> clusters	156
<b>Figure 6.5:</b>	TGA-DSC curves for (a) Au <sub>6</sub> Pd clusters and (b) Au <sub>8</sub> Sn clusters	157
<b>Figure 6.6:</b>	ESI-MS spectra of <b>Au<sub>9</sub></b> , <b>Au<sub>13</sub></b> , <b>Au<sub>6</sub>Pd</b> and <b>Au<sub>8</sub>Sn</b> clusters	159
<b>Figure 6.7:</b>	XRD patterns of uncalcined, calcined at 300 °C and calcined at 500 °C, (a) <b>Au<sub>9</sub></b> , (b) <b>Au<sub>6</sub>Pd</b> and (c) <b>Au<sub>8</sub>Sn</b> on SiO <sub>2</sub> nanospheres	160
<b>Figure 6.8:</b>	Best fit between experimental Au L <sub>III</sub> edge EXAFS and theory/calculated data for <b>Au<sub>6</sub>Pd</b> ; [(PPh <sub>3</sub> )Pd(AuPh <sub>2</sub> P( <i>p</i> -tol)) <sub>6</sub> ](NO <sub>3</sub> ) <sub>2</sub> clusters (top).	161
<b>Figure 6.9:</b>	Best fit between experimental Pd K edge EXAFS and theory/calculated data for <b>Au<sub>6</sub>Pd</b> ; [(PPh <sub>3</sub> )Pd(AuPh <sub>2</sub> P( <i>p</i> -tol)) <sub>6</sub> ](NO <sub>3</sub> ) <sub>2</sub> clusters (top) and [Pd(AuPPh <sub>3</sub> ) <sub>8</sub> ](NO <sub>3</sub> ) <sub>2</sub> clusters (bottom). On the right corresponding Fourier transforms of the experimental and calculated data are shown.	163
<b>Figure 6.10:</b>	Comparison between experimental Pd K edge EXAFS data for <b>Au<sub>6</sub>Pd</b> ; [(PPh <sub>3</sub> )Pd(AuPh <sub>2</sub> P( <i>p</i> -tol)) <sub>6</sub> ](NO <sub>3</sub> ) <sub>2</sub> clusters (top) and [Pd(AuPPh <sub>3</sub> ) <sub>8</sub> ](NO <sub>3</sub> ) <sub>2</sub> clusters (bottom). Corresponding Fourier transforms and XANES of the experimental data are shown.	165
<b>Figure 6.11:</b>	Comparison of % conversion of benzyl alcohol using 4.0 wt. % Au of <b>Au<sub>6</sub>Pd</b> supported catalysts uncalcined, calcined at 300 °C and calcined at 500 °C	167

- 
- Figure 6.12:** Comparison of % conversion of benzyl alcohol using 4.0 wt. % Au of **Au<sub>8</sub>Sn** supported catalysts uncalcined, calcined at 300 °C and calcined at 500 °C. 168
- Figure 6.13:** Selectivity of each product obtained by 4.0 wt. % Au of **Au<sub>6</sub>Pd** supported catalyst calcined at 300 °C 169
- Figure 6.14:** Selectivity of each product obtained by 4.0 wt. % Au of **Au<sub>8</sub>Sn** supported catalyst calcined at 300 °C 170
- Chapter 7 Conclusions and Future Works**
- Figure 7.1:** Crystal structure of (a) **Au<sub>9</sub>** and (b) **Au<sub>13</sub>** clusters from literature. Carbons and hydrogens were omitted for clarity 175
- Figure 7.2:** TEM images of (a) **Au<sub>13</sub>** cluster on SiO<sub>2</sub> (WI) nanospheres calcined at 300 °C and (b) **Au<sub>13</sub>** cluster on SiO<sub>2</sub> (TBHP) nanospheres uncalcined
- Figure 7.3:** High resolution of TEM images of **Au<sub>13</sub>** clusters catalyst deposited on SiO<sub>2</sub> nanospheres *via* TBHP method uncalcined showing the self-assembled particles organization 178
- Figure 7.4:** Kinetic comparison between uncalcined catalysts prepared using wet impregnation (WI) method and TBHP method over 4 hours of catalysis reaction. Experiment was done in 3 replicates and the average values were plotted. 180
- Figure 7.5:** Comparison of % conversion of benzyl alcohol using 4.0 wt. % Au of **Au<sub>8</sub>Sn** supported catalysts uncalcined, calcined at 300 °C and calcined at 500 °C 181

---

## List of Schemes

### **Chapter 2    Synthesis and Characterization of Gold Molecular Clusters and Gold Nanoparticulate Catalysts**

**Scheme 2.1:** Reaction scheme of **Au<sub>9</sub>** clusters synthesis 35

**Scheme 2.2:** Reaction scheme of **Au<sub>13</sub>** clusters synthesis 37

### **Chapter 5    Catalysis – Oxidation of Benzyl Alcohol: Clusters Effect and Comparison of TBHP Deposition Precipitation vs. Wet Impregnation Method**

**Scheme 5.1:** Oxidation of benzyl alcohol 119

---

## List of Tables

<b>Chapter 1</b>	<b>General Introduction</b>	
<b>Table 1.1:</b>	Summary of some of known gold cluster cations with their polyhedral geometry arrangement <sup>90</sup>	18
<b>Chapter 3</b>	<b>Gold Molecular Clusters – Structure, Stability and Size Effects on Nanoparticle Catalyst Generation by the Wet Impregnation Method</b>	
<b>Table 3.1:</b>	Elemental analysis data of the synthesized clusters	64
<b>Table 3.2:</b>	<sup>1</sup> H-NMR chemical shift	66
<b>Table 3.3:</b>	<sup>1</sup> H-NMR chemical shift	66
<b>Table 3.4:</b>	<sup>31</sup> P{ <sup>1</sup> H} NMR chemical shift	67
<b>Table 3.5:</b>	Comparison of clusters stability according to TGA-DSC analysis	71
<b>Table 3.6:</b>	Structural parameters derived from the analysis of Au L <sub>III</sub> edge EXAFS data	78
<b>Table 3.7:</b>	Structural parameters derived from the analysis of Au L <sub>III</sub> edge EXAFS data for <b>Au<sub>9</sub></b> clusters physically mixed with Al <sub>2</sub> O <sub>3</sub> in-situ heating up to 450 °C	82
<b>Table 3.8:</b>	Structural parameters derived from the analysis of Au L <sub>III</sub> edge EXAFS data for <b>Au<sub>13</sub></b> clusters physically mixed with Al <sub>2</sub> O <sub>3</sub> in-situ heating up to 450 °C	85
<b>Table 3.9:</b>	Average particle sizes of gold nanoparticles measured by TEM	86

---

**Chapter 4** *tert*-Butyl Hydroperoxide (TBHP) Assisted Deposition-Precipitation – A New Low Temperature Method for Generating Gold Nanoparticulate Catalysts

**Table 4.1:** FWHM values derived from powder XRD patterns using *fit(y)k* software of **Au<sub>9</sub>** and **Au<sub>13</sub>** catalysts deposited onto SiO<sub>2</sub> nanospheres and Al<sub>2</sub>O<sub>3</sub> support by TBHP method 99

**Table 4.2:** Average particle sizes of gold nanoparticles measured by TEM 105

**Chapter 5** Catalysis – Oxidation of Benzyl Alcohol: Clusters Effect and Comparison of TBHP Deposition Precipitation vs. Wet Impregnation Method

**Table 5.1:** Calculated and actual gold loading of **Au<sub>9</sub>** clusters on SiO<sub>2</sub> nanospheres prepared by wet impregnation method. 123

**Table 5.2:** Average particle sizes of **Au<sub>9</sub>** and **Au<sub>13</sub>** clusters on Al<sub>2</sub>O<sub>3</sub> and SiO<sub>2</sub> nanospheres catalysts prepared by wet impregnation and TBHP method determined using TEM analysis 126

**Table 5.3:** Initial rates of reaction for WI and TBHP prepared catalysts on SiO<sub>2</sub> nanospheres support. Initial rate determined by  $(TON_{t_1} - TON_{t_0}) / (15\text{min})$   $t_1=30$  and  $t_0=15$ . <sup>a</sup>Taken at  $t_1=60$  and  $t_0=45$  130

**Table 5.4:** TON and TOF after 4 hours of catalytic oxidation benzyl alcohol reaction 133

**Table 5.5:** Leaching of gold and % conversion of benzyl alcohol after six times catalyst recycled 137

---

**Chapter 6 Heterobimetallic Gold-Metal Clusters and Nanoparticles -  
Synthesis, Characterization and Catalysis**

<b>Table 6.1:</b>	<sup>1</sup> H-NMR chemical shift	154
<b>Table 6.2:</b>	<sup>31</sup> P{ <sup>1</sup> H} NMR chemical shift	155
<b>Table 6.3:</b>	Calculated <i>m/z</i> values of clusters	158
<b>Table 6.4:</b>	Structural parameters derived from the analysis of Au L <sub>III</sub> edge EXAFS data of <b>Au<sub>6</sub>Pd</b> clusters	162
<b>Table 6.5:</b>	Structural parameters derived from the analysis of Pd K edge EXAFS data of <b>Au<sub>6</sub>Pd</b> clusters	164

---

## Acknowledgement

I would like to express my gratitude to all those who gave me the possibility to complete this thesis. My supervisors, Dr Graeme Hogarth and Prof Gopinathan Sankar, I am truly indebted with all the guidance, knowledge and “tough love” you have given to me.

To all friends now and then, John Kilmartin, Martin Martis, Nazarudin, Tiffany, Jeff Chao, Vladimir Martis and Husna Islam, thank you for brighten up my day, every day for the past 45 months! I truly valued the discussions and knowledge shared among us, in all sorts of way. To Tom Daley, not the diver, thank you for proofing my writings and always listen to my complaints. To my ex-housemate for 36 months, Nurul Izza Nordin, thank you for being such a great friend and sister for me in this country. My Ph.D life could not be so meaningful without all of you wonderful people!

Throughout the journey, I am very grateful to have my father, Sarip Dolah, my mother, Norhayati Kassim and my siblings to be there during ups and downs. To my husband, Mohd KhairulHisyam Mohd Mahadzir, thank you for the unconditional love. *“I know it is not your dream but you always believe in me”*. My best friend, forever and ever, Salhafizah Yaacob, thank you so much to always understand and be the shoulder to cry on, 23 years of friendship and still counting!

I want to thank all of the staffs at Department of Chemistry, University College London that had helped me with various issues. Former colleagues and friends in 308 office of Christopher Ingold Building, you guys are much appreciated.

This thesis is explicitly sentimental for me... who, for uncounted times had doubted myself to be able to pull it through. *Alhamdulillah...*

---

*This is for my mom, Norhayati Kassim, my dad, Sarip Dolah and my husband, Mohd*

*KhairulHisyam Mohd Mahadzir*

---

## Chapter 1

### General Introduction

#### 1.0 Overview

Nanochemistry is an exciting and rapidly developing discipline with important applications in the area of heterogeneous catalysis. Thus, nanoparticles of the late transition elements; ruthenium, platinum, palladium and gold show particularly high activity in a range of important catalytic processes<sup>1-3</sup>. They can be prepared in a number of ways but one attractive way of controlling their precise nature and size, hence their activity and selectivity as catalysts, is *via* a bottom-up approach. This involves the initial preparation of homogeneous molecular clusters which can be tailored to have specific molecular parameters such as the number and arrangement of metal atoms. These complexes are not catalysts since the supporting ligand shell blocks the active sites; however, they can be activated by heating or chemical oxidation to give “naked” nanoparticles with high activity.

To introduce these molecular clusters to solid supports, there are three major procedures; namely, incipient wetness impregnation or the wet impregnation method, the deposition-precipitation method (immobilization) and the grafting or anchoring method. The wet impregnation method involves the support being brought into contact with a solution of the precursor and then removal of the solvent followed by calcination. This method is commonly used as it allows the active phase to be deposited onto a specially shaped or structured support<sup>4</sup>. The deposition-precipitation

method involves a precursor solution being mixed with a solid support; with the use of a precipitating agent then simultaneous precipitation of both the support and the active phase through adjustment of the pH. The precipitating agents used being typically NaOH or urea<sup>5</sup>.

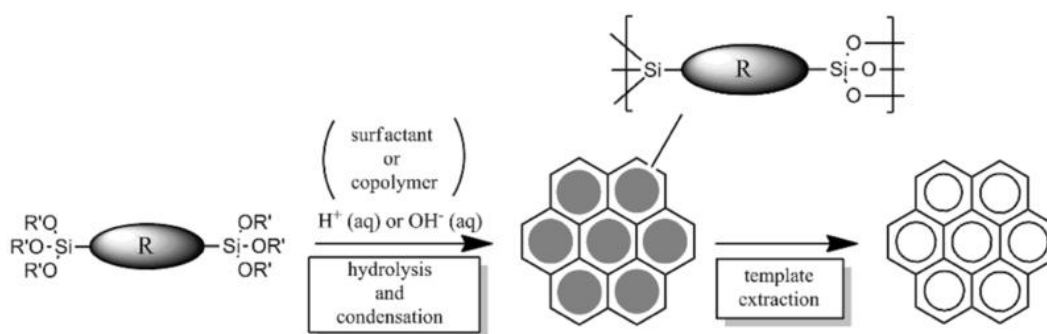


**Figure 1.1:** Grafting or anchoring process of supported catalyst<sup>6</sup>

Grafting or anchoring method requires support to be surface modified or functionalized with specific functional group which then allows the metal complexes to be chemically bonded to the support (Figure 1.1). This method is normally employed when using zeolite or mesoporous silica as a support. The organic structures in their framework provide adjustable reactive surfaces. Organic functional groups, typically organosilanes or alkoxyorganosilanes, are reacted with the assembled silicon mesostructure with or without the surfactant template present<sup>7</sup>. If the template is still present, the grafting process will involve simultaneously removing the template and attaching the functional group. However, the pores of the material can be blocked during this process so a one-pot synthesis using the necessary components is more advantageous. This one-pot synthesis is known as co-condensation, in which the desired organosilyl functional groups are combined with the surfactant or other structure-directing agent. In this method, the material becomes

---

structured and functionalized. Co-condensation gives rise to periodicity with the mesostructure, and it accommodates larger organic groups as well as larger pore sizes because of the one-step assembly process<sup>8</sup>.

Molecular gold clusters have been widely studied as precursors to gold nanoparticles<sup>9-18</sup>, with phosphine and thiolate derivatives being employed<sup>19-23</sup>. The gold clusters can be tailored to have specific atom frameworks by introducing different ligands. An important challenge in cluster-based catalyst research is to understand how the cluster behaves when deposited onto the support. Does the unique framework retain or collapse and undergo framework rearrangement resulting in different cluster sizes and shape that show different catalytic properties? Figure 1.2 shows development of cluster based catalysts.

Besides the potential of tailoring the molecular gold clusters in order to give highly disperse, supported gold nanoparticles, other low-valent transition metal atoms can be introduced into the molecular cluster which allows activity to be further tuned, while they can also act as the “hook” towards anchoring the species onto the support. This is required since often the catalytically active metals do not adhere strongly to the support and hence deactivation *via* aggregation can be rapid. One way to tackle this is to use a linking element which binds strongly to both support and nanoparticle. There are a number of possible elements which fulfil this role such as copper<sup>24-26</sup>, ruthenium<sup>1, 27</sup> and tin<sup>28, 29</sup>. Further, many other mixed-metal gold catalysts are known to enhance the catalytic performance with the synergistic effect offered for different types of catalysis reaction<sup>30-32</sup>.

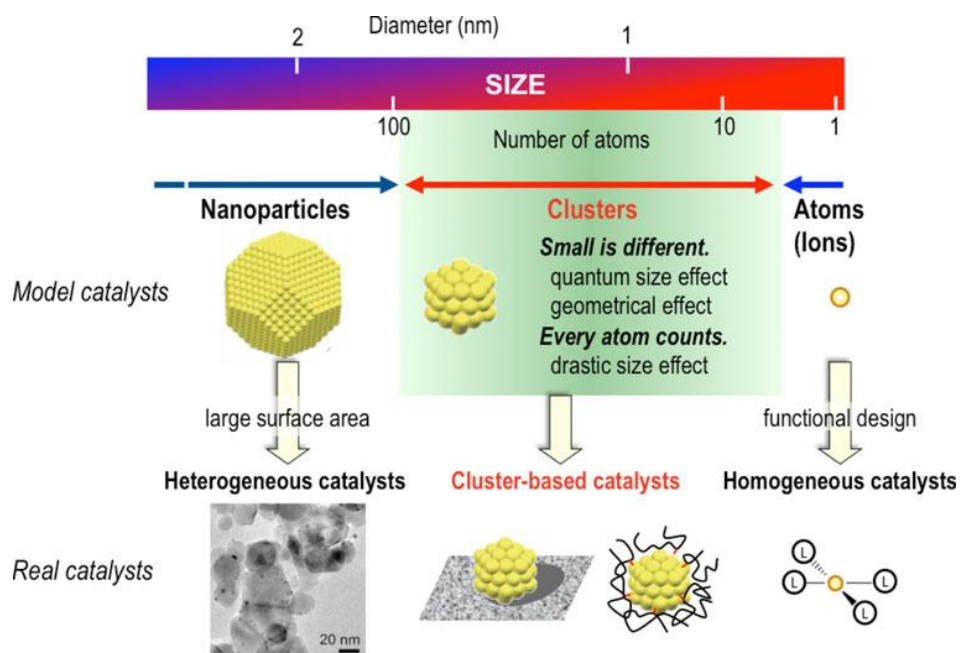


**Figure 1.2:** Development of cluster-based catalysts<sup>33</sup>

## 1.1 Catalysts and Catalysis : Concepts

A catalyst can be defined as a substance that alters the rate of a chemical reaction. The process of acceleration or deceleration of a chemical reaction due to the presence of a catalyst is called catalysis. For the occurrence of any process an activation energy is required (Figure 1.3). For reactants, it is a necessity to achieve this activation energy in order to be converted into the final products. This energy barrier of a reaction is called the activation energy,  $E_a$ . When a catalyst is present it generally decreases the activation energy allowing the reaction to proceed at a faster rate<sup>34</sup>.

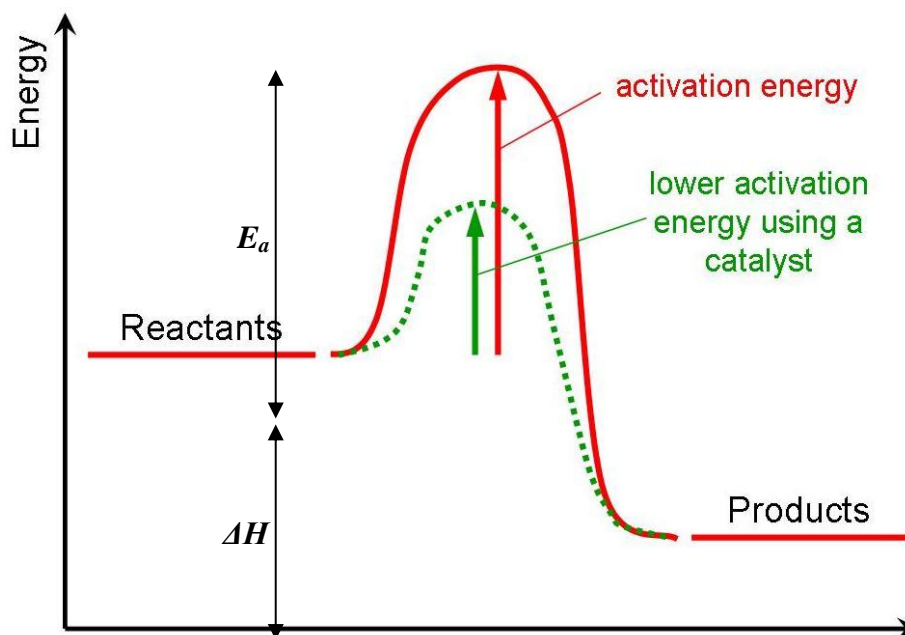


**Figure 1.3:** The relationship between activation energy ( $E_a$ ) and enthalpy of formation ( $\Delta H$ ) with and without a catalyst<sup>6</sup>

However, there are also some “*negative*” catalysts, which decelerate reaction rates<sup>35</sup>. “*Negative*” catalysts are best termed “inhibitors” as the use of the term “*negative*” has always drawn to a misleading judgement. These catalysts have great uses in medical science, slowing down various detrimental biochemical reactions. The mechanism of action for these catalysts is such that they generally provide a new path for the formation of products from reactants with higher activation energy compared to the energy needed for the reaction mechanism among reactants alone. The catalyst will combine with intermediates in a chain reaction in such a way as to break the reaction chain that results in the retardation of the reaction. Enzymes are inhibitors that are widely used in the treatment of cancer, slowing down the growth process of the cancerous cell<sup>36</sup>.

---

## 1.2 Homogeneous vs. Heterogeneous Catalysis

Homogeneous catalysts are those that are in the same phase as the substrate, which is generally a liquid. These catalysts have the advantage of mixing with the substrate better than heterogeneous catalysts. In homogeneous catalysis, the speed at which the reaction takes place is generally proportional to the concentration of catalyst<sup>37</sup>. The active molecules tend to be mononuclear species with labile ligands. Homogeneous catalysts are frequently used in organic synthesis and have been found to be particularly useful for asymmetric synthesis as the ligands on the active centre can be carefully selected to allow only one stereoisomer to be formed<sup>38</sup>. Homogeneous catalysts are often highly selective and operate with high turnover numbers, although catalyst recycling can be uneconomical. Problems with homogeneous catalysts are that they are normally difficult to separate from the reactants as they are in the same phase, and rates are relatively slow.

A heterogeneous catalyst is one that is in a different phase to the reactants. The catalysts are usually solid with the substrates in either gas or liquid form. In heterogeneous catalysis, the speed at which the reaction takes place is proportional to the area of the catalytic surface<sup>34, 39, 40</sup>. The rates of diffusion of the reactants and products on the catalytic surface, as well as the rate of activity at the site of the catalyst, are all important factors in heterogeneous catalysis. Heterogeneous catalysts are generally preferred for industrial processes since they can be easily separated and reused in a subsequent cycle.

Heterogeneous catalysts come in different forms depending on their use. There are two main types of heterogeneous catalyst; bulk catalysts and supported

---

catalysts<sup>41</sup>. In heterogeneous catalysis the rate of diffusion is generally slow, but the catalytic rates are high. A major problem with heterogeneous catalysts is that surface phenomena lead to catalytic deactivation, either in bulk or in dispersed metal systems. Deactivation can be caused by species such as oxygen, carbon monoxide, halogens, sulphur, hydrocarbons or even the reaction products<sup>42</sup>. This occurs because only a small fraction of the catalytic surfaces are ‘active sites’<sup>43-45</sup>. These are often associated with geometric lattice defects or adjacent regions in different oxidation states. If these ‘active sites’ become ‘poisoned’ by the irreversible adsorption of molecules onto them, they become unavailable for further catalysis. Catalytic metals are not equally susceptible to poisoning, for example, molecular oxygen poisons gold to a lesser extent than other platinum group metals<sup>46</sup>.

Heterogenizing homogeneous catalysts is a trend toward the development of chemically homogeneous but physically heterogeneous catalysts. The beauty of such catalysts is that they offer a hybrid organic-inorganic system. The attachment of homogeneous catalysts to insoluble supports, such as zeolites<sup>8</sup> or mesoporous materials,<sup>47, 48</sup> helps retain the reactivity yet aids catalyst separation. These catalysts can also be tuned to a specific shape, size or isomer to enhance product selectivity<sup>48, 49</sup>. Corma *et. al* have reported many hybrid catalysts that are highly active towards oxidation, epoxidation or hydrogenation reactions<sup>50</sup>. One example is an alkanethiol-capped gold organic-inorganic supported on silica catalyst (Figure 1.4) that was synthesized with an average particle size of 2-4 nm which is highly active in CO oxidation<sup>51</sup>. The high surface area and properties of the three component catalyst system make it interesting for further studies in organic reactions. Although a major

---

downside of this system is that the synthetic procedure is complicated and challenging<sup>52</sup>.

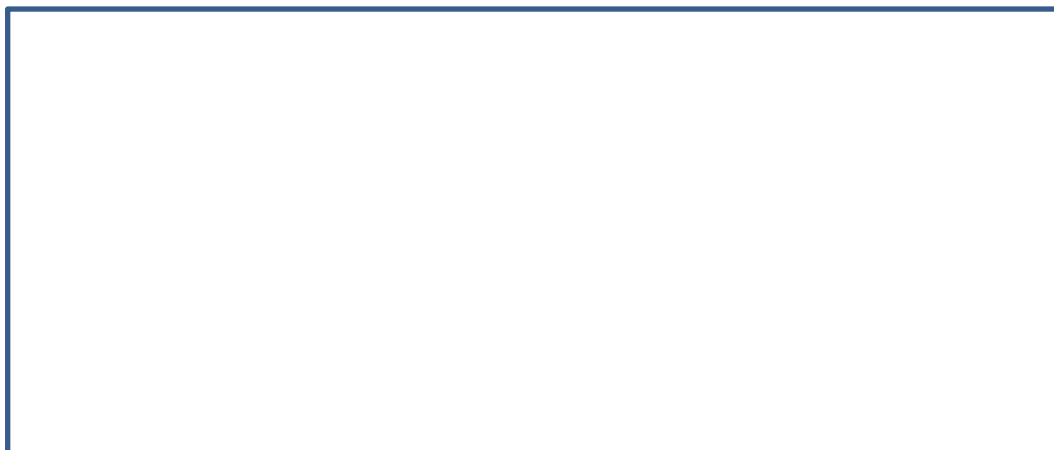


**Figure 1.4:** Gold nanoparticles capped with alkanethiol supported on SiO<sub>2</sub> structure. Alkanethiols shown as thick lines (right), provides the organic links between the metal particles and the inorganic mesoporous silica<sup>51</sup>

### 1.3 Gold in Catalysis

Catalysis by gold being superior to other catalysts was first noted by Bond in 1973<sup>53</sup>. They used gold supported on silica and alumina prepared by wet impregnation to catalyse the hydrogenation of olefins. In 1987, Haruta *et al.* discovered that gold could be highly active in CO oxidation at low temperatures when not in the bulk<sup>54</sup>. Later in 1988, Hutchings found gold to be highly effective as a heterogeneous catalyst in the hydrochlorination of ethyne to vinyl chloride<sup>55</sup>.

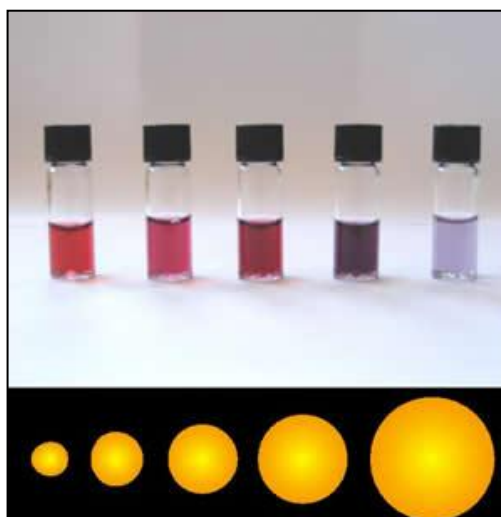


**Figure 1.5:** Different size gold nanoparticles appear different colours in solution<sup>56</sup>

Gold in bulk exist in a very striking yellow in colour that makes it attractive especially as expensive jewellery. However, smaller size particle of gold gives different colours ranging from red to purple in solution depending on the size and oxidation state of the gold (Figure 1.5)<sup>56</sup> that consequently makes gold possess unique chemical properties particularly in catalysis. What makes gold strikingly active as a catalyst is the existence of very small and fine particles. Thus, gold in the bulk is not generally active in catalyzing chemical reactions<sup>18, 57-63</sup>. In the early years, the wet impregnation method was widely used to synthesize these heterogeneous gold catalysts. However, control over size and particle distribution on supports is difficult using this method<sup>60, 64-66</sup>. Hence, the deposition–precipitation and co-precipitation methods are used and provide the desired intimacy of contact between metal and support. The high activity may originate on sites at the gold–support interface, with the support making a vital contribution.

Gold catalysts also have potential for both the selective and non-selective oxidation of hydrocarbons. For example methanol synthesis *via* hydrogenation of

---

carbon monoxide or dioxide, the water–gas shift, and the reduction of nitric oxide by hydrogen, propene or carbon monoxide<sup>61, 63, 67-71</sup>. The hydrogenation of unsaturated hydrocarbons also occurs on highly dispersed gold catalysts<sup>53, 72-74</sup>. As mentioned earlier, the remarkable catalytic behaviour shown by gold depends upon forming small particles. Presumably the bulk metal or large particles cannot chemisorb typical reactant molecules; this only occurs when a sufficient number of low-coordination surface atoms are present on particles so small that they lack full metallic character. The long neglect of gold as a catalyst is due to the failure to appreciate the importance of creating particles that are sufficiently small and, for oxidations, of selecting the correct support<sup>40, 42, 75</sup>. The preparation methods for heterogeneous catalysts also play an important role in determining particle sizes and support-surface interactions. Other relevant factors are the high mobility of surface atoms on small particles and the electronegative character of gold, both influenced from the relativistic contraction of the *s*-electron orbitals<sup>76-78</sup>.

It is difficult, bordering on impossible, to prepare a collection of metallic particles that are monodisperse, that is with exactly the same size, and it is difficult to recognize size effects when the size distribution is broad. Small metal particles are unstable with respect to aggregation, the driving force responsible for sintering being equal in magnitude but opposite in sign to the work done breaking metal–metal bonds to form the small particles<sup>4, 74</sup>. Consequently, the metal particles are often supported on a suitable high-surface-area solid which keeps them apart, but their interaction with the support may affect some changes in the properties and behaviour of the particles.

---

The term ‘cluster’ can mean either a small metallic particle containing up to a few tens of atoms or multinuclear organometallic complexes, where the array of metal atoms is stabilised by suitable ligands<sup>79</sup>. Clusters fall into the category between molecules and nanoparticles. They can be considered as large molecules or small, monodisperse nanoparticles. Gold clusters have been known since the 1960s, but it has only been recently that their applications have been explored<sup>65</sup>. From a structural and theoretical point of view, gold clusters are particularly interesting because they do not conform to the structural patterns which have emerged for metal carbonyl cluster compounds. This is due to two unique properties of gold namely, the relativistic effect and aurophilicity. Besides, there are four pre-determined differences in their chemistry which are that; (i) aggregation and degradation reactions of the gold clusters are much more favourable, (ii) potential energy surfaces appear to be much softer, (iii) gold clusters frequently adopt more open structures and (iv) the addition of electron pairs to gold cluster cation does not lead to geometric changes compared to the metal carbonyl clusters<sup>80</sup>.

### *1.3.1 Relativistic Effects and Aurophilicity*

Relativistic effects are most important for understanding the chemistry and physics of gold<sup>78</sup>. Its molecular chemistry is dominated by complexes of the oxidation states  $\text{Au}^+$  and  $\text{Au}^{3+}$ . The former are generally found to be two-coordinate with a linear geometry of the two donor atoms. The  $d$  orbitals of gold atoms participate in gold cluster formation affording high stabilities of such systems and increasing the ionic character of intermetallic gold clusters<sup>78</sup>. While the ready access to the higher oxidation states of gold ( $\text{Au}^{3+}$  and  $\text{Au}^{5+}$ ) is best rationalized by invoking relativistic contributions, the coordination number and geometry of  $\text{Au}^{3+}$  and  $\text{Au}^{5+}$

---

are not exceptional. The  $5d^8$  and  $5d^6$  electron configurations require square planar tetracoordinate and octahedral hexacoordinate complexation which is confirmed by virtually all stoichiometries and structures reported to date in an already vast literature<sup>16, 81, 82</sup>. This is analogous to findings for isoelectronic metal cations such as  $Pt^{2+}$  ( $5d^8$ ) and  $Pt^{4+}$  ( $5d^6$ ) in the  $5d$  transition metal series, but also for  $Ni^{2+}$  ( $3d^8$ ) or  $Fe^{3+}$  ( $3d^6$ ) in the  $3d$  block<sup>83, 84</sup>. However, for platinum and the gold analogues the relativistic  $5d$  expansion /  $6s$  contractions as well as the spin-orbit coupling effects are significant contributions enhancing the basic trends in the periodic table.

The inability of  $f$  electrons to screen increasing nuclear charge from the  $s$ ,  $p$  and  $d$  electrons (*the lanthanide contraction*) accounts for many properties of the third row heavy elements such as gold ( $Z = 79$ ). A large nuclear charge has a large electrostatic field which leads to increased inner electron velocities. These average velocities approach the speed of light and hence increased relative masses. Thus relativistic mass increase of electrons leads to the stabilisation and contraction of the inner  $s$  electrons. These inner electrons shield the  $d$  and  $f$  electrons from the nuclear charge resulting in the expansion and destabilisation of  $d$  and  $f$  (high angular momentum) orbitals. Since the lower electron  $s$  shells must be orthogonal with respect to the higher shells, the  $6s$  (and  $6p$ ) electrons are also drawn closer to the nuclear charge. These effects are greatest in gold which is the most electronegative metal with a value of 1.691 V for the  $Au^+/Au^0$  couple, and a high first ionisation energy<sup>13, 78, 85-87</sup>.

Another important factor affecting the synthesis of gold clusters is the aurophilic interaction. Aurophilicity is defined as the tendency of closed-shell gold(I)

---

atoms to aggregate at distances shorter than the *van der Waals* radii<sup>88</sup>. The energy of aurophilic molecules is comparable to that of a hydrogen bond<sup>86, 88</sup>. The aggregation is an intrinsic effect of the metal centres and is not imposed by the ligand architecture. So in principle, gold-gold interactions could be used to control supramolecular structure and their dimensionality. Nevertheless, in most cases the formation of polymeric structures or the ligand architecture plays a significant role in the aggregation of the metal centres.

### 1.3.2 Molecular Gold Cluster

$[\text{Au}_{11}(\text{PPh}_3)_7\text{I}_3]^{89}$  was the first example of a molecular gold cluster synthesized and since then the area expanded rapidly. Many of the known cluster entities are stabilised by tertiary phosphine, ( $\text{PR}_3$ ) and halide ligands, ( $\text{X}$ )<sup>90</sup>. Nevertheless, research has also been carried out on clusters stabilised by other ligands, particularly thiolates. The largest molecular gold cluster known to date is  $[\text{Au}_{102}(\text{p-mba})_{44}]$  (*p-mba* = *para*-mercapto benzoic acid) (Figure 1.6)<sup>91</sup>. The surface coverage of the thiol ligands is relatively large at 70% of the 23 surface gold atoms. The thiol monolayer is not only stabilized by bonds with the gold surface, but also by interactions between the *p-mba* ligands. At the center of the 79 atom core, the gold is arranged in an *fcc* arrangement also found in metallic gold.



**Figure 1.6:** X-ray crystal structure for  $[\text{Au}_{102}(\text{p-mba})_{44}]^{91}$

This cluster was discovered whilst researching thiol-stabilised nanoparticles which are similar to clusters only larger and generally non-uniform in size and geometry. The cluster  $[\text{Au}_{102}(\text{p-mba})_{44}]$  is of great importance because it was the first reported monoatomically dispersed nanoparticle. This is a huge area of research due to gold nanoparticles unique optical, electrochemical and photophysical properties. Thiol-stabilised gold nanoparticles are usually prepared through the reduction of AuSR species by  $\text{NaBH}_4$  but this can give a range of particle sizes<sup>92</sup>. Control over the average core size can be exhibited by monitoring the ratio of Au:SR. The size of the particles formed is highly sensitive to the reactions conditions during their synthesis. The length of the SR ligands is another major factor controlling the particle size.

---

### 1.3.3 Phosphine-stabilised Molecular Gold Clusters

Phosphine ligands play an important role in determining the clusters framework. Thus, changing substituents on phosphine ligands can cause marked changes in the behaviour of the metal clusters. Molecular structures, rate and equilibrium constants, nuclear magnetic resonance (NMR) chemical shifts and even relative infrared (IR) intensities have been correlated with ligand cone angle<sup>93</sup>. The latter is a measure of the size of a ligand defined as the solid angle formed with the metal at the vertex and the hydrogen atoms at the perimeter of the cone (Figure 1.7).

For phosphine-stabilised gold cluster cations, the extent of cluster growth is primarily limited by the steric demands of the peripheral ligands<sup>80, 94</sup>. When small ions such as chloride or bromide replace one of the bulkier phosphine ligands then the cluster growth can proceed until it is limited by the steric demands of the new ligand set. Hence, in a bottom-up approach towards gold nanoclusters, designing the gold clusters by appropriate ligand choice with a specific cone angle is promising. For example, exchanging PPh<sub>3</sub> ligand with Ph<sub>2</sub>P(*o*-tolyl) ligand leads to the formation of [Au<sub>6</sub>(Ph<sub>2</sub>P(*o*-tolyl))<sub>6</sub>](NO<sub>3</sub>)<sub>2</sub> (**Au<sub>6</sub>**), rather than [Au<sub>9</sub>(PPh<sub>3</sub>)<sub>8</sub>](NO<sub>3</sub>)<sub>3</sub> (**Au<sub>9</sub>**). In Ph<sub>2</sub>P(*o*-tolyl) ligand, the cone angle ( $\theta = 185^\circ$ ) is greater than PPh<sub>3</sub> ligand ( $\theta = 145^\circ$ )<sup>93</sup> making it more congested hence decreasing the binding ability. Thus, the conclusion can be made that steric effects occurring in the ligand environment cause the aurophilic interaction to be less favourable leading to the formation of smaller clusters.

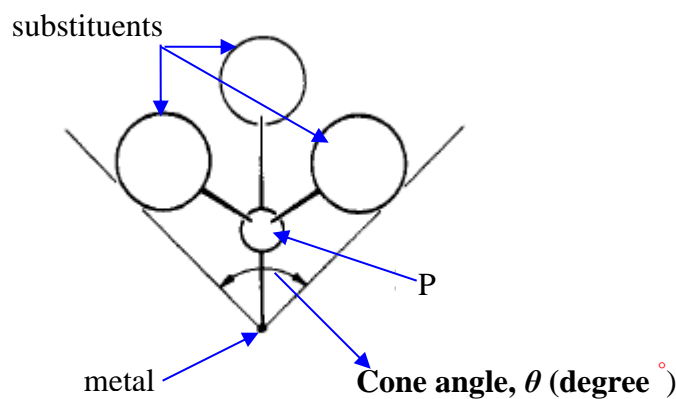


**Figure 1.7:** The ligand cone angle

Phosphine-stabilised gold clusters are generally synthesized by the reduction of mononuclear gold phosphine complexes,  $\text{AuX}(\text{PR}_3)$  and the most commonly used reducing agent has been  $\text{NaBH}_4$ . The type of reducing agent used is also an important factor affecting the formation of the gold cluster. From the same gold-phosphine complex precursor, a number of different complexes can be obtained if a different reducing agent was employed. For example, the reduction of  $(\text{PPh}_3)\text{AuCl}$  by  $[\text{Ti}(\eta\text{-C}_5\text{H}_5\text{Me})_2]$  leads to the formation of  $[\text{Au}_9(\text{PPh}_3)_8]^{+3}$ ,<sup>95</sup> whereas reduction of the same compound with  $\text{B}_2\text{H}_6$  gives a larger gold phosphine cluster  $[\text{Au}_{55}(\text{PPh}_3)_{12}\text{Cl}_6]$ <sup>96</sup>.

Two gold complexes were commonly used as the starting material in synthesizing phosphine-stabilised gold clusters,  $[\text{Au}(\text{PPh}_3)]\text{Cl}$ <sup>15</sup> and  $[\text{Au}(\text{PPh}_3)]\text{NO}_3$ <sup>14, 97</sup>. The most stable compound derived from  $\text{AuCl}$  is in fact  $[\text{Au}(\text{PPh}_3)]\text{Cl}$  but with an excess of phosphine,  $[\text{Au}(\text{PPh}_3)_2]\text{Cl}$  could also be obtained<sup>94, 98-101</sup>. Meanwhile, the nitrogen-oxygen stretching bands in  $[\text{Au}(\text{PPh}_3)]\text{NO}_3$  seems to indicate that the nitrate group does not act as ligand and it is not covalently bonded to the metal<sup>102</sup>. Other synthetic routes to gold clusters include; reactions of carbonyl metalates with  $\text{AuPR}_3\text{X}$  ( $\text{X}$  = halide or weakly coordinating anion)<sup>103</sup>,

---

replacement of metal hydride ligands by  $\text{AuPR}_3^+$  units<sup>104</sup>, and formation of new clusters by the reduction of  $\text{AuPR}_3^+$  moieties in the presence of a coordinately unsaturated transition metal compounds<sup>105</sup>.

Another unique feature of phosphine-stabilised gold clusters is the way that the size and geometry adopted by the cluster is highly dependant upon the ligands in the complex, depending on the specific ligand cone angle. Table 1.1 summarizes some examples of common structural geometries associated with specific gold clusters. The main form of bonding occurring within gold clusters is the overlap of the  $6s$  orbitals and is of a multicentre nature. Thus for the clusters to be at their most stable, bonding occurs in all directions. This leads to the shape of clusters of low nuclearity being condensed deltahedral polyhedral, while higher nuclearity clusters contain an additional metal atom at the centre of polyhedron<sup>80, 90, 106, 107</sup>. By slight alteration of the phosphine group on the gold(I) precursor, a large change can be seen in the cluster core. For example, the reduction of  $[\text{Au}(\text{PPh}_3)](\text{NO}_3)$  by  $\text{NaBH}_4$  gives the cluster compound,  $[\text{Au}_9(\text{PPh}_3)_8](\text{NO}_3)_3$ <sup>108</sup>, whereas if  $[\text{Au}(\text{PCyPh}_2)](\text{NO}_3)$  is reduced under the same conditions,  $[\text{Au}_6(\text{PCyPh}_2)_6](\text{NO}_3)_2$  is formed<sup>109</sup>. Geometric rearrangement has also been demonstrated through electrochemical reduction of the gold cluster<sup>110</sup>.  $[\text{Au}_9(\text{PPh}_3)_8]^{3+}$  was reduced by a two-step charge transfer at a platinum electrode to give  $[\text{Au}_9(\text{PPh}_3)_8]^+$ . The solid structure of the cluster had reordered significantly as a result of the reduction process.

**Table 1.1:** Summary of some of known gold cluster cations with their polyhedral geometry arrangement<sup>90</sup>

Stoichiometry	Polyhedral Geometry
Non-centred polyhedral:	
- $[\text{Au}_4(\text{PPh}_3)_4(\mu\text{-I})_2]^{111}$	- tetrahedral
- $[\text{Au}_7(\text{PPh}_3)_7]^{2+ 112}$	- pentagonal bi-pyramid
Condensed non-centred polyhedral:	
- $[\text{Au}_6(\text{PPh}_3)_6]^{2+ 109}$	- edge-sharing bi-tetrahedral
- $[\text{Au}_6(\text{dppp})_4]^{2+ 113}$	- di-edged-bridged tetrahedral
Toroidal centred clusters:	
- $[\text{Au}_{10}(\text{PCy}_2\text{Ph})_6\text{Cl}_3]^+ 114$	- tri-edged-bridged centred chair
Spherical centred clusters:	
- $[\text{Au}_{13}(\text{PMe}_2\text{Ph})_{10}\text{Cl}_2]^+ 115$	- icosahedron

#### 1.3.4 Molecular Gold Clusters as Catalyst Precursors

The application of phosphine-stabilised molecular gold clusters has an increasing attention in a wide range of heterogeneous nanoparticle catalysts due to their unique catalytic properties<sup>66, 71</sup>. In principle, the molecular catalyst can be tailored to a specific (selective) reaction requirement in almost infinite detail. However, most gold nanoparticles catalysts synthesised to date utilise the reduction of a gold salt leading to lack of control over the size and shape of the nanoparticles<sup>18, 116, 117</sup>. Molecular gold clusters, especially phosphine-stabilised gold clusters have clearly defined and tunable sizes and shapes potentially allowing the synthesis of monodisperse nanoparticles. In 1996, Iwasawa<sup>59</sup> utilized the **Au<sub>9</sub>** cluster as precursor

---

for preparation of supported catalysts on various inorganic oxides such as TiO<sub>2</sub>,  $\alpha$ -Fe<sub>2</sub>O<sub>3</sub> and SiO<sub>2</sub>, which were found to be active for CO oxidation.

Highly active and stable gold nanoparticles catalysts have been synthesized by the interaction of **Au<sub>6</sub>** cluster with TiO<sub>2</sub> support for CO oxidation<sup>118</sup>. The CO oxidation activity is strongly influenced by the catalyst preparation methods normally involving the pre-calcination step. However, it was found that even under that high temperature pre-treatment condition, the gold catalyst obtained was still in the range of <5 nm and highly dispersed on a conventional TiO<sub>2</sub> support<sup>119</sup>. The nanoparticles generated were found to be uniform in size as compared to gold nanoparticle catalyst derived from reduced gold salt as a precursor<sup>57, 59</sup>. This insight shows that it is the cluster-derived nanoparticles that results in their small size uniformity and enhanced catalytic activity.

A number of important developments in this area have occurred during the work described in this thesis. Thus, a simple, effective method has been demonstrated to immobilize Au clusters within mesoporous silica (SBA-15, MCF and HMS) using triphenylphosphine-protected clusters, [Au<sub>11</sub>(PPh<sub>3</sub>)<sub>7</sub>]Cl<sub>3</sub> (**Au<sub>11</sub>**) as precursors, which were deposited on the silica surface in an organic medium<sup>120</sup>. A unique feature of this method is the ability to disperse Au<sub>11</sub> homogeneously over a large silica surface area by optimizing the solvent-mediated interaction. The gold particle size supported on SBA-15 was measured to be ~0.8 nm. It exhibited catalytic activity for oxidation of various alcohols by H<sub>2</sub>O<sub>2</sub> under microwave irradiation and were found to be reusable. Another **Au<sub>11</sub>** cluster used as a precursor to gold nanoparticle catalyst is [Au<sub>11</sub>(P<sup>^</sup>P)<sub>4</sub>Cl<sub>2</sub>]Cl species (P<sup>^</sup>P = chiral atropisomeric

---

diphosphine ligand)<sup>121</sup>. In such system, chloride abstraction performed to generate Au<sup>+</sup> active sites induced the Au<sub>11</sub> cluster evolution to nanoparticles. The nanoparticles generated are reported to be highly active in catalyzing the tandem hydroarylation-carbocyclization reaction with minimal sintering being observed. This findings hint at the possibility that highly active, homogeneously dispersed and practical gold catalysts can be developed if the cluster is used as nanoparticles precursor and the size is reduced to below 1 nm<sup>122</sup>.

The development of gold cluster precursors towards nanoparticle catalysts expands with the use of bigger clusters in producing smaller nanoparticles. Catalysts with very small gold entities (<1.4 nm) derived from [Au<sub>55</sub>(PPh<sub>3</sub>)<sub>12</sub>]Cl<sub>6</sub> (**Au<sub>55</sub>**) gold clusters and supported on inert materials were found to be efficient and robust catalysts for selective oxidation reactions<sup>123</sup>. Minimal nanoparticle aggregation was reported when using Au<sub>55</sub> clusters as the catalyst precursor supported on TiO<sub>2</sub>. A study by Jiang *et. al* showed that there is a size threshold for these particles in styrene epoxidation, where larger particles are relatively inactive<sup>124</sup>. The catalytic activity arises from the altered electronic structures intrinsic to gold clusters. The DFT technique was employed to simulate the styrene epoxidation on Au<sub>55</sub> and Au<sub>38</sub> clusters and showed that the Au<sub>38</sub> cluster was more likely the size threshold. The high catalytic activity of the Au<sub>38</sub> cluster as compared to Au<sub>55</sub> is due to their different adsorption structures of O<sub>2</sub> and styrene resulting from its geometry<sup>125</sup>. Little or no cluster aggregation occurred upon deposition or during catalysis, indicating that the gold mobility on the surface of the oxide support was limited by the core of the gold cluster providing a clear vindication of the cluster precursor approach.

---

## 1.4 Heterobimetallic Gold-Metal Cluster as Catalyst

The increasing interest in heterobimetallic gold-metal clusters is based on the idea that they contain a variety of novel structures and promising reactivity for homogenous and heterogeneous catalytic processes. One of the catalytic reactions that have been reported to be activated by the heterobimetallic Pt-Au cluster is the H<sub>2</sub>-D<sub>2</sub> equilibration reaction. Generally, the clusters have great potential as models for the activation of H<sub>2</sub> by supported Pt-Au catalysts. Studies on Pt-centred, crown-shaped geometry of [Pt(AuPPh<sub>3</sub>)<sub>8</sub>](NO<sub>3</sub>)<sub>2</sub> clusters in the solid state showed that the cluster reacts rapidly and fully reversibly at ambient temperature and pressure with H<sub>2</sub><sup>126</sup>.

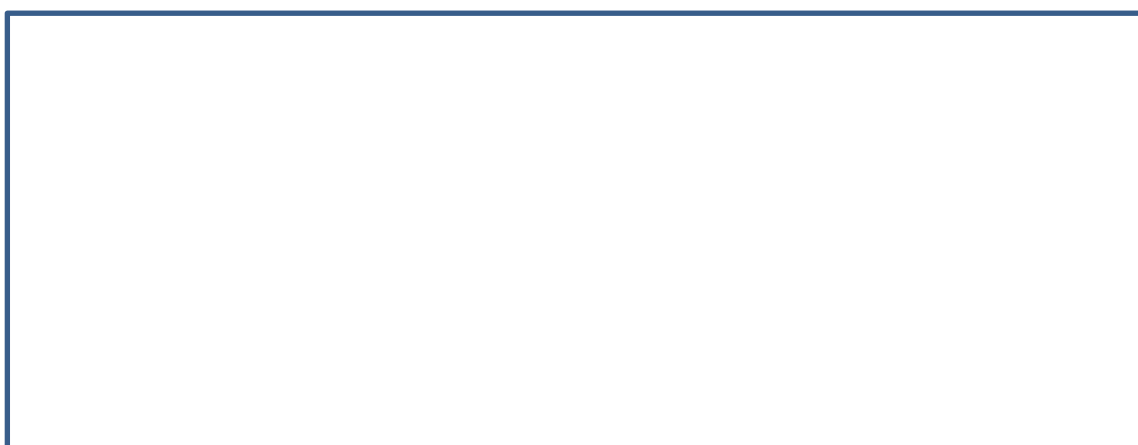


**Figure 1.8:** Solid state structures of Pt(AuP)<sub>x</sub> cores of the clusters (1) [Pt(AuPPh<sub>3</sub>)<sub>8</sub>](NO<sub>3</sub>)<sub>2</sub>, (2) [(PPh<sub>3</sub>)Pt(AuPPh<sub>3</sub>)<sub>6</sub>](NO<sub>3</sub>)<sub>2</sub><sup>15</sup>

Instead of catalyzing the H<sub>2</sub>-D<sub>2</sub> equilibration reaction, a number of reports have demonstrated the use of gold-based catalysts for CO oxidation<sup>59, 127</sup>, methane oxidation<sup>128</sup>, propylene epoxidation<sup>129</sup> and hydrogenation<sup>2, 130</sup>. The Pt-Au clusters; [Pt(AuPPh<sub>3</sub>)<sub>8</sub>](NO<sub>3</sub>)<sub>2</sub> and [(PPh<sub>3</sub>)Pt(AuPPh<sub>3</sub>)<sub>6</sub>](NO<sub>3</sub>)<sub>2</sub> (Figure 1.8) when immobilized on silica supports showed excellent performance in catalyzing CO oxidation but the

---

same clusters are less catalytically active<sup>15</sup>. Consequently, it is of interest to determine the effect of support on the structure and reactivity of the clusters. Although supported molecular compounds are not likely to be a practical catalysts themselves due to their relatively instability, the study of their surface chemistry can provide useful insight into cluster reactivity and the mechanism of thermal activation. Adding to that, it was found that the catalyst was more active than single metal nanoparticles mainly because of the co-existence of two metals in dispersed form (synergistic effect). Hence, when synthesizing mixed-metal catalysts, the way that two metals clustered together is another important factor to be carefully chosen.

### 1.5 Research Aim

The aim of this project is to prepare a series of gold molecular clusters starting from **Au<sub>9</sub>** and **Au<sub>13</sub>** core clusters as well as heterobimetallic gold-metal clusters, namely gold-palladium and gold-tin clusters. Characterisation techniques such as nuclear magnetic resonance (NMR) spectroscopy will be employed with the precise geometries of the atoms being probed by X-ray crystallography. These molecular clusters will then be absorbed onto oxide supports and nanoparticles generated. A few important factors will be investigated throughout the research such as average particle size and distribution of particles size of the gold deposited on support (*i.e* the method of gold deposition and support used in the supported gold nanoparticle catalysts) as well as the calcination temperatures (*i.e* method of catalysts activation). The precise nature (size, constitution and metal arrangement) of these clusters will be probed using extended X-ray absorption fine structure analysis (EXAFS) and then tested as catalysts in benzyl alcohol oxidation reaction.

---

## 1.6 References

1. B. D. Alexander, M. P. Gomez-Sal, P. R. Gannon, C. A. Blaine, P. D. Boyle, A. M. Mueting and L. H. Pignolet, *Inorganic Chemistry*, 1988, **27**, 3301-3308.
2. B. D. Chandler, L. I. Rubinstein and L. H. Pignolet, *Journal of Molecular Catalysis A: Chemical*, 1998, **133**, 267-282.
3. L. H. Pignolet, M. A. Aubart, K. L. Craighead, R. A. T. Gould, D. A. Krogstad and J. S. Wiley, *Coordination Chemistry Reviews*, 1995, **143**, 219-263.
4. M. Bowker, A. Nuhu and J. Soares, *Catalysis Today*, 2007, **122**, 245-247.
5. R. Zanella, S. Giorgio, C.-H. Shin, C. R. Henry and C. Louis, *Journal of Catalysis*, 2004, **222**, 357-367.
6. G. Rothenberg, *Catalysis - Concepts and Green Applications*, Wiley-VCH Verlag GmbH & Co. KGaA, Weinheim, 2008.
7. K. Qian, W. Huang, Z. Jiang and H. Sun, *Journal of Catalysis*, 2007, **248**, 137-141.
8. V. Ayala, A. Corma, M. Iglesias, J. A. Rincan and F. Sanchez, *Journal of Catalysis*, 2004, **224**, 170-177.
9. F. Cariati, L. Naldini, G. Simonetta and L. Malatesta, *Inorganica Chimica Acta*, 1967, **1**, 315-318.
10. D. V. J. W. A. Van, J. J. Bour, F. A. Vollenbroek, P. T. Beurskens and J. M. M. Smits, *Journal of Chemical Society, Chemical Communications*, 1979, 1162-1163.
11. J. W. A. V. D. Velden, F. A. Vollenbroek, J. J. Bour, P. T. Beurskens, J. M. M. Smits and W. P. Bosman, *Recueil, Journal of the Royal Netherlands Chemical Society*, 1981, **100**, 148-152.
12. D. V. J. W. A. Van, J. J. Bour, J. J. Steggerda, P. T. Beurskens, M. Roseboom and J. H. Noordik, *Inorganic Chemistry*, 1982, **21**, 4321-4324.
13. A. Goerling, N. Roesch, D. E. Ellis and H. Schmidbaur, *Inorganic Chemistry*, 1991, **30**, 3986-3994.
14. Y. Yang and P. R. Sharp, *Journal of the American Chemical Society*, 1994, **116**, 6983-6984.

- 
15. I. V. G. Graf, J. W. Bacon, M. B. Consugar, M. E. Curley, L. N. Ito and L. H. Pignolet, *Inorganic Chemistry*, 1996, **35**, 689-694.
  16. M. A. Omary, M. A. Rawashdeh-Omary, C. C. Chusuei, J. P. Fackler and P. S. Bagus, *Journal of Chemical Physics*, 2001, **114**, 10695-10702.
  17. P. Schwerdtfeger, *Angewandte Chemie, International Edition*, 2003, **42**, 1892-1895.
  18. G. Schmid and B. Corain, *Eur. Journal of Inorganic Chemistry*, 2003, 3081-3098.
  19. K. Ikeda, Y. Kobayashi, Y. Negishi, M. Seto, T. Iwasa, K. Nobusada, T. Tsukuda and N. Kojima, *Journal of the American Chemical Society*, 2007, **129**, 7230-7231.
  20. Y. Shichibu, Y. Negishi, T. Watanabe, N. K. Chaki, H. Kawaguchi and T. Tsukuda, *Journal of Physical Chemistry C*, 2007, **111**, 7845-7847.
  21. H. Tsunoyama, P. Nickut, Y. Negishi, K. Al-Shamery, Y. Matsumoto and T. Tsukuda, *Journal of Physical Chemistry C*, 2007, **111**, 4153-4158.
  22. M. Walter, J. Akola, O. Lopez-Acevedo, P. D. Jadzinsky, G. Calero, C. J. Ackerson, R. L. Whetten, H. Gronbeck and H. Hakkinen, *Proceedings of the National Academy of Sciences*, 2008, **105**, 9157-9162.
  23. Y. Pei, Y. Gao and X. C. Zeng, *Journal of the American Chemical Society*, 2008, **130**, 7830-7832.
  24. G. Van Koten and J. G. Noltes, *Journal of Organometallic Chemistry*, 1974, **82**, C53-C55.
  25. M. F. J. Schoondergang, J. J. Bour, P. P. J. Schlebos, A. W. P. Vermeer, W. P. Bosman, J. M. M. Smits, P. T. Beurskens and J. J. Steggerda, *Inorganic Chemistry*, 1991, **30**, 4704-4709.
  26. T. G. M. M. Kappen, P. P. J. Schlebos, J. J. Bour, W. P. Bosman, J. M. M. Smits, P. T. Beurskens and J. J. Steggerda, *Journal of the American Chemical Society*, 1995, **117**, 8327-8334.
  27. B. D. Alexander, B. J. Johnson, S. M. Johnson, P. D. Boyle, N. C. Kann, A. M. Mueting and L. H. Pignolet, *Inorganic Chemistry*, 1987, **26**, 3506-3513.
  28. Z. Demidowicz, R. L. Johnston, J. C. Machell, D. M. P. Mingos and I. D. Williams, *Dalton Transactions*, 1988, 1751-1756.

- 
29. S. Hagen, L. Wesemann and I. Pantenburg, *Chemical Communications*, 2005, 1013-1015.
  30. D. T. Thompson, *Platinum Metals Review*, 2004, **48**, 169-172.
  31. L. Prati, A. Villa, F. Porta, D. Wang and D. Su, *Catalysis Today*, 2007, **122**, 386-390.
  32. S. A. Kondrat, G. Shaw, S. J. Freakley, Q. He, J. Hampton, J. K. Edwards, P. J. Miedziak, T. E. Davies, A. F. Carley, S. H. Taylor, C. J. Kiely and G. J. Hutchings, *Chemical Science*, 2012, **3**, 2965-2971.
  33. H. Tsunoyama, Y. Liu, T. Akita, N. Ichikuni, H. Sakurai, S. Xie and T. Tsukuda, *Catalysis Surveys from Asia*, 2011, **15**, 230-239.
  34. J. R. H. Ross, *Heterogeneous Catalysis Fundamentals and Applications*, Elsevier, 2012.
  35. H. Singh and K. L. Mittal, *Journal of Chemical Education*, 1969, **46**, 185.
  36. A. K. Larsen, A. E. Escargueil and A. Skladanowski, *Pharmacology & Therapeutics*, 2003, **99**, 167-181.
  37. P. Lahtinen, H. Korpi, E. Haavisto, M. Leskelä and T. Repo, *Journal of Combinatorial Chemistry*, 2004, **6**, 967-973.
  38. M. Shibasaki, H. Sasai and T. Arai, *Angewandte Chemie International Edition in English*, 1997, **36**, 1236-1256.
  39. M. Bowker, *The Basis and Applications of Heterogeneous Catalysis*, Oxford University Press Inc., New York, Oxford, 1998.
  40. M. Comotti, P. C. Della, R. Matarrese and M. Rossi, *Angewandte Chemie, International Edition*, 2004, **43**, 5812-5815.
  41. G. V. Smith and F. Notheisz, *Heterogeneous Catalysis in Organic Chemistry*, Academic Press, Orlando, Florida, 1999.
  42. P. C. Della, E. Falletta, M. Rossi and A. Sacco, *Journal of Catalysis*, 2009, **263**, 92-97.
  43. W. Yan, S. M. Mahurin, B. Chen, S. H. Overbury and S. Dai, *The Journal of Physical Chemistry B*, 2005, **109**, 15489-15496.
  44. C.-H. Tu, A.-Q. Wang, M.-Y. Zheng, X.-D. Wang and T. Zhang, *Applied Catalysis A: General*, 2006, **297**, 40-47.
  45. M. P. Casaletto, A. Longo, A. Martorana, A. Prestianni and A. M. Venezia, *Surface and Interface Analysis*, 2006, **38**, 215-218.

- 
46. F. Wang, J. Xu, X. Li, J. Gao, L. Zhou and R. Ohnishi, *Advanced Synthesis & Catalysis*, 2005, **347**, 1987-1992.
  47. M. Alvaro, A. Corma, D. Das, V. Fornés and H. García, *Chemical Communications*, 2004, 956-957.
  48. C. González-Arellano, A. Corma, M. Iglesias and F. Sánchez, *European Journal of Inorganic Chemistry*, 2008, **2008**, 1107-1115.
  49. A. Arnanz, C. Gonzalez-Arellano, A. Juan, G. Villaverde, A. Corma, M. Iglesias and F. Sanchez, *Chemical Communications*, 2010, **46**, 3001-3003.
  50. A. Corma and H. Garcia, *Advanced Synthesis & Catalysis*, 2006, **348**, 1391-1412.
  51. G. Budroni and A. Corma, *Angewandte Chemie, International Edition*, 2006, **45**, 3328-3331.
  52. A. Corma, *Catalysis Reviews*, 2004, **46**, 369-417.
  53. G. C. Bond, P. A. Sermon, G. Webb, D. A. Buchanan and P. B. Wells, *Journal of the Chemical Society, Chemical Communications*, 1973, 444b-445.
  54. M. Haruta, T. Kobayashi, H. Sano and N. Yamada, *Chemistry Letters*, 1987, 405-408.
  55. B. Nkosi, N. J. Coville and G. J. Hutchings, *Journal of the Chemical Society, Chemical Communications*, 1988, 71-72.
  56. E. M. Larsson, C. Langhammer, I. Zoric and B. Kasemo, *Science of Advanced Materials*, 2009, **326**, 1091-1094.
  57. M. Haruta, N. Yamada, T. Kobayashi and S. Iijima, *Journal of Catalysis*, 1989, **115**, 301-309.
  58. M. A. Aubart and L. H. Pignolet, *Journal of the American Chemical Society*, 1992, **114**, 7901-7903.
  59. Y. Yuan, K. Asakura, H. Wan, K. Tsai and Y. Iwasawa, *Catalysis Letters*, 1996, **42**, 15-20.
  60. G. C. Bond and D. T. Thompson, *Catalysis Reviews*, 1999, **41**, 319-388.
  61. C. Milone, R. Ingoglia, G. Neri, A. pistone and S. Galvagno, *Applied Catalysis A: General*, 2001, **211**, 251-257.
  62. M. Haruta and M. Data, *Applied Catalysis A: General*, 2001, **222**, 427-437.
  63. S. Biella, L. Prati and M. Rossi, *Journal of Catalysis*, 2002, **206**, 242-247.

- 
64. G. J. Hutchings, *Catalysis Today*, 2005, **100**, 55-61.
  65. G. J. Hutchings and M. Haruta, *Applied Catalysis A: General*, 2005, **291**, 2-5.
  66. M. Haruta, *Journal of the Vacuum Society of Japan*, 2008, **51**, 721-726.
  67. L. A. Larew and D. C. Johnson, *Journal of Electroanalytical Chemistry, Interfacial Electrochemistry*, 1989, **262**, 167-182.
  68. A. I. Kozlov, A. P. Kozlova, H. Liu and Y. Iwasawa, *Applied Catalysis A: General*, 1999, **182**, 9-28.
  69. H. G. Boyen, G. Kastle, F. Weigl, B. Koslowski, C. Dietrich, P. Ziemann, J. P. Spatz, S. Riethmuller, C. Hartmann, M. Moller, G. Schmid, M. G. Garnier and P. Oelhafen, *Science*, 2002, **297**, 1533-1536.
  70. S. Biella, G. L. Castiglioni, C. Fumagalli, L. Prati and M. Rossi, *Catalysis Today*, 2002, **72**, 43-49.
  71. H. Berndt, A. Martin, I. Pitsch, U. Prusse and K. D. Vorlop, *Catalysis Today*, 2004, **91-92**, 191-194.
  72. W. Fang, J. Chen, Q. Zhang, W. Deng and Y. Wang, *Chemistry – A European Journal*, 2011, **17**, 1247-1256.
  73. G. Diaz, A. Gomez-Cortes, O. Hernandez-Cristobal, J. J. Murcia, G. Borda and H. Rojas, *Topics in Catalysis*, 2011, **54**, 467-473.
  74. E. Castillejos, E. Gallegos-Suarez, B. Bachiller-Baeza, R. Bacsá, P. Serp, A. Guerrero-Ruiz and I. Rodríguez-Ramos, *Catalysis Communications*, 2012, **22**, 79-82.
  75. K. Qian, J. Fang, W. Huang, B. He, Z. Jiang, Y. Ma and S. Wei, *Journal of Molecular Catalysis A: Chemical*, 2010, **320**, 97-105.
  76. P. Schwerdtfeger and P. D. W. Boyd, *Inorganic Chemistry*, 1992, **31**, 327-329.
  77. O. D. Haeberlen, H. Schmidbaur and N. Roesch, *Journal of the American Chemical Society*, 1994, **116**, 8241-8248.
  78. H. Schmidbaur, S. Cronje, B. Djordjevic and O. Schuster, *Chemical Physics*, 2005, **311**, 151-161.
  79. G. Hogarth, S. E. Kabir and E. Nordlander, *Dalton Transactions*, 2010, **39**, 6153-6174.
  80. D. M. P. Mingos, *Polyhedron*, 1984, **3**, 1289-1297.

- 
81. M. Walter, J. Akola, O. Lopez-Acevedo, P. D. Jadzinsky, G. Calero, C. J. Ackerson, R. L. Whetten, H. Gräßlinbeck and H. Häkkinen, *Proceedings of the National Academy of Sciences*, 2008, **105**, 9157-9162.
  82. G. Shafai, S. Hong, M. Bertino and T. S. Rahman, *Journal of Physical Chemistry C*, 2009, **113**, 12072-12078.
  83. R. P. F. Kanters, J. J. Bour, P. P. J. Schlebos, W. P. Bosman, H. Behm, J. J. Steggerda, L. N. Ito and L. H. Pignolet, *Inorganic Chemistry*, 1989, **28**, 2591-2594.
  84. O. Rossell, M. Seco, G. Segalés, M. A. Pellinghelli and A. Tiripicchio, *Journal of Organometallic Chemistry*, 1998, **571**, 123-128.
  85. R. Boca, *Journal of the Chemical Society, Dalton Transactions*, 1994, 2061-2064.
  86. P. Pykkö, *Angewandte Chemie, International Edition*, 2004, **43**, 4412-4456.
  87. J. Granatier, M. Urban and A. J. Sadlej, *Chemical Physics Letters*, 2010, **484**, 154-159.
  88. A. Codina, E. J. Fernandez, P. G. Jones, A. Laguna, J. M. Lopez-de-Luzuriaga, M. Monge, M. E. Olmos, J. Perez and M. A. Rodriguez, *Journal of the American Chemical Society*, 2002, **124**, 6781-6786.
  89. L. Malatesta, *Gold Bulletin*, 1975, **8**, 48-52.
  90. D. M. P. Mingos, *Gold Bulletin*, 1984, **17**, 5-12.
  91. P. D. Jadzinsky, G. Calero, C. J. Ackerson, D. A. Bushnell and R. D. Kornberg, *Science of Advanced Materials*, 2007, **318**, 430-433.
  92. M. Brust, M. Walker, D. Bethell, D. J. Schiffrin and R. Whyman, *Journal of Chemical Society, Chemical Communications*, 1994, 801-802.
  93. C. A. Tolman, *Chemical Reviews*, 1977, **77**, 313-348.
  94. D. M. P. Mingos, *Philosophical Transactions of the Royal Society of London. Series A, Mathematical and Physical Sciences*, 1982, **308**, 75-83.
  95. P. J. Dyson and D. M. P. Mingos, *Homonuclear Clusters and Colloids of Gold: Synthesis, Reactivity, Structural and Theoretical Considerations in Gold; Progress in Chemistry, Biochemistry and Technology*, Wiley, Chichester., 1999.

- 
96. G. Schmid, R. Pfeil, R. Boese, F. Bandermann, S. Meyer, G. H. M. Calis and W. A. Vandervelden, *Chemische Berichte-Recueil*, 1981, **114**, 3634-3642.
  97. F. A. Vollenbroek, J. J. Bour and d. V. J. W. A. Van, *Recueil des Travaux Chimiques des Pays-Bas*, 1980, **99**, 137-141.
  98. F. Cariati and L. Naldini, *Journal of the Chemical Society, Dalton Transactions*, 1972, 2286 - 2287.
  99. F. A. Vollenbroek, J. J. Bour, J. M. Trooster and J. W. A. v. d. Velden, *Journal of the Chemical Society, Chemical Communications*, 1978, 907-909.
  100. F. A. Vollenbroek, W. P. Bosman, J. J. Bour, J. H. Noordik and P. T. Beurskens, *Journal of Chemical Society, Chemical Communications*, 1979, 387-388.
  101. D. V. J. W. A. Van, J. J. Bour, W. P. Bosman and J. H. Noordik, *Journal of Chemical Society, Chemical Communications*, 1981, 1218-1219.
  102. L. Malatesta, L. Naldini, G. Simonetta and F. Cariati, *Coordination Chemistry Reviews*, 1966, **1**, 255-262.
  103. B. F. G. Johnson, D. A. Kaner, J. Lewis, P. R. Raithby and M. J. Taylor, *Polyhedron*, 1982, **1**, 105-107.
  104. A. L. Casalnuovo, J. A. Casalnuovo, P. V. Nilsson and L. H. Pignolet, *Inorganic Chemistry*, 1985, **24**, 2554-2559.
  105. P. D. Boyle, B. J. Johnson, A. Buehler and L. H. Pignolet, *Inorganic Chemistry*, 1986, **25**, 5-7.
  106. D. M. P. Mingos, *Journal of the Chemical Society, Dalton Transactions*, 1976, 1163-1169.
  107. K. P. Hall, D. I. Gilmour and D. M. P. Mingos, *Journal of Organometallic Chemistry*, 1984, **268**, 275-293.
  108. F. Cariati and L. Naldini, *Journal of Chemical Society - Dalton Transactions*, 1972, 2286-2287.
  109. C. E. Briant, K. P. Hall, D. M. P. Mingos and A. C. Wheeler, *Journal of Chemical Society - Dalton Transactions*, 1986, 687-692.
  110. J. G. M. Vanderlinden, M. L. H. Paulissen and J. E. J. Schmitz, *Journal of the American Chemical Society*, 1983, **105**, 1903-1907.
  111. F. Demartin, M. Manassero, L. Naldini, R. Ruggeri and M. Sansoni, *Journal of Chemical Society - Chemical Communications*, 1981, 222-223.

- 
112. J. W. A. Vandervelden, P. T. Beurskens, J. J. Bour, W. P. Bosman, J. H. Noordik, M. Kolenbrander and J. Buskes, *Inorganic Chemistry*, 1984, **23**, 146-151.
113. J. W. A. Vandervelden, J. J. Bour, J. J. Steggerda, P. T. Beurskens, M. Roseboom and J. H. Noordik, *Inorganic Chemistry*, 1982, **21**, 4321-4324.
114. C. E. Briant, K. P. Hall, A. C. Wheeler and D. M. P. Mingos, *Journal of Chemical Society - Chemical Communications*, 1984, 248-250.
115. C. E. Briant, B. R. C. Theobald, J. W. White, L. K. Bell and D. M. P. Mingos, *Journal of Chemical Society - Chemical Communications*, 1981, 201-202.
116. P. Mukherjee, C. R. Patra, R. Kumar and M. Sastry, *Physical Chemistry Communications*, 2001, **5**, 1-2.
117. F. Caruso, M. Spasova, V. Salgueiriño-Maceira and L. M. Liz-Marzán, *Advanced Materials*, 2001, **13**, 1090-1094.
118. C. C. Chusuei, X. Lai, K. A. Davis, E. K. Bowers, J. P. Fackler and D. W. Goodman, *Langmuir*, 2001, **17**, 4113-4117.
119. T. V. Choudhary, C. Sivadinarayana, C. C. Chusuei, A. K. Datye, J. P. Fackler and D. W. Goodman, *Journal of Catalysis*, 2002, **207**, 247-255.
120. Y. Liu, H. Tsunoyama, T. Akita and T. Tsukuda, *The Journal of Physical Chemistry C*, 2009, **113**, 13457-13461.
121. E. S. Andreiadis, M. R. Vitale, N. Mezailles, X. L. Goff, P. L. Floch, P. Y. Toullec and V. Michelet, *Dalton Transactions*, 2010, **39**, 10608-10616.
122. Y. Liu, H. Tsunoyama, T. Akita and T. Tsukuda, *Chemistry Letters*, 2010, **39**, 159-161.
123. M. Turner, V. B. Golovko, O. P. H. Vaughan, P. Abdulkin, A. Berenguer-Murcia, M. S. Tikhov, B. F. G. Johnson and R. M. Lambert, *Nature*, 2008, **454**, 981-983.
124. P.-J. Li, S.-A. Dong, C. Tang, S.-C. Yang, Y.-W. Gu and K.-Z. Li, *Huaxue Xuebao*, 2006, **64**, 1140-1144.
125. W. Gao, X. F. Chen, J. C. Li and Q. Jiang, *Journal of Physical Chemistry C*, 2010, **114**, 1148-1153.
126. T. G. M. M. Kappen, J. J. Bour, P. P. J. Schlebos, A. M. Roelofsen, J. G. M. Van der Linden, J. J. Steggerda, M. A. Aubart, D. A. Krogstad, M. F. J.

- 
- Schoondergang and L. H. Pignolet, *Inorganic Chemistry*, 1993, **32**, 1074-1075.
127. C.-W. Chiang, A. Wang and C.-Y. Mou, *Catalysis Today*, 2006, **117**, 220-227.
128. S. Jafari, H. Asilian Mahabady and H. Kazemian, *Catalysis Letters*, 2009, **128**, 57-63.
129. H. Jiahui, A. Tomoki, F. Jérémy, F. Tadahiro, T. Takashi and H. Masatake, *Angewandte Chemie, International Edition*, 2009, **48**, 7862-7866.
130. T. Joseph, K. Vijay Kumar, A. V. Ramaswamy and S. B. Halligudi, *Catalysis Communications*, 2007, **8**, 629-634.
131. M. Wolf and H. Knozinger, *Journal of Molecular Catalysis*, 1984, **25**, 273-283.

---

## Chapter 2

### Synthesis and Characterization of Gold Molecular Clusters and Gold Nanoparticulate Catalysts

#### 2.0 Abstract

Gold phosphine molecular clusters were used during this research as precursors to gold nanoparticle catalysts. The reasoning behind using molecular clusters as precursors is to be able to control nanoparticle size and distribution. Two gold-phosphine molecular clusters were used namely,  $[\text{Au}_9\{\text{Ph}_2\text{P}(p\text{-tolyl})\}_8](\text{NO}_3)_3$  (**Au<sub>9</sub>**) and  $[\text{Au}_{13}(\text{dppm})_6](\text{NO}_3)_4$  (**Au<sub>13</sub>**) with dppm being 1,1-bis(diphenylphosphino)methane (dppm). Two methods were utilised towards heterogenization of the clusters onto supports, namely, the classic wet impregnation method (WI) and *tert*-butylhydroperoxide deposition precipitation method (TBHP) which we first developed and reported<sup>1</sup>. Two different supports were also used, SiO<sub>2</sub> nanospheres and Al<sub>2</sub>O<sub>3</sub>. Concise synthetic procedures and characterization techniques that were used are discussed in this chapter.

#### 2.1 Introduction

Highly dispersed gold nanoparticles have been demonstrated to be highly active catalysts for a number of important chemical reactions ranging from selective oxidation<sup>2</sup> to hydrogenation<sup>3</sup> and hydrochlorination<sup>4</sup>. It is crucial to get narrow size and shape distributions of gold nanoparticles since catalytic activities have been

---

shown to be strongly dependent on both factors<sup>5</sup>. In order to achieve the controlled synthesis of gold nanoparticles within a narrow size range, several methods have been developed<sup>6-10</sup>. These include, co-precipitation from an aqueous solution of  $\text{HAuCl}_4$ <sup>11</sup>, deposition-precipitation using precipitation agents<sup>12</sup> and chemical vapour deposition of gold nanoparticles<sup>13</sup>.

For catalytic applications, nanoparticles are normally either formed on external surfaces of the oxide particles<sup>14, 15</sup> or embedded in microporous oxide matrices such as zeolites<sup>16, 17</sup>. Gold nanoparticles on external surfaces are susceptible to aggregation because of a lack of space confinements,<sup>18, 19</sup> while in zeolites they can become inaccessible to reactants for effective catalytic reactions<sup>20, 21</sup>. Our approach towards minimizing aggregation and accessibility issues was to use molecular clusters as catalyst precursors and the development of methodology for the controlled synthesis of gold nanoparticulate catalysts *via* chemical modification.

This approach has been successfully used to produce a variety of mono and bimetallic clusters<sup>1, 22-24</sup>. However, these clusters are generally inherently unstable and not easily accessible. In order to use them for catalysis they have to be activated by removing the capping agent and attaching to a support which is often a finely-divided metal oxide, such as silica or titania. The support has a number of functions, but the major role is to prevent particle aggregation which can lead to significant loss of catalytic activity.

---

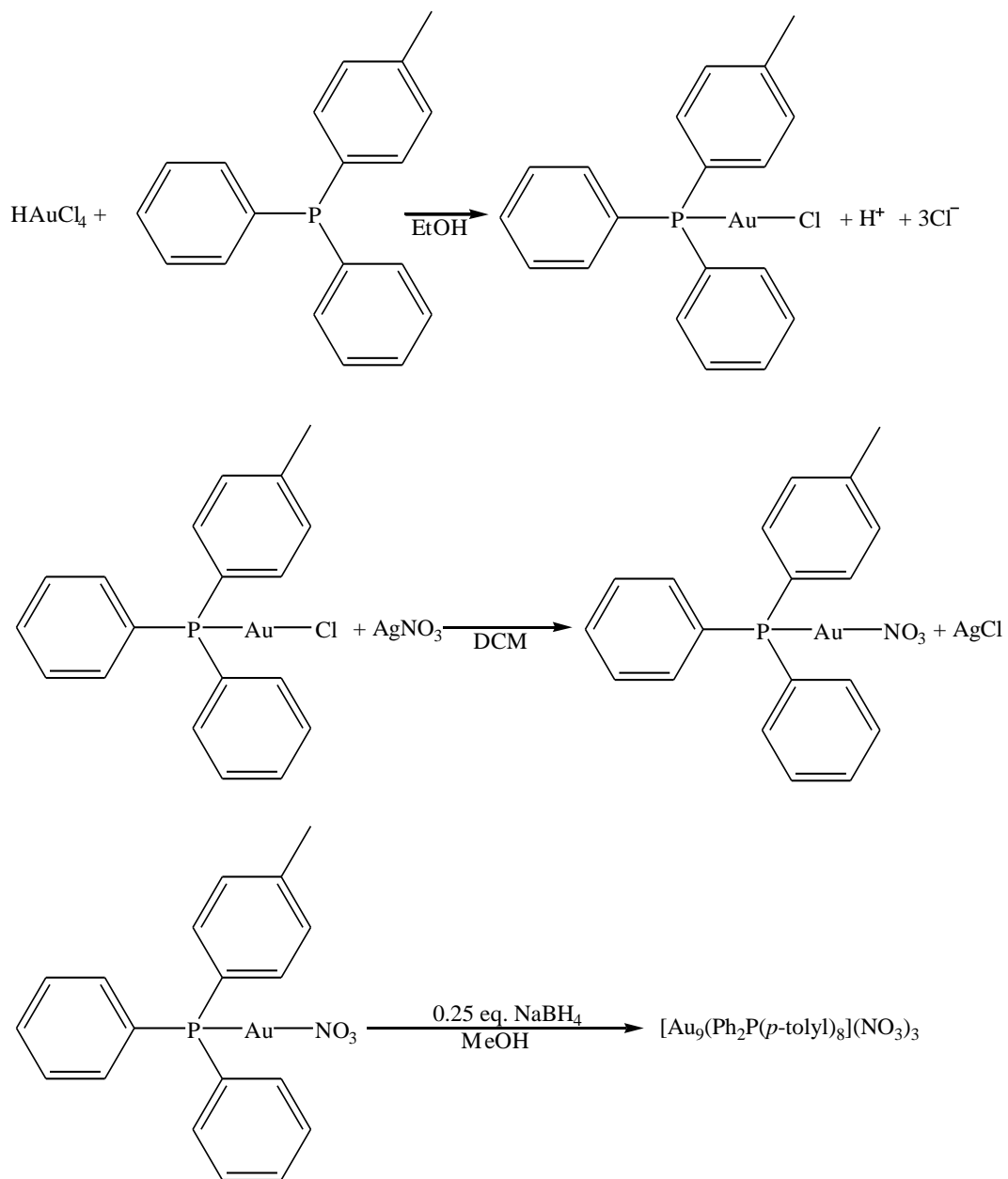
## 2.2 Synthesis of Gold Molecular Clusters

Gold clusters have been synthesized with two different phosphine ligands namely diphenyl-*p*-tolylphosphine and bis(diphenylphosphino)methane (dppm). Their synthesis involved three steps starting with the gold chloride complexes ( $\text{Au}(\text{L})\text{Cl}$ ;  $\text{L} = \text{Ph}_2\text{P}(p\text{-tol})$  or  $\text{Au}_2(\text{L})\text{Cl}_2$ ;  $\text{L} = \text{dppm}$ ) prepared from hydrogen tetrachloroaurate trihydrate ( $\text{HAuCl}_4 \cdot 3\text{H}_2\text{O}$ ) and the ligand. The chloride ligand was then exchanged for nitrate by reacting the chloride complexes with silver nitrate ( $\text{AgNO}_3$ ). Clusters were then obtained by reducing the gold nitrate complexes with stoichiometric amounts of sodium borohydride ( $\text{NaBH}_4$ ).

We utilised a synthetic method reported in the literature but with an adjustment of the ligand system<sup>25, 26</sup>. The use of diphenyl-*p*-tolyl-phosphine (*p*-tol) instead of triphenylphosphine ( $\text{PPh}_3$ ) ligand was to generate a clearer NMR spectrum for monitoring the changes occurred. Besides that, the solubility of the clusters especially in non-chlorinated solvent is one of the important parameters that needed attention. The presence of the methyl group in the *p*-tol ligand affords greater solubility due to its non-symmetrical structure. Hence, the rearrangement of the gold core geometry<sup>27</sup>, also degradation of the clusters<sup>28</sup> that tends to happen in solution especially with the presence of chlorinated solvents, can be minimised.

All experiments were carried out using the standard Schlenk-line techniques under a purified  $\text{N}_2$  atmosphere unless mentioned otherwise. Solvents used were dried and  $\text{O}_2$ -free if necessary. No any other special precautions were taken to exclude air or moisture from the synthetic procedures. All chemicals were used as purchased from Sigma-Aldrich, BDH or Alfa Aesar.

### 2.2.1 Synthesis of Au<sub>9</sub> Clusters



**Scheme 2.1:** Reaction scheme of Au<sub>9</sub> clusters synthesis

$[\text{Au}_9(\text{Ph}_2\text{P}(p\text{-tol}))_8](\text{NO}_3)_3$  was prepared as described in the literature<sup>26</sup> with a slight modification.  $\text{Au}(\text{Ph}_2\text{P}(p\text{-tol}))\text{NO}_3$  (0.2522 g, 0.467 mmol) in ethanol (10 ml) was placed in round bottom flask. A solution of  $\text{NaBH}_4$  (0.0049 g, 0.119 mmol) in

---

ethanol (10 ml) was added to the stirring slurry of  $\text{Au}(\text{Ph}_2\text{P}(p\text{-tol}))\text{NO}_3$ . The solution immediately turned to dark red-brown. It was stirred until all the white solid has fully reacted. Evaporation of the solvents to dryness gave a brown solid (0.2060 g) which was then washed with tetrahydrofuran (10 ml) and filtered off under vacuum giving the dark green solid. % yield: 78% based on gold.  $^1\text{H}$ -NMR (MeOD):  $\delta$  (ppm) aromatic protons; 7.39-6.51(m);  $-\text{CH}_3$ ; 2.10(s).  $^{31}\text{P}\{^1\text{H}\}$ -NMR:  $\delta$  (ppm) 56.6(s). Elemental analysis gives C, 43.52%; H, 2.97%; N, 1.00%; as  $\text{Au}_9\text{P}_8\text{C}_{152}\text{H}_{136}\text{N}_3\text{O}_9$  requires C, 43.79%; H, 3.29%; N, 1.01%.

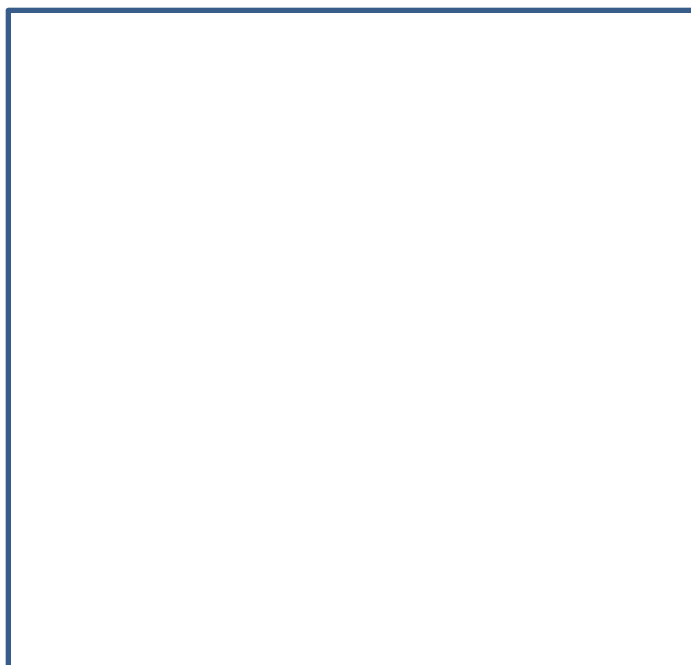
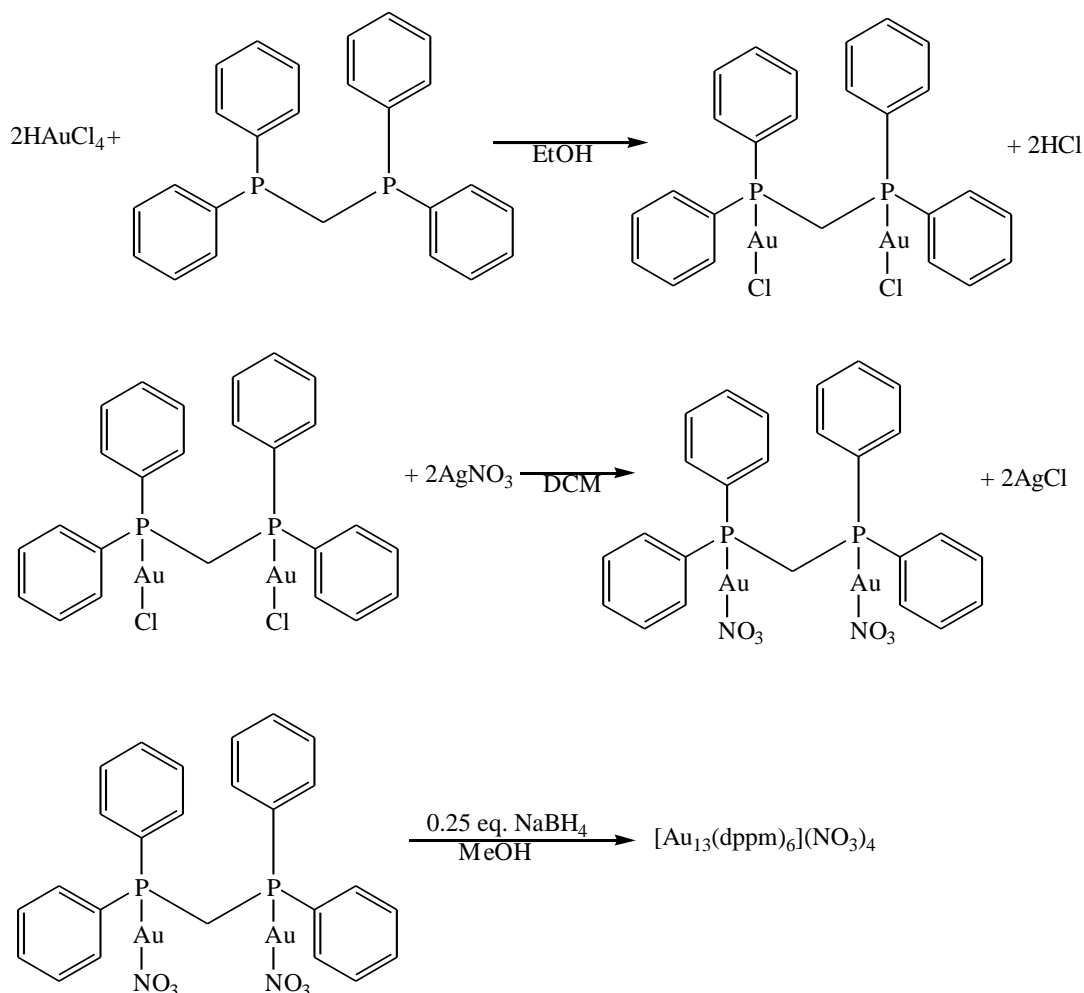


**Figure 2.1:** Crystal structure of  $[\text{Au}_9(\text{PPh}_3)_8](\text{NO}_3)_3$  clusters referenced from literature. Hydrogen and carbon atoms omitted for clarity<sup>29</sup>

## 2.2.2 Synthesis of Au<sub>13</sub> Clusters



**Scheme 2.2:** Reaction scheme of Au<sub>13</sub> clusters synthesis

The synthesis of  $[\text{Au}_{13}(\text{dppm})_6](\text{NO}_3)_4$  was carried out according to a literature<sup>30</sup> procedure.  $\text{Au}_2(\text{dppm})(\text{NO}_3)_2$  was prepared in an analogous manner to  $\text{Au}(\text{PPh}_3)\text{NO}_3$ <sup>26</sup>.  $\text{NaBH}_4$  (0.0059 g, 0.150 mmol) dissolved in 30 ml ethanol was slowly added to a stirred solution of  $\text{Au}_2(\text{dppm})(\text{NO}_3)_2$  (0.2701 g, 0.299 mmol) in 50 ml ethanol. The reaction mixture turned green and was then filtered and the filtrate set aside. Evaporation of the solvents of the filtrate produced a greenish-brown solid (0.2015 g) which was dried in ambient temperature. % yield: 63% based on gold. <sup>1</sup>H-

---

NMR (MeOD):  $\delta$  (ppm) aromatic protons; 7.85-7.07(m);  $-\text{CH}_2-$ ; 3.80(t).  $^{31}\text{P}\{^1\text{H}\}$ -NMR:  $\delta$  (ppm) 35.9(s). Elemental analysis gives C, 34.11%; H, 2.62%; N, 1.07%; as  $\text{Au}_{13}\text{P}_{12}\text{C}_{150}\text{H}_{132}\text{N}_4\text{O}_{12}$  requires C, 35.22%; H, 2.60%; N, 1.10%.

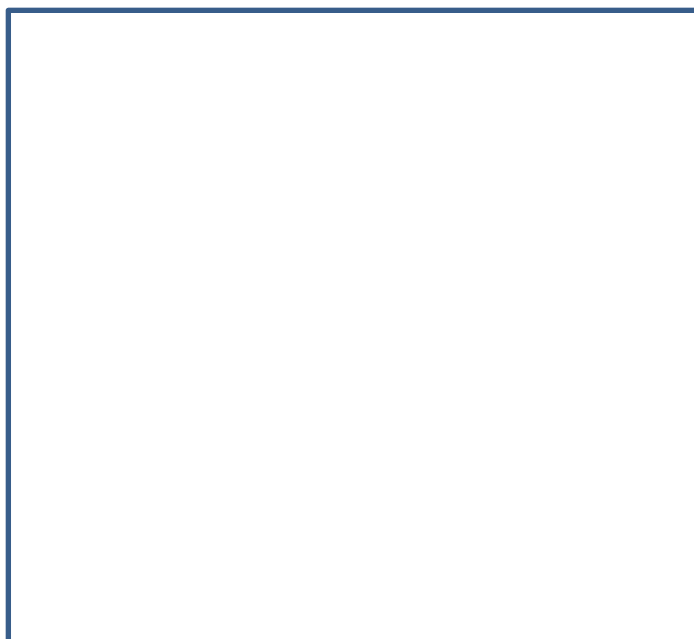


**Figure 2.2:** Crystal structure of  $[\text{Au}_{13}(\text{dppm})_6](\text{NO}_3)_4$  clusters referenced from literature. Hydrogen and carbon atoms omitted for clarity<sup>31</sup>

### 2.3 Synthesis of Gold Nanoparticle Catalysts

Heterogeneous catalysts are often synthesized using capillary impregnation or dry impregnation or commonly called the incipient wetness impregnation method. The procedure requires the active metal precursor first to be dissolved in an aqueous or organic solution before being added to a slurry of the catalyst support in the same solvent. It is called capillary impregnation when the capillary action draws the solution into the pores and then changes to a diffusion process, which is much slower. In order to be able to process changes, solutions must be added in excess of the support pore volume. To isolate the catalyst, it is then dried or calcined to remove all the volatile components as well as depositing the metal onto the support. The

---

main drawbacks of this method are the limited loading of the metal being limited by the solubility of the precursor in the solution and the mass transfer conditions within the support pore or surface during the impregnation and drying that determined the concentration of the impregnated compound<sup>32</sup>. Nevertheless, the simplicity of the procedure often makes it the initial choice for scientist in preparing heterogeneous catalysts.

The deposition precipitation method in contrast is usually employed to prepare highly dispersed gold particles on oxide supports. It involves heating (from 70°C to 100°C) and pH adjustment processes to 7 or 8 by adding a base, such as NaOH or urea as a precipitating agent. The precursor and solid support is mixed and aged between one to twelve hours and washed with distilled water to remove residuals before drying and calcined at the required temperature. Despite the more detailed procedure including pre-treatment and calcination that significantly influence the properties of the gold catalysts, this method still seems to be the most efficient for preparing highly active gold catalysts<sup>12, 33-37</sup>.

### *2.3.1 Wet Impregnation (WI) Method*

The clusters were deposited on SiO<sub>2</sub> spheres or CATAPAL-A Al<sub>2</sub>O<sub>3</sub> with different loading percentages of gold (0.1, 1.0 and 4.0 % wt). A proper amount of support was immersed in ethanol (5 ml) and stirred for 5 minutes. The slurry was then placed in an ultrasonic bath for 5 minutes to generate a relatively equal dispersion of the support. An appropriate amount of clusters (0,1 wt. %, 1.0 wt. % or 4.0 wt. %) was dissolved in methanol (5 ml) and added to the SiO<sub>2</sub> slurry while stirring. The mixture was stirred for 30 minutes then placed into an ultrasonic bath

---

for another 5 minutes. The products were recovered by drying out the solvents using rotary evaporator or Schlenk-line vacuum and then finely ground into a powder to get the visibly homogenized sample. The catalysts were calcined at 300 °C and 500 °C at 10 °C/min for 1 hour.

### 2.3.2 *tert-butylhydroperoxide Deposition-Precipitation (TBHP) Method*

The clusters were deposited on SiO<sub>2</sub> spheres or CATAPAL-A Al<sub>2</sub>O<sub>3</sub> with a calculated of 4.0 % wt. Au loading. An amount of support (1.0 g) was immersed in TBHP (5 ml) and stirred for 5 minutes. The slurry was then put into an ultrasonic bath for 5 minutes to generate a relatively equal dispersion of the support. An appropriate amount of the cluster was dissolved in TBHP (5 ml) then added to the support slurry while stirring. The mixture was stirred for 10 minutes then placed in an ultrasonic bath for another 5 minutes. An excess of TBHP (5 ml) was then added to the mixture which was refluxed at 90 °C for 3 hours. The products were recovered by vacuum filtration, dried in an oven at 100 °C for 1 hour then finely ground to a powder to give a visibly homogenized sample. Half of the catalyst samples were calcined at 300 °C at 10 °C/min for 1 hour with the remaining being uncalcined.

## 2.4 Characterization Techniques

Characterisation of the synthesized compounds was carried out using several techniques and instruments at University College London. Elemental analyses were measured by Jill Maxwell. Proton-decoupled <sup>31</sup>P{<sup>1</sup>H} NMR spectra were recorded in either CDCl<sub>3</sub>, CD<sub>2</sub>Cl<sub>2</sub> or MeOD on a Bruker Avance 400MHz spectrometer at room temperature. Electrospray ionization mass spectrometry (ESI-MS) was carried out on a Micromass Quattro Micro. Samples were diluted in methanol/water at a

---

concentration of  $\sim 1$  ng/ $\mu$ L. Thermogravimetric and differential scanning calorimetric (TGA-DSC) were measured on Netzsch system under an argon atmosphere up to 600 °C with increasing rate of 2 °C/min. Transmission electron micrograph (TEM) images of the nanoparticles were taken using a JEOL 100 keV transmission electron microscope. X-ray powder diffraction (XRD) pattern were measured using Bruker D4 X-ray diffractometer with Cu  $K_{\alpha}$  radiation over the  $2\theta$ -range of 5 to 90°, 0.05sec/step size.

Au  $L_3$ -edge extended X-ray absorption fine structure (EXAFS) analysis were recorded at DUBBLE BM26 beamline, ESRF Synchrotron Centre Grenoble, France and SAMBA beamline, SOLEIL Synchrotron Centre Paris, France and DIAMOND Light Source, Oxford, UK. The samples were measured at room temperature for *ex-situ* study and *in-situ* heating up to 300 °C in a transmission mode. Alternate XRD patterns were recorded after every one complete EXAFS scan. The data analysis was carried out using Athena and EXCURVE software. Detailed procedure to analyse the data was employed according to literature<sup>38</sup>.

#### 2.4.1 Carbon, Hydrogen, Nitrogen (CHN) Elemental Analysis

The first method employed to characterise the clusters prepared was elemental analysis. Basically, this technique can be qualitative, that is to detect elements present in the compound, and can also be quantitative, determining the percentage of each elements present. We determined the mass fraction of carbon, hydrogen and nitrogen in the clusters. It is the first insight whether we managed to incorporate the ligand and the metal as complexes than clusters without breaking the

---

structure of the ligand used. This information helps us to determine the structure as well as ascertain the purity of synthesized clusters.

This technique is accomplished by combustion analysis where a small amount of cluster (*ca.* 15 – 20 mg) is burned in excess of oxygen with various traps attached to collect the combustion products. The mass fractions data gathered were then used to calculate the composition of the clusters. Results were analysed by determining the ratio of each elements from within the clusters and working out an empirical formula that fits with those ratios. Comparison of this data with the expected calculated data confirms the purity of the clusters. The accepted deviation of elemental analysis results from the calculated is 0.4%<sup>39</sup>.

#### 2.4.2 Ultraviolet-Visible (UV-Vis) Spectroscopy

Another spectroscopic method utilised in the characterisation of gold molecular clusters was ultraviolet-visible (UV-Vis) spectroscopy. One of the characteristics of gold molecular clusters is their colour. The relativistic effects (as discussed in Chapter 1) become dominant in gold because of the *5d* character that makes the *s* and *p* sub-shells more contracted while *d* and *f* are destabilized and more diffuse. This relativistic stabilization results in gold not only being yellow in colour but also existing as red, blue, green, purple, brown and even black gold. Therefore, UV-Vis spectroscopy can be used to give preliminary insight of the electronic properties of gold molecular clusters synthesized.

The molecular moieties that are likely to absorb light in the UV-Vis region (200-800nm) are  $\pi$ -electron functions and hetero atoms having non-bonding valence-

shell electron pairs that are referred to as chromophores<sup>40</sup>. It is difficult to obtain much information about the gold molecular clusters using only this technique. Hence, other analytical techniques should be employed together but this technique is of importance as a first characterization of a newly formed compound as it is simple and economic<sup>41</sup>. Mingos *et al.* used UV-Vis spectroscopy to distinguish the clusters in solution from differences in band maxima which differ for **Au<sub>9</sub>**, **Au<sub>11</sub>** and **Au<sub>13</sub>** clusters<sup>42</sup>. Recently, Haiss *et al.* reported that UV-Vis spectroscopy can be used in size determination of gold nanoparticles<sup>43</sup>.

### 2.4.3 <sup>1</sup>H and <sup>31</sup>P Nuclear Magnetic Resonance (NMR) Spectroscopy

Nuclear magnetic resonance (NMR) spectroscopy is a unique technique in that it explores the nuclei of a sample and not the electrons. NMR takes advantages of the magnetic properties of specific nuclei to yield chemical information. Nuclei that have an overall spin can be probed by NMR spectroscopy. When a magnetic field is applied to an atom, the magnetic moment of the nucleus will either align with or against the applied magnetic field<sup>40</sup>. It is applicable to any kind of sample that contains nuclei possessing spin.

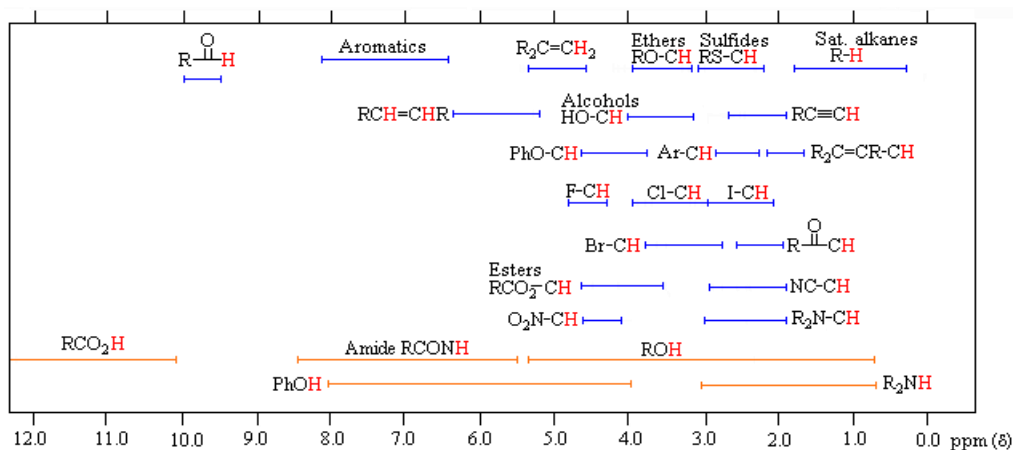


**Figure 2.3:** Proton Chemical Shift Ranges<sup>40</sup>

---

The phosphine stabilized gold molecular clusters that we synthesized were probed by NMR measurement for two different active nuclei, proton and phosphorus. The nuclei will absorb electromagnetic radiation at frequency characteristic of the specific isotope namely  $^1\text{H}$  and  $^{31}\text{P}$  with spin quantum number of  $\frac{1}{2}$ . Proton NMR was generally straight forward determining the type of proton present in the ligand. The assignments of the peaks were done with reference to proton chemical shift ranges, as shown in Figure 2.3.

For spin  $\frac{1}{2}$  nuclei, the energy difference between the two spin states at a given magnetic field strength are proportional to their magnetic moments. However, even if all protons have the same magnetic moments, they do not give resonant signals at the same values. This is because this is dependent on the electrons surrounding the proton in covalent compounds. Upon application of an external magnetic field, these electrons move in response to the field and generate local magnetic fields that oppose the much stronger applied field. This local field thus 'shield' the proton from the applied magnetic field, which must therefore be increased in order to achieve resonance. Such increments are very small, usually in parts per million (ppm)<sup>40</sup>. The chemical shift provides information of every neighbouring atom (proton) therefore detail of the structure of the molecule can be achieved.

We have demonstrated the uses of elemental analysis and UV-Vis spectroscopy as the preliminary tools for characterisation of gold molecular clusters. It was found to be of limited use to identify and to verify the purity of gold clusters. Vollenbroek *et. al* however proved that  $^{31}\text{P}\{^1\text{H}\}$  NMR spectroscopy to be very useful

---

in giving better information about the structure of phosphine-stabilized gold molecular clusters<sup>44</sup>. This spectroscopic method was also used to investigate the reaction of phosphine-stabilized gold molecular clusters<sup>27, 45, 46</sup> and to obtain information about chemical bonding and dynamical properties of the clusters.

#### *2.4.4 Thermogravimetric Analysis-Differential Scanning Calorimetry (TGA-DSC)*

Thermal analysis is widely used in materials science where the properties of materials are studied as they change with temperature. In this research, we use thermogravimetric analysis (TGA) to observe the mass change in the sample, together with differential scanning calorimetry (DSC) which records the heat differences, while ramping the sample at increasing temperature under controlled condition (Figure 2.4). Both TGA and DSC were used simultaneously on the same sample in a single instrument. The test conditions are perfectly identical for the TGA and DSC signals which include the same atmosphere, gas flow rate, vapor pressure of the sample and heating rate.

TGA is a process that utilizes heat and stoichiometry ratios to determine the percent by mass of a solute<sup>47</sup>. Analysis is carried out by raising the temperature of the sample gradually and plotting weight (in percentage value) against temperature or time. The temperature in many testing methods routinely reaches 1000°C or higher. After the data are obtained, curve smoothing and other operations may be done to find the exact points of inflection.

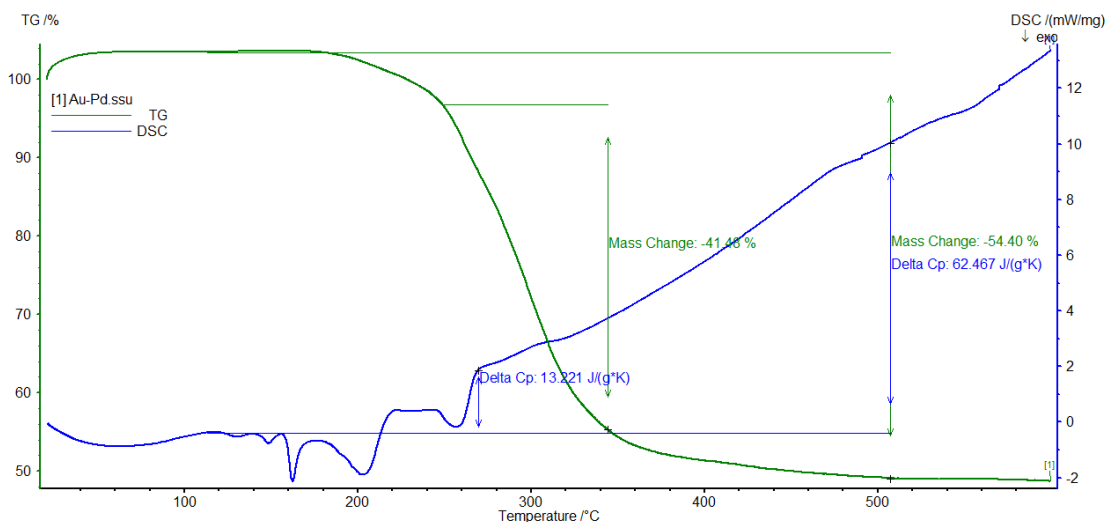


**Figure 2.4:** Example of TGA-DSC curve of **Au<sub>9</sub>** cluster that measured simultaneously

DSC measures the difference in the amount of heat required to increase the temperature of a sample and reference as a function of temperature<sup>47, 48</sup>. Both the sample and reference are maintained at nearly the same temperature throughout the experiment. Generally, the sample holder temperature increases linearly as a function of time. The reference sample should have a well-defined heat capacity over the range of temperature to be scanned. The basic principle underlying this technique is that when the sample undergoes a physical transformation such as phase transitions, more or less heat will need to flow to it than the reference to maintain both at the same temperature. The amount of heat required to flow throughout the sample depends on whether the process is exothermic or endothermic.

In our work, TGA-DSC analysis was used to determine the temperature to activate the catalyst or to get the naked gold clusters. The existence of ligand as precursor for gold molecular cluster to tailor the specific geometry and

---

hypothetically the size of gold cluster can somehow affect the activity of the catalyst. Therefore, this technique is needed to determine the required temperature to strip off ligands from molecular clusters as well as activating the catalyst. Sintering and aggregation of gold clusters can occur at high temperature<sup>18,19</sup>. It is crucial to control the sintering process and simultaneously activate the catalyst with heat treatment at ideal temperature.

#### 2.4.5 *Electrospray Ionization-Mass Spectrometry (ESI-MS)*

Mass spectrometry (MS) is another spectroscopic technique that measures mass-to-charge ratio of charged particles which determined the mass, elemental composition as well as elucidating the chemical structures of a molecule. Electrospray ionization (ESI) on the other hand is one of the techniques used in MS to produce ions especially macromolecules because it can overcome the propensity of molecules to fragment when ionized. The samples were diluted in an appropriate solvent (typically mixed water with volatile organic liquor, such as methanol and acetonitrile) and then dispersed by electrospray into a fine aerosol. The initial droplet size has to be very small therefore compounds that increase the conductivity, such as acetic acid are customarily added to the solution.

The ions observed by ESI-MS may be quasimolecular ions  $[M+H]^+$  or another cation such as sodium ion  $[M+Na]^+$  or the removal of a proton  $[M-H]^-$ . Often observed in ESI-MS spectrum is multiply charged ions, such as  $[M+H]^{n+}$ . Furthermore, for macromolecules, there are also many charge states observed resulting in a characteristic charge state envelope. All these are even-electron ion species which is electrons alone that are not added or removed unlike in some other

---

ionization sources. Adding to that, the analytes are sometimes involved in the electrochemical processes leading to shifts of the corresponding peaks in the mass spectrum<sup>49, 50</sup>.

Traeger *et al.* review illustrates the wide and comprehensive uses of the ESI technique not only well suited to ionic compounds in solution but also to neutral compounds that may be detected following their conversion of closely related ionic species in organometallic compounds<sup>51</sup>. Usually, there is a correlation between the observed mass spectra and the species known to be present in the solution hence the addition of this technique to the other complimentary techniques, such as X-ray crystallography and NMR spectroscopy, can give better information in structure characterisation. Besides, sometimes the soft nature of the electrospray process indicates that ESI-MS can provide a better understanding of structure nomenclature particularly when the more traditional methods are either inappropriate or unable to use.

ESI-MS is often used for the qualitative determination of compounds, nevertheless several researchers have demonstrated successful quantitative application<sup>52</sup>. In our work, ESI-MS was used to qualitatively analyse the gold molecular clusters synthesized. However, the inaccuracies of the data that we obtained due to large molecular mass of the clusters do not permit a clear-cut determination of the mass fraction of the compound. Besides that, clusters that we synthesized also known to be easily decompose or fragment to other clusters especially in solution with halogenated solvents<sup>27, 53</sup>. Hence, we utilised the ESI-MS

---

data as a fingerprinting characterisation of gold molecular clusters that were synthesized.

#### 2.4.6 X-ray Diffraction (XRD) Spectroscopy

XRD is used for identifying the crystalline phases as well as estimating particle sizes. It is based on the elastic scattering of X-ray photons by atoms in a periodic lattice. A beam of X-rays (wavelength  $\lambda$  ca. 0.5-2 Å) hits the catalyst sample and is diffracted by the crystalline phases in the catalyst according to *Bragg's* law (Equation 2.1) where  $n = 1, 2, \dots$ ,  $d$  is the spacing between atomic planes in the crystalline phase and  $\theta$  is the diffraction angle.

$$n\lambda = 2d \sin \theta \quad \text{Equation 2.1}$$

The intensity of the diffracted X-rays is plotted as a function of the diffraction angle and the sample orientation. This diffraction pattern is used for identifying the crystalline phases and measuring the size and lattice spacing of the crystallites. Since XRD is based on interference between reflecting X-rays from lattice planes, it requires sufficient long range order. Non-crystalline catalysts or amorphous will show either broad, weak diffraction lines or even no diffraction at all.

We will discuss extensively the use of XRD in our research in Chapter 3 and 4. We often employed XRD with EXAFS as an *in-situ* analysis method in order to follow the creation of gold nanoparticulate catalyst from molecular clusters. XRD is more useful in the characterization of catalyst rather than the gold molecular precursor because we often observed the clusters to be amorphous and not really crystalline as we record the XRD pattern of the sample as synthesized.

---

#### 2.4.7 *Transmission Electron Microscopy (TEM)*

Electron microscopy is used to determining the size, shape and composition of supported particles. Transmission electron microscopy (TEM) is a microscopy technique whereby a beam of electrons is transmitted through an ultra-thin specimen interacting with the specimen as it passes through. An image is formed from the interaction of the electrons transmitted through the specimen. The image is magnified and focused onto an imaging device such as a fluorescent screen, on a layer of photographic film or to be detected by a sensor such as CCD camera<sup>54</sup>.

A TEM is like an optical microscope which the optical lenses have been replaced by electromagnetic ones. An electron beam hits the sample and transmitted electrons are magnified by the electromagnetic lenses. The optics brings the scattered electrons from the same point in the sample to the same point in the image (bright-field image). A conventional TEM can magnify 300 000 times with a resolution of 0.5 nm (Figure 2.5 (b)) whereas a high-resolution apparatus can magnify 1 000 000 times giving atomic resolution (Figure 2.5 (a)).

The contrast in the image reflects the different scattering processes and the interactions between the transmitted electrons and different atoms in the sample (typical the metal has much higher electron density than the support and appears darker in the TEM image). Thus, supported metal particles appear as dark spots while the support itself appears as a lighter background. TEM is crucially useful in our research to get an insight of the particles size and dispersion of gold nanocatalyst on support. Gold as a very dense element gives advantage on analysing the particles

using TEM. Information gathered from XRD regarding the particle size of the catalyst can be confirmed with TEM images.

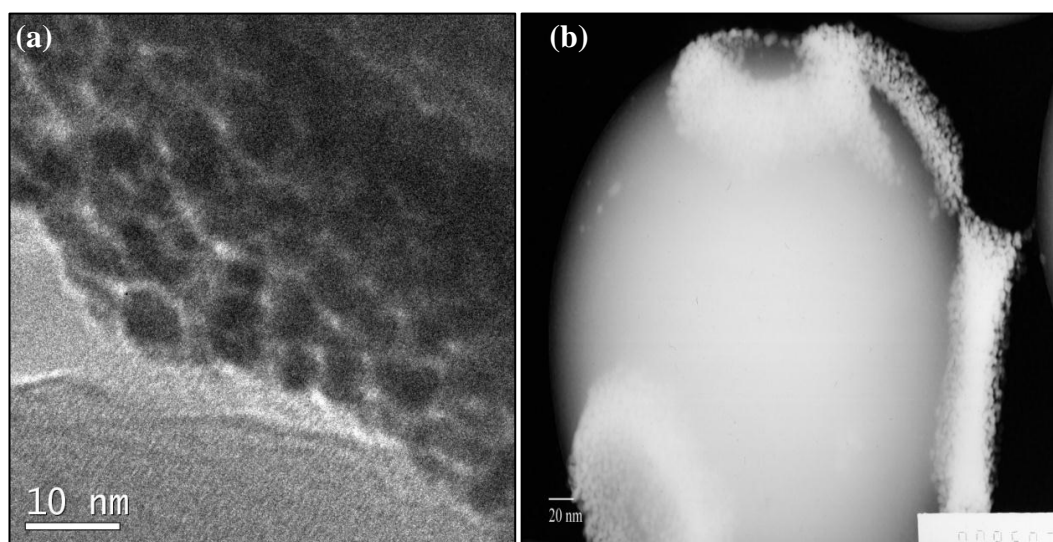


**Figure 2.5:** Example of TEM images of  $\text{Au}_{13}$  clusters on  $\text{SiO}_2$  nanospheres (TBHP method) (a) high resolution bright field TEM up to  $1 \times 10^6$  times magnification (b) conventional negative film dark field TEM up to  $1 \times 10^3$  times magnification

#### 2.4.8 X-ray Absorption Near Edge Structure (XANES)

X-ray absorption fine structure (XAFS) spectroscopy is a unique tool for studying, at the atomic and molecular scale, the local structure around selected elements that are contained within a material. The term XAFS is a broad one that comprise several different techniques namely; EXAFS (extended X-ray absorption fine structure), XANES (X-ray absorption near edge structure), NEXAFS (near edge XAFS) and SEXAFS (surface EXAFS). XAFS is an intrinsically quantum mechanical phenomenon that is based on the X-ray photoelectric effect. An X-ray

---

photon incident on an atom within a sample is absorbed and liberates an electron from an inner atomic orbital<sup>38</sup>.

XAFS is a measurement unique to each specific element in the periodic table. It can give information about the oxidation state of the metal ion under consideration, coordination number of the selected ion as well as the bond lengths of first few neighbours. Using this technique is an advantage in particular when the metal ion concentration is low and may not be crystalline, since this technique does not depend on the long-range order. An absorption spectrum comprises of three main regions namely the pre-edge, edge and post edge (typical X-ray absorption spectrum is given in Figure 2.6). The first part pre-edge and edge regions are also called XANES and the post-edge is termed as EXAFS. The absorption process is due to incoming X-ray photons exciting a bound or occupied electron from the core energy level to a vacant state.

The XANES region is associated with an initial decrease in absorption due to mass absorption followed by a sudden increase caused by absorption of X-rays causing electrons in the core-level to be excited to a vacant or partially occupied states. Different classes of absorption are observed depending on whether the X-ray energy excites the electron from the  $1s$  level (called K-edge) or  $2s$ ,  $2p_{1/2}$  or  $2p_{3/2}$ , resulting in  $L_I$ ,  $L_{II}$  or  $L_{III}$  absorption edges, respectively<sup>38, 55, 56</sup>. In our case for gold, we utilised  $L_{III}$  edge.

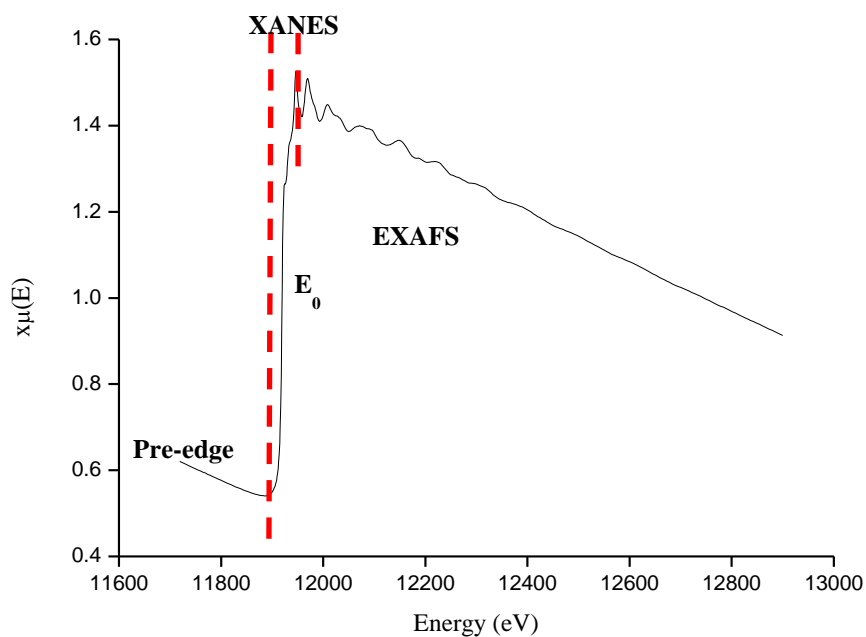


**Figure 2.6:** Experimental L<sub>III</sub>-edge XAS spectrum of Au foil showing the regions observed for characterising a material

Information regarding the oxidation state, coordination number and local structure of the absorbing atom can be determined using XANES. Nevertheless, the quantitative accuracy of XANES calculations and structure determination is not as good as EXAFS, since the theory is poorly understood. Therefore, features in the XANES are used to determine coordination environment based on the study of various appropriate model compounds.

---

#### 2.4.9 Extended X-ray Absorption Fine Structure (EXAFS)

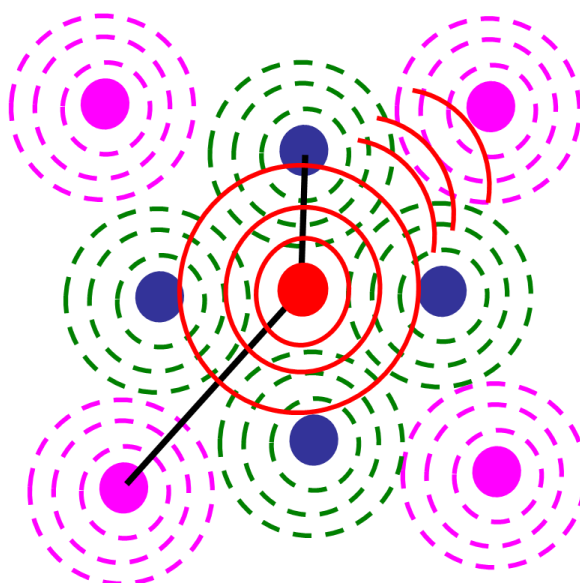


**Figure 2.7:** Outgoing photoelectron waves (solid lines) propagate to neighbouring atoms represented by open circles. The back-scattered waves (dashed lines) modify the wave function at the central atom<sup>38</sup>.

EXAFS is observed as oscillations over a wide energy range in the X-ray absorption spectra, 50-1000eV above the edge<sup>55</sup>. Above the absorption edge the ejected photoelectrons possess a kinetic energy ( $E_{ke}$ ). The oscillations observed (Figure 2.7) arise due to interference between the outgoing electron wave from the absorbing atom and the incoming back-scattered wave from the neighbouring atoms.

We used EXAFS as a means of determining local structure (first few neighbours) for the supported gold catalysts. In addition, we demonstrate the power of combined EXAFS and XRD data collection using *in-situ techniques* to study the formation of gold nanoparticulate supported catalyst from gold molecular clusters as precursor. Only first shell analysis was carried out using EXCURVE which is

sufficient to determine whether phosphine ligands are present in the system and the nature of the gold nanoparticulates in the supported catalysts. Nonetheless, this technique is very important in our work as we gather information that put a mutual conclusion to our hypothesis together with other information obtained from other characterisation techniques involved.

The analysis of XANES and EXAFS is carried out typically using two processing methods. In the first part of the analysis, the background due to mass absorption is removed by fitting a linear line. Subsequently the post edge background (representing a single atom without neighbours) is simulated by fitting a spline or a polynomial and subtracted from the data. Finally the data is normalised with respect to the edge jump giving rise to the final normalised data which is used for further analysis. The process described here is shown in Figure 2.8.

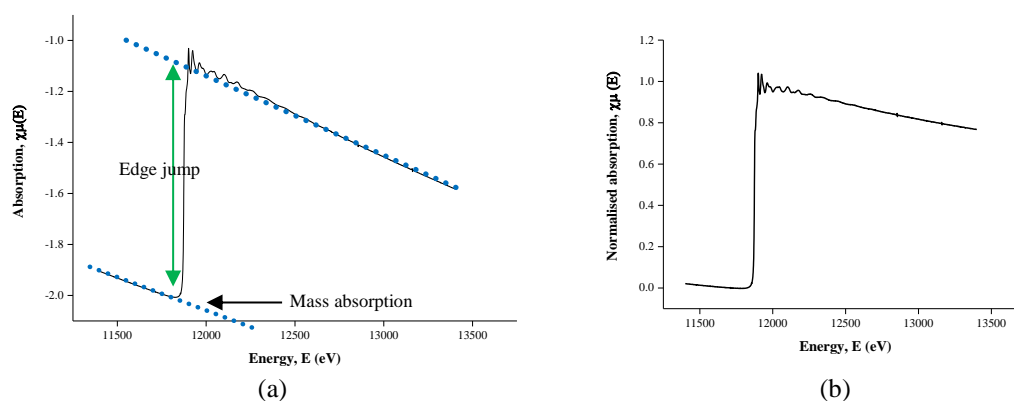


**Figure 2.8:** Plot of (a) raw data showing mass absorption obtained from EXAFS experiment (b) normalised fitting for analysis

Once the normalised data is obtained, XANES data can be used to determine oxidation state, coordination geometry by comparing with crystallographically well

known model compounds (Figure 2.9). Similarly EXAFS data is processed, more in detail using methods developed over the last 20 years. Here, first a model structure (which is closed to an expected one) is created and the EXAFS data is calculated using the following expression (Equation 2.2) and compared with the experimental data.

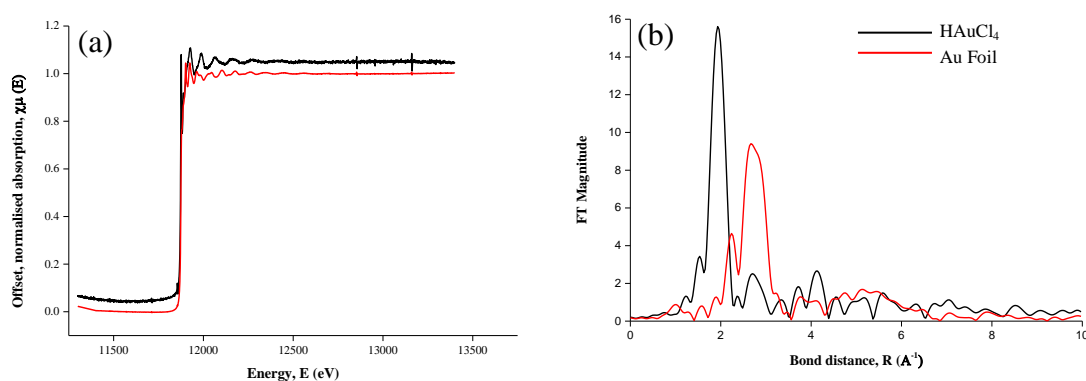


**Figure 2.9:** Plot of (a) XANES and (b) Fourier Transform of model compound (standard); HAuCl<sub>4</sub> and Au foil

$$\chi(k) = \sum_j \frac{N_j f_j(k) e^{-2k^2 \sigma_j^2}}{k R_j^2} \sin[2k R_j + \delta_j(k)] \quad \text{Equation 2.2}$$

$N$  = coordination number

$R$  = interatomic distance – bond distance

$\sigma$  = mean square deviation in distance

$f$  = back scattering amplitude

$\delta$  = phase shift

If the match is not acceptable, the coordination numbers, interatomic distances and mean square deviation (also referred as Debye-Waller factor) is refined in the EXCURVE program to achieve the best match between experimental and

---

computed data. This procedure allows us to extract the interatomic distances, coordination number and disorder associated with the distance. Throughout this thesis, the analysis procedure described above is used.

## 2.5 Conclusion

**Au<sub>9</sub>** and **Au<sub>13</sub>** clusters were prepared as the molecular precursor towards generating controlled size gold nanoparticles. A simplified method has been used to synthesize the clusters and various characterizations techniques were used throughout the project. The clusters were first carefully characterised at molecular level before incorporating it onto solid support to get heterogeneous gold catalysts. More than one type of solid support also has been used in order to study the support effect in catalytic reaction. Instead of practising a well-known technique to prepare heterogeneous catalyst which is wet impregnation method, we also demonstrate a new approach *via* chemical modification using TBHP to deposit the gold nanoparticles onto support. Complete characterizations and comparison between catalysts prepared using two methods will be critically discussed in Chapter 3 and Chapter 4 of this thesis.

## 2.6 References

1. J. Kilmartin, R. Sarip, R. Grau-Crespo, D. Di Tommaso, G. Hogarth, C. Prestipino and G. Sankar, *American Chemical Society Catalysis*, 2012, **2**, 957-963.
2. P. C. Della, E. Falletta and M. Rossi, *American Chemical Society - Conference Proceedings*, 2008.
3. E. Castillejos, E. Gallegos-Suarez, B. Bachiller-Baeza, R. Bacsa, P. Serp, A. Guerrero-Ruiz and I. Rodríguez-Ramos, *Catalysis Communications*, 2012, **22**, 79-82.

- 
4. M. Conte, A. F. Carley, G. Attard, A. A. Herzing, C. J. Kiely and G. J. Hutchings, *Journal of Catalysis*, 2008, **257**, 190-198.
  5. G. Schmid and B. Corain, *European Journal of Inorganic Chemistry*, 2003, 3081-3098.
  6. P.-J. Li, S.-A. Dong, C. Tang, S.-C. Yang, Y.-W. Gu and K.-Z. Li, *Huaxue Xuebao*, 2006, **64**, 1140-1144.
  7. K. Qian, W. Huang, Z. Jiang and H. Sun, *Journal of Catalysis*, 2007, **248**, 137-141.
  8. J. Gu, W. Fan, A. Shimojima and T. Okubo, *Journal of Solid State Chemistry*, 2008, **181**, 957-963.
  9. *Tokyo Metropolitan University, Japan Pat.*, JP2009220017A, 2009.
  10. K. Guillois, L. Burel, A. Tuel and V. Caps, *Applied Catalysis A: General*, 2012, **415-416**, 1-9.
  11. M. Haruta, N. Yamada, T. Kobayashi and S. Iijima, *Journal of Catalysis*, 1989, **115**, 301-309.
  12. K. Qian, J. Fang, W. Huang, B. He, Z. Jiang, Y. Ma and S. Wei, *Journal of Molecular Catalysis A: Chemical*, 2010, **320**, 97-105.
  13. S. Vallejos, T. Stoycheva, P. Umek, C. Navio, R. Snyders, C. Bittencourt, E. Llobet, C. Blackman, S. Moniz and X. Correig, *Chemical Communications*, 2011, **47**, 565-567.
  14. I. V. G. Graf, J. W. Bacon, M. B. Consugar, M. E. Curley, L. N. Ito and L. H. Pignolet, *Inorganic Chemistry*, 1996, **35**, 689-694.
  15. A. Mirescu, H. Berndt, A. Martin and U. Pruesse, *Applied Catalysis, A*, 2007, **317**, 204-209.
  16. S. Jafari, H. Asilian Mahabady and H. Kazemian, *Catalysis Letters*, 2009, **128**, 57-63.
  17. M. ZahmakIran and S. Özkar, *Materials Chemistry and Physics*, 2010, **121**, 359-363.
  18. M. Comotti, P. C. Della, R. Matarrese and M. Rossi, *Angewandte Chemie, International Edition*, 2004, **43**, 5812-5815.
  19. Y. Yang, S. Matsubara, M. Nogami and J. Shi, *Materials Science & Engineering. B, Solid-State Materials for Advanced Technology*, 2007, **140**, 172-176.

- 
20. A. B. Laursen, K. T. Højholt, L. F. Lundegaard, S. B. Simonsen, S. Helveg, F. Schüth, M. Paul, J.-D. Grunwaldt, S. Kegnæs, C. H. Christensen and K. Egeblad, *Angewandte Chemie International Edition*, 2010, **49**, 3504-3507.
  21. K. T. Højholt, A. B. Laursen, S. Kegnæs and C. H. Christensen, *Topics in Catalysis*, 2011, **54**, 1026-1033.
  22. Y. Yuan, K. Asakura, H. Wan, K. Tsai and Y. Iwasawa, *Catalysis Letters*, 1996, **42**, 15-20.
  23. B. D. Chandler, L. I. Rubinstein and L. H. Pignolet, *Journal of Molecular Catalysis A: Chemical*, 1998, **133**, 267-282.
  24. C. C. Chusuei, X. Lai, K. A. Davis, E. K. Bowers, J. P. Fackler and D. W. Goodman, *Langmuir*, 2001, **17**, 4113-4117.
  25. L. Malatesta, L. Naldini, G. Simonetta and F. Cariati, *Coordination Chemistry Reviews*, 1966, **1**, 255-262.
  26. F. Cariati and L. Naldini, *J. Chem. Soc., Dalton Transactions*, 1972, 2286 - 2287.
  27. F. A. Vollenbroek, J. J. Bour, J. M. Trooster and J. W. A. v. d. Velden, *Journal of the Chemical Society, Chemical Communications*, 1978, 907-909.
  28. O. E. Briant, K. P. Hall and D. M. P. Mingos, *Journal of Organometallic Chemistry*, 1982, **229**, C5-C8.
  29. F. Wen, U. Englert, B. Gutrath and U. Simon, *European Journal of Inorganic Chemistry*, 2008, **2008**, 106-111.
  30. J. W. A. V. D. Velden, F. A. Vollenbroek, J. J. Bour, P. T. Beurskens, J. M. M. Smits and W. P. Bosman, *Recueil, Journal of the Royal Netherlands Chemical Society*, 1981, **100**, 148-152.
  31. Y. Shichibu and K. Konishi, *Small*, 2010, **6**, 1216-1220.
  32. M. Bowker, A. Nuhu and J. Soares, *Catalysis Today*, 2007, **122**, 245-247.
  33. N. S. Patil, B. S. Uphade, P. Jana, R. S. Sonawane, S. K. Bhargava and V. R. Choudhary, *Catalysis Letters*, 2004, **94**, 89-93.
  34. W.-C. Li, M. Comotti and F. Schüth, *Journal of Catalysis*, 2006, **237**, 190-196.
  35. V. Choudhary and D. Dumbre, *Topics in Catalysis*, 2009, **52**, 1677-1687.
  36. W. Fang, J. Chen, Q. Zhang, W. Deng and Y. Wang, *Chemistry – A European Journal*, 2011, **17**, 1247-1256.

- 
37. L. S. Roselin, F.-W. Chang, W.-S. Chen and H.-C. Yang, *Science of Advanced Materials*, 2011, **3**, 893-900.
  38. G. Bunker, *Introduction to XAFS : A Practical Guide to X-ray Absorption Fine Structure Spectroscopy*, Cambridge University Press, 2010.
  39. G. M. Hieftje, S. J. Ray and R. A. Meyers, in *Encyclopedia of Analytical Chemistry : Applications, Theory, and Instrumentation*, John Wiley and Sons, Inc., Editon edn., 2000, vol. 1.
  40. M. Hesse, H. Meier and B. Zeeh, *Spectroscopic Methods in Organic Chemistry*, Georg Thieme Verlag Stuttgart, New York, 1997.
  41. J. M. M. Smits, P. T. Beurskens and J. J. Steggerda, *Journal of Crystallographic and Spectroscopic Research*, 1983, **13**, 381-384.
  42. D. M. P. Mingos, *Polyhedron*, 1984, **3**, 1289-1297.
  43. W. Haiss, N. T.H.Thanh, J. Aveyard and D. G. Fernig, *Analytical Chemistry*, 2007, **79**, 4215-4221.
  44. F. A. Vollenbroek, d. B. J. P. Van, d. V. J. W. A. Van and J. J. Bour, *Inorganic Chemistry*, 1980, **19**, 2685-2688.
  45. F. A. Vollenbroek, W. P. Bosman, J. J. Bour, J. H. Noordik and P. T. Beurskens, *Journal of Chemical Society, Chemistry Communication*, 1979, 387-388.
  46. D. Stefanescu, D. Glueck, R. Siegel and R. Wasylishen, *Journal of Cluster Science*, 2008, **19**, 445-458.
  47. E. L. Charsley, S. B. Warrington and S. Thermal Analysis Consultancy, *Thermal analysis: techniques and applications*, Royal Society of Chemistry, 1992.
  48. M. E. Brown and P. K. Gallagher, *Applications to Inorganic and Miscellaneous Materials*, Elsevier Science Limited, 2003.
  49. C. J. McNeal, J. M. Hughes, L. H. Pignolet, L. T. J. Nelson, T. G. Gardner, J. P. Fackler, R. E. P. Winpenny, L. H. Irgens, G. Vigh and R. D. Macfarlane, *Inorganic Chemistry*, 1993, **32**, 5582-5590.
  50. E. S. Andreiadis, M. R. Vitale, N. Mezailles, X. L. Goff, P. L. Floch, P. Y. Toullec and V. Michelet, *Dalton Transactions*, 2010, **39**, 10608-10616.
  51. J. C. Traeger, *International Journal of Mass Spectrometry*, 2000, **200**, 387-401.

- 
52. I. I. Stewart, *Spectrochimica Acta Part B: Atomic Spectroscopy*, 1999, **54**, 1649-1695.
  53. F. A. Vollenbroek, J. J. Bour and d. V. J. W. A. Van, *Recl. Trav. Chim. Pays-Bas*, 1980, **99**, 137-141.
  54. D. B. Williams and C. B. Carter, *Transmission Electron Microscopy: A Textbook for Materials Science*, 2nd Edition edn., Springer, 2009.
  55. R. E. Benfield, D. Grandjean, M. Kroll, R. Pugin, T. Sawitowski and G. Schmid, *The Journal of Physical Chemistry B*, 2001, **105**, 1961-1970.
  56. A. Frenkel, *Z. Kristallogr.*, 2007, **222**, 605-611.

---

## Chapter 3

### Gold Molecular Clusters – Structure, Stability and Size Effects on Nanoparticle Catalyst Generation by the Wet Impregnation Method

#### 3.0 Abstract

Phosphine-stabilised gold molecular clusters,  $[\text{Au}_9\{\text{Ph}_2\text{P}(p\text{-tolyl})\}_8](\text{NO}_3)_3$  (**Au<sub>9</sub>**) and  $[\text{Au}_{13}(\text{dppm})_6](\text{NO}_3)_4$  (**Au<sub>13</sub>**) were synthesized and characterized by elemental analysis,  $^1\text{H}$  and  $^{31}\text{P}$  NMR spectroscopy. Both clusters were then deposited onto  $\text{SiO}_2$  nanospheres and  $\text{Al}_2\text{O}_3$  supports before being transformed into nanoparticles. The incipient wetness impregnation or wet impregnation method was employed which includes catalyst activation *via* high temperature calcination (at  $300^\circ\text{C}$  and  $500^\circ\text{C}$ ). Particle-support interactions play an important role in controlling the deposition of the size and morphology of gold nanoparticles, the formation of different surface gold species and their electronic properties as well as their catalytic performance (see Chapter 5). Consequently, we scrutinized the structure-stability of the gold clusters and controlled particle size formation *via in-situ* heating using instantaneous XRD-EXAFS analysis. Structural parameters such as coordination number and atom-atom bond distances were derived utilising Athena and EXCURVE software. The gold nanoparticles prepared by this method were relatively large ( $> 5\text{ nm}$ ) being bigger than those prepared using co-precipitation or deposition-precipitation methods.

---

### 3.1 Introduction

Heterogeneous gold catalysts prepared by depositing gold nanoparticles onto various solid supports have received much attention in recent years<sup>1-5</sup>. There are many different methods<sup>6-8</sup> employed to prepare these catalysts including incipient wetness impregnation also known as the wet impregnation method. This involves a metal precursor or complex, usually  $\text{HAuCl}_4$  for gold, being dissolved in an organic solvent and stirred with the support followed by solvent removal and evaporation. Although the procedure is simple, a disadvantage is that it does not allow control over particle size. Gold nanoparticles produced by this method are often  $> 10$  nm in size and can enlarge up to  $> 100$  nm resulting in poor catalytic activity.

Consequently, catalysts produced by the wet impregnation method generally have poor activities and thus it is necessary to use other methods, such as deposition-precipitation to produce more active materials. Further, activation of the catalyst involves calcination at high temperature resulting in excessive sintering and thus limiting access to catalytically active sites. Bowker *et. al.* have shown that it is indeed possible to synthesize high activity supported gold catalysts by the wet impregnation method if care is taken to remove chloride during the process<sup>9</sup>. They achieved this by employing a double impregnation method where chloroauric acid and a base are precipitated out to give gold hydroxide within the pores of the catalysts followed by limited washing. Nevertheless, the sizes of nanoparticles that they obtained were of the order of 30 nm and above.

Molecular gold clusters have been widely investigated and phosphine-stabilized examples have attracted much interest<sup>10-15</sup>. These clusters contain a well-

defined group of metal atoms that are held together by direct metal-metal bonds and certain non-metal atoms may also be incorporated<sup>16</sup>. For the phosphine-stabilized gold molecular clusters the phosphine ligands can be tailored to give number-specific gold clusters. The use of monodentate or bidentate phosphines with different Tolman cone angles results in different clusters both structurally and chemically<sup>17</sup> (see Chapter 1). The ability to release these ligands at relatively low temperatures leaving naked gold clusters motivated us to use them as nanoparticle precursors. In this chapter, we attempt the size-controlled formation of gold nanoparticles using phosphine-stabilized gold molecular clusters prepared *via* wet impregnation methods. Structural stability and size effects were carefully considered and discussed in both the gold nitrate precursors and the corresponding clusters. Two different gold molecular clusters used in this research were **Au<sub>9</sub>** and **Au<sub>13</sub>** clusters by monodentate and bidentate phosphine ligands respectively.

### 3.2 Characterizations of Gold Molecular Clusters

All experimental procedures and characterization techniques have been precisely outlined and discussed in Chapter 2.

#### 3.2.1 Elemental Analysis

**Table 3.1:** Elemental analysis data of the synthesized clusters

Clusters	% C		% H		%N	
	Calculated	Found	Calculated	Found	Calculated	Found
<b>Au<sub>9</sub></b>	43.79	43.52	3.29	2.97	1.01	1.00
<b>Au<sub>13</sub></b>	35.22	34.11	2.60	2.62	1.10	1.07

---

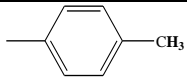
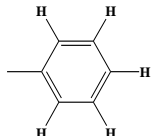
Elemental analysis is a useful technique to give the first insight into the empirical formula of the clusters. The actual stoichiometry of the clusters, however, is difficult to predict due to their large molecular masses.

We obtained relatively good yields for the two clusters synthesized; **Au<sub>9</sub>** was isolated as dark green powder<sup>18</sup> in 78% yield, while **Au<sub>13</sub>** was as a greenish brown solid<sup>19</sup> in 63% yield (based on gold). Elemental analysis data (Table 3.1) for both clusters gave % C % H and % N values in agreement with the calculated values. Purification of the clusters was done by multiple re-crystallizations since slightly higher % N were found at first, probably due to the NaNO<sub>3</sub> produced not being fully separated.

### 3.2.2 <sup>1</sup>H and <sup>31</sup>P{<sup>1</sup>H} nuclear magnetic resonance

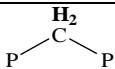
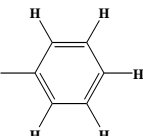
The <sup>1</sup>H NMR spectrum of the ligands and complexes were monitored throughout the synthetic procedure in order to confirm that no degradation occurred at any stage. The spectra were recorded on solutions of corresponding ligand and complexes in MeOD. Table 3.2 lists <sup>1</sup>H NMR resonances for **Au<sub>9</sub>** complexes. For the phosphine ligand, two types of <sup>1</sup>H NMR resonance were observed, namely the aromatic protons and –CH<sub>3</sub> group. The resonance for –CH<sub>3</sub> group in *p*-tol ligand of **Au<sub>9</sub>** clusters is shifted further upfield (δ 2.10) as compared to the ligand and the intermediate Au-nitrate complex.

**Table 3.2:**  $^1\text{H}$ -NMR chemical shift

Type of $^1\text{H}$	$\delta$ (ppm)			
	$\text{Ph}_2\text{P}(p\text{-tol})$	$(\text{Ph}_2\text{P}(p\text{-tol}))\text{AuCl}$	$(\text{Ph}_2\text{P}(p\text{-tol}))\text{Au}(\text{NO}_3)$	$\text{Au}_9$
	2.38 (s)	2.43 (s)	2.44 (s)	2.10 (s)
	7.19-7.37 (m)	7.28-7.56 (m)	7.30-7.66 (m)	6.51- 7.39 (m)

For the formation of  $\text{Au}_{13}$  clusters, *bis*(diphenylphosphino)methane (dppm) was used as the ligand. Resonances for the  $-\text{CH}_2$  and aromatic groups were observed (Table 3.3). The protons resonate shifted downfield upon  $\text{Au}_{13}$  formation. The  $-\text{CH}_2$  peak appeared as simple triplet in the ligand and intermediate gold complexes.

**Table 3.3:**  $^1\text{H}$ -NMR chemical shift

Type of $^1\text{H}$	$\delta$ (ppm)			
	(dppm)	$\text{Au}_2(\text{dppm})\text{Cl}_2$	$\text{Au}_2(\text{dppm})(\text{NO}_3)_2$	$\text{Au}_{13}$
	2.83 (t)	3.63 (t)	3.77 (t)	3.91 (t)
	7.31-7.48 (m)	7.41-7.68 (m)	7.39-7.68 (m)	7.08-7.83 (m)

The use of phosphine ligands gives an advantage in cluster characterization as  $^{31}\text{P}\{^1\text{H}\}$  NMR can be utilised giving clearer information on cluster formation. A full comparison of the  $^{31}\text{P}\{^1\text{H}\}$  NMR data is listed in Table 3.4. For  $\text{Au}_9$  clusters, the

values observed were at 56.6 ppm similar to literature reports of 54.8 ppm for  $[\text{Au}_9(\text{PPh}_3)_8](\text{PF}_6)_3$  in  $\text{CD}_2\text{Cl}_2$ <sup>20</sup>. For the corresponding **Au<sub>13</sub>** clusters, the  $^{31}\text{P}\{^1\text{H}\}$  NMR resonance was also in agreement with the literature (35.8 ppm)<sup>21, 22</sup>.

**Table 3.4:**  $^{31}\text{P}\{^1\text{H}\}$  NMR chemical shift

Compound	Chemical shift (ppm)
(Ph <sub>2</sub> P( <i>p</i> -tol)) ligand	-6.4 (s)
(Ph <sub>2</sub> P( <i>p</i> -tol))AuCl	32.4 (s)
(Ph <sub>2</sub> P( <i>p</i> -tol))Au(NO <sub>3</sub> )	26.9 (s)
<b>Au<sub>9</sub></b>	56.6 (s)
(dppm) ligand	-22.6 (s)
Au <sub>2</sub> (dppm)Cl <sub>2</sub>	24.3 (s)
Au <sub>2</sub> (dppm)(NO <sub>3</sub> ) <sub>2</sub>	24.2 (s)
<b>Au<sub>13</sub></b>	35.9 (s)

The singlet observed for **Au<sub>9</sub>** clusters is explained by the dominant *trans* influence of the central gold atom upon the chemical shift of the phosphines coordinated to the peripheral gold atoms as described by Bour *et. al.*<sup>20, 23</sup>. For **Au<sub>13</sub>**, the singlet was due to all twelve phosphorus atoms that are equivalent due to symmetrical nature of the icosahedral geometry<sup>22, 24</sup>. An identical one signal spectrum was observed even after heating the solution at 50°C for a day and also after being left for more than a month, indicating that the cluster skeleton possesses high structural stability in methanol.

### 3.2.3 Electrospray Ionisation-Mass Spectroscopy (ESI-MS) analysis

To aid determination of the elemental composition of the clusters synthesized, a mass spectrometric study using electrospray ionization (ESI) was used as the method of choice. Figure 3.1 and 3.2 showed the ESI-MS spectrum of **Au<sub>9</sub>** and **Au<sub>13</sub>** clusters respectively. The calculated  $m/z$  value of  $[\text{Au}_9(\text{Ph}_2\text{P}(p\text{-tol}))_8]^{3+}$  is 3983.1906 while  $[\text{Au}_{13}(\text{dppm})_6]^{4+}$  is 4866.8992. Since clusters have a large molecular masses, often the mass spectra can be difficult to interpret. Unfortunately, we were unable to identify any multiply charged clusters in the  $m/z$  range up to calculated mass value for each cluster.

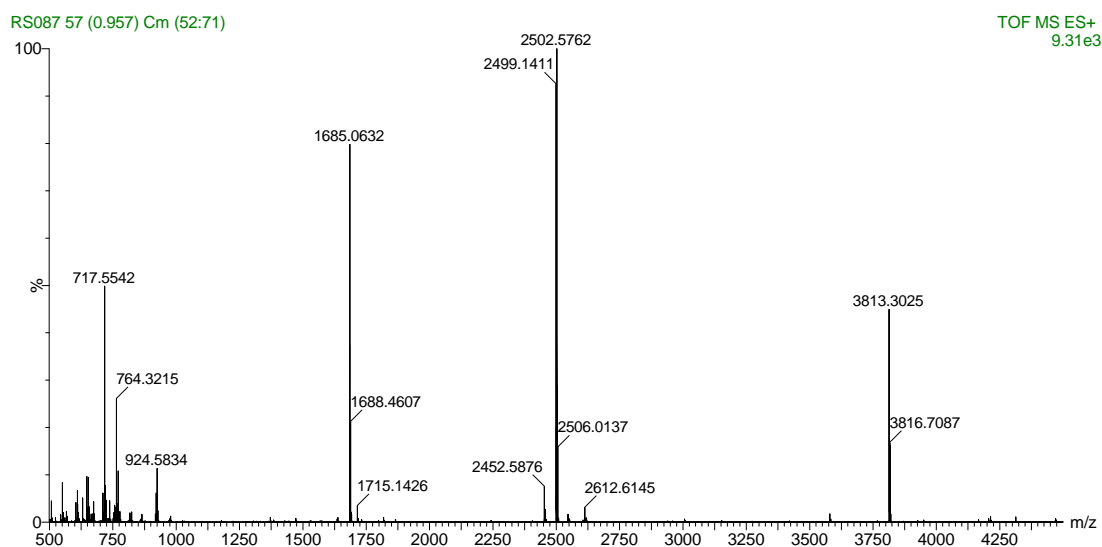


**Figure 3.1:** ESI-MS spectrum of **Au<sub>9</sub>** cluster;  $[\text{Au}_9(\text{Ph}_2\text{P}(p\text{-tol}))_8]^{3+}$ .

The clusters are easily fragmented in gas-phase giving many peaks in the lower  $m/z$  region<sup>25</sup>. Furthermore, there is a high possibility of mix clusters species existing and also being fragmented. Various research groups have previously reported similar fragmentation pattern in small clusters as well as differences in sample composition in large clusters were observed and studied using ESI-MS<sup>22, 25-29</sup>.

Nevertheless, apart from that, we did observe peaks in the expected  $m/z$  region for each cluster, close enough to the calculated value. Hence, we suggested the use of ESI-MS technique as finger printing pattern in clusters synthesis.

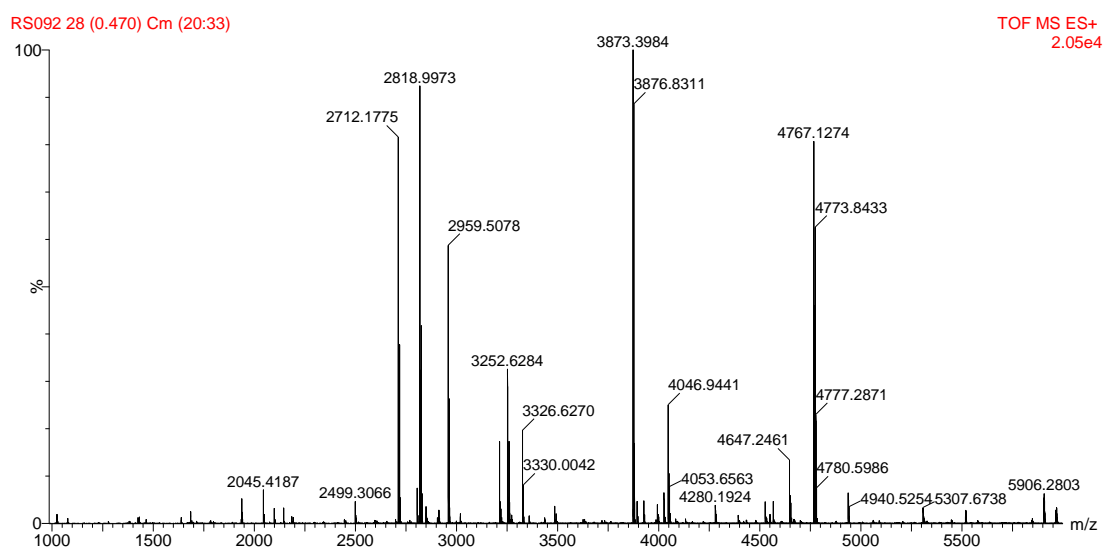


**Figure 3.2:** ESI-MS spectrum of  $\text{Au}_{13}$  cluster;  $[\text{Au}_{13}(\text{dppm})_6]^{4+}$ .

### 3.3 Catalyst Activation

Gold molecular clusters were used as precursors towards bottom-up approach to gold nanoparticles generation. In wet impregnation method of catalyst preparation, the prepared clusters were deposited onto  $\text{SiO}_2$  nanospheres and  $\text{Al}_2\text{O}_3$  support in methanol that was then being removed by solvent evaporation method. As the ligands were still attached to the clusters, it cannot directly be used in catalytic reactions. The bulky structure of the ligands limit the accessibility to Au active sites that is crucially important in catalysis<sup>17</sup>. Besides, it may also act as catalyst surface poison<sup>30</sup>. Pre-treatment or activation of the catalysts is typically carried out by calcination in air at  $300^\circ\text{C}$  and  $500^\circ\text{C}$  for 1 hour. The phosphine ligands were stripped off and removed upon heat treatment at *ca.*  $300^\circ\text{C}$  resulting in naked gold

---

nanoparticles. Further calcination at 500°C was done in order to investigate the effect of temperature treatment on structural stability, particles size effect at higher temperature and on catalytic properties<sup>7, 31</sup>.

### 3.4 Stability of Clusters

Clusters stability was investigated further using several techniques including *in-situ* heating XRD-EXAFS analysis. Au-nitrate complexes that were initially intermediate precursor to clusters were also carefully studied to determine structure formation towards nanoparticles generation.

#### 3.4.1 Structural Rearrangements Study by Thermogravimetric Analysis-Differential Scanning Calorimetry (TGA-DSC)

Thermogravimetric analysis (TGA) of each sample was carried out with the aim of determining appropriate temperatures needed for cluster decomposition *via* ligand loss. In order to generate nanoparticles from these clusters, ligands were removed by heating leaving the naked clusters. TGA was carried out in argon, heating samples up to 600°C by 2°C/min. Differential scanning calorimetry (DSC) was measured simultaneously with TGA giving insight into the thermal reactions of the clusters.

Data listed in Table 3.5 shows at 245.6°C about 45.1% mass loss of the **Au<sub>13</sub>** clusters and 53.0% for **Au<sub>9</sub>** clusters at 298.3°C. This mass loss corresponds to the eight (*p*-tolyl) and six dppm ligands respectively. Thus the **Au<sub>13</sub>** clusters decompose at relatively lower temperatures as compared to **Au<sub>9</sub>** clusters. This might be important as aggregation is more likely to occur at higher temperatures<sup>32</sup>. Thus, the

---

lower temperature needed for cluster decomposition at molecular level is an advantage in controlling the particles agglomeration that leads to greater particle size of the gold nanoparticulates<sup>14</sup>.

**Table 3.5:** Comparison of clusters stability according to TGA-DSC analysis

Clusters	Temperature (°C)	Time (min)	DSC (mW/mg)	Mass Lost (%)
<b>Au<sub>9</sub></b>	298.3	27.8	2.3	53.0
<b>Au<sub>13</sub></b>	245.6	22.1	-117.4	45.1

Comparing the DSC curves of the two clusters, significant changes in the behaviour of the clusters towards thermal changes were observed. Figure 3.3 compares the TGA-DSC curve for the **Au<sub>9</sub>** and **Au<sub>13</sub>** clusters. The dramatic mass loss in the TGA curve for **Au<sub>13</sub>** clusters supported by significant increase of heat is seen in DSC curve which indicates that all ligands were stripped off simultaneously instead of gradually as seen in **Au<sub>9</sub>**; as the ligands are being removed, the metallic cluster core tends to rearrange similar to the one observed for **Au<sub>6</sub>** by computational study reported in an earlier work<sup>33, 34</sup>. This metastability of clusters may be influenced by aurophilicity and relativistic effect<sup>11, 35-38</sup>.

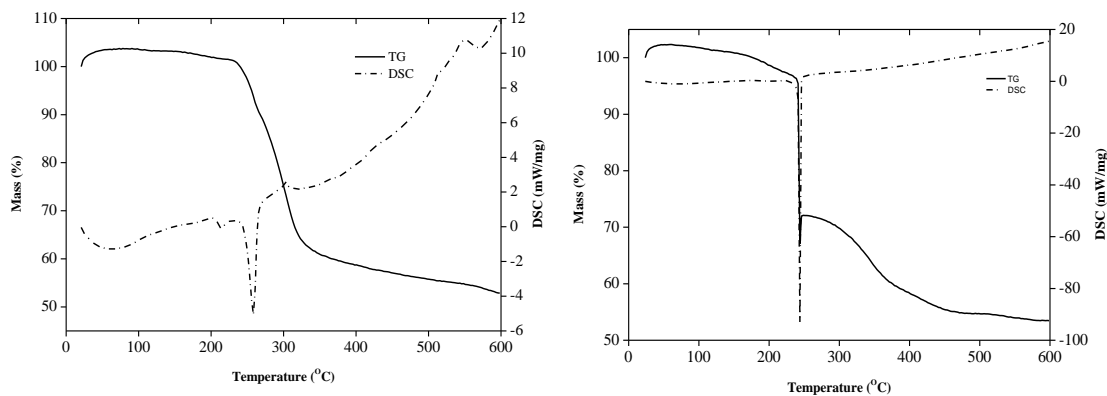


**Figure 3.3:** TGA-DSC curve of **Au<sub>9</sub>** (left) and **Au<sub>13</sub>** clusters (right) ramping at 2 °C/min rate to 600 °C

The **Au<sub>9</sub>** clusters have a cluster-core geometry of bicapped centred chair<sup>39</sup> as compared to the rigid icosahedral<sup>24, 40</sup> geometry of **Au<sub>13</sub>** suggesting the presence of slow kinetics in intramolecular atom rearrangement processes occurred in **Au<sub>9</sub>** cluster. Few studies have been carried out on non-icosahedral gold clusters that showed the ability of cluster core rearrangement by replacing or adding one or more ligands<sup>23, 41</sup> or applying heat<sup>34</sup> on the system as well as the use of different solvent<sup>42</sup> resulting clusters growth or dwindled, fragmented into mixture of clusters. Instead, **Au<sub>13</sub>** structure was rather rigid hence the structural rearrangement is unlikely to happen<sup>21, 22, 24, 40</sup> and the removal of ligand became a one-step process, explained in TGA-DSC plot.

### 3.4.2 Gold Nanoparticles Formation Monitored by X-ray Diffraction (XRD) Spectroscopy

X-ray diffraction of clusters and gold nitrate complexes were measured during *in-situ* heating in a custom made cell up to 450 °C and parallel we measured the EXAFS data at the Au L<sub>III</sub> edge. Au foil was used as standard in calibrating the

diffractometer. The main peaks observed in the XRD pattern of gold are Au (111), (200), (220) and (311) reflections and the corresponding  $2\theta$  (degree) values for Au foil are  $25.9^\circ$ ,  $30.0^\circ$ ,  $42.9^\circ$  and  $50.8^\circ$ , respectively.

Often  $\text{HAuCl}_4$  was used as nanoparticle precursor but controlling the particle growth has always been a problem<sup>43-46</sup>. In order to determine whether mononuclear  $\text{Ph}_2\text{P}(p\text{-tol})\text{Au}(\text{NO}_3)_2$  can be converted to gold nanoparticle, the precursor compound was deposited onto  $\text{Al}_2\text{O}_3$  by the wet impregnation method the decomposition behaviour was studied.

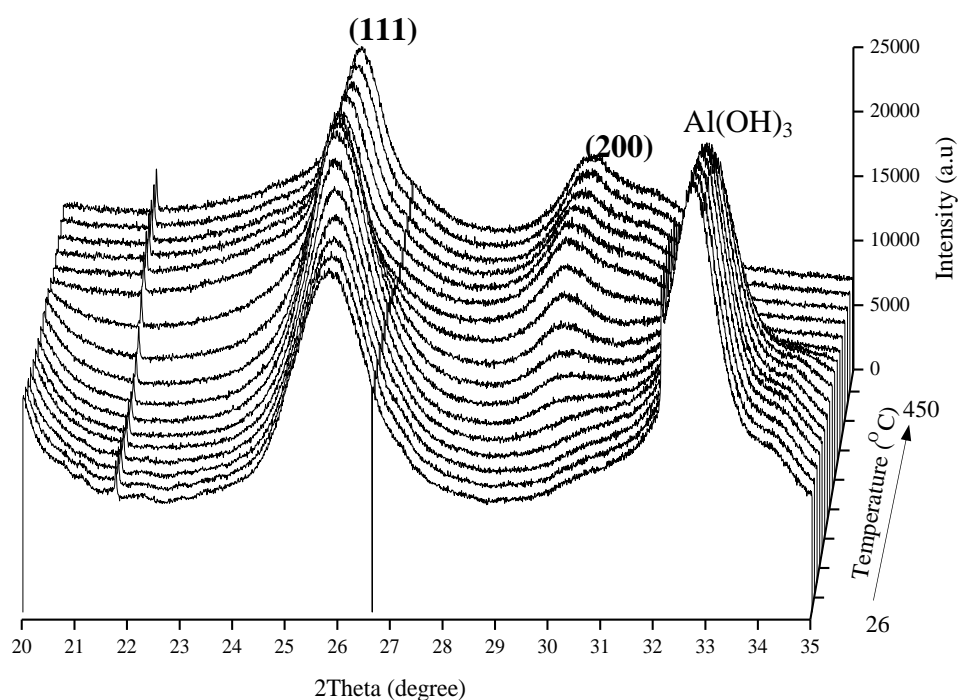


**Figure 3.4:** XRD patterns of  $\text{Au}_9$  precursor ( $\text{Ph}_2\text{P}(p\text{-tol})\text{AuNO}_3$  complex) prepared by the wet impregnation on  $\text{Al}_2\text{O}_3$  in-situ heating up to  $450^\circ\text{C}$ .

Figure 3.4 shows stacked XRD patterns recorded during the combined XRD/XAS measurement while increasing the temperature. After heating to *ca.*

295 °C, peak associated with Au (200) reflection has begun to make its appearance (it was difficult to see Au (111) reflection since it appears along with broad alumina reflections). However, there was slight shift in  $2\theta$ , compared to pure metal foil, is observed that could be due to temperature resulting from lattice expansion. This indicated that the gold has undergone chemical changes presumably transformed to nano metallic clusters or aggregates producing more crystalline compound. In order to determine whether a physical mixture of the complex precursor compound behave similar way, we investigated a physical mixture of the  $\text{Au}_{13}$  precursor complex  $\text{Au}_2(\text{dppm})(\text{NO}_3)_2$  was physically mixed with the  $\text{Al}_2\text{O}_3$  support and probed to *in-situ* heating XRD-EXAFS experiment. In Figure 3.5 we show the XRD pattern recorded during in situ heating of the physical mixture.

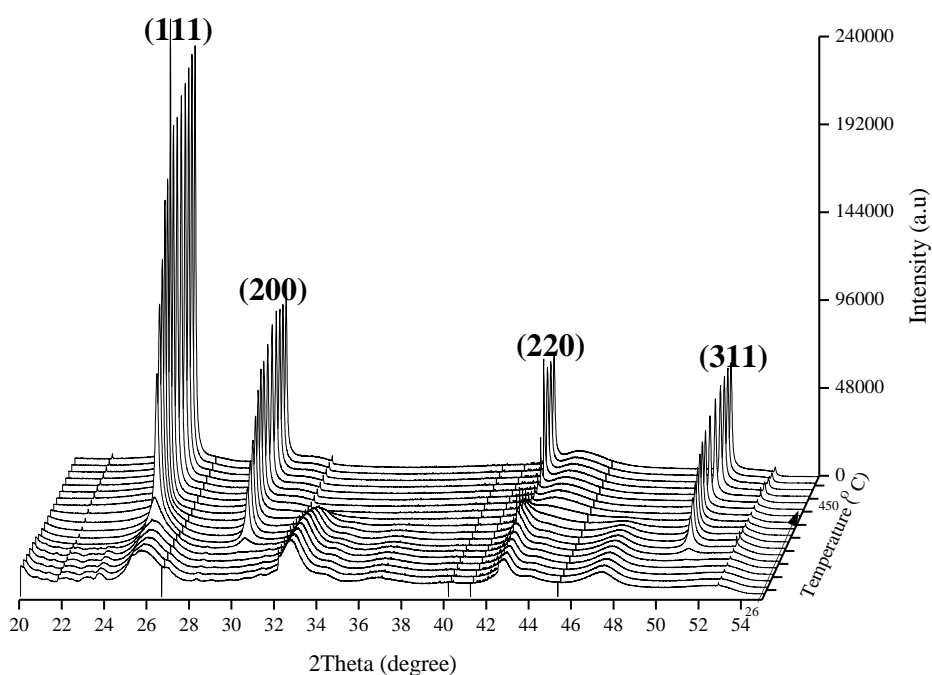


**Figure 3.5:** XRD patterns of  $\text{Au}_{13}$  precursor physically mixed with  $\text{Al}_2\text{O}_3$  in-situ heating up to 450 °C

All four gold reflections are seen to appear as the temperature was increased. The amount of crystalline gold metal particles gradually increases with temperature. It is clear that the wet impregnation method produced smaller gold particles compared to the physically mixed sample. Similarly, we also investigated a physical mixture of the gold cluster compounds, **Au<sub>9</sub>** and **Au<sub>13</sub>** mixed with alumina to investigate the stability of the cluster compounds and the temperature at which they decompose to yield gold nanoparticles. Figure 3.6 shows stacked XRD patterns in which four peaks are assigned to gold reflections which gradually increase in intensity as temperature increases. The Au (200) plane began to rise when temperature reached *ca.* > 200 °C uniform in both **Au<sub>9</sub>** and **Au<sub>13</sub>** clusters. However, **Au<sub>13</sub>** clusters transformed to nanoparticles at slightly lower temperature (240 °C) compared to **Au<sub>9</sub>** clusters (295 °C). This finding is in mutual consensus with TGA-DSC data where ligands removal took place at temperature between 200 °C and 300 °C.

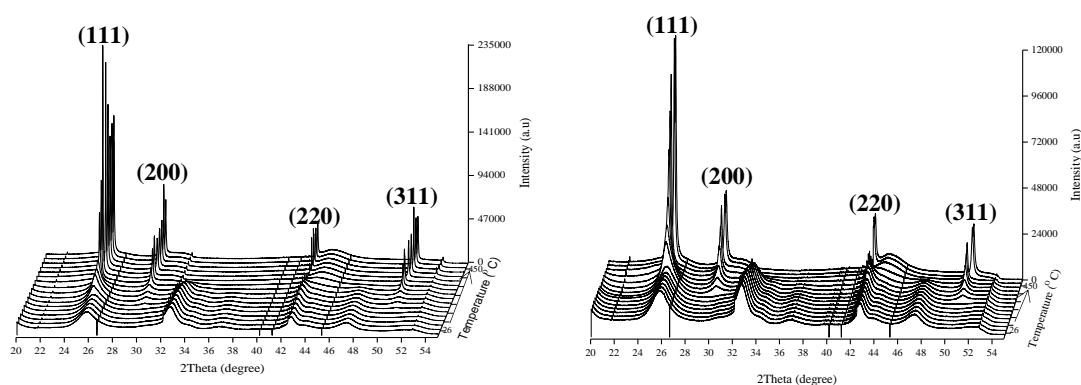


**Figure 3.6:** XRD patterns of **Au<sub>9</sub>** clusters physically mixed with Al<sub>2</sub>O<sub>3</sub> in-situ heating up to 450 °C (left) and **Au<sub>13</sub>** clusters physically mixed with Al<sub>2</sub>O<sub>3</sub> in-situ heating up to 450 °C (right).

---

### 3.4.3 X-ray Absorption Spectroscopy; XANES and EXAFS

Although XRD revealed the formation of gold nanoparticles, this technique failed to show the presence of the cluster compound at the initial stages, probably due to lack of long-range order. XAS is an ideal technique to determine the structure of the precursor compound since it does not depend on the long-range order. Furthermore, XAS will also allow us to determine the structure of evolving gold nanoparticles that may complement the XRD results.

The stability of the gold-nitrate complex precursor and molecular clusters was monitored by *in-situ* heating of Au L<sub>III</sub> edge EXAFS instantaneously with XRD at B18 beamline of Diamond Light Source. The furnace was programmed to ramp from room temperature to 450 °C at 10 °C/min with 30 minutes dwell time before being cooled down. XRD was measured before each EXAFS was taken as plotted and discussed in section 3.4.2.

The Au L<sub>III</sub> XANES data recorded *in-situ* is shown in Figure 3.7. Here we plot the data recorded at room temperature and after heating for both precursor compounds along with the model compounds. XANES data clearly shows the starting material has features similar to the one which has ligands and the heated samples were found to be closely similar to the metallic gold. However, it is difficult to extract from XANES whether the metallic gold is nano sized or close to bulk and hence a detailed analysis of the EXAFS data was carried out.

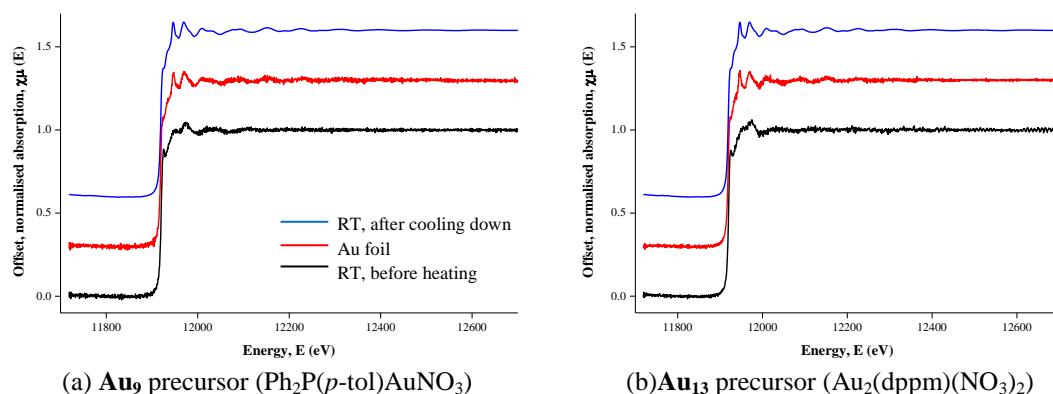


**Figure 3.7:** Au  $L_{\text{III}}$  XANES plot for both precursor complexes recorded at room temperature and after heating along with the Au foil standard

The stability of supported  $\text{Ph}_2\text{P}(p\text{-tol})\text{AuNO}_3$  onto  $\text{Al}_2\text{O}_3$  by wet impregnation method and  $\text{dppmAu}_2(\text{NO}_3)_2$  physically mixed with  $\text{Al}_2\text{O}_3$  support were first to be analysed before the corresponding clusters. Figure 3.8 illustrates the best fit between experimental and calculated Fourier transforms for the  $\text{Ph}_2\text{P}(p\text{-tol})\text{AuNO}_3$ . Figure 3.8 show that the theory and structural geometry modelled by EXCURVE matched well with the experimental data.

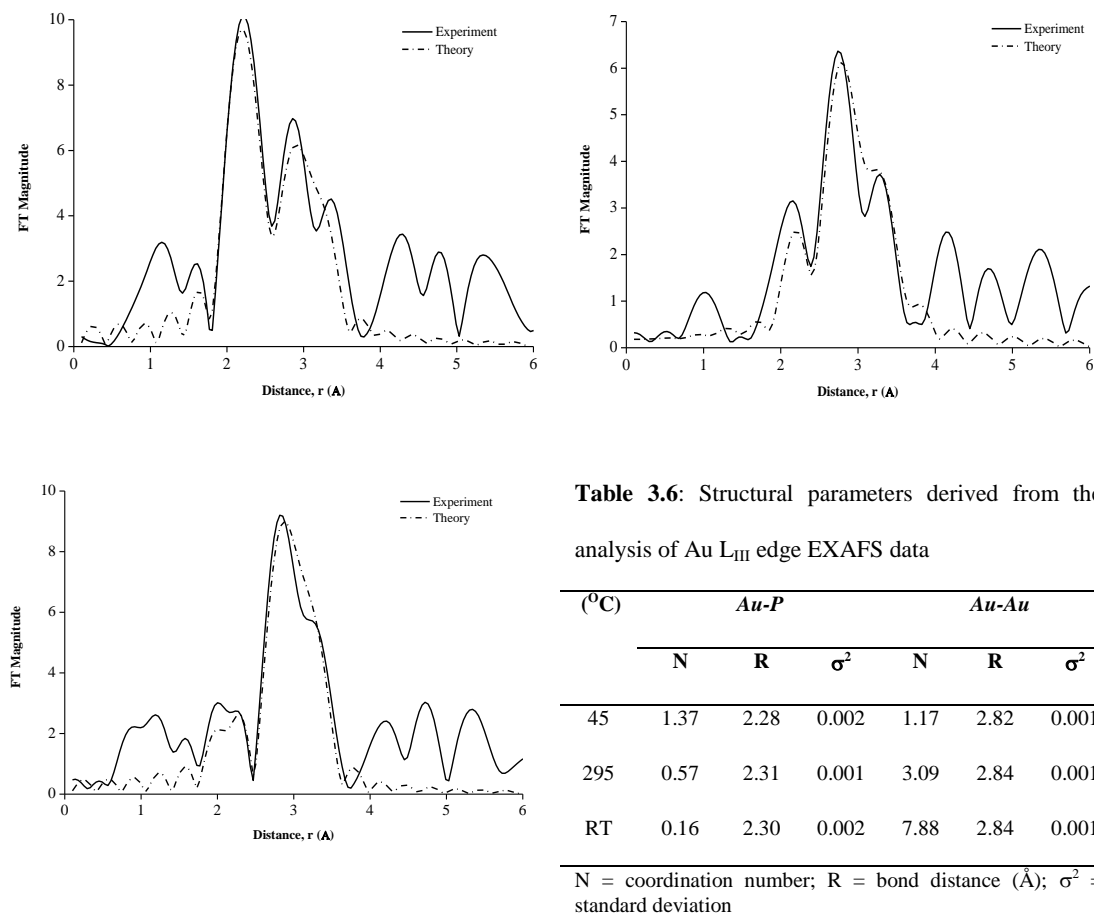


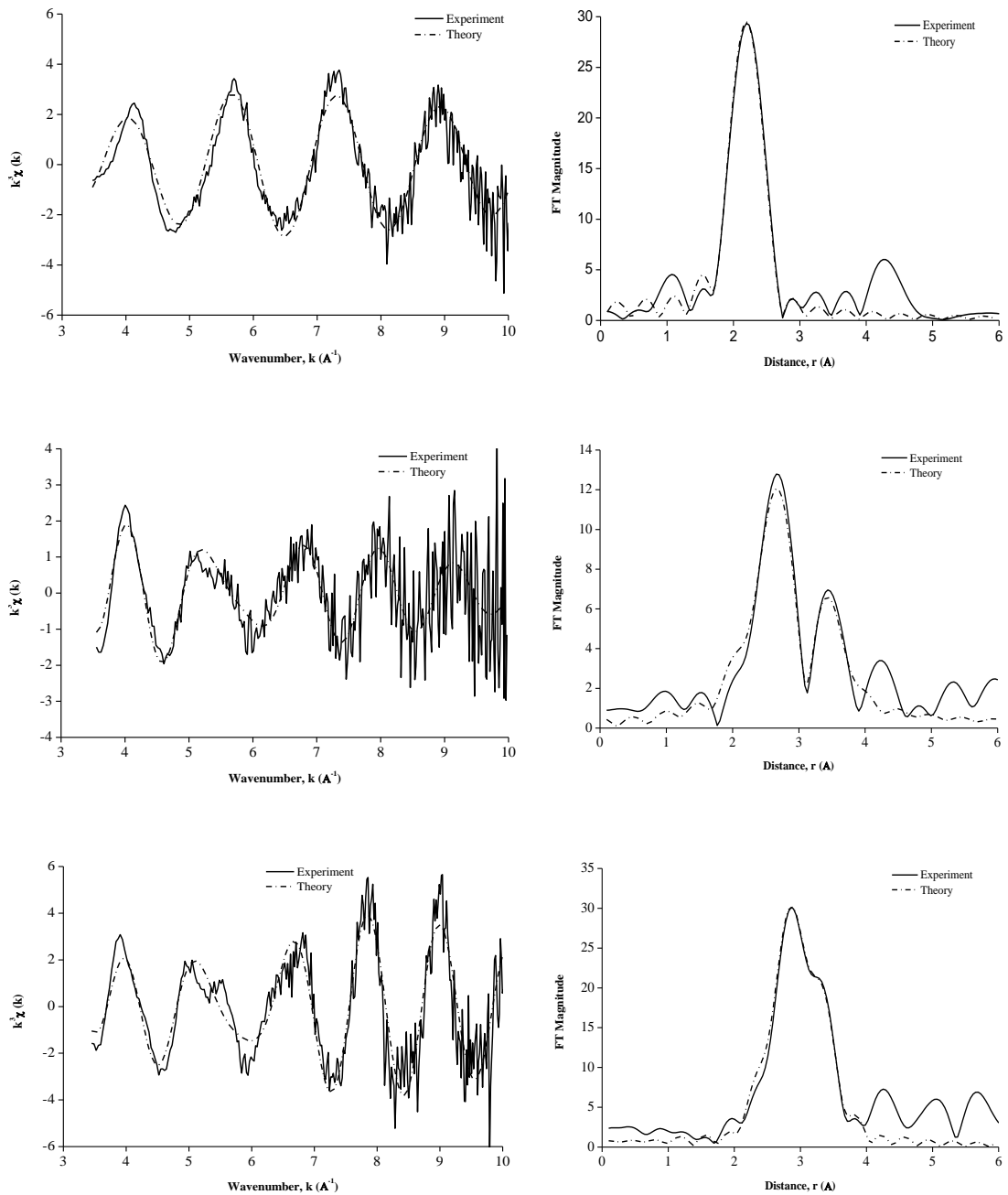
**Figure 3.8:** Best fit corresponding Au L<sub>III</sub> edge EXAFS; Fourier transforms of the experimental and calculated data are shown for Ph<sub>2</sub>P(*p*-tol)AuNO<sub>3</sub> prepared by wet impregnation on Al<sub>2</sub>O<sub>3</sub> *in-situ* heating up to 450 °C; at 45 °C (top left), 295 °C (top right) and after cooling down (bottom).

According to the structural parameters derived (listed in Table 3.6), the coordination number of the phosphorus atom ( $N_{\text{Au-P}}$ ) decreases with increasing temperature and an increase for the gold ( $N_{\text{Au-Au}}$ ) is seen. At *ca.* 295 °C, the Au-P coordination number is 0.57 with a distance of 2.31 Å, while the Au-Au coordination number is 3.09 with 2.84 Å. With these findings, it further confirmed the observation made earlier using TGA-DSC and XRD data that the complex transformed to gold nanoparticles at *ca.* 295 °C. The gold nanoparticles after cooling down from 450 °C

---

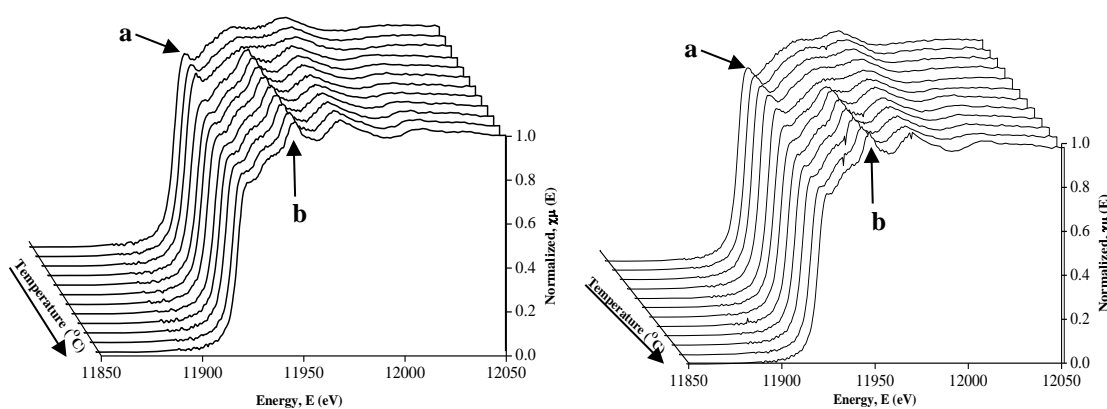
seem to have features similar to metallic gold with  $N_{\text{Au-Au}}$  of ca 7.88 at 2.84 Å ( $R_{\text{Au-Au}}$ ). The particle sizes however were still in the nanoparticle regime as the coordination number is lower than bulk gold ( $N_{\text{Au-Au}}$  bulk is 12 derived from EXAFS of gold foil).

Figure 3.9 shows EXAFS plot for  $\text{dppmAu}_2(\text{NO}_3)_2$  physically mixed with  $\text{Al}_2\text{O}_3$  in-situ heating up to 450°C. Before heating, at 35°C, only one peak was observed associated with gold-phosphine interactions with  $N_{\text{Au-P}}$  of ca 2.04,  $R_{\text{Au-P}}$  of ca 2.28 Å. This was expected as the two phosphorus atoms are chemically equivalent. Transformation begins to happen at ca. 240°C where mixed features of Au-P and Au-Au are observed in the FT plot (see Figure 3.9 middle). This agrees well with TGA-DSC and XRD data for the temperature required for diphosphine removal being ca. 245°C is lower than that for the *p*-tolyl ligand (ca. 290°C).



**Figure 3.9:** Best fit between experimental Au L<sub>III</sub> edge EXAFS and theory/calculated data for dppmAu<sub>2</sub>(NO<sub>3</sub>)<sub>2</sub> physically mixed with Al<sub>2</sub>O<sub>3</sub> in-situ heating up to 450°C; at 35°C (top), 240°C (middle) and after cooled down 62°C (bottom). On the right corresponding Fourier transforms of the experimental and calculated data are shown.

Metallic gold features with no Au-P peaks were observed after  $\text{dppmAu}_2(\text{NO}_3)_2$  was cooled down to room temperature. The  $N_{\text{Au-Au}}$  after cooling is 11.58 with  $R_{\text{Au-Au}}$  of 2.86 Å which is closely similar to that observed for the Au foil standard suggesting that the gold generated is in bulk. This result is consistent with XRD results that physically mixed compounds produce large particles compared to wet-impregnated preparation.



**Figure 3.10:** XANES plot of  $\text{Au}_9$  clusters physically mixed with  $\text{Al}_2\text{O}_3$  in-situ heating up to  $450^\circ\text{C}$  (left) and  $\text{Au}_{13}$  clusters physically mixed with  $\text{Al}_2\text{O}_3$  in-situ heating up to  $450^\circ\text{C}$  (right).

Information obtained from both precursors lead us to XANES and EXAFS study on their corresponding clusters. Transformations from phosphine-stabilized molecular clusters to naked gold nanoparticles were monitored using real time *in-situ* heating in a QEXAFS experiment. The small peak (shoulder) marked (a) in Figure 3.10 is due to the transitions from the  $2p_{2/3}$  to the  $5d$  level, which appear to be higher for the cluster and less for metallic system. Similar feature with a strong intensity has been observed for chlorine landed and gold hydroxide systems. This appears to be a

signature for direct ligand coordination. It can be seen that the peak intensity is gradually diminished as the temperature rises and these resemble metallic gold.

The charge on **Au<sub>9</sub>** clusters is +3, while for **Au<sub>13</sub>** is +4 giving the gold atom charges of +1/3 and *ca.* +1/4 each respectively thus making the peak more prominent than for naked gold nanoparticles. This explains the feature (a) present in the starting material, which is related to the presence of density of unoccupied states. Features labelled (b) in Figure 3.10 present in the XANES becomes sharper as temperature increases. These represent the metallic gold state that became more dominant above 200°C. This change is in agreement with the TGA-DSC and XRD data confirming the formation of gold nanoparticles upon heating the supported clusters compounds. Thus, it is possible to directly link the calcination conditions to catalyst activation for these samples.

**Table 3.7:** Structural parameters derived from the analysis of Au L<sub>III</sub> edge EXAFS data for **Au<sub>9</sub>** clusters physically mixed with Al<sub>2</sub>O<sub>3</sub> in-situ heating up to 450°C

Temperature, (°C)	<i>Au-P</i>			<i>Au-Au</i>		
	N	R, (Å)	$\sigma^2, (\text{Å}^2)$	N	R, (Å)	$\sigma^2, (\text{Å}^2)$
69	1.00	2.29	0.001	2.72	2.69	0.002
299	0.03	2.26	0.001	8.18	2.83	0.003
RT	-	-	-	8.54	2.86	0.002

N = coordination number; R = bond distance (Å);  $\sigma^2$  = standard deviation

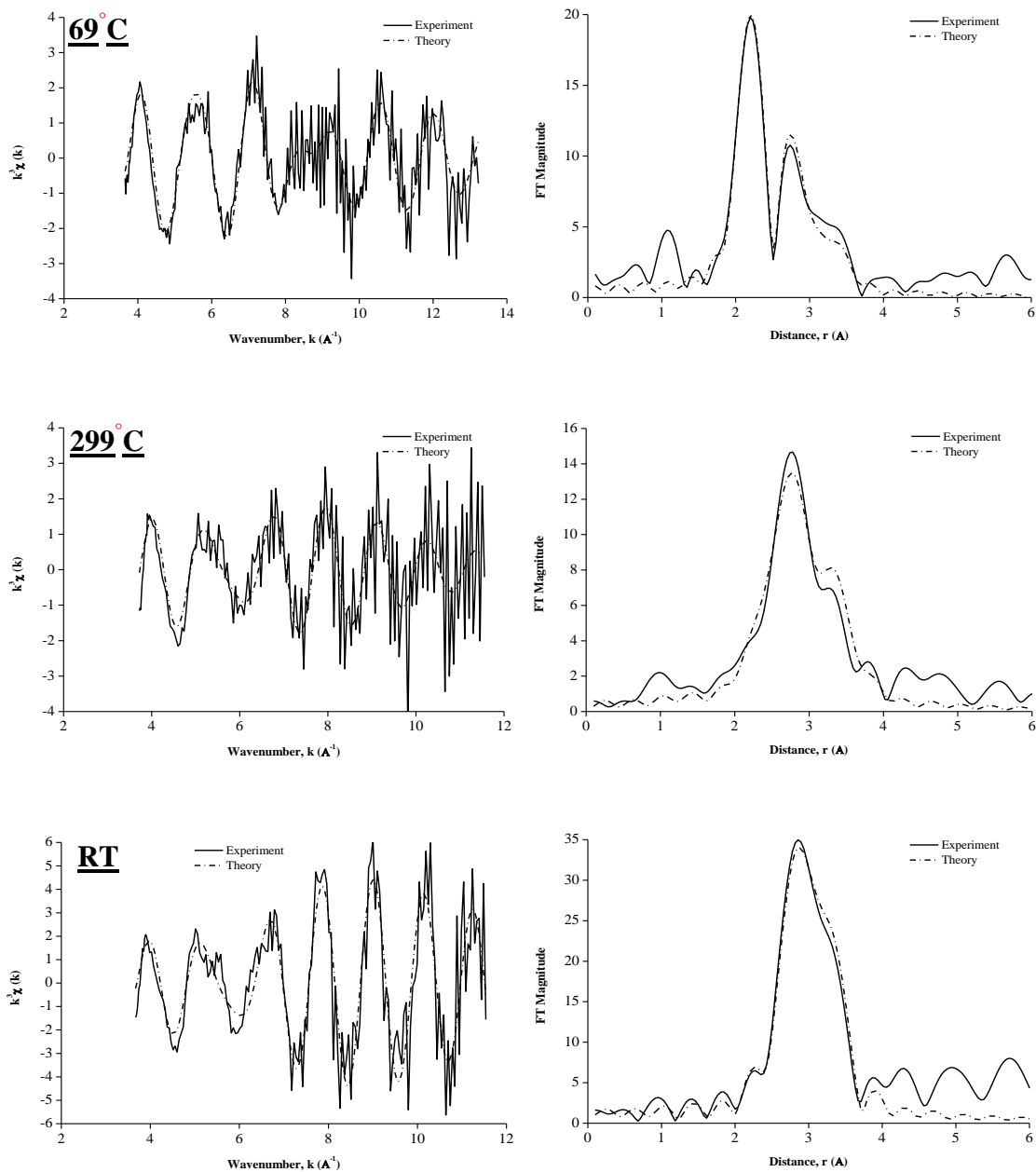


**Figure 3.11:** Best fit corresponding Au L<sub>III</sub> edge EXAFS; Fourier transforms of the experimental and calculated data are shown for **Au<sub>9</sub>** clusters physically mixed with Al<sub>2</sub>O<sub>3</sub> in-situ heating up to 450°C

Table 3.7 lists structural parameters derived from EXAFS analysis for **Au<sub>9</sub>** clusters, while Table 3.8 gives the same information for **Au<sub>13</sub>** clusters. The patterns are similar with Au-P features observed before heating being diminished upon

---

heating in the experiment leaving only a dominant Au-Au feature in the FT plot. However,  $N_{\text{Au-Au}}$  (8.54) with  $R_{\text{Au-Au}}$  2.85 Å for **Au<sub>9</sub>** after cooling is lower than the value for **Au<sub>13</sub>**  $N_{\text{Au-Au}}$  (12.54) with  $R_{\text{Au-Au}}$  2.86 Å. This result suggest that small particles are produced when **Au<sub>9</sub>** cluster was used compared to the **Au<sub>13</sub>**, which is consistent with XRD results. The Au-Au bond distances for both clusters are in agreement with Au foil standard confirming that metallic gold is present<sup>31, 47</sup>. These were indeed very promising results supporting our initial hypothesis that control of size and formation conditions of gold nanoparticles was possible using phosphine-stabilized gold molecular cluster precursors.

The Fourier transformed Au L<sub>III</sub> edge EXAFS data shown in Figure 3.11 gives a good overall view of the transformation taking place with the **Au<sub>9</sub>** cluster. It can be seen that as the temperature increases, the intensity of Au-P peak decreases due to the gradual loss of the phosphines. The peak assigned to Au-Au interactions shows increased in intensity at 299°C. This is in agreement with the data obtained from the XANES, that is, during the initial stages of heating the phosphine ligands were removed.

Further evidence for the transformation of the cationic gold molecular cluster, **Au<sub>13</sub>** to metallic gold was gained considering the change in coordination number and bond distances of Au-P and Au-Au atom pairs (Figure 3.12). In the cationic state, it is common for the Au-Au bond distance to be below 2.70 Å<sup>13, 48</sup>. In an uncharged metallic state, this bond distance is 2.88 Å for gold foil. In Figure 3.11, it can be seen that as the temperature increases from 250°C to 300°C, the Au-Au bond distance

increases from 2.60 Å to 2.80 Å. Upon cooling back down to room temperature, the Au-Au bond distance remains near 2.80 Å.

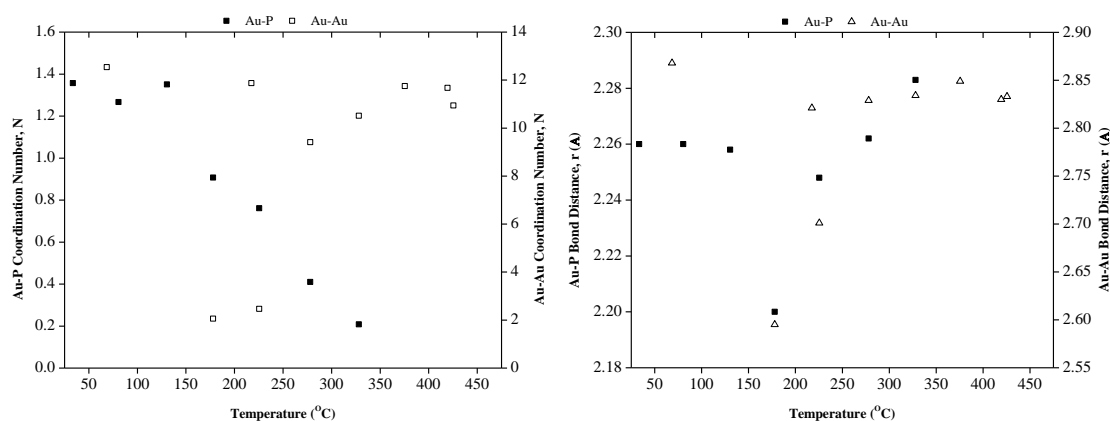


**Table 3.8:** Structural parameters derived from the analysis of Au L<sub>III</sub> edge EXAFS data for Au<sub>13</sub> clusters physically mixed with Al<sub>2</sub>O<sub>3</sub> in-situ heating up to 450 °C

°C	<i>Au-P</i>			<i>Au-Au</i>		
	N	R	$\sigma^2$	N	R	$\sigma^2$
28	1.36	2.26	0.001	-	-	-
RT*	-	-	-	12.54	2.86	0.002

\*temperature after being cooled down from 450 °C

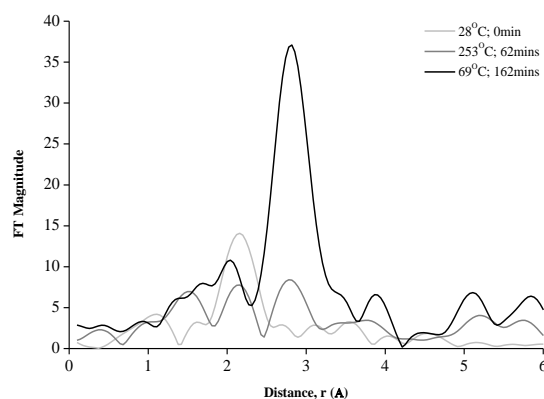


**Figure 3.12:** Plot of the change in coordination number (top left), bond distances (top right) of Au-P and Au-Au atom pair and corresponding Fourier transforms (bottom left) of the experimental data according to different temperatures collected for Au<sub>13</sub> clusters physically mixed with Al<sub>2</sub>O<sub>3</sub> in-situ heating up to 450 °C. N = coordination number; R = bond distance (Å);  $\sigma^2$  = standard deviation

This value is slightly lower than that of bulk metallic gold (gold foil) possibly due to the size of the gold particles as Au-Au bond lengths in small particles (<50

nm) are lower than that observed for the bulk. Considering the Au-Au bond distance before (2.76 Å) and after (2.86 Å) the calcination process, there is further evidence that calcination at 450°C increases the size of the gold particles<sup>49</sup>. This is in good agreement with the Au-Au coordination number data described earlier.

### 3.5 Size Effect

Table 3.9 presents the average particle sizes obtained for the catalysts synthesised from **Au<sub>9</sub>** and **Au<sub>13</sub>** clusters by the wet impregnation method using TEM measurements. This data highlights two points. Firstly, increasing the calcination temperature increases the average gold particle size and secondly increasing the number of gold atoms in the cluster gives smaller gold particles on SiO<sub>2</sub> supports while the opposite is true for Al<sub>2</sub>O<sub>3</sub> supports. It is difficult to obtain TEM images for any of the uncalcined catalysts as the gold clusters were too small to observe.

**Table 3.9:** Average particle sizes of gold nanoparticles measured by TEM

Samples		Mean Particle Size (nm)	
		Calcined at 300°C	Calcined at 500°C
SiO <sub>2</sub>	<b>Au<sub>9</sub></b>	51	78
	<b>Au<sub>13</sub></b>	15	19
Al <sub>2</sub> O <sub>3</sub>	<b>Au<sub>9</sub></b>	8	20
	<b>Au<sub>13</sub></b>	16	24

The TEM images (Figure 3.13) show the broad size distribution of the gold particles. For example, **Au<sub>9</sub>** on SiO<sub>2</sub> support after calcination at 300°C and 500°C gives average particles size in the range of 51 to 78 nm. This in contrast to those

supported on  $\text{Al}_2\text{O}_3$  where the average particle size is only between 8 to 20 nm after calcination at  $300^\circ\text{C}$  and  $500^\circ\text{C}$ . This indicates that the gold is highly mobile on the surface of the silica during calcination and that there is no strong gold-support interaction.

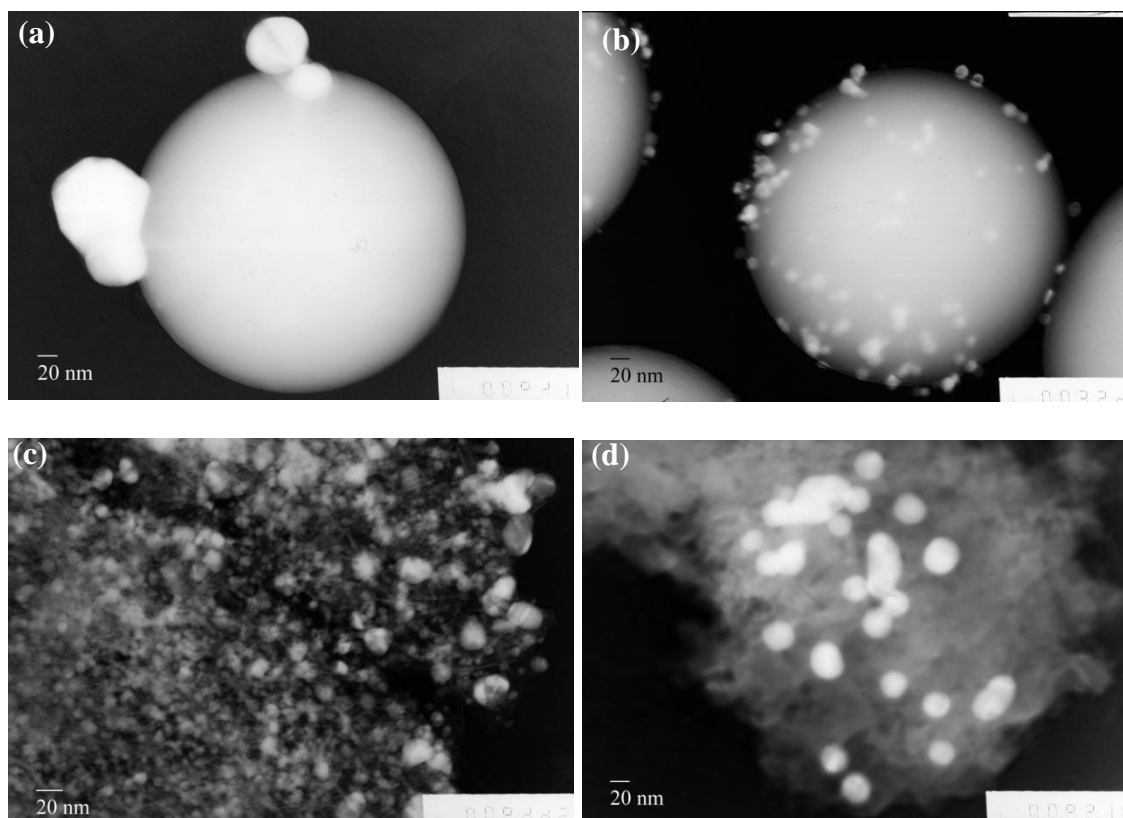


**Figure 3.13:** TEM images of (a)  $\text{Au}_9$  clusters on  $\text{SiO}_2$  nanospheres calcined at  $300^\circ\text{C}$ ; (b)  $\text{Au}_{13}$  clusters on  $\text{SiO}_2$  nanospheres calcined at  $300^\circ\text{C}$ ; (c)  $\text{Au}_9$  clusters on  $\text{Al}_2\text{O}_3$  calcined at  $300^\circ\text{C}$ ; (d)  $\text{Au}_{13}$  clusters on  $\text{Al}_2\text{O}_3$  calcined at  $300^\circ\text{C}$

In contrast,  $\text{Au}_{13}$  catalysts showed more uniform sizes regardless of the support type used in this work. The range of average particle sizes was smaller being between 15 to 25 nm after calcinations at  $300^\circ\text{C}$  and  $500^\circ\text{C}$ . This suggests that either  $\text{Al}_2\text{O}_3$  is better support than  $\text{SiO}_2$  or the  $\text{Au}_{13}$  cluster icosahedral geometry makes it more stable thus avoiding structural rearrangements which may limit the aggregation

---

to bigger nanoparticles. Nonetheless, the wet impregnation method employed in this research was incapable of producing small gold nanoparticles (< 10 nm) even when phosphine-stabilized gold molecular clusters were used as precursors. We find that 300°C is an optimum catalyst activation temperature, which in agreement with data provided by TGA-DSC, XRD and *in-situ* EXAFS analysis.

### 3.6 Conclusions

Using the wet impregnation method towards the bottom-up approach to gold nanoparticles is possible to obtain some size-control when particles interact well with the support. This method involves activation at high temperature which tends to promote larger particles but no evidence was observed in this research that particle sizes enlarge > 100 nm. The use of phosphine-stabilized clusters as precursors that tailored the molecular clusters in the initial stage of particles formation also helps avoiding gold atoms to sinter further upon calcination. It appeared to be in very good agreement with coordination number analysed by EXAFS for both precursor complexes and clusters visualizing strong structural stability and limitation in mobility of gold on support surface. We believe that our hypothesis of having control over nanoparticles size generation by using gold molecular cluster as a precursor is relevant but the method used in preparing the catalyst has to be optimised. There may be several advantages of this kind of approach for preparing fine size gold nanoparticles catalysts, such as the likely of loss of Au in the preparation which is reported elsewhere<sup>9</sup>. Having used gold molecular clusters as a precursor added another advantage. Careful consideration on the type of clusters to be used, method of preparation and appropriate solid support lead to the production of widely dispersed and small gold nanoparticles catalyst.

---

### 3.7 References

1. M. Comotti, P. C. Della, R. Matarrese and M. Rossi, *Angewandte Chemie, International Edition*, 2004, **43**, 5812-5815.
2. Y. Onal, S. Schimpf and P. Claus, *Journal of Catalysis*, 2004, **223**, 122-133.
3. S. Kim, S. W. Bae, J. S. Lee and J. Park, *Tetrahedron*, 2009, **65**, 1461-1466.
4. W. Fang, J. Chen, Q. Zhang, W. Deng and Y. Wang, *Chemistry – A European Journal*, 2011, **17**, 1247-1256.
5. K. Guillois, L. Burel, A. Tuel and V. Caps, *Applied Catalysis A: General*, 2012, **415-416**, 1-9.
6. L. S. Roselin, F.-W. Chang, W.-S. Chen and H.-C. Yang, *Science of Advanced Materials*, 2011, **3**, 893-900.
7. W.-C. Li, M. Comotti and F. Schüth, *Journal of Catalysis*, 2006, **237**, 190-196.
8. K. Qian, J. Fang, W. Huang, B. He, Z. Jiang, Y. Ma and S. Wei, *Journal of Molecular Catalysis A: Chemical*, 2010, **320**, 97-105.
9. M. Bowker, A. Nuhu and J. Soares, *Catalysis Today*, 2007, **122**, 245-247.
10. P. D. Boyle, Copyright (C) 2011 American Chemical Society (ACS). All Rights Reserved., 1988.
11. O. D. Haerberlen, H. Schmidbaur and N. Roesch, *Journal of American Chemical Society*, 1994, **116**, 8241-8248.
12. I. V. G. Graf, J. W. Bacon, M. B. Consugar, M. E. Curley, L. N. Ito and L. H. Pignolet, *Inorganic Chemistry*, 1996, **35**, 689-694.
13. Y. Yuan, K. Asakura, H. Wan, K. Tsai and Y. Iwasawa, *Catalysis Letters*, 1996, **42**, 15-20.
14. C. C. Chusuei, X. Lai, K. A. Davis, E. K. Bowers, J. P. Fackler and D. W. Goodman, *Langmuir*, 2001, **17**, 4113-4117.
15. M. Walter, J. Akola, O. Lopez-Acevedo, P. D. Jadzinsky, G. Calero, C. J. Ackerson, R. L. Whetten, H. Gronbeck and H. Hakkinen, *Proceedings of the National Academy of Sciences*, 2008, **105**, 9157-9162.
16. D. F. Shriver, H. D. Kaesz and R. D. Adams, in *The Chemistry of Metal Cluster Complexes*, eds. D. F. Shriver, H. D. Kaesz and R. D. Adams, VCH Publishers, Inc., New York, Editon edn., 1990, pp. 11-120.
17. C. A. Tolman, *Chemical Reviews*, 1977, **77**, 313-348.

- 
18. F. Cariati and L. Naldini, *Journal of Chemical Society, Dalton Transactions*, 1972, 2286 - 2287.
  19. J. W. A. V. D. Velden, F. A. Vollenbroek, J. J. Bour, P. T. Beurskens, J. M. M. Smits and W. P. Bosman, *Recueil, Journal of the Royal Netherlands Chemical Society*, 1981, **100**, 148-152.
  20. F. A. Vollenbroek, d. B. J. P. Van, d. V. J. W. A. Van and J. J. Bour, *Inorganic Chemistry*, 1980, **19**, 2685-2688.
  21. C. E. Briant, B. C. Theobald, J. W. White, L. K. Bell and D. M. P. Mingos, *Journal of the Chemical Society, Chemical Communications*, 1981, **5**, 201-201.
  22. Y. Shichibu and K. Konishi, *Small*, 2010, **6**, 1216-1220.
  23. F. A. Vollenbroek, J. J. Bour and d. V. J. W. A. Van, *Recl. Trav. Chim. Pays-Bas*, 1980, **99**, 137-141.
  24. G. Shafai, S. Hong, M. Bertino and T. S. Rahman, *Journal of Physical Chemistry C*, 2009, **113**, 12072-12078.
  25. J. S. Golightly, L. Gao, A. W. C. Jr., D. E. Bergeron, J. W. Hudgens, R. J. Magyar and C. A. Gonzalez, *The Journal of Physical Chemistry C*, 2007, **111**, 14625-14627.
  26. C. J. McNeal, J. M. Hughes, L. H. Pignolet, L. T. J. Nelson, T. G. Gardner, J. P. Fackler, R. E. P. Winpenny, L. H. Irgens, G. Vigh and R. D. Macfarlane, *Inorganic Chemistry*, 1993, **32**, 5582-5590.
  27. P. Sevillano, O. Fuhr, O. Hampe, S. Lebedkin, E. Matern, D. Fenske and M. M. Kappes, *Inorganic Chemistry*, 2007, **46**, 7294-7298.
  28. M. F. Bertino, Z.-M. Sun, R. Zhang and L.-S. Wang, *The Journal of Physical Chemistry B: Letters*, 2006, **110**, 21416-21418.
  29. E. S. Andreiadis, M. R. Vitale, N. Mezailles, X. L. Goff, P. L. Floch, P. Y. Toullec and V. Michelet, *Dalton Transactions*, 2010, **39**, 10608-10616.
  30. A. Quintanilla, V. C. L. Butselaar-Orthlieb, C. Kwakernaak, W. G. Sloof, M. T. Kreutzer and F. Kapteijn, *Journal of Catalysis*, 2010, **271**, 104-114.
  31. S. H. Overbury, V. Schwartz, D. R. Mullins, W. Yan and S. Dai, *Journal of Catalysis*, 2006, **241**, 56-65.
  32. A. I. Kozlov, A. P. Kozlova, H. Liu and Y. Iwasawa, *Applied Catalysis A: General*, 1999, **182**, 9-28.

- 
33. J. Kilmartin, Thesis, University College London, 2010.
  34. J. Kilmartin, R. Sarip, R. Grau-Crespo, D. Di Tommaso, G. Hogarth, C. Prestipino and G. Sankar, *American Chemical Society: Catalysis*, 2012, **2**, 957-963.
  35. P. Pyykkoe, *Angewandte Chemie, International Edition*, 2004, **43**, 4412-4456.
  36. P. Pyykko and N. Runeberg, *Angewandte Chemie, International Edition*, 2002, **41**, 2174-2176.
  37. A. Goerling, N. Roesch, D. E. Ellis and H. Schmidbaur, *Inorganic Chemistry*, 1991, **30**, 3986-3994.
  38. P. Schwerdtfeger and P. D. W. Boyd, *Inorganic Chemistry*, 1992, **31**, 327-329.
  39. D. M. P. Mingos, *Polyhedron*, 1984, **3**, 1289-1297.
  40. Y. Shichibu, K. Suzuki and K. Konishi, *Nanoscale*, 2012, **4**, 4125-4129.
  41. F. A. Vollenbroek, J. J. Bour, J. M. Trooster and J. W. A. v. d. Velden, *Journal of the Chemical Society, Chemical Communications*, 1978, 907-909.
  42. P. Schwerdtfeger, *Angewandte Chemie, International Edition*, 2003, **42**, 1892-1895.
  43. M. Haruta, N. Yamada, T. Kobayashi and S. Iijima, *Journal of Catalysis*, 1989, **115**, 301-309.
  44. M. H. Rashid and T. K. Mandal, *Advanced Functionalised Materials*, 2008, **18**, 2261-2271.
  45. H. Zhang, J.-J. Xu and H.-Y. Chen, *Journal of Physical Chemistry C*, 2008, **112**, 13886-13892.
  46. S. Jafari, H. Asilian Mahabady and H. Kazemian, *Catalysis Letters*, 2009, **128**, 57-63.
  47. R. E. Benfield, D. Grandjean, M. Kroll, R. Pugin, T. Sawitowski and G. Schmid, *The Journal of Physical Chemistry B*, 2001, **105**, 1961-1970.
  48. Y. Yuan, K. Asakura, H. Wan, K. Tsai and Y. Iwasawa, *Journal of Molecular Catalysis A: Chemical*, 1997, **122**, 147-157.
  49. J. T. Miller, A. J. Kropf, Y. Zha, J. R. Regalbuto, L. Delannoy, C. Louis, E. Bus and J. A. van Bokhoven, *Journal of Catalysis*, 2006, **240**, 222-234.

---

## Chapter 4

### ***tert*-Butyl Hydroperoxide (TBHP) Assisted Deposition-Precipitation – A New Low Temperature Method for Generating Gold Nanoparticulate Catalysts**

#### **4.0 Abstract**

This chapter highlights the development of a new deposition-precipitation method assisted by *tert*-butyl hydroperoxide (TBHP). We investigate the role of TBHP in the ligand removal for phosphine-stabilized gold molecular clusters at relatively low temperatures *ca.* 95°C. Catalyst activation was possible without the needs of a calcination step potentially limits particle agglomeration. *In-situ* EXAFS was employed to monitor nanoparticle creation. Differences in cluster precursors particle was studied using both **Au<sub>9</sub>** and **Au<sub>13</sub>** as well as on different supports (SiO<sub>2</sub> nanospheres and Al<sub>2</sub>O<sub>3</sub>). Very small (< 5 nm) and finely dispersed gold nanoparticles were observed for as-synthesized catalysts as compared to calcined (300°C) catalysts. TEM images of supported catalysts on SiO<sub>2</sub> nanospheres showed interesting patterns that might due to a self-assembly effect.

#### **4.1 Introduction**

There has been an ever-expanding effort in the field of catalysis by gold, ever since the report of Haruta *et al.* on high activity of gold for certain reactions under low temperature conditions<sup>1</sup>. From this first report it was evident that the catalyst preparation method was a crucial factor in determining the efficiency of the gold heterogeneous catalysts. It was shown that one of the best catalysts for the latter

---

reaction was Au/TiO<sub>2</sub> and that this was successfully used to oxidise CO below ambient temperature<sup>2, 3</sup>. However, such activity was only achieved when using the method of deposition–precipitation which involves increasing the pH of a dilute slurry containing the support, usually using ammonia, NaOH or Na<sub>2</sub>CO<sub>3</sub> to a certain pH depending on the support. At this point Au(OH)<sub>3</sub> is precipitated from solution onto the surface of the support.

Most literature reports claim that the optimum gold particle size was in the range of 2-3 nm<sup>4-9</sup>. Such sizes can be achieved by careful control of the preparation conditions. Until now, the most practical and reliable method for the preparation of supported gold catalysts has been deposition-precipitation using NaOH<sup>2, 10</sup>. This method allows the size of gold particles to be adjusted by controlling pH and the calcination temperature. Furthermore, the deposition-precipitation method using sodium hydroxide has been also shown to produce very small gold particles<sup>11</sup>. The main advantage of this method over that of deposition-precipitation with NaOH is that all the gold from solution is deposited onto the support so that higher gold loadings can be reached.

The calcination step is crucial in the conventional deposition-precipitation method whether using NaOH or Na<sub>2</sub>CO<sub>3</sub>. From the literature, the optimal calcination temperature is in the range of 200-500°C but most reported that highly active gold must be calcined at temperature, above 300°C<sup>2, 6, 7, 12</sup>. Many authors have suggested that the catalytic activity of gold catalysts strongly depends upon the size of the gold particles with a maximum of activity usually observed for a particle sizes *ca.* 3 nm. Indeed, it was found that the catalysis reaction markedly increases with a decrease in

---

the diameter of the Au particles<sup>13-17</sup>. It was summarised that the effect of the oxidation state of gold was at least as important as that of the particle size. However, the oxidation state of the gold in the active catalysts is unclear. It is very difficult to obtain gold nanoparticles in a state of high dispersion as the melting point of gold particles with diameter of *ca.* 2 nm is lowered to 573 K (*ca.* 300 °C) due to quantum size effect<sup>13</sup>.

In this work, we developed a novel deposition-precipitation method assisted by *tert*-butyl hydroperoxide at relatively low temperature (95 °C). We illustrate how to convert the phosphine-stabilized gold molecular clusters to a denuded active catalyst without the need for a calcination step. Finely dispersed and small gold particles were achieved by this method (*ca.* 2 nm). Furthermore, an interesting self-assembled of gold particles was observed for **Au<sub>13</sub>** deposited on SiO<sub>2</sub> nanospheres using this method. The goal of this study was threefold; (i) to control the gold particle size by a bottom-up approach using phosphine-stabilized gold molecular clusters, (ii) to minimise the gold agglomeration by avoiding a high temperature calcination step, and (iii) to develop a one pot, single step, catalyst preparation procedure at low temperature.

## 4.2 Experimental

Detailed procedures of synthesis and characterisation techniques of the synthesized compound are discussed in Chapter 2. Transmission electron micrograph (TEM) image of the nanoparticles were taken using JEOL 100 keV transmission electron microscope and high resolution JEM 2100 Electron Microscope. X-ray powder diffraction (XRD) pattern were measured using Bruker D4 X-Ray

---

diffractometer with Cu  $K_{\alpha}$  radiation over the  $2\theta$ -range of 5 to  $90^{\circ}$ , 0.05sec/step size. Au  $L_{III}$  edge X-ray absorption spectroscopy (XAS) analysis was recorded at BM26 beam line of DUBBLE, ESRF Synchrotron Centre Grenoble, France, SAMBA beam line of SOLEIL Synchrotron Centre Paris, France and B18 beam line of Diamond Light Source, Didcot, United Kingdom. The samples were measured at room temperature for *ex-situ* study and *in-situ* heating up to  $500^{\circ}\text{C}$  in a transmission mode.

#### 4.2.1 *Generating Au nanoparticles with tert-butyl hydroperoxide (TBHP)*

The  $\text{Au}_9$  and  $\text{Au}_{13}$  clusters were deposited on  $\text{SiO}_2$  nanospheres or commercially available CATAPAL-A  $\text{Al}_2\text{O}_3$  with a percentage of calculated 4.0 % wt. Au loading. Approximately 1.0 g of support was immersed in TBHP (5 ml) and stirred for 5 minutes. An appropriate amount of clusters *ca.* 0.1g was dissolved in TBHP (5 ml) then added to the support slurry while stirring. The mixture was stirred for 10 minutes. An excess of TBHP (5 ml) was then added and the mixture heated to  $90^{\circ}\text{C}$  for 3 hours. The solids were isolated by vacuum filtration and dried at  $100^{\circ}\text{C}$  for 1 hour then finely ground to give a visibly homogenized sample. Half of the solid was calcined at  $300^{\circ}\text{C}$  at  $10^{\circ}\text{C}/\text{min}$  for one hour with the remaining was uncalcined.

## 4.3 Results and Discussion

### 4.3.1 Study of formation of gold nano particles

In order to establish the process of formation of gold nanoparticle by TBHP method, first we react the gold cluster (dissolved in TBHP) at 95°C and periodically removed the sample and examined by Au L<sub>3</sub> X-ray absorption spectroscopy. Stacked Au L<sub>III</sub> edge XANES data (normalised) for Au<sub>13</sub> clusters dissolved in TBHP plotted at different time interval is shown in Figure 4.1. These spectra shows that the features marked (*a*) present at the start of the reaction are those of gold in a phosphine-stabilised cationic cluster. During the course of the reaction, this feature undergoes changes. The spectrum of the samples reacted for 6 hours resembles that of metallic gold.

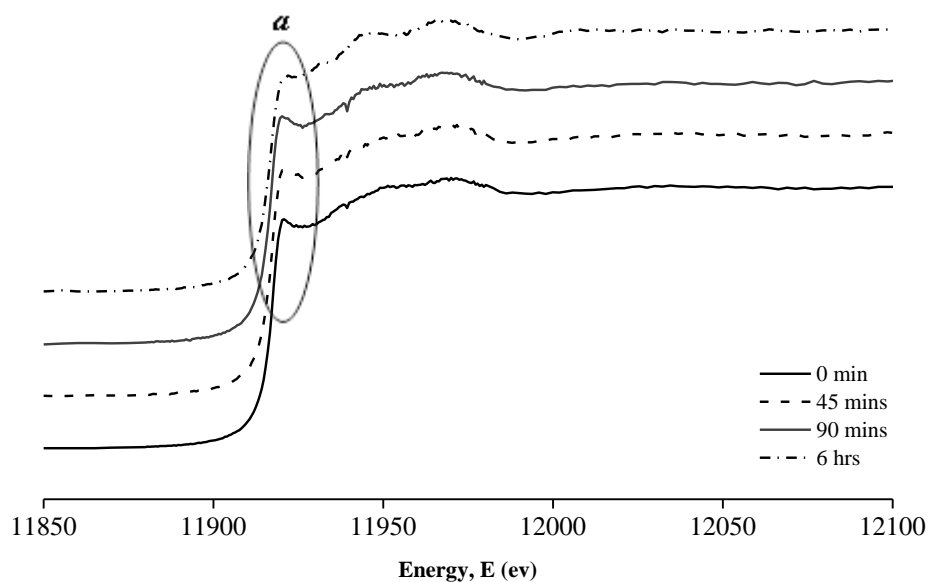


**Figure 4.1:** XANES spectra of Au<sub>13</sub> clusters dissolved in TBHP *ex-situ* heating up to 95°C for 6 hours

Following the experiment of dissolving the  $\text{Au}_{13}$  clusters in TBHP (Figure 4.1), we then introduced supports ( $\text{SiO}_2$  or  $\text{Al}_2\text{O}_3$ ) to the solution to follow nanoparticle creation. The cluster solution in TBHP was introduced to appropriate amount of support before being refluxed at  $95^\circ\text{C}$  for 3 hours. The EXAFS was recorded for samples that have been filtered and dried (Figure 4.2).

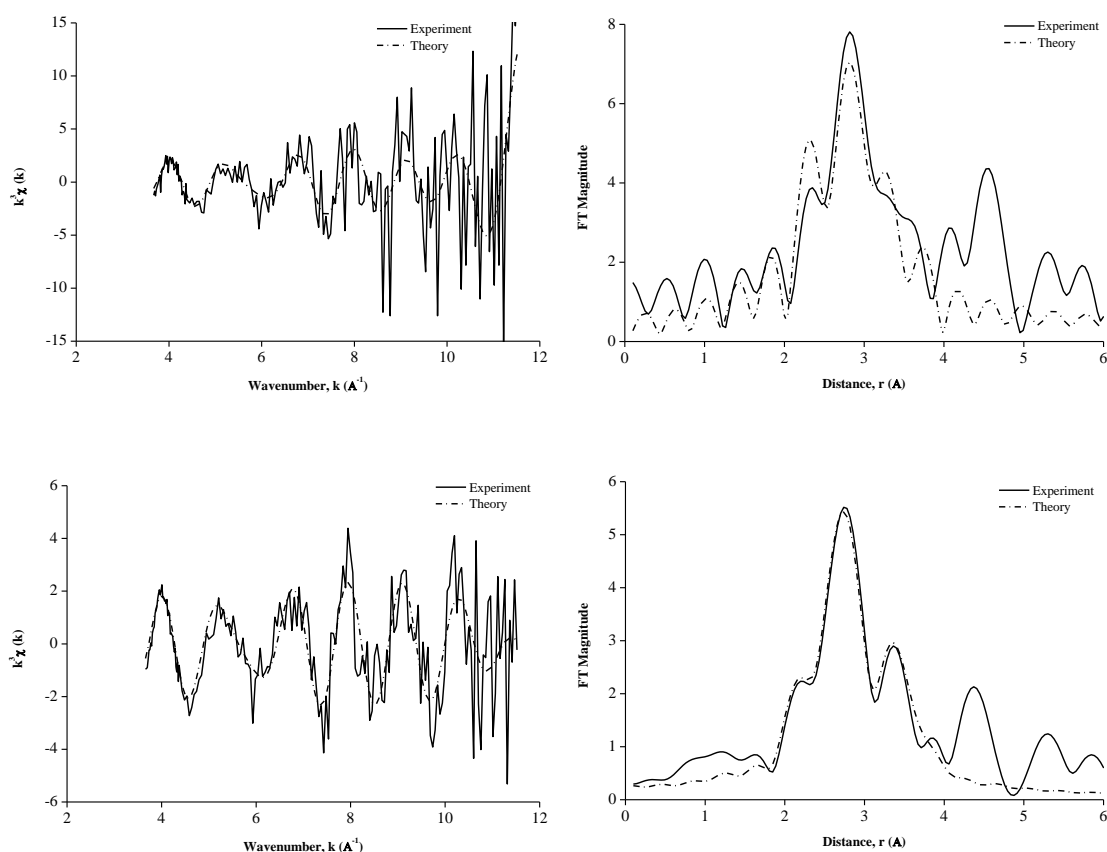


**Figure 4.2:** Best fit between experimental Au L<sub>III</sub> edge EXAFS and theory/calculated data for  $\text{Au}_{13}$  deposited on  $\text{SiO}_2$  (top) and  $\text{Al}_2\text{O}_3$  (bottom) reacted with TBHP at  $95^\circ\text{C}$  after 3 hours (catalyst was filtered and dried before analysis). On the right corresponding Fourier transform of the experimental and calculated data are shown.

The analysis of the EXAFS data indicate that after 3 hours, gold nanoparticles were deposited onto supports and Au-P features were found to be absent. The Au-Au coordination number for supported catalyst on Al<sub>2</sub>O<sub>3</sub> was found to be 6.58 with bond distance being 2.82 Å. The catalyst supported on SiO<sub>2</sub> gave slightly different values, 7.62 for Au-Au coordination number with a bond distance of 2.82 Å. This confirms that the nanoparticle formation has occurred during the deposition process directed by TBHP. Following this study we prepared a series of supported catalyst using this deposition-precipitation method and investigated, *ex situ*, the nature of gold on the supports using XRD, XANES, EXAFS and TEM techniques.

#### 4.3.2 X-ray Diffraction (XRD)

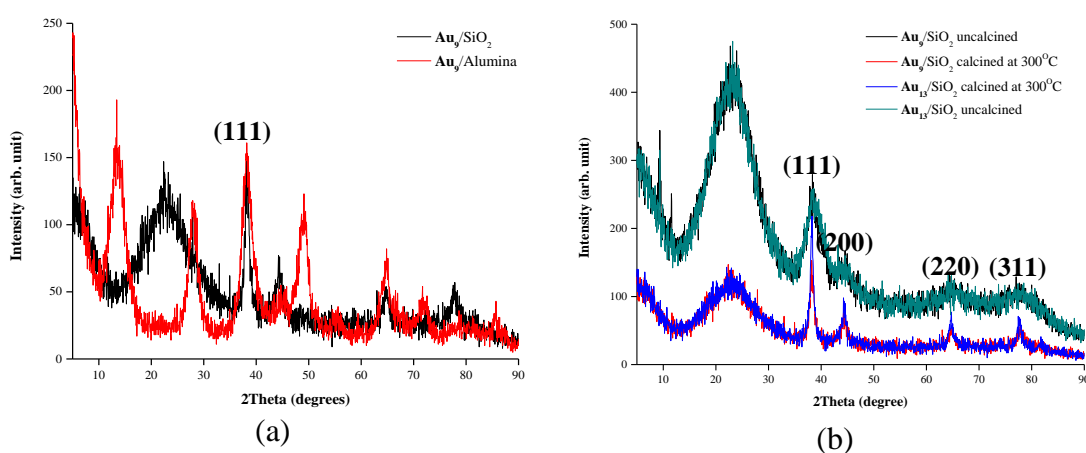


**Figure 4.3:** (a) comparison of **Au<sub>9</sub>** clusters on SiO<sub>2</sub> nanospheres support and alumina support; (b) **Au<sub>9</sub>** and **Au<sub>13</sub>** clusters on SiO<sub>2</sub> nanospheres uncalcined and calcined at 300 °C

X-ray diffraction studies of gold cluster deposited on alumina and silica were investigated. However, the data on alumina could not be interpreted due to the

appearance of broad reflections of  $\text{Al}_2(\text{OH})_3$  in the region where major reflections from gold particles are seen. A typical XRD plot recorded for deposited gold nanoparticles on alumina and silica are shown in Figure 4.3. It is clear from the figure that major gold reflections appear at  $2\theta$  values closely similar to that of alumina preventing any detailed determination of FWHM and particle size. Therefore, only samples prepared on silica are discussed here.

The full width at half maximum (FWHM) values obtained from powder XRD of selected catalysts are reported in Table 4.1. Very broad diffraction peaks for the Au (111) plane of the *fcc* structure of gold were found in the uncalcined  $\text{SiO}_2$  supported materials corresponding to very small gold nanoparticles. Slightly larger gold nanoparticles (size > 5 nm) were detected in calcined at  $300^\circ\text{C}$  on  $\text{SiO}_2$  nanospheres (Table 4.1). This corresponds well with findings described in literatures showing high temperature treatment lead to gold aggregation<sup>7, 18</sup>.

**Table 4.1:** FWHM values derived from powder XRD patterns using *fit(y)k* software of **Au<sub>9</sub>** and **Au<sub>13</sub>** catalysts deposited onto  $\text{SiO}_2$  nanospheres and  $\text{Al}_2\text{O}_3$  support by TBHP method

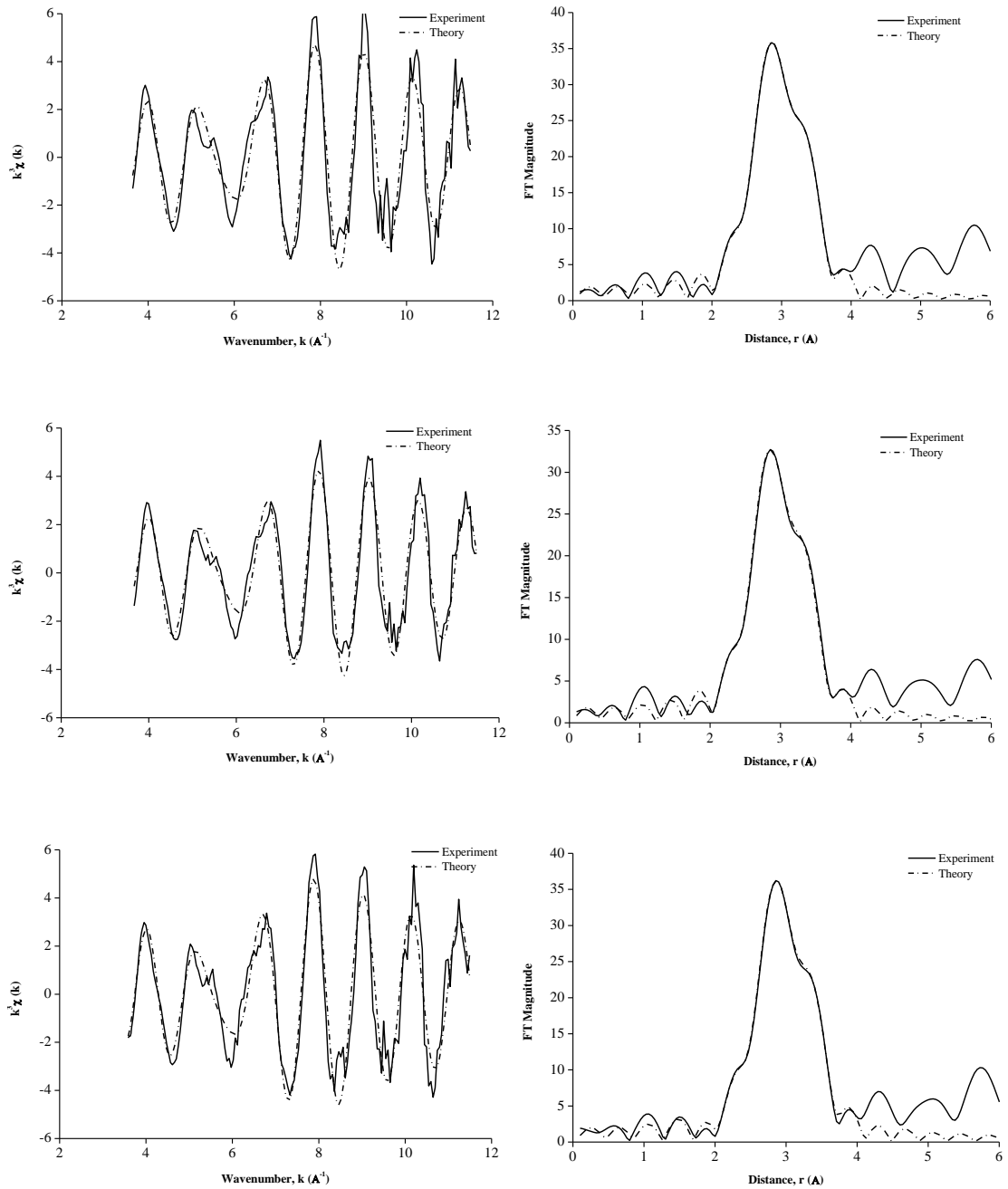
Samples	(111)		Estimated Particle
	$2\theta$ ( $^\circ$ )	FWHM	Size (nm)
<b>Au<sub>9</sub></b> on $\text{SiO}_2$ uncalcined	23.08	3.0	2.7
<b>Au<sub>9</sub></b> on $\text{SiO}_2$ calcined at $300^\circ\text{C}$	22.96	1.0	8.9
<b>Au<sub>13</sub></b> on $\text{SiO}_2$ uncalcined	23.05	3.0	1.9
<b>Au<sub>13</sub></b> on $\text{SiO}_2$ calcined at $300^\circ\text{C}$	23.03	1.0	13.4

---

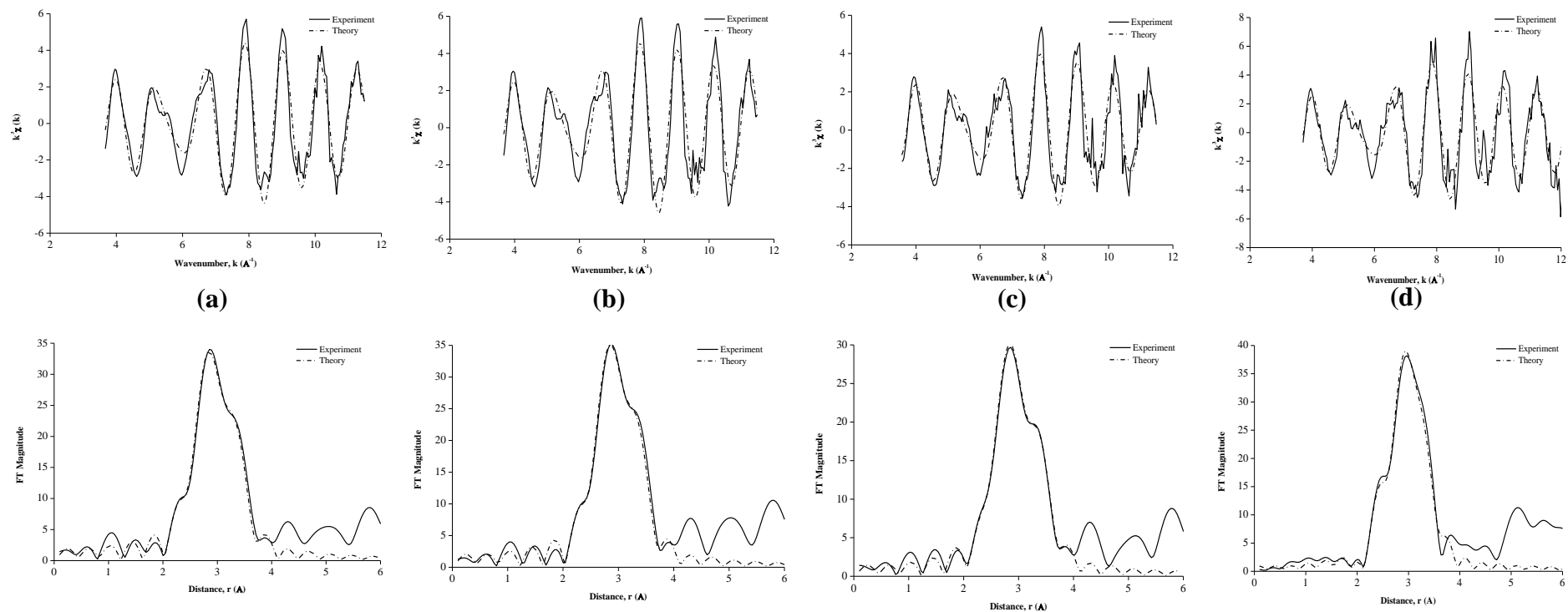
### 4.3.3 X-ray Absorption Spectroscopy; XANES and EXAFS

EXAFS spectra of **Au<sub>9</sub>** deposited on SiO<sub>2</sub> and Al<sub>2</sub>O<sub>3</sub> were measured for the uncalcined and calcined at 300°C (Figure 4.4). The best fit gives a coordination number for Au-Au atom pair of 11.85 (calcined at 300°C **Au<sub>9</sub>** on SiO<sub>2</sub>), 10.96 (uncalcined **Au<sub>9</sub>** on Al<sub>2</sub>O<sub>3</sub>) and 11.94 (calcined at 300°C **Au<sub>9</sub>** on Al<sub>2</sub>O<sub>3</sub>) with bond distances of 2.85 Å for all species. Coordination numbers for Au-P atom pairs reach zero indicating complete loss of phosphines. These findings show that formation of metallic gold nanoparticles was complete even before calcination.

A similar investigation was carried out for **Au<sub>13</sub>** supported catalysts. Figure 4.5 shows the EXAFS best fit for **Au<sub>13</sub>** catalysts deposited on SiO<sub>2</sub> and Al<sub>2</sub>O<sub>3</sub>, uncalcined and calcined at 300°C. The plots for each catalyst are almost identical with  $N_{\text{Au-Au}}$  approaching bulk (*ca.* 11) and  $R_{\text{Au-Au}}$  values being 2.85 Å. All exhibit the typical Fourier transform pattern of *fcc* gold. These findings further show that the TBHP deposition-precipitation method requires one less step than conventional deposition-precipitation.



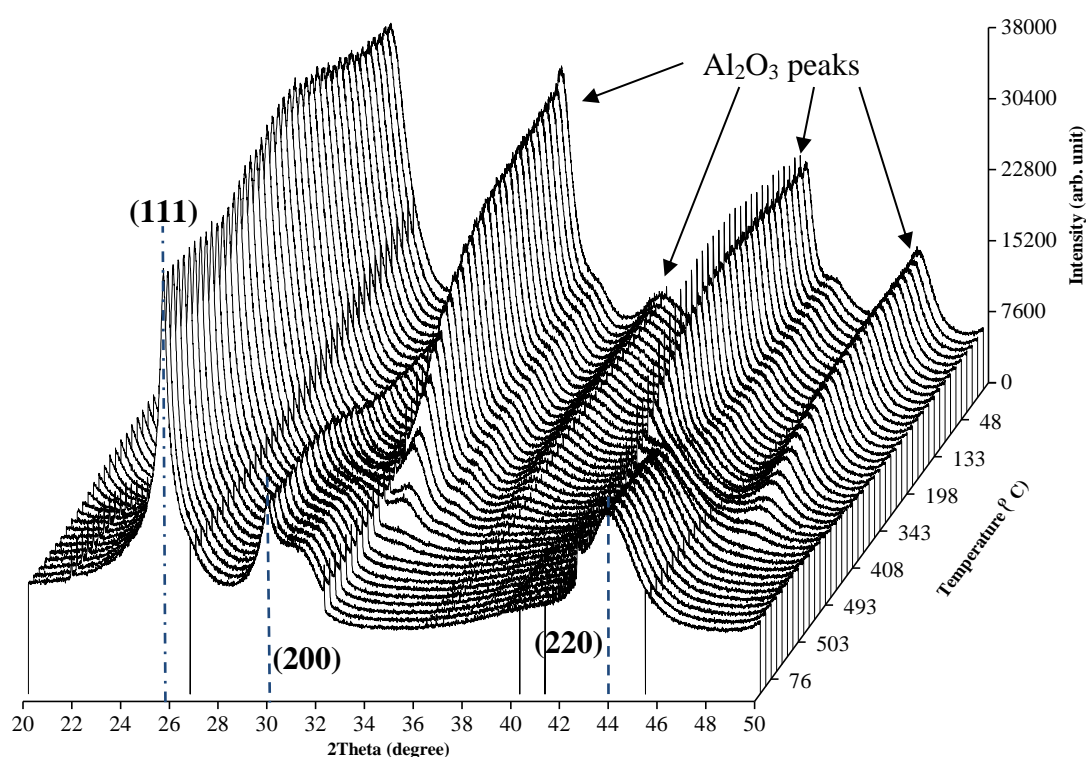
**Figure 4.4:** Best fit between experimental Au L<sub>III</sub> edge EXAFS and theory/calculated data for **Au<sub>9</sub>** deposited on SiO<sub>2</sub> calcined at 300 °C (top), Al<sub>2</sub>O<sub>3</sub> uncalcined (middle) and Al<sub>2</sub>O<sub>3</sub> calcined at 300 °C (bottom) by TBHP method. On the right corresponding Fourier transform of the experimental and calculated data are shown.



**Figure 4.5:** Best fit between experimental Au L<sub>III</sub> edge EXAFS and theory/calculated data for  $\text{Au}_{13}$  deposited on  $\text{SiO}_2$  (a) uncalcined and (b) calcined at  $300^\circ\text{C}$ ,  $\text{Al}_2\text{O}_3$  (c) uncalcined and (d) calcined at  $300^\circ\text{C}$  by TBHP method. On the bottom corresponding Fourier transform of the experimental and calculated data are shown.

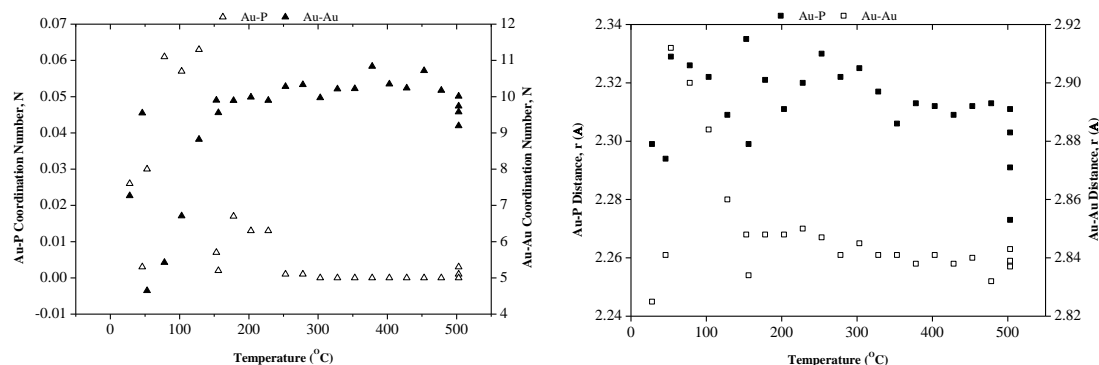
#### 4.3.4 *In-situ* Studies of Au<sub>9</sub> Deposited on Alumina

Figure 4.6 illustrates the diffraction patterns of Au<sub>9</sub> clusters deposited onto Al<sub>2</sub>O<sub>3</sub> using the TBHP method followed by *in-situ* heating to 500°C. Although it appears that some broad reflections of Au (200) and Au (220) planes can be observed even before the heating was started, it is difficult to interpret the data due to the presence of reflections from alumina support.



**Figure 4.6:** XRD patterns of Au<sub>9</sub> clusters catalyst deposited on Al<sub>2</sub>O<sub>3</sub> by TBHP method *in-situ* heating to 500°C

Analysis of the *in-situ* EXAFS data collected during heating yields more information on the changes undergone by the gold in the cluster during the calcination process.



**Figure 4.7:** Plot of the changes in coordination number (left) and bond distances (right) of Au-P and Au-Au atom pair collected at different temperature in-situ heating **Au<sub>9</sub>** clusters deposited on Al<sub>2</sub>O<sub>3</sub> by TBHP method

Figure 4.7 shows changes in coordination number and bond distances observed for **Au<sub>9</sub>** clusters deposited on Al<sub>2</sub>O<sub>3</sub> by the TBHP method. There was a general decrease in the Au-P coordination number up to *ca.* 250 °C although this value (<1) reached zero after 250 °C. However, the Au-Au coordination number is approximately *ca.* 10 constant throughout the heat treatment. This indicates that metallic gold nanoparticles have been prepared on the support surfaces even before calcination.

#### 4.3.5 Transmission Electron Microscopy (TEM) Analysis

Table 4.2 gives the average particle sizes obtained for materials synthesised from **Au<sub>9</sub>** and **Au<sub>13</sub>** clusters by the TBHP method. This data highlights three points. Firstly, uncalcined catalysts have transformed to nanoparticles which can be seen under electron microscope as opposed to uncalcined WI method catalysts (Chapter 3). Secondly, increasing calcination temperature increases the average gold particle size and thirdly, increasing the number of gold atoms in the clusters (**Au<sub>13</sub>** vs. **Au<sub>9</sub>**)

gives smaller gold particles on SiO<sub>2</sub> nanospheres support but the opposite is seen on Al<sub>2</sub>O<sub>3</sub>.

**Table 4.2:** Average particle sizes of gold nanoparticles measured by TEM

Samples		Mean Particle Size (nm)	
		Uncalcined	Calcined at 300 °C
SiO <sub>2</sub>	Au <sub>9</sub>	3	9
	Au <sub>13</sub>	2	13
Al <sub>2</sub> O <sub>3</sub>	Au <sub>9</sub>	6	11
	Au <sub>13</sub>	3	20

The TEM images (Figure 4.8) show a highly uniform and narrow size distribution of gold particles on the supported catalysts. Au<sub>9</sub> on SiO<sub>2</sub> uncalcined and calcined at 300 °C gives average particles sizes of 3 nm and 9 nm respectively. In contrast, on Al<sub>2</sub>O<sub>3</sub> mean particle sizes observed are much bigger being 6 nm uncalcined and 11 nm after calcination at 300 °C. This indicates that the gold particles are highly mobile on the surface of the alumina support as compared to silica nanospheres and agglomeration occurs after calcination<sup>2</sup>.

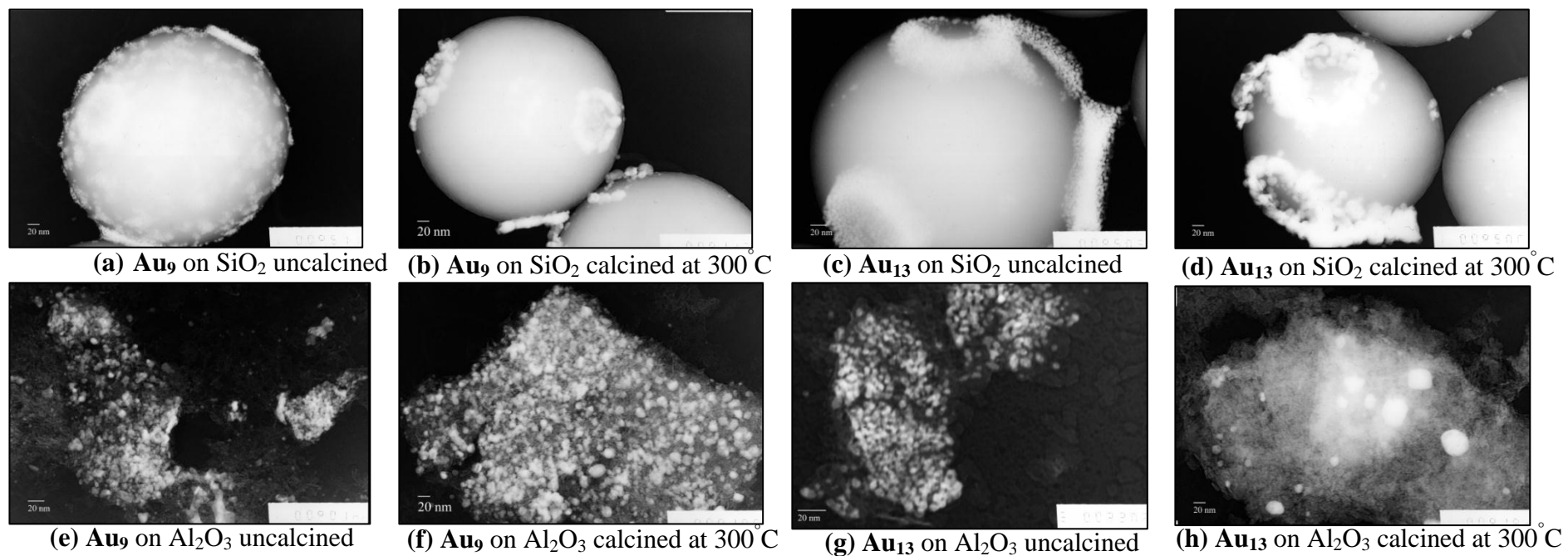


**Figure 4.8:** Film negative TEM images of  $\text{Au}_9$  and  $\text{Au}_{13}$  deposited onto  $\text{SiO}_2$  nanospheres and  $\text{Al}_2\text{O}_3$  support *via* TBHP method; uncalcined and calcined at  $300^\circ\text{C}$

---

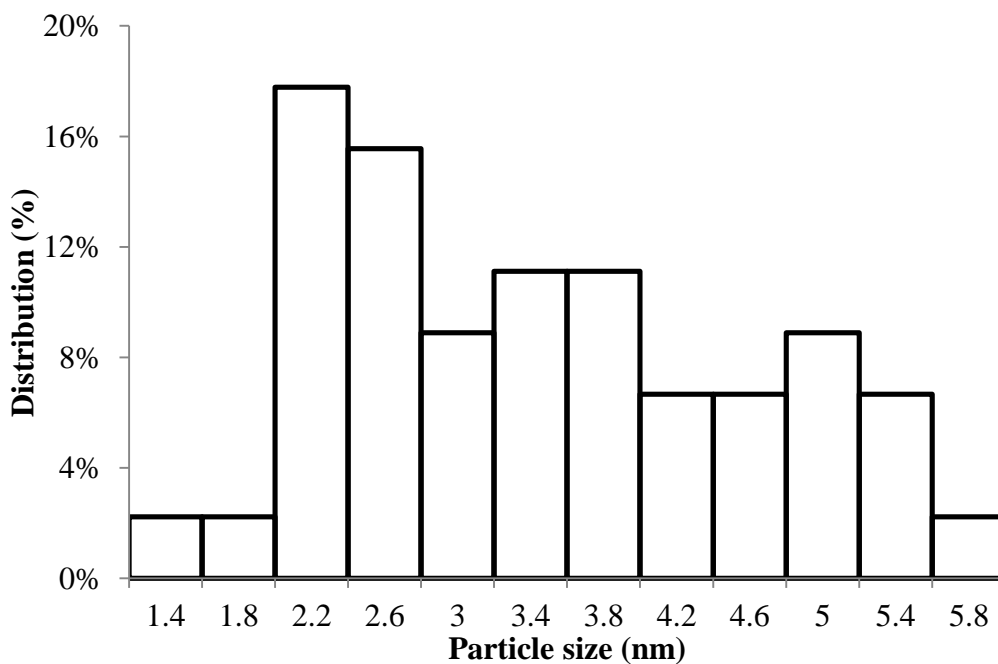
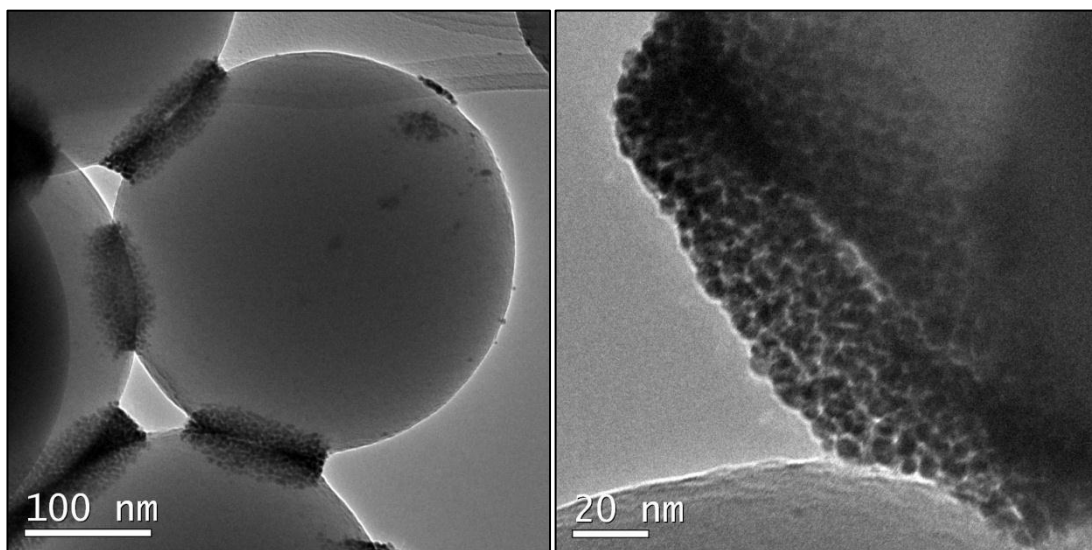
**Au<sub>13</sub>** generated nanoparticles were smaller for uncalcined catalysts both on SiO<sub>2</sub> or Al<sub>2</sub>O<sub>3</sub> supports. The range of particles sizes observed was between 2-4 nm for the uncalcined catalysts. However, when calcined at 300 °C, catalysts prepared by the TBHP method was bigger in size compared to similar **Au<sub>9</sub>** generated catalysts. This shows that the **Au<sub>13</sub>** clusters icosahedral geometry<sup>23-25</sup> makes it more stable hence avoiding structural rearrangement leading to aggregation.

Figure 4.8 (images (a), (b), (c) and (d)) shows a very interesting distribution of gold particles on SiO<sub>2</sub> nanospheres support especially for **Au<sub>13</sub>** catalysts. The particles seem to clump together in a “crown”-shaped building block while still remaining finely dispersed. This presumably explains why particles are more mobile on alumina rather than silica nanospheres. In order to investigate this phenomenon we examined the **Au<sub>13</sub>** on SiO<sub>2</sub> nanospheres both uncalcined (Figure 4.9) and calcined at 300 °C (Figure 4.10) under high resolution TEM.

The high resolution TEM images for uncalcined **Au<sub>13</sub>** catalysts supported on SiO<sub>2</sub> nanospheres shows that the particles assemble in a layered, “crown”-shaped manner at the edge of the support surfaces. This formation is maintained even after calcination at 300 °C, but the particle size increases. Average particle size of 2.2 nm (histogram in Figure 4.9) for the uncalcined catalysts increase by *ca.* 80% to 12.5 nm (histogram in Figure 4.10).

Many self-assembled gold nanoparticles have been reported involving ligands act as linker or temperature treatment or solvent evaporation as well as non-covalent

interactions<sup>26-29</sup>. In our case, the driving force for this unique self-assembly of nanoparticles is still an open area to be discovered.



**Figure 4.9:** High resolution TEM images of  $\text{Au}_{13}$  clusters catalyst deposited on  $\text{SiO}_2$  nanospheres *via* TBHP method uncalcined and histogram of particles size distribution

---

We believe that there is some kind of self-assembly processes occurring especially for catalysts supported on SiO<sub>2</sub> nanospheres which we cannot fully explain. The differences in SiO<sub>2</sub> nanospheres being uniformly shaped as compared to Al<sub>2</sub>O<sub>3</sub> and in addition, charge on silica particles created during deposition process by TBHP might influence this organization to happen. In regards to **Au<sub>9</sub>** catalysts prepared under the same condition as **Au<sub>13</sub>**, the process of self-assemble seems to occur but was much slower compared to **Au<sub>13</sub>** system.

As can be seen in Figure **4.8** (a), uncalcined **Au<sub>9</sub>** on SiO<sub>2</sub> catalyst showed relatively dispersed nanoparticles on the support with some part of it showing the “crown”-shaped organization beginning to build. When this sample calcined at 300 °C Figure **4.8** (b), not only the particle size increase but the assembly became more obvious. We did not observe this phenomenon when catalysts were produced *via* wet impregnation method (Chapter **3**). Further detailed study is necessary to determine the cause of this self-organisation which may assist the design of synthesis of self-assembled gold nano particles.

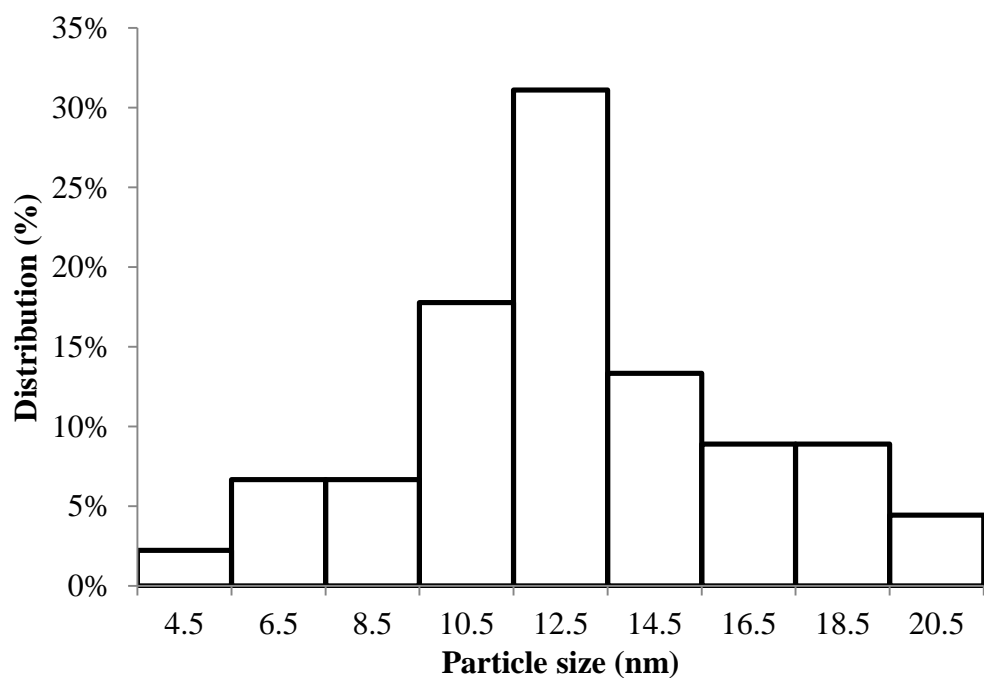
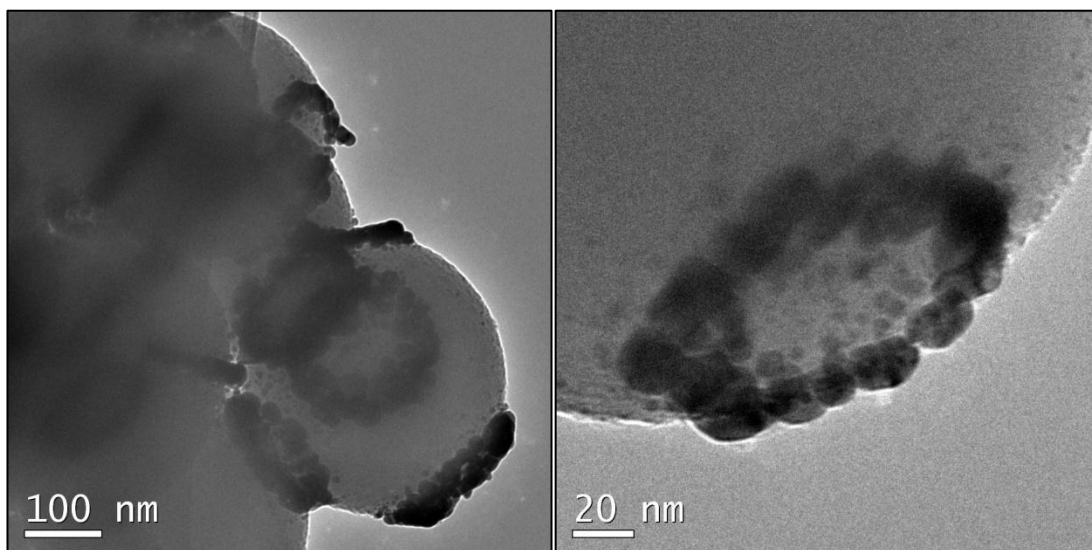


**Figure 4.10:** High resolution TEM images of Au<sub>13</sub> clusters catalyst deposited on SiO<sub>2</sub> nanospheres *via* TBHP method calcined at 300°C and histogram of particles size distribution

---

#### 4.4 Conclusion

In conclusion, TBHP deposition-precipitation method is very promising in producing finely dispersed and relatively small gold nanoparticulate catalysts. The most widely applicable discovery of this work has been the development of a new chemical treatment method for ligands removal at low temperature (95 °C) and a one-step procedure to produce active gold catalysts. This method may prove to be viable for the activation of a range of ligand-stabilised clusters catalysts that are able to minimise gold particles agglomeration. However, further detailed investigation should be carried out in order to study the particle-support interactions between clusters and SiO<sub>2</sub> nanospheres *via* this method that presumably promotes self-assembly nanoparticles as observed by high resolution TEM. The catalytic activities of catalysts prepared are extensively discussed in Chapter 5 of this thesis.

#### 4.5 References

1. M. Haruta, T. Kobayashi, H. Sano and N. Yamada, *Chemistry Letters*, 1987, 405-408.
2. R. Zanella, S. Giorgio, C.-H. Shin, C. R. Henry and C. Louis, *Journal of Catalysis*, 2004, **222**, 357-367.
3. W. Yan, S. M. Mahurin, B. Chen, S. H. Overbury and S. Dai, *The Journal of Physical Chemistry B*, 2005, **109**, 15489-15496.
4. G. Schmid and B. Corain, *Eur. Journal of Inorganic Chemistry*, 2003, 3081-3098.
5. M. Comotti, P. C. Della, R. Matarrese and M. Rossi, *Angewandte Chemie, International Edition*, 2004, **43**, 5812-5815.
6. C.-H. Tu, A.-Q. Wang, M.-Y. Zheng, X.-D. Wang and T. Zhang, *Applied Catalysis A: General*, 2006, **297**, 40-47.
7. S. H. Overbury, V. Schwartz, D. R. Mullins, W. Yan and S. Dai, *Journal of Catalysis*, 2006, **241**, 56-65.

- 
8. J. T. Miller, A. J. Kropf, Y. Zha, J. R. Regalbuto, L. Delannoy, C. Louis, E. Bus and J. A. van Bokhoven, *Journal of Catalysis*, 2006, **240**, 222-234.
  9. M. Haruta, JP2007197591A, 2007.
  10. N. S. Patil, B. S. Uphade, P. Jana, S. K. Bharagava and V. R. Choudhary, *Journal of Catalysis*, 2004, **223**, 236-239.
  11. N. S. Patil, B. S. Uphade, P. Jana, R. S. Sonawane, S. K. Bhargava and V. R. Choudhary, *Catalysis Letters*, 2004, **94**, 89-93.
  12. K. Qian, J. Fang, W. Huang, B. He, Z. Jiang, Y. Ma and S. Wei, *Journal of Molecular Catalysis A: Chemical*, 2010, **320**, 97-105.
  13. P. Buffat and J. P. Borel, *Physical Review A*, 1976, **13**, 2287-2298.
  14. P. Haider, B. Kimmerle, F. Krumeich, W. Kleist, J.-D. Grunwaldt and A. Baiker, *Catalysis Letters*, 2008, **125**, 169-176.
  15. A. B. Laursen, K. T. Højholt, L. F. Lundegaard, S. B. Simonsen, S. Helveg, F. Schüth, M. Paul, J.-D. Grunwaldt, S. Kegnæs, C. H. Christensen and K. Egeblad, *Angewandte Chemie International Edition*, 2010, **49**, 3504-3507.
  16. K. T. Højholt, A. B. Laursen, S. Kegnæs and C. H. Christensen, *Topics in Catalysis*, 2011, **54**, 1026-1033.
  17. E. Castillejos, E. Gallegos-Suarez, B. Bachiller-Baeza, R. Bacsá, P. Serp, A. Guerrero-Ruiz and I. Rodríguez-Ramos, *Catalysis Communications*, 2012, **22**, 79-82.
  18. T. Castro, R. Reifengerger, E. Choi and R. P. Andres, *Physical Review B*, 1990, **42**, 8548-8556.
  19. M. S. Kwon, N. Kim, C. M. Park, J. S. Lee, K. Y. Kang and J. Park, *Organic Letters*, 2005, **7**, 1077-1079.
  20. J.-F. Chen, Y.-H. Wang, F. Guo, X.-M. Wang and C. Zheng, *Industrial & Engineering Chemistry Research*, 2000, **39**, 948-954.
  21. P. K. Sharma, M. H. Jilavi, D. Burgard, R. Nass and H. Schmidt, *Journal of the American Ceramic Society*, 1998, **81**, 2732-2734.
  22. M. G. Gee, *Wear*, 1992, **153**, 201-227.
  23. L. D. Menard, F. Xu, R. G. Nuzzo and J. C. Yang, *Journal of Catalysis*, 2006, **243**, 64-73.
  24. G. Shafai, S. Hong, M. Bertino and T. S. Rahman, *Journal of Physical Chemistry C*, 2009, **113**, 12072-12078.

- 
25. Y. Shichibu, K. Suzuki and K. Konishi, *Nanoscale*, 2012, **4**, 4125-4129.
  26. S. Liu, T. Zhu, R. Hu and Z. Liu, *Physical Chemistry Chemical Physics*, 2002, **4**, 6059-6062.
  27. F. Caruso, M. Spasova, V. Salgueiriño-Maceira and L. M. Liz-Marzán, *Advanced Materials*, 2001, **13**, 1090-1094.
  28. A. K. Boal, F. Ilhan, J. E. DeRouchey, T. Thurn-Albrecht, T. P. Russell and V. M. Rotello, *Nature*, 2000, **404**, 746-748.
  29. S. Lin, M. Li, E. Dujardin, C. Girard and S. Mann, *Advanced Materials*, 2005, **17**, 2553-2559.

---

## Chapter 5

### Catalysis – Oxidation of Benzyl Alcohol: Clusters Effect and Comparison of TBHP Deposition Precipitation vs. Wet Impregnation Method

#### 5.0 Abstract

Heterogeneous catalysts prepared *via* two different methods described in the previous chapters, utilising two different gold molecular clusters (**Au<sub>9</sub>** and **Au<sub>13</sub>**), were tested for catalytic performance for the oxidation of benzyl alcohol. The oxidation reaction has been investigated in the presence of *tert*-butylhydroperoxide as oxidant at 95 °C for 4 hours. Selective oxidation to benzaldehyde was observed for almost all catalysts. The appearance of benzoic acid and benzyl benzoate as by-products was sometimes detected especially for catalyst supported on Al<sub>2</sub>O<sub>3</sub> prepared by the wet impregnation (WI) method. Throughout this chapter, we will discuss the effect of particle size towards catalysis, the initial induction period observed for uncalcined catalysts prepared by the WI method, support effects, leaching of gold into the reaction solution and catalyst recyclability. Towards the end of this chapter, we give the best gold molecular clusters heterogeneous catalyst system for benzyl alcohol oxidation reaction based on our findings. Our new TBHP catalyst preparation method also will be discussed in detail regarding how it affects the catalytic reaction as compared to traditional WI methods.

---

## 5.1 Introduction

In Chapters 2-4 we have shown the detailed synthesis and characterizations of  $\text{Au}_9$  and  $\text{Au}_{13}$  molecular clusters on  $\text{SiO}_2$  nanospheres or  $\text{Al}_2\text{O}_3$  supports prepared *via* two different methods, namely wet impregnation (WI) and TBHP deposition precipitation (TBHP). A detailed investigation using TEM and EXAFS analysis confirmed that both methods produce significant differences in physical and chemical properties of the catalyst. The TBHP method was developed based on the observed of an induction period for the first 45 minutes of the catalytic reaction using uncalcined WI catalysts.

Benzaldehyde has been widely used in industrial processes especially in perfumery and fragrances<sup>1-3</sup> and as a precursor to other organic compounds ranging from pharmaceuticals<sup>4,5</sup> to plastic additives<sup>6</sup>. There are numerous ways to produce benzaldehyde such as the partial oxidation of benzyl alcohol<sup>7,8</sup>, alkali hydrolysis of benzyl chloride, carbonylation of benzene<sup>9</sup> and liquid phase chlorination and oxidation of toluene<sup>10</sup>. However, long reaction times and mixture of by-products cause problems in all other routes.

The most economical way of producing benzaldehyde is from oxidation of benzyl alcohol<sup>11</sup>. This requires mild reaction conditions such as temperature and pressure. Generally, benzyl alcohol is used as the solvent due to its polarity, low toxicity and low vapour pressure but with the presence of an oxidant it can break down and create aldehydes that are more useful in many important chemical processes. Throughout the years, many researchers had developed catalysts that can be used to enhance the benzyl alcohol oxidation process by improving the selectivity

---

towards benzaldehyde formation<sup>12</sup>. Prior to that, homogeneous catalysts were used such as Schiff-base or salen catalysts<sup>13</sup>, ionic liquids<sup>14,15</sup> and various other metal complexes<sup>16, 17</sup>. However, there are many drawbacks in using homogenous catalysts as discussed in Chapter 1, especially in separating the catalyst from end products. Therefore, the use of hybrid supported catalysts<sup>18</sup> that has advantage of homogeneous and heterogeneous catalyst as well as precious metal heterogeneous catalysts such as Pt<sup>19</sup>, Pd<sup>20</sup> and Au<sup>21</sup> together with bimetallic cluster catalysts<sup>12, 20, 22, 23</sup> have attracted much attention in order to produce a high performance, recyclable, robust yet economical catalyst system.

Gold, as first discovered by Haruta, can be very reactive in catalytic reactions, especially CO oxidation when dispersed in a fine size and not in the bulk<sup>24</sup>. By definition, the gold nanoparticles regime is in the range 1 nm to 1  $\mu$ m. Small gold clusters are usually considered as large molecules while large clusters, are defined as monodisperse nanoparticles<sup>25, 26</sup>. The rapid growth in nanoscience has led to important developments in physical and chemical technologies by offering advanced tools for arranging atoms in specific molecular and supramolecular structures. Gold catalysis has attracted much attention especially for tailoring solid nanostructured surfaces that show unsuspected catalytic properties. Supported gold catalysts shows a great improvement in selectivity and stability and therefore represent a second generation of catalysts for alcohol oxidation, thus becoming viable substitutes for platinum group metals<sup>27-29</sup>.

The growing attention on catalytic activity of gold supported catalyst covers a few main parameters. Besides the effect of particles size, catalyst preparation method

---

and nature of the support is also reported to influence the catalytic performance<sup>30</sup>. Optimization has been made by many researchers in developing the best method of producing gold nanoparticle catalysts. The traditional well-known methods such as incipient wetness impregnation, co-precipitation and deposition precipitation while reported to be successful in producing highly effective gold nanoparticle catalysts, certain drawbacks still need to be overcome such as their agglomeration and mono-dispersed particles<sup>31-34</sup>. The temperature treatment (calcination) involved in the catalyst preparation is indeed the crucial part where it decides the particle size of the particle, support interaction as well as surface nature of the catalysts. All of these factors are important in determining the activity of a catalyst towards reaction selectivity of producing only the desired product. It is known that gold supported catalysts show excellent performance in gas phase oxidations<sup>12</sup> however, their potential in liquid phase catalytic oxidation reactions has also been reported<sup>18, 35-37</sup>. The main parameters that have to be carefully chosen in the liquid phase system are solvents and oxidants. Both factors can either enhance the catalytic performance of the catalyst or disturb the catalytic mechanism.

In this research, we developed a new deposition-precipitation method in synthesizing gold nanoparticles using TBHP. We can control two main factors in producing the nanoparticles, namely their size and distribution by using gold clusters as nanoparticle precursors and chemical modification at low temperature (95°C). A comparison with wet impregnation prepared catalysts was carried out with the aim of highlighting the advantages of our new preparation method.

---

## 5.2 Experimental

Catalytic activity was studied for the oxidation of benzyl alcohol using *tert*-butylhydroperoxide (TBHP) in decane as oxidant. Dodecane was added as a gas chromatography GC internal standard. Reactions were carried out in a Mettler Toledo batch reactor at 95°C with continuous stirring for up to 24 hours. Samples were taken every 15 minutes for the first hour followed by once every hour thereafter, being injected in Perkin Elmer Clarus 500 Gas Chromatograph (Figure 5.1) to determine the percentage of substrate conversion, product selectivity and yield. Calibration curves for each substrate and possible products were first plotted to determine the catalytic performance of each catalyst.

### 5.2.1 Oxidation of Benzyl Alcohol

In a typical catalytic reaction, 0.20 g of catalyst was introduced into the reactor containing benzyl alcohol (5.4 ml, 52 mmol) and *tert*-butyl hydroperoxide (11.4 ml, 10 mmol) 5.0-6.0 M solution in decane as the oxidant. The catalytic reaction was followed for 4-24 hours at 95°C. Scheme 5.1 illustrates oxidation reaction that took place.





**Figure 5.1:** Perkin Elmer Clarus 500 GC with WCOT fused silica 60m × 0.25mm internal diameter (CP7818) column. Temperature program: starting at 80°C for 5 minutes then ramping at 10°C/min to 250°C for 8 minutes.

GC operates like a highly accurate oven with a separation column that can be set with a certain temperature program to accelerate the rate at which compounds passing through the column. The flow rate of the carrier gas is adjusted in order to get a better separation of compounds analysed. Every compound takes a different time to pass through the column that is known as retention time,  $r_t$ . Therefore, the output of GC chromatogram will be the retention time vs. the ionization current that given as a series of peaks with peak area proportional to the amount of compound present.

Figure 5.2 showed calibration curves of benzyl alcohol, dodecane, benzaldehyde, benzoic acid and benzyl benzoate that have been plotted as concentration vs. peak area gained from GC chromatogram. The calibration was done first by injecting pure standard samples of expected compound into GC to assign the individual retention time. In principal, equal quantity of pure compounds injected

should give the same peak size with equal peak area. However, some compounds have a better response in GC than others which is known as response factor,  $r_f$ . Therefore, to determine the response factor for each compound, mixtures of known quantities or ratios of each individual compound were injected into the GC and determined the peak area of the respective compounds was determined corresponding to the injected moles of each compound. Details of the calibration curve are given in Figure 5.2.

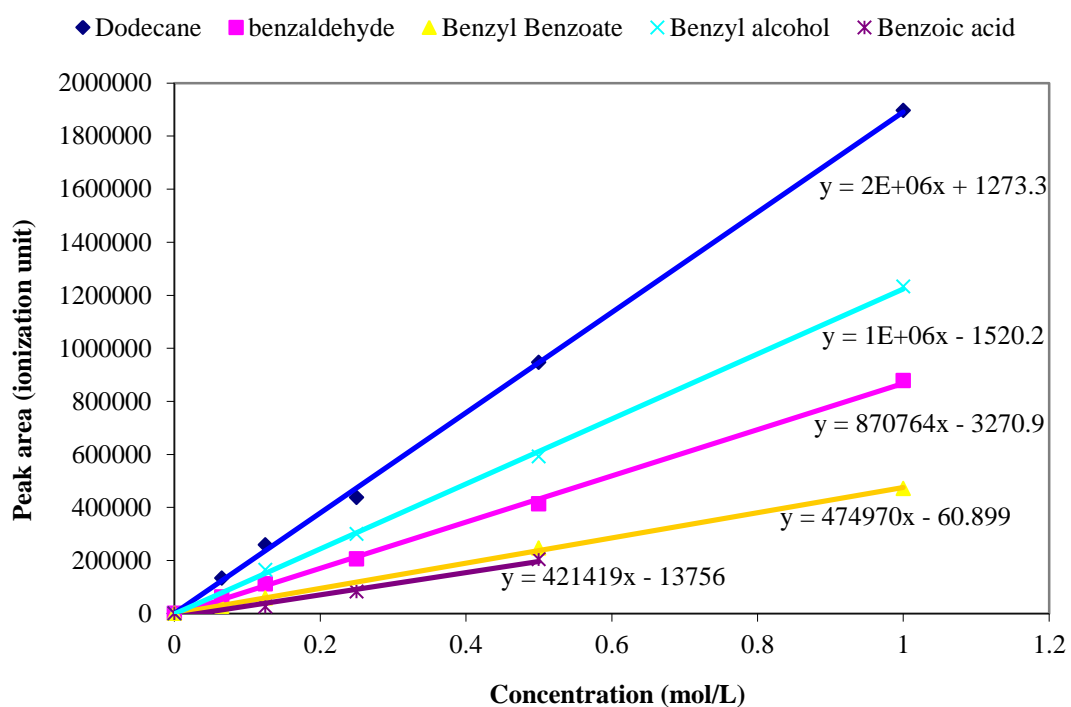


**Figure 5.2:** Calibration curves of substrate, internal standard and expected products in oxidation of benzyl alcohol

The relative quantity of each compound in a sample mixture was then determined by injecting a series of different concentrations of each compound. The peak area that corresponds to the compound of interest was normalised with respect to a known quantity of internal standard that does not vary throughout the reaction.

---

Plots of concentration *vs.* normalised peak area were then used in qualitative analysis of catalytic performance. The calculation formula to determine gold loading (mmol/g), % conversion of benzyl alcohol, % selectivity of product, initial rate of reaction, turnover number (TON) and turnover frequency (TOF) are listed in Appendix A. In the absence of catalyst or when using the support in the absence of gold no oxidation was observed, confirming that the presence of gold was essential for catalytic oxidation.

## 5.3 Results and Discussions

### 5.3.1 Gold Loading Optimization

Our first consideration in order to investigate catalytic performances was the amount of gold needed in the heterogeneous catalyst system. **Au<sub>9</sub>** on SiO<sub>2</sub> nanospheres prepared by WI method was the first system synthesized therefore various gold loadings were introduced. We started with 0.1wt. % Au followed by 1.0 wt. % Au and finally 4.0 wt. % Au. Such percentages were chosen based on studies reported in various literature studies, suggested to be sufficient amounts for catalysis using active gold nanoparticle catalysts<sup>11, 36, 39-43</sup>. However, the actual amount present in the support was determined using atomic absorption spectroscopy (AAS) as listed in Table 5.1. Actual gold loading as determined from AAS showed that not all the gold that we started with was deposited onto the support. The estimated values were found to be well within the error limits.

**Table 5.1:** Calculated and actual gold loading of **Au<sub>9</sub>** clusters on SiO<sub>2</sub> nanospheres prepared by wet impregnation method.

Expected (wt. %)	Calculated (mmol/g) $\times 10^{-3}$	<sup>a</sup> Actual (mmol/g) $\times 10^{-4}$		
		Uncalcined	Calcined at 300 °C	Calcined at 500 °C
0.1	0.001	0.002	0.002	0.002
1.0	0.133	0.202	0.202	0.201
4.0	2.124	4.026	4.020	4.019

<sup>a</sup>Determined from AAS analysis for 0.20 g catalyst used for the catalytic reaction.

Figure 5.3 illustrates the comparison of % conversion of benzyl alcohol achieved between nine **Au<sub>9</sub>** on SiO<sub>2</sub> WI prepared catalysts. 4.0 wt % catalyst calcined at 300 °C and 500 °C gives the highest conversion compared to 1.0 wt % and 0.1 wt. % catalyst. However, 4.0 wt % uncalcined catalyst achieved the lowest conversion of all presumably since the gold active sites are still covered with ligands. In all cases (uncalcined and calcined catalysts) 0.1 wt. % did not promote high benzyl alcohol conversion (not more than 50%). For 1.0 wt. % gold loaded catalysts, it seems that the calcinations temperature does not affect the catalytic activity as the conversion remains between 50-55%.

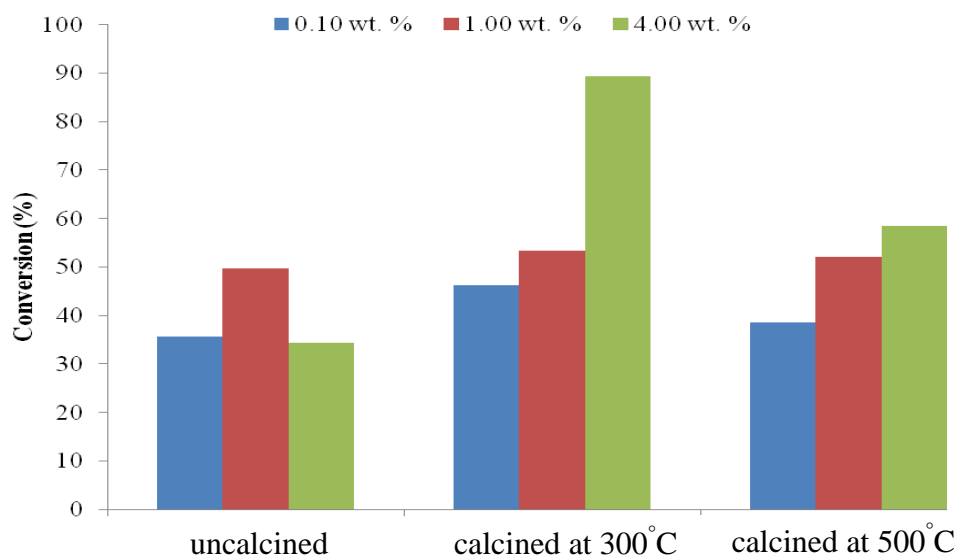


**Figure 5.3:** Comparison of % conversion of benzyl alcohol using **Au<sub>9</sub>** catalysts on SiO<sub>2</sub> prepared by wet impregnation method with different gold loading calcined at different temperature.

Catalysts that were calcined at 500°C gave lower conversion as compared to those calcined at 300°C. This is mainly due to agglomeration. The degree of aggregation can be controlled not only by introducing a bottom-up approach using gold molecular clusters but also by careful choice of calcination temperature<sup>44</sup>. This aspect will be discussed further later in this chapter (section 5.3.2). The highest % conversion of benzyl alcohol achieved was when using 4.0 wt % **Au<sub>9</sub>** on SiO<sub>2</sub> calcined at 300°C, agrees well with our hypothesis. The calcination temperature (300°C) was ideal as it lead to the full removal of all the protecting phosphine ligands (as discussed in Chapter 3, proven with TGA-DSC analysis) and yet minimised the particles aggregation. Hence, the 4.0 wt. % gold loading percentage offers more gold active sites for catalytic reaction. The increase in catalytic activity with gold content within the range of gold loadings reported in a few other

---

studies<sup>11,36</sup>. Milone *et. al.*, showed that the increase of the specific activity with the gold loading is due to the enhancement of the reducibility of the catalyst involved in the oxidation of benzyl alcohol<sup>45</sup>. Therefore, we demonstrate 4.0 wt % of Au in all other catalysts investigated in this research.

### 5.3.2 Catalyst Activation and Particle Size Effect

The idea behind our research is to control the size of gold nanoparticles formation from bottom-up approach as well as during catalyst activation. While this work was in progress, Tsukuda group in Japan reported studies on **Au<sub>11</sub>** clusters supported on mesoporous silica SBA-15<sup>44</sup> as well as **Au<sub>25</sub>** clusters immobilized on hydroxyapatite<sup>46</sup> and various other Au cluster system with different protecting ligands<sup>47,48</sup> for a bottom-up approach towards synthesizing controlled size of gold nanoparticulate catalysts. **Au<sub>9</sub>** and **Au<sub>13</sub>** were chosen in our research as a continuation to our investigation before with **Au<sub>6</sub>** phosphine-stabilized clusters system<sup>49</sup>. Furthermore, **Au<sub>9</sub>** and **Au<sub>13</sub>** are precursors to larger clusters<sup>50-53</sup> or the smallest core structure exists in larger Au clusters compound<sup>54-60</sup>.

In Chapter 3 and 4 we discussed the detailed characterization of catalysts prepared by WI and TBHP methods. Table 5.2 summarises the average particle sizes observed under TEM. As can be seen, WI catalysts calcined at 500 °C lead to the nanoparticles becoming bigger ranging from 20-80 nm. This explained the lower % conversion of benzyl alcohol as reported earlier in Figure 5.1. A study by Liu *et. al.* is in agreement with our findings that the catalytic activity for benzyl alcohol oxidation decreased monotonically with the increase in nanoparticle size<sup>44</sup>.

**Table 5.2:** Average particle sizes of **Au<sub>9</sub>** and **Au<sub>13</sub>** clusters on Al<sub>2</sub>O<sub>3</sub> and SiO<sub>2</sub> nanospheres catalysts prepared by wet impregnation and TBHP method determined using TEM analysis

Samples	Mean Particle size (nm)	Wet Impregnation		TBHP	
		SiO <sub>2</sub>	Al <sub>2</sub> O <sub>3</sub>	SiO <sub>2</sub>	Al <sub>2</sub> O <sub>3</sub>
Uncalcined	<b>Au<sub>9</sub></b>	-	-	3	6
	<b>Au<sub>13</sub></b>	-	-	3	4
Calcined at 300°C	<b>Au<sub>9</sub></b>	51	8	9	11
	<b>Au<sub>13</sub></b>	15	17	13	20
Calcined at 500°C	<b>Au<sub>9</sub></b>	78	20	-	-
	<b>Au<sub>13</sub></b>	19	25	-	-

**Au<sub>9</sub>** and **Au<sub>13</sub>** molecular clusters that we used as a precursor towards naked gold nanoparticles reported to be around 5.5-6 Å in size<sup>61, 62</sup>. Therefore, uncalcined catalysts prepared by WI method cannot be observed under TEM as the particles are too small for detection. Activation of catalyst *via* calcinations at 300°C or 500°C especially in WI method helps aids the stripping off the ligand spheres leaving only naked gold nanoparticles. However, with TBHP method, the ligands are being oxidised to become phosphine oxide, which then dissociate from the clusters resulting in naked gold nanoparticles<sup>49</sup> similar to what we achieved by calcination. In comparison, low temperature (95°C; uncalcined) catalyst activation by the TBHP method produces smaller nanoparticles (in the range of 2-20 nm) compared to 8-50 nm through WI method (calcined at 300°C). It has been reported by M. Turner *et. al.* that larger gold nanoparticles were obtained by an incipient wetness impregnation method<sup>63</sup>. Heat treatment is known to be associated with the growth of particles size and have been reported previously<sup>64</sup>. The diameter of gold particles is tuneable by

---

choosing the calcinations temperature for the gold catalysts according to theoretical calculations and experimental results<sup>65, 66</sup>.

Comparing between **Au<sub>9</sub>** and **Au<sub>13</sub>** catalysts system, we noticed that in most cases **Au<sub>13</sub>** catalysts produced smaller particles than **Au<sub>9</sub>** catalysts. The icosahedral geometry of **Au<sub>13</sub>** clusters may be responsible for this as structure rearrangement is less likely to occur hence avoiding cluster to enlargement<sup>60</sup>. Various reports have shown that gold clusters smaller than 2 nm can oxidize various alcohols using O<sub>2</sub> in air<sup>67-71</sup>. One rational approach to gold oxidation catalysts is to utilize the potential ability of small clusters to activate O<sub>2</sub><sup>72</sup>. However, there are reports showing that gold nanoparticles in the size range of 2-30 nm can be catalytically active towards various oxidations including benzyl alcohol oxidation<sup>73-76</sup> using different sources of oxygen as oxidant. Nonetheless, it is generally accepted that the best catalytic performance is exhibited by the smaller particles (between ~1-10 nm)<sup>36, 77</sup>. Boronat *et. al.* investigated this effect using DFT method and experimental procedure concluding that as the particle size decreases, the number of coordinated atoms that are considered to be active sites in alcohol oxidation to aldehydes increases<sup>75</sup>. Nevertheless, with the TBHP method that we developed, highly uniform (refer to TEM results and discussions in Chapter 3) and relatively small gold nanoparticles (<20 nm) can be achieved.

### 5.3.3 Catalytic Performances : % Conversion of Benzyl Alcohol

We have demonstrated that a 4.0 wt % gold loading activated at lower temperature (300°C for WI method and 95°C for TBHP method) gives smaller gold nanoparticles and good catalytic activity for oxidation of benzyl alcohol. The

---

comparison between the WI and TBHP methods was further investigated in the form of % conversion of benzyl alcohol. Figure 5.4 compares the % conversion achieved using uncalcined catalysts prepared by WI and TBHP methods. Earlier in Figure 5.3 we illustrated that uncalcined catalyst by WI method gives the lowest % conversion comparing with other calcined catalysts. This was again seen in all cases regardless of whether **Au<sub>9</sub>** or **Au<sub>13</sub>** clusters on SiO<sub>2</sub> or Al<sub>2</sub>O<sub>3</sub> supports, the % benzyl alcohol conversion achieved being lower than that from the TBHP method. The highest % conversion (*ca.* 70%) for WI method uncalcined catalyst was accomplished by **Au<sub>9</sub>** on Al<sub>2</sub>O<sub>3</sub> support (Figure 5.4 (c)).

Our bottom-up approach utilising phosphine-stabilized clusters as precursors to size-controlled gold nanoparticles necessarily means that prior to calcination the organic ligands still attached to the gold clusters acting as a capping agent. This will limit the exposure of gold active sites necessary for catalysis. The capping agents may induce diffusion limitations by hindering the approach to the active site due to the formation of stagnant structure, may compete with the reactant for the adsorption on the active site or even both<sup>78</sup>. This explains recent findings that we obtained with WI catalysts. However, the same situation does not occur when using uncalcined TBHP catalysts. After 4 hours of reaction, the % benzyl alcohol conversion was almost 60% for all four uncalcined catalysts. We observed also that reaction begins as early as 15 minutes after reagent addition giving *ca.* 30% conversion for **Au<sub>9</sub>** on SiO<sub>2</sub> and Al<sub>2</sub>O<sub>3</sub> catalysts, while **Au<sub>13</sub>** on SiO<sub>2</sub> and Al<sub>2</sub>O<sub>3</sub> gave *ca.* 90% conversion. Thus it appears that the TBHP prepared catalyst was readily activated without the

need for calcination and supporting our preliminary report<sup>49</sup>. Indeed, this initial finding leads us to developing the TBHP method initially.

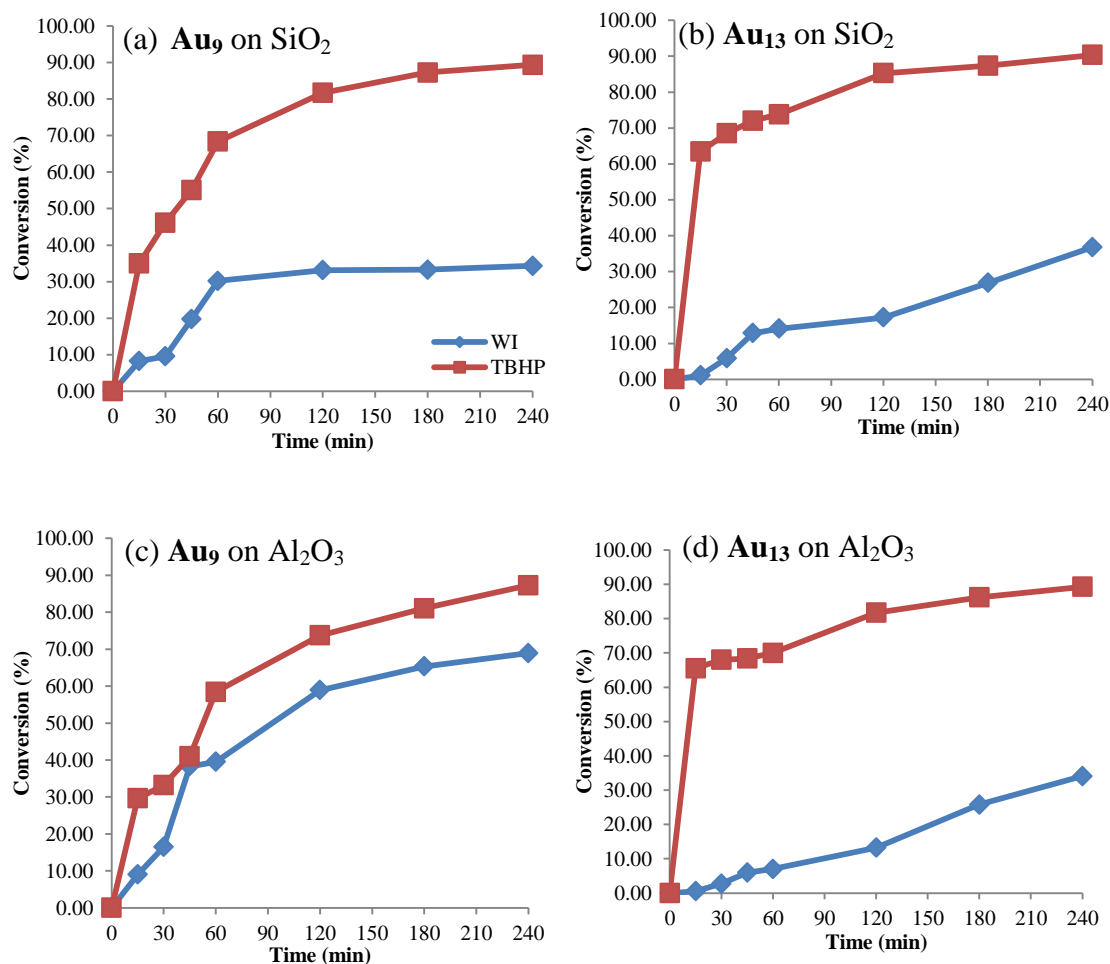


**Figure 5.4:** Kinetic comparison between uncalcined catalysts prepared using wet impregnation (WI) method and TBHP method over 4 hours of catalysis reaction. Experiment was done in 3 replicates and the average values were plotted.

From the Figure 5.4, the catalytic conditions and initial rate of reactions have been estimated (Table 5.3) for all catalysts. The induction stage was observed for all WI prepared catalysts (Figure 5.4) being up to 45 minutes for Au<sub>13</sub> catalysts. The

initial rate was calculated only on the % conversion of benzyl alcohol consumed over the actual gold loading (TON) for the first 15 minutes of reaction.

Table 5.3 clearly suggests that the catalytic reaction takes place immediately for all uncalcined TBHP prepared catalysts used compared to WI catalysts. The highest rate of reaction obtained for uncalcined catalyst was **Au<sub>9</sub>** on SiO<sub>2</sub> TBHP prepared catalysts which was  $49.5 \times 10^2 \text{ min}^{-1}$  compared to only  $18.7 \times 10^2 \text{ min}^{-1}$  for the same catalyst prepared *via* the WI method.

**Table 5.3:** Initial rates of reaction for WI and TBHP prepared catalysts on SiO<sub>2</sub> nanospheres support. Initial rate determined by  $(\text{TON}_{t_1} - \text{TON}_{t_0}) / (15 \text{ min})$   $t_1=30$  and  $t_0=15$ . <sup>a</sup>Taken at  $t_1=60$  and  $t_0=45$

Support	Condition	Catalyst	Initial rate ( $\text{min}^{-1}$ ) $\times 10^2$	
			WI	TBHP
SiO <sub>2</sub>	Uncalcined	<b>Au<sub>9</sub></b>	18.7 <sup>a</sup>	49.5
		<b>Au<sub>13</sub></b>	5.8 <sup>a</sup>	13.8
	Calcined at 300 <sup>o</sup> C	<b>Au<sub>9</sub></b>	13.1	73.7
		<b>Au<sub>13</sub></b>	2.5	43.2
	Uncalcined	<b>Au<sub>9</sub></b>	5.4 <sup>a</sup>	18.0
		<b>Au<sub>13</sub></b>	3.8 <sup>a</sup>	8.8
Al <sub>2</sub> O <sub>3</sub>	Calcined at 300 <sup>o</sup> C	<b>Au<sub>9</sub></b>	16.9	48.8
		<b>Au<sub>13</sub></b>	15.7	27.1

TBHP was used as the oxidant. These results suggest that for uncalcined WI catalysts, TBHP was largely responsible for activating the catalysts during the initial 45 minutes. This induction period is obvious for uncalcined **Au<sub>13</sub>** catalysts compared

---

to **Au<sub>9</sub>**. According to the previous computational results with the **Au<sub>6</sub>** system<sup>49, 79</sup> we predict that structural rearrangement also occurs for **Au<sub>9</sub>** and **Au<sub>13</sub>** clusters catalysts. Being more rigid in structural geometry (icosahedron), for **Au<sub>13</sub>** catalysts the ‘*in-situ*’ activation by TBHP during the oxidation reaction is somewhat slower than for **Au<sub>9</sub>**. Supported by TGA-DSC data (Chapter 3), all the ligands for **Au<sub>13</sub>** were removed simultaneously, rather than sequentially as seen for **Au<sub>9</sub>**. Therefore, the gold active sites of **Au<sub>9</sub>** clusters catalysts exposed slightly earlier than **Au<sub>13</sub>** explaining the higher conversion achieved even during the induction period (Figure 5.4). These observations confirmed that TBHP can be used to chemically transform gold clusters into nanoparticles without high temperature treatment.

In order to confirm and support the results found with the uncalcined catalyst regarding induction period, we also did the investigation of the catalytic performance in term of % benzyl alcohol conversion attained by catalysts calcined at 300 °C. The initial rate of reaction was listed in Table 5.3 while the % conversion vs. time was plotted in Figure 5.5. Observed that there were no delays in converting the benzyl alcohol therefore all initial rate of reaction were calculated for the 0-15 minutes.

The absence of an induction period for WI prepared catalysts was due to calcination. The initial rates of reaction for catalysts calcined at 300 °C *via* the TBHP method were still higher as compared to the same catalyst prepared *via* the WI method. This is possibly related to the smaller particle size for TBHP compared to WI catalysts as discussed in Section 5.3.2. The particle size effects the % conversion of benzyl alcohol; the 300 °C calcined catalysts were slightly lower (*ca.* 80%) than

uncalcined (*ca.* 90%). It was established that the catalytic reaction kinetics was determined not only by catalyst activation step but also the particles size.

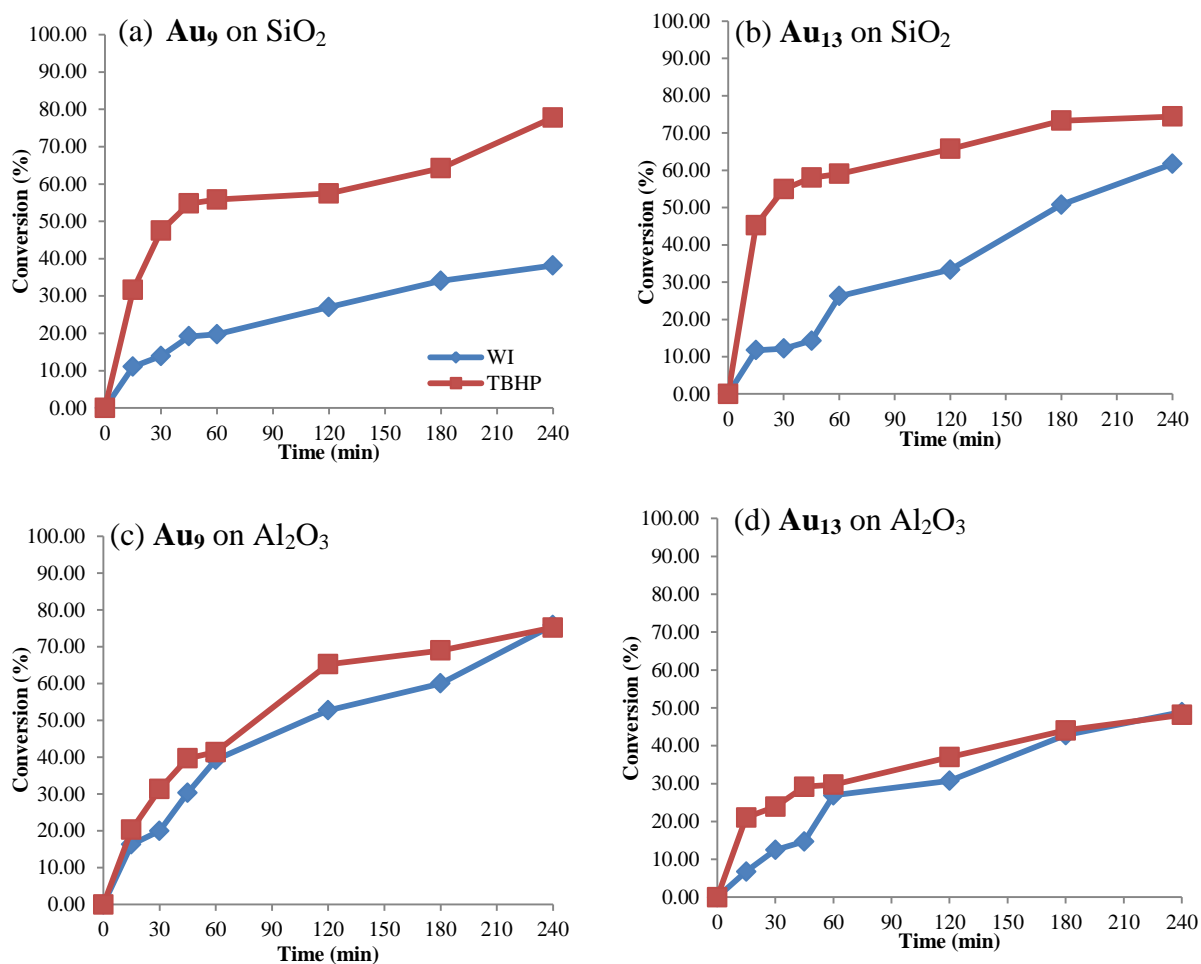


**Figure 5.5:** Kinetic comparison between calcined at 300°C catalysts prepared using wet impregnation (WI) method and TBHP method over 4 hours of catalysis reaction. Experiment was done in 3 replicates and average values were plotted.

#### 5.3.4 Turnover Number (TON) and Turnover Frequency (TOF)

In catalysis, to measure the catalytic performance of catalysts instead of reporting the % conversion of the substrate, there are two important terms to be considered namely turnover number (TON) and turnover frequency (TOF). TON is

defined as the number of moles of substrate that a mole of catalyst can convert before becoming inactivated. Theoretically, an ideal catalyst would have an infinite TON in this sense because it would not ever be consumed but in actual practice one often sees TON which goes from 100 up to millions depending on how efficient the catalyst is. It is more precise to report turnover number in order to compare one catalyst which another especially involving different metal loading in heterogeneous catalyst. On the other hand, TOF is used to refer the turnover per unit time either in seconds, minutes or hours. TOF value gives an idea of the rate of substrate being converted into product for every mole of catalyst used.

**Table 5.4:** TON and TOF after 4 hours of catalytic oxidation benzyl alcohol reaction

Support	Condition	Catalyst	TON ( $\times 10^5$ )		TOF ( $\text{min}^{-1}$ )	
			WI	TBHP	WI	TBHP
SiO <sub>2</sub>	Uncalcined	Au <sub>9</sub>	1.75	5.17	730	2153
		Au <sub>13</sub>	1.69	5.04	703	2102
	Calcined at 300°C	Au <sub>9</sub>	2.64	5.45	1102	2269
		Au <sub>13</sub>	4.18	4.98	1743	2074
Al <sub>2</sub> O <sub>3</sub>	Uncalcined	Au <sub>9</sub>	3.55	5.09	1480	2121
		Au <sub>13</sub>	1.70	4.97	709	2072
	Calcined at 300°C	Au <sub>9</sub>	4.22	5.21	1760	2171
		Au <sub>13</sub>	3.35	3.34	1396	1392

Table 5.4 lists the TON and TOF of all catalysts tested for the oxidation of benzyl alcohol after 4 hours. Actual gold loadings were measured by AAS as listed in Appendix B. According to conversion vs. time plots in Figure 5.4 and 5.5,

---

catalysts that give high conversion in both methods are **Au<sub>13</sub>** on SiO<sub>2</sub> prepared by the uncalcined TBHP method (90.35%), **Au<sub>9</sub>** on SiO<sub>2</sub> uncalcined TBHP method (89.39%), **Au<sub>9</sub>** on Al<sub>2</sub>O<sub>3</sub> calcined at 300 °C by the WI method (75.85%) and **Au<sub>13</sub>** on SiO<sub>2</sub> calcined at 300 °C WI method (61.73%). The findings for WI catalysts are the same as those found with the % conversion, however, for TBHP method, two catalysts that gives high TON and TOF are **Au<sub>9</sub>** on SiO<sub>2</sub> calcined at 300 °C ( $5.45 \times 10^5$  and  $2269 \text{ min}^{-1}$ ) and **Au<sub>9</sub>** on Al<sub>2</sub>O<sub>3</sub> calcined at 300 °C ( $5.21 \times 10^5$  and  $2171 \text{ min}^{-1}$ ).

As we discussed in *Section 5.3.1* after calcination, there is a certain degree of gold loss. Even though the loss is not significant, calculating the TON and TOF, the 300 °C calcined TBHP catalyst gives higher values. This is because the % conversion is somewhat comparable with the uncalcined catalyst regardless of the decrease in gold content. This explains the situation occurring when the **Au<sub>9</sub>** on SiO<sub>2</sub> calcined at 300 °C and **Au<sub>9</sub>** on Al<sub>2</sub>O<sub>3</sub> calcined at 300 °C gave higher TON and TOF values as compared to **Au<sub>13</sub>** on SiO<sub>2</sub> uncalcined TBHP method, **Au<sub>9</sub>** on SiO<sub>2</sub> uncalcined TBHP method that initially gives higher % conversion. Nonetheless, comparing the two methods, it is confirmed that TBHP catalysts give higher TON and TOF values hence are more efficient than WI catalysts. These results support our previous finding regarding the catalyst activation, particle size effect and % conversion of benzyl alcohol.

### 5.3.5 Support and Selectivity Effect

In our work, we have used both SiO<sub>2</sub> and Al<sub>2</sub>O<sub>3</sub> supports. Although we did not investigate thoroughly the support interaction effect but a comparison of the two supports employed two different methods of preparing the catalysts can be made

according to the catalytic activity achieved. The gold particle size is controlled by a combined effect produced by the interactions between the gold particles themselves and gold-support interactions (which are expected to control the surface mobility of the gold particles); the lower the mobility of the gold particles, the larger the gold dispersion or smaller the gold particles on the surface. Other have found that the interaction of gold with oxide supports plays a vital role in determining the unique properties of supported gold nanoparticulate catalysts as well as the preparation method<sup>21, 36, 80-82</sup>.

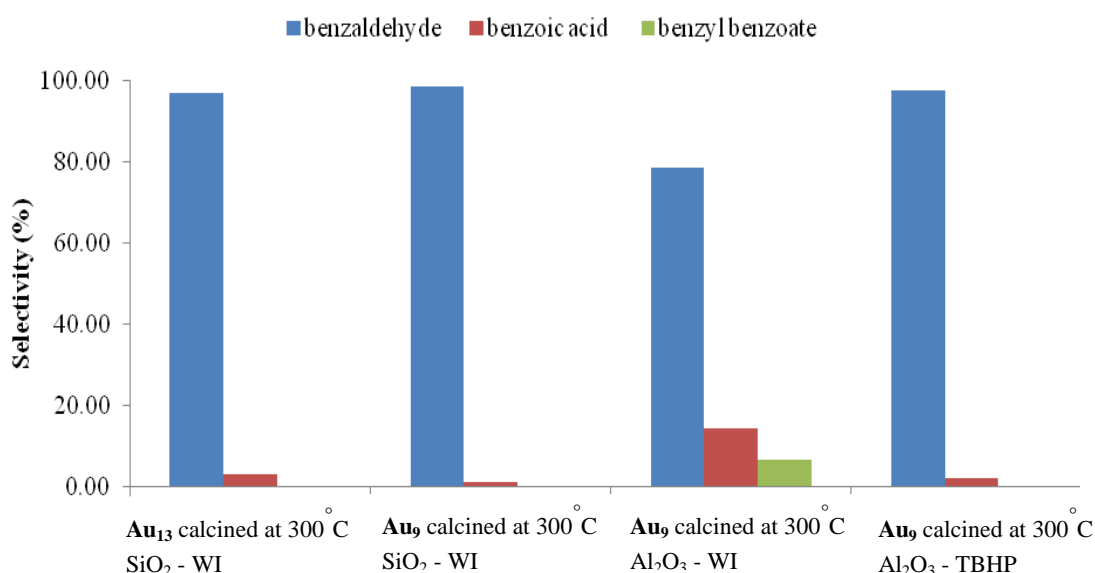


**Figure 5.6:** Product selectivity from oxidation of benzyl alcohol after 4 hours

Comparing between the SiO<sub>2</sub> nanospheres and Al<sub>2</sub>O<sub>3</sub> supports that we used, TBHP method prepared catalysts on SiO<sub>2</sub> produced smaller particle sizes while for WI method, catalysts on Al<sub>2</sub>O<sub>3</sub> gives smaller particles. Comparing the surface area (measured by BET surface area analysis) of SiO<sub>2</sub> nanospheres (149.9883 m<sup>2</sup>/g) and Al<sub>2</sub>O<sub>3</sub> (258.3253 m<sup>2</sup>/g), the latter support with WI method preparation agrees with what has been reported by Choudhary *et. al.*<sup>39</sup>. However, with TBHP method, the

---

lower mobility of gold particles produced from chemical modification at lower temperature promoted by TBHP resulting gold supported on SiO<sub>2</sub> nanospheres to be smaller in size compared to Al<sub>2</sub>O<sub>3</sub> supported catalysts. High temperature encourages gold mobility and aggregation (by calcinations especially in WI method preparation) to happened hence surface area becomes the limiting factor for gold particles to enlarge.

We relate the support effect with the product selectivity. Oxidation of benzyl alcohol will produce benzaldehydes as the main product but two other products are prone to be produced, which are benzoic acid and benzyl benzoate. Figure 5.6 showed the product selectivity of two best catalysts from WI and TBHP method. We always found that our catalysts gives high selectivity of benzaldehyde but in some cases especially catalyst supported on Al<sub>2</sub>O<sub>3</sub> prepared by WI method, also produced benzoic acid and sometimes benzyl benzoate as by-products. Benzyl benzoate appeared later in the reaction normally after 3 hours that is when enough benzaldehyde produced reacted with benzyl alcohol to form benzyl benzoate. Hence, we conclude that TBHP method produced not only high activity of catalysts but also selective towards producing benzaldehyde.

### 5.3.6 *Leaching and Recyclability*

Taking into considerations of all the findings discussed before, two most ideal catalyst systems were investigated further for their recyclability and leaching issues. Those catalysts are TBHP prepared **Au<sub>9</sub>** on SiO<sub>2</sub> nanospheres calcined at 300 °C and WI prepared **Au<sub>13</sub>** on SiO<sub>2</sub> nanospheres calcined at 300 °C. The average particles size of the first catalyst mentioned is 8.99 nm while the latter is 15.35 nm explaining the

slightly higher TON and TOF for the smaller particulate catalyst ( $5.45 \times 10^5$  and  $2269 \text{ min}^{-1}$  compared to  $4.98 \times 10^5$  and  $2074 \text{ min}^{-1}$ ). We observed that  $\text{Al}_2\text{O}_3$  supported gold catalyst gives higher particulate sizes and slightly lower benzaldehyde selectivity towards catalytic oxidation of benzyl alcohol. Hence, we did not pursue on investigating leaching and recyclability of any  $\text{Al}_2\text{O}_3$  supported gold nanoparticles catalyst.

**Table 5.5:** Leaching of gold and % conversion of benzyl alcohol after six times catalyst recycled

	<b>Au<sub>9</sub></b> on SiO <sub>2</sub> calcined at 300 °C – TBHP method	<b>Au<sub>13</sub></b> on SiO <sub>2</sub> calcined at 300 °C – WI method
Au loading <b>before</b> 1 <sup>st</sup> catalysis reaction (mmol/g)	$4.0198 \times 10^{-4}$	$4.0375 \times 10^{-4}$
Au loading <b>after</b> 1 <sup>st</sup> catalysis reaction (mmol/g)	$3.9697 \times 10^{-4}$	$3.9841 \times 10^{-4}$
	1 <sup>st</sup> used	61.73
	2 <sup>nd</sup> used	60.03
<b>% benzyl alcohol conversion (after 4hours)</b>	3 <sup>rd</sup> used	59.06
	4 <sup>th</sup> used	58.45
	5 <sup>th</sup> used	58.02
	6 <sup>th</sup> used	54.76

It is important for the heterogeneous catalyst system to stay intact on the support and that it does not leach into the reaction solution during catalysis in order to avoid disadvantages of homogeneous catalyst to encounter. Since the interaction between metal and support surface is not chemical interaction (does not involves chemical bonding), the particles are prone to leave the support surface and mix well in the reaction solution. To investigate this phenomenon, we employed two

---

techniques. The first technique was to measure the gold loading for the catalyst after being used in catalysis reaction and the second one was filtering the catalyst after 2 hours of catalysis reaction and to then let the reaction resume for another 24 hours while monitoring the % conversion of benzyl alcohol. Table 5.5 shows the differences in gold loading before and after catalysis reaction as determined by AAS spectroscopy.

Both catalysts system were started with 4.0 wt. % Au loading which were then determined by AAS to be  $4.0198 \times 10^{-4}$  mmol/g (**Au<sub>9</sub>** on SiO<sub>2</sub> calcined at 300°C – TBHP method) and  $4.0375 \times 10^{-4}$  mmol/g (**Au<sub>13</sub>** on SiO<sub>2</sub> calcined at 300°C – WI method). After 4 hours of reaction, the catalyst was recovered and dried before analysing the gold content again with AAS. It was confirmed that only about 2% of gold content were leached out during the catalytic reaction. This was a relatively high percentage compared to what has been reported by Hutchings *et. al.* utilising Au/SiO<sub>2</sub> catalyst prepared by coprecipitation procedure<sup>83</sup>. However, in order to support the spectroscopic evidence and prove that there was no significant decrease in catalytic reaction, we carried out the leaching experiment to get the experimental evidence.

Figure 5.7 shows the plot of % conversion vs. time with catalyst being filtered after 2 hours of reaction determined by GC analysis. In agreement with our AAS results, no significant leaching was observed as the % conversion does not increase with disappearance of catalyst used. After 120 minutes, the % conversion of benzyl alcohol obtained by **Au<sub>9</sub>** on SiO<sub>2</sub>, calcined at 300°C prepared by TBHP method, was in agreement with what we had achieved before. There was no major increase in

conversion observed even after 24 hours of reaction. Both catalysts (TBHP prepared  $\text{Au}_9$  on  $\text{SiO}_2$  nanospheres calcined at  $300^\circ\text{C}$  and WI prepared  $\text{Au}_{13}$  on  $\text{SiO}_2$  nanospheres calcined at  $300^\circ\text{C}$ ) displayed the same pattern indicating that either WI or TBHP method does not affect the physical interactions between gold and support. These also ensure that the catalytic activity was accomplished by heterogeneous gold nanoparticles embedded on support not homogeneously with free gold particles that leached out into the reaction solution.

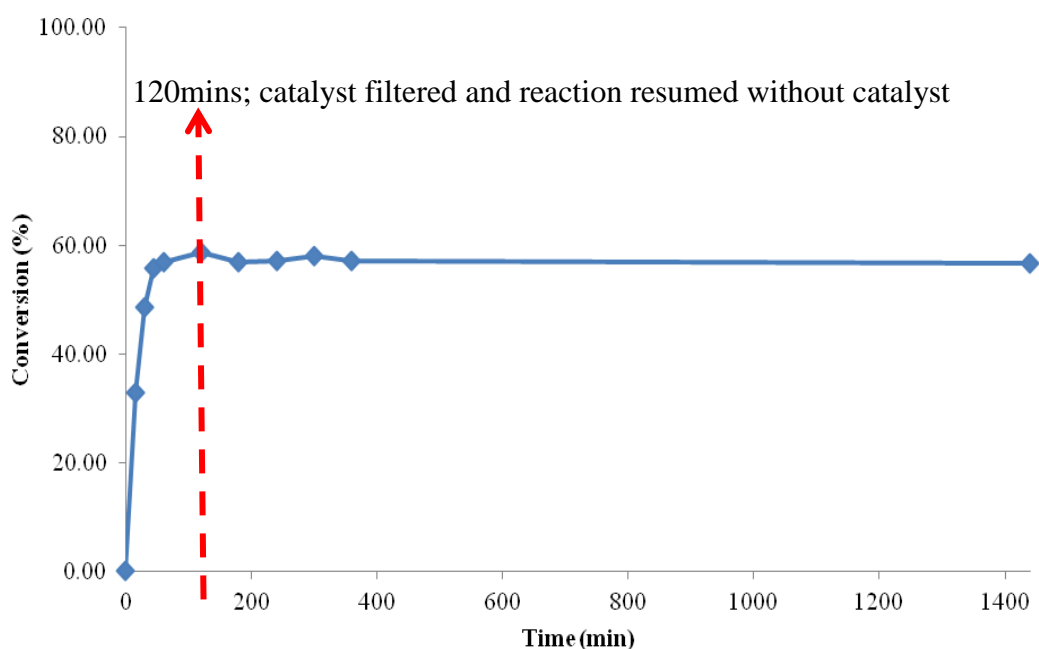


**Figure 5.7:** Leaching test, oxidation of benzyl alcohol for  $\text{Au}_9$  on  $\text{SiO}_2$  calcined at  $300^\circ\text{C}$  prepared by TBHP method

The catalysts were also tested for their recyclability. Both catalysts were recycled six times and the % conversion of benzyl alcohol was determined after 4 hours of reaction using GC (Table 5.5). Even in the sixth use, no large decrease in

---

catalytic activity was observed. Therefore, this showed that the <2% gold leached as observed was irrelevant due to the insignificant loss of the catalytic activity.

#### **5.4 Conclusion**

From the works discussed above, the following conclusions can be drawn:

1. Gold nanoparticles ranging from 1-20 nm showed excellent catalytic performance in terms of % substrate conversion. Nevertheless, gold nanoparticles below 5 nm proved to be the best catalysts judging from the % substrate conversion, % product selectivity, TON, TOF and recyclability.
2. The TBHP method that we have developed is promising and allows the synthesis of finely dispersed gold nanoparticles with minimised agglomeration. Regardless of differences in solid supports or gold molecular cluster precursors the TBHP prepared catalysts always gave better catalytic performance.
3. Leaching of gold nanoparticles into the reaction solution seems to be minimised and catalyst can be recycled up to six times.
4. The use of phosphine-stabilized molecular gold clusters allows control over the size of the gold nanoparticles provided the activation of the catalyst step is carefully chosen; for example, by avoiding high temperature activation. This is the crucial stage in catalyst preparation and we achieved it with the TBHP method at only 95°C.

#### **5.5 References**

1. T. Eltz, Y. Zimmermann, C. Pfeiffer, J. Pech, R. Twele, W. Francke, J. J. G. Quezada-Euan and K. Lunau, *Current Biology*, 2008, **18**, 1844.

- 
2. V. G. Mata, P. B. Gomes and A. E. Rodrigues, *Flavour and Fragrance Journal*, 2005, **20**, 465-471.
  3. E. Brenna, *Agro Food Industry Hi Tech*, 2005, **16**, 18-20.
  4. J. Karthikeyan, P. P. Naik and A. N. Shetty, *Environmental Monitoring and Assessment*, **176**, 419-426.
  5. Y. Liu, T. Lv, J. Ren, M. Wang, Q. Q. Wu and D. M. Zhu, *Steroids*, **76**, 1136-1140.
  6. R. Buchalla, C. Boess and K. W. Bogl, *Radiation Physics and Chemistry*, 1999, **56**, 353-367.
  7. M. N. Missaghi, J. M. Galloway and H. H. Kung, *Applied Catalysis. A, General*, 2011, **391**, 297-304.
  8. H. Berndt, A. Martin, I. Pitsch, U. Prusse and K. D. Vorlop, *Catalysis Today*, 2004, **91-92**, 191-194.
  9. A. J. Kunin and R. Eisenberg, *Journal of the American Chemical Society*, 1986, **108**, 535-536.
  10. F. Wang, J. Xu, X. Li, J. Gao, L. Zhou and R. Ohnishi, *Advanced Synthesis & Catalysis*, 2005, **347**, 1987-1992.
  11. V. R. Choudhary, D. K. Dumbre and S. K. Bhargava, *Industrial & Engineering Chemistry Research*, 2009, **48**, 9471-9478.
  12. C. Della Pina, E. Falletta and M. Rossi, *Journal of Catalysis*, 2008, **260**, 384-386.
  13. G. Wu, X. Wang, J. Li, N. Zhao, W. Wei and Y. Sun, *Catalysis Today*, 2008, **131**, 402-407.
  14. A. C. Herath and J. Y. Becker, *Electrochimica Acta*, 2008, **53**, 4324-4330.
  15. A. C. Herath and J. Y. Becker, *Journal of Electroanalytical Chemistry*, 2008, **619-620**, 98-104.
  16. P. Lahtinen, H. Korpi, E. Haavisto, M. Leskel and T. Repo, *Journal of Combinatorial Chemistry*, 2004, **6**, 967-973.
  17. S.-S. Weng, M.-W. Shen, J.-Q. Kao, Y. S. Munot and C.-T. Chen, *Proceedings of National Academic of Science*, 2006, **103**, 3522-3527.
  18. M. Salavati-Niasari, *Journal of Molecular Catalysis A: Chemical*, 2006, **245**, 192-199.

- 
19. A. Tarasov, L. Kustov, V. Isaeva, A. Kalenchuk, I. Mishin, G. Kapustin and V. Bogdan, *Kinetics and Catalysis*, 2011, **52**, 273-276.
  20. S. Marx and A. Baiker, *The Journal of Physical Chemistry C*, 2009, **113**, 6191-6201.
  21. M. Comotti, P. C. Della, R. Matarrese and M. Rossi, *Angewandte Chemie, International Edition*, 2004, **43**, 5812-5815.
  22. M. Wolf and H. Knozinger, *Journal of Molecular Catalysis*, 1984, **25**, 273-283.
  23. N. Ahmed, T. Olivier, B. Jean Pierre, R. Jacky, B. Pierre, W. Richard and D. Marc, *Chemistry - A European Journal*, 2008, **14**, 2355-2362.
  24. M. Haruta, T. Kobayashi, H. Sano and N. Yamada, *Chemistry Letters*, 1987, 405-408.
  25. G. Hogarth, S. E. Kabir and E. Nordlander, *Dalton Transactions*, 2010, **39**, 6153-6174.
  26. M. C. Gimeno, in *Modern Supramolecular Gold Chemistry: Gold-Metal Interactions and Applications*, ed. A. Laguna, Wiley-VCH Verlag GmbH & Co. KGaA, Weinheim, Germany, Editon edn., 2008, pp. 1-63.
  27. R. P. F. Kanters, P. P. J. Schlebos, J. J. Bour, W. P. Bosman, H. J. Behm and J. J. Steggerda, *Inorganic Chemistry*, 1988, **27**, 4034-4037.
  28. M. A. Aubart and L. H. Pignolet, *Journal of the American Chemical Society*, 1992, **114**, 7901-7903.
  29. B. D. Chandler, L. I. Rubinstein and L. H. Pignolet, *Journal of Molecular Catalysis A: Chemical*, 1998, **133**, 267-282.
  30. G. C. Bond and D. T. Thompson, *Catalysis Reviews*, 1999, **41**, 319-388.
  31. W.-C. Li, M. Comotti and F. Schüth, *Journal of Catalysis*, 2006, **237**, 190-196.
  32. M. Bowker, A. Nuhu and J. Soares, *Catalysis Today*, 2007, **122**, 245-247.
  33. K. Qian, J. Fang, W. Huang, B. He, Z. Jiang, Y. Ma and S. Wei, *Journal of Molecular Catalysis A: Chemical*, 2010, **320**, 97-105.
  34. L. S. Roselin, F.-W. Chang, W.-S. Chen and H.-C. Yang, *Science of Advanced Materials*, 2011, **3**, 893-900.
  35. S. Biella, G. L. Castiglioni, C. Fumagalli, L. Prati and M. Rossi, *Catalysis Today*, 2002, **72**, 43-49.

- 
36. V. Choudhary and D. Dumbre, *Topics in Catalysis*, 2009, **52**, 1677-1687.
  37. K. Premalatha, P. S. Raghavan and B. Viswanathan, *Applied Catalysis A: General*, 2012, **419-420**, 203-209.
  38. H. M. McNair and J. M. Miller, *Basic Gas Chromatography: Techniques in Analytical Chemistry*, Second Edition edn., John Wiley & Sons, New York, 2009.
  39. N. S. Patil, B. S. Uphade, P. Jana, R. S. Sonawane, S. K. Bhargava and V. R. Choudhary, *Catalysis Letters*, 2004, **94**, 89-93.
  40. A. Habrioux, E. Sibert, K. Servat, W. Vogel, K. B. Kokoh and N. Alonso-Vante, *Journal of Physical Chemistry B*, 2007, **111**, 10329-10333.
  41. J.-J. Yu, S. Lu, J.-W. Li, F.-Q. Zhao and B.-Z. Zeng, *Journal of Solid State Electrochemistry*, 2007, **11**, 1211-1219.
  42. K. Qian, W. Huang, Z. Jiang and H. Sun, *Journal of Catalysis*, 2007, **248**, 137-141.
  43. E. Castillejos, E. Gallegos-Suarez, B. Bachiller-Baeza, R. Bacsá, P. Serp, A. Guerrero-Ruiz and I. Rodríguez-Ramos, *Catalysis Communications*, 2012, **22**, 79-82.
  44. Y. Liu, H. Tsunoyama, T. Akita and T. Tsukuda, *Chemistry Letters*, 2010, **39**, 159-161.
  45. C. Milone, R. Ingoglia, G. Neri, A. Pistone and S. Galvagno, *Applied Catalysis A: General*, 2001, **211**, 251-257.
  46. Y. Liu, H. Tsunoyama, T. Akita and T. Tsukuda, *Chemical Communications*, 2010, **46**, 550-552.
  47. P. Maity, T. Wakabayashi, N. Ichikuni, H. Tsunoyama, S. Xie, M. Yamauchi and T. Tsukuda, *Chemical Communications*, 2012, **48**, 6085-6087.
  48. Y. Levi-Kalisman, P. D. Jadzinsky, N. Kalisman, H. Tsunoyama, T. Tsukuda, D. A. Bushnell and R. D. Kornberg, *Journal of the American Chemical Society*, 2011, **133**, 2976-2982.
  49. J. Kilmartin, R. Sarip, R. Grau-Crespo, D. Di Tommaso, G. Hogarth, C. Prestipino and G. Sankar, *American Chemical Society: Catalysis*, 2012, **2**, 957-963.
  50. F. A. Vollenbroek, J. J. Bour, J. M. Trooster and J. W. A. v. d. Velden, *Journal of the Chemical Society, Chemical Communications*, 1978, 907-909.

- 
51. F. A. Vollenbroek, J. J. Bour and d. V. J. W. A. Van, *Recl. Trav. Chim. Pays-Bas*, 1980, **99**, 137-141.
  52. M. Schulz-Dobrick and M. Jansen, *European Journal of Inorganic Chemistry*, 2006, 4498-4502.
  53. P. Sevilano, O. Fuhr, M. Kattannek, P. Nava, O. Hampe, S. Lebedkin, R. Ahlrichs, D. Fenske and M. M. Kappes, *Angewandte Chemie, International Edition*, 2006, **45**, 3702-3708.
  54. L. D. Menard, F. Xu, R. G. Nuzzo and J. C. Yang, *Journal of Catalysis*, 2006, **243**, 64-73.
  55. Y. Shichibu, Y. Negishi, T. Watanabe, N. K. Chaki, H. Kawaguchi and T. Tsukuda, *Journal of Physical Chemistry C*, 2007, **111**, 7845-7847.
  56. G. Schmid, *Chem. Soc. Rev.*, 2008, **37**, 1909-1930.
  57. M. Walter, J. Akola, O. Lopez-Acevedo, P. D. Jadzinsky, G. Calero, C. J. Ackerson, R. L. Whetten, H. Gronbeck and H. Hakkinen, *Proceedings of National Academic of Science U. S. A.*, 2008, **105**, 9157-9162.
  58. Y. Pei, Y. Gao and X. C. Zeng, *Journal of American Chemical Society*, 2008, **130**, 7830-7832.
  59. M. W. Heaven, A. Dass, P. S. White, K. M. Holt and R. W. Murray, *Journal of American Chemical Society*, 2008, **130**, 3754-3755.
  60. G. Shafai, S. Hong, M. Bertino and T. S. Rahman, *Journal of Physical Chemistry C*, 2009, **113**, 12072-12078.
  61. F. Wen, U. Englert, B. Guttrath and U. Simon, *European Journal of Inorganic Chemistry*, 2008, **2008**, 106-111.
  62. J. W. A. V. D. Velden, F. A. Vollenbroek, J. J. Bour, P. T. Beurskens, J. M. M. Smits and W. P. Bosman, *Recueil, Journal of the Royal Netherlands Chemical Society*, 1981, **100**, 148-152.
  63. M. Turner, V. B. Golovko, O. P. H. Vaughan, P. Abdulkin, A. Berenguer-Murcia, M. S. Tikhov, B. F. G. Johnson and R. M. Lambert, *Nature*, 2008, **454**, 981-983.
  64. S. H. Overbury, V. Schwartz, D. R. Mullins, W. Yan and S. Dai, *Journal of Catalysis*, 2006, **241**, 56-65.
  65. T. Castro, R. Reifengerger, E. Choi and R. P. Andres, *Physical Review B*, 1990, **42**, 8548-8556.

- 
66. C. L. Cleveland, W. D. Luedtke and U. Landman, *Physical Review B*, 1999, **60**, 5065-5077.
  67. H. Tsunoyama, N. Ichikuni, H. Sakurai and T. Tsukuda, *Journal of the American Chemical Society*, 2009, **131**, 7086.
  68. H. Tsunoyama, N. Ichikuni and T. Tsukuda, *Langmuir*, 2008, **24**, 11327.
  69. H. Tsunoyama, H. Sakurai and T. Tsukuda, *Chemical Physics Letters*, 2006, **429**, 528-532.
  70. H. Tsunoyama, H. Sakurai, Y. Negishi and T. Tsukuda, *Journal of the American Chemical Society*, 2005, **127**, 9374.
  71. H. Jiahui, A. Tomoki, F. Jérémy, F. Tadahiro, T. Takashi and H. Masatake, *Angewandte Chemie International Edition*, 2009, **48**, 7862-7866.
  72. H. Tsunoyama, Y. Liu, T. Akita, N. Ichikuni, H. Sakurai, S. Xie and T. Tsukuda, *Catalysis Surveys from Asia*, 2011, **15**, 230-239.
  73. N. S. Patil, B. S. Uphade, P. Jana, S. K. Bharagava and V. R. Choudhary, *Journal of Catalysis*, 2004, **223**, 236-239.
  74. S. Meenakshisundaram, E. Nowicka, P. J. Miedziak, G. L. Brett, R. L. Jenkins, N. Dimitratos, S. H. Taylor, D. W. Knight, D. Bethell and G. J. Hutchings, *Faraday Discussion, The Royal Society of Chemistry*, 2010, **145**, 341-356.
  75. M. Boronat, A. Corma, F. Illas, J. Radilla, T. Rodenas and M. J. Sabater, *Journal of Catalysis*, 2011, **278**, 50-58.
  76. F. Ying, S. Wang, C.-T. Au and S.-Y. Lai, *Gold Bulletin*, 2010, **43**, 241-251.
  77. Z. Ma and S. Dai, *Nano Research*, 2011, **4**, 3-32.
  78. A. Quantanilla, V. C. L. Butselar-Orthlieb, C. Kwarkernaan, W. G. Sloof, M. T. Kreutzer and F. Kapteijn, *Journal of Catalysis*, 2010, **271**, 104-114.
  79. J. Kilmartin, University College London, 2010.
  80. A. I. Kozlov, A. P. Kozlova, H. Liu and Y. Iwasawa, *Applied Catalysis A: General*, 1999, **182**, 9-28.
  81. M. Haruta, *Journal of Vac. Society Japan.*, 2008, **51**, 721-726.
  82. P. C. Della, E. Falletta, M. Rossi and A. Sacco, *Journal of Catalysis*, 2009, **263**, 92-97.
  83. D. I. Enache, D. W. Knight and G. J. Hutchings, *Catalysis Letters*, 2005, **103**, 43-52.

---

## Chapter 6

### Heterobimetallic Gold-Metal Clusters and Nanoparticles - Synthesis, Characterization and Catalysis

#### 6.0 Abstract

Two heterobimetallic gold clusters compounds,  $[(PPh_3)Pd\{AuPh_2P(p\text{-tol})\}_6][NO_3]_2$  (**Au<sub>6</sub>Pd**) and  $[Au_8(PPh_3)_7(SnCl_3)]_2[SnCl_6]$  (**Au<sub>8</sub>Sn**) were synthesized and deposited onto silica nanospheres. Characterization of the supported clusters was carried out using elemental analysis, UV-Vis spectroscopy,  $^1H$  and  $^{31}P$  NMR, TGA-DSC, ESI-MS, powder X-ray diffraction and X-ray absorption fine structure techniques. The wet impregnation method was utilised to deposit clusters onto silica nanospheres. Nanoparticle generation was achieved after activation *via* calcination at 300°C and 500°C. Some difficulties were encountered in the synthesis and characterization of **Au<sub>8</sub>Sn** clusters and are reported in this chapter. The reactivity of the supported catalysts for benzyl alcohol oxidation was investigated using similar reaction conditions as discussed in Chapter 5. The preliminary results were used to understand and compare the catalytic properties of pure gold clusters and heterobimetallic gold-metal species. These showed that the Au-Pd catalyst was reactive in promoting benzyl alcohol oxidation but not the Au-Sn species. Significant synergistic properties of both metals towards catalysis are unclear and open to further investigation.

---

## 6.1 Introduction

There has been considerable interest in the synthesis of heterobimetallic compounds due to the synergistic effects shown when used as catalysts. Corma and co-workers<sup>1-4</sup> have shown that an Au-Pd catalyst was active for the selective oxidation of alcohols to aldehydes and ketones and that the oxidation of aldehydes to acid was in the absence of base and under solvent-free conditions. The number of high nuclearity heterobimetallic gold-metal clusters being structurally characterised has steadily increased in recent years.

It has become clear from the growing number of mixed metal-gold clusters that the transition metal to gold bond is thermodynamically favourable<sup>5</sup>. Recent work by Hutchings *et. al.* demonstrated the role of gold in gold-palladium alloy catalysts towards benzyl alcohol oxidation<sup>6-9</sup> under solvent-free gas-phase conditions. Three common explanations have been proposed to account for catalytic enhancement by heterobimetallic compounds: (i) the geometric effect, in which atomic ensembles act as active sites; (ii) the electronic effect, in which interactions among surrounding atoms give rise to electron density dislocation and (iii) the bifunctional effect, in which each metal promotes a different step of the surface reaction<sup>10</sup>.

A coordinatively unsaturated transition-metal moiety, produced for example by hydride loss or ligand dissociation, can either trap a gold cluster fragment or participate directly in cluster growth, thereby forming a mixed-metal cluster. A number of heterobimetallic gold-metal clusters have been studied including Au-Pt<sup>11-14</sup>, Au-Pd<sup>15, 16</sup>, Au-Rh<sup>17-19</sup>, Au-Fe<sup>20, 21</sup>, Au-Co<sup>22</sup>, Au-Sn<sup>23, 24</sup> and Au-Os<sup>25-27</sup>. The introduction of heterometallic gold-metal bonding into these clusters leads to an

---

increase in the polarity of the molecule, which probably results in the enhancement of the catalytic activity. Generally, there are two types of heterobimetallic gold-metal clusters, namely, metal-rich and gold-rich heterobimetallic molecular clusters. In our research, we were more interested in gold-rich heterobimetallic clusters.

Platinum-gold clusters have previously been reported to be active catalysts for the H<sub>2</sub>-D<sub>2</sub> equilibration reaction<sup>28</sup>. The Pt-centred, crown-shaped cluster of [Pt(AuPPh<sub>3</sub>)<sub>8</sub>](NO<sub>3</sub>)<sub>2</sub> is highly reactive towards H<sub>2</sub> and is an excellent H<sub>2</sub>-D<sub>2</sub> equilibration catalyst at room temperature and 1 atm of H<sub>2</sub> pressure. Other M-Au clusters also have been reported to show similar reactivity towards H<sub>2</sub>. These include [Pt(AuPPh<sub>3</sub>)<sub>8</sub>(CuCl)]<sup>2+</sup><sup>29</sup> and [Pt(AuPPh<sub>3</sub>)<sub>8</sub>(Ag)]<sup>3+</sup><sup>30</sup>.

In our research, we aimed to synthesize Au-Pd and Au-Sn heterobimetallic catalysts using gold-phosphine nitrate complexes and phosphine-stabilized **Au**<sub>9</sub> clusters as precursors. Both heterobimetallic clusters systems have been reported previously but to our knowledge, no catalytic studies have been carried out using this system.

## 6.2 Experimental

All experiments were carried out using the standard Schlenk-line technique under a purified N<sub>2</sub> atmosphere unless mentioned otherwise. Solvents used were dried and O<sub>2</sub>-free if necessary. No any other special precautions were taken to exclude air or moisture from the synthetic procedures. All chemicals were used as purchased from Sigma-Aldrich, BDH or Alfa Aesar. Details on characterizations techniques were described in Chapter 2 of this thesis.

---

### 6.2.1 Synthesis of Heterobimetallic Gold-Metal Clusters

Two clusters - gold-palladium;  $[(PPh_3)Pd\{AuPh_2P(p-tol)\}_6][NO_3]_2$  (**Au<sub>6</sub>Pd**) and  $[Pd(AuPPh_3)_8](NO_3)_2$  (**Au<sub>8</sub>Pd**) also one from gold-tin;  $[Au_8(Ph_2P(p-tol))_7(SnCl_3)]_2[SnCl_6]$  (**Au<sub>8</sub>Sn**) were synthesized.  $(PPh_3)AuNO_3$ ,  $\{Ph_2P(p-tol)\}AuNO_3$  complexes or **Au<sub>9</sub>** cluster were utilised as starting material. The method of synthesizing both precursors has been described in Chapter 2.

#### 6.2.1.1 Synthesis of Au<sub>6</sub>Pd Clusters

The procedure for the synthesis of **Au<sub>6</sub>Pd** was followed as described in literature<sup>16</sup>. The **Au<sub>6</sub>Pd** that we synthesized was  $[(PPh_3)Pd\{AuPh_2P(p-tol)\}_6][NO_3]_2$  (Figure 6.1).

A 100 ml three-necked round bottom flask was charged with  $[PdCl_2(PPh_3)_2]$  (0.0812 g, 0.115 mmol),  $[Ph_2P(p-tol)AuNO_3]$  (0.3024 g, 0.560 mmol) and 10 ml dichloromethane with a continuous flow of N<sub>2</sub>. A methanol solution of NaBH<sub>4</sub> (10 ml, 0.0137 g, 0.276 mmol) was added dropwise to the mixture. The solution was stirred for about 30 minutes during which the colour gradually changed from yellow to dark red to brown. A drop of distilled water was added to quench the reaction. Solvents were removed on a rotary evaporator and methanol (7 ml) added. This dissolved the crude mixture which was filtered through celite to remove any precipitates. The dark brown filtrate was reduced to dryness and acetone (5 ml) was added to dissolve the dark red-purple solid to give a dark brown solution. The solution was filtered again through celite and the dark brown filtrate was once again evaporated to dryness. A brown microcrystalline solid was obtained by liquid diffusion using a minimum amount of methanol to dissolve the solid then layering

---

with diethyl ether. The solid (0.1541 g) was isolated on a fritted funnel, washed with diethyl ether and dried under vacuum. % yield: 71% based on gold. The crystal structure of similar clusters was reported by Sotelo *et. al.*<sup>31</sup>. <sup>1</sup>H-NMR (CD<sub>2</sub>Cl<sub>2</sub>): δ (ppm) aromatic protons; 7.75-6.39(m); -CH<sub>3</sub>; 2.17(s). <sup>31</sup>P{<sup>1</sup>H}-NMR: δ (ppm) 61.3(m); 49.2(s). Elemental analysis gives C, 47.14%; H, 3.49%; N, 1.12%; as PdAu<sub>6</sub>P<sub>7</sub>C<sub>132</sub>H<sub>117</sub>N<sub>2</sub>O<sub>6</sub> requires C, 47.58%; H, 3.54%; N, 0.84%.



**Figure 6.1:** (a) **Au<sub>6</sub>Pd<sup>31</sup>** and (b) **Au<sub>8</sub>Pd<sup>16</sup>** crystal structure from literature. Carbons and hydrogens were omitted for clarity.

#### 6.2.1.2 Synthesis of Au<sub>8</sub>Sn Clusters

We encountered difficulties in preparing **Au<sub>8</sub>Sn** clusters according to method described by Demidowicz *et. al.* This utilised the direct reaction of **Au<sub>9</sub>** cluster and SnCl<sub>2</sub>·2H<sub>2</sub>O<sup>24</sup>. The **Au<sub>9</sub>** cluster (0.4134 g, 0.099mmol) was suspended in acetone (30 ml) under the N<sub>2</sub> atmosphere. The mixture was stirred for 15 minutes and then SnCl<sub>2</sub>·2H<sub>2</sub>O (0.2013 g, 0.892 mmol) was added to give a slurry. The green suspension turned red and stirring was continued for 2.5 hours. In our hands, however after 3 minutes, the red precipitate that should separate out did not appear.

---

Rather, after 1 hour the solution turned purple then an orange precipitate developed. The reaction was repeated three times following the procedure reported. Unfortunately, the expected red precipitate was not produced.



**Figure 6.2:** Crystal structure of  $\text{Au}_8\text{Sn}$  from literature<sup>24</sup>. Carbons and hydrogens were omitted for clarity.

We then employed an alternate method utilising  $\text{Au}_9$  cluster and  $[\text{NEt}_4]\text{SnCl}_3$ , the latter being synthesized according to literature<sup>32</sup> (Figure 6.2). The cluster  $[\text{Au}_9\{\text{Ph}_2\text{P}(p\text{-tol})\}_8][\text{NO}_3]_3$  (0.1836 g, 0.0460 mmol) was suspended in acetone (30 ml) under a  $\text{N}_2$  atmosphere. The mixture was stirred for 15 minutes,  $[\text{NEt}_4]\text{SnCl}_3$  (0.0084 g, 0.0020 mmol) was added, and the solution was stirred for 30 minutes. The solution lightened in colour and an orange-red precipitate separated out. Solvent evaporation gave a red-orange solid (0.4838 g) which was dried under vacuum (61% yield based on gold). Mingos *et. al.* had reported the detailed structural characterisation on the similar envisioned cluster<sup>24</sup>.  $^1\text{H-NMR}$  ( $\text{CD}_2\text{Cl}_2$ ):  $\delta$  (ppm)

---

aromatic protons; 7.61-7.32(m); -CH<sub>3</sub>; 2.45(s). <sup>31</sup>P{<sup>1</sup>H}-NMR: δ (ppm) 32.4(s). Elemental analysis: C, 31.56%; H, 2.66%; Cl, 4.97%; as Au<sub>16</sub>C<sub>266</sub>H<sub>238</sub>P<sub>14</sub>Sn<sub>3</sub>Cl<sub>12</sub> for **Au<sub>8</sub>Sn** requires C, 30.95%; H, 3.07%; Cl, 5.45%.

### 6.2.2 *Synthesis of Heterobimetallic Gold-Metal Nanoparticle Catalysts*

Heterobimetallic clusters were deposited onto SiO<sub>2</sub> nanospheres using the wet impregnation method as described in Chapter 2. Gold loading was 4.0 wt. % and catalysts were activated by calcination at 300 °C and 500 °C; 10 °C/min for 1 hour.

## 6.3 Results and Discussions

### 6.3.1 *Carbon, Hydrogen, Nitrogen (CHN) Elemental Analysis*

The stoichiometry of clusters is difficult to predict due to the large molecular mass. We managed to obtain relatively high yields (> 60%) for both clusters synthesized. The heterobimetallic gold-metal cluster, **Au<sub>6</sub>Pd** was collected as a brown microcrystalline solid in 71% yield and **Au<sub>8</sub>Sn** as red-orange solid in 61% yield (based on gold). There is a slight difference in value for % N found according to elemental analysis for **Au<sub>6</sub>Pd** clusters. However, the % C and % H values were in agreement with the calculated values. The higher nitrogen content may be because of the NaNO<sub>3</sub> formed during the cluster preparation was not fully separated. Nonetheless, for **Au<sub>8</sub>Sn** clusters, the elemental analysis data on carbon, hydrogen and chlorine is in agreement with calculated values.

### 6.3.2 Ultraviolet-Visible (UV-Vis) Spectroscopy

UV-Vis spectroscopy for precursor clusters was carried out in solution. **Au<sub>6</sub>Pd** was dissolved in methanol. Unfortunately, there was a solubility issue with **Au<sub>8</sub>Sn** and no UV-Vis spectrum could be recorded. The **Au<sub>6</sub>** cluster was synthesized according to our previous work<sup>33, 34</sup>. Both **Au<sub>6</sub>** and **Au<sub>6</sub>Pd** spectra were recorded in methanol in the range 300-800 nm. A comparison between the two spectra is shown in Figure 6.3.

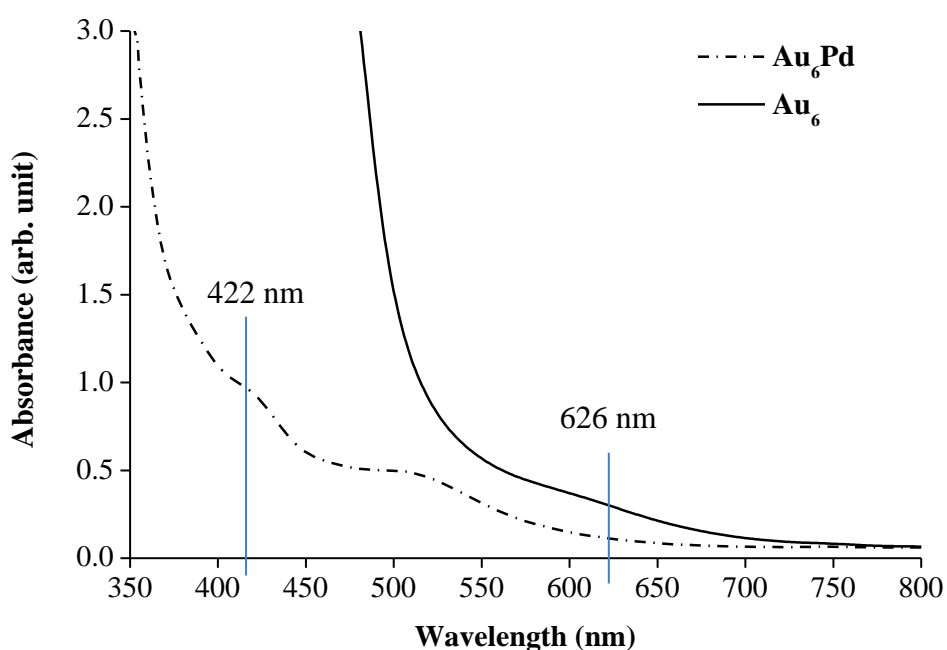


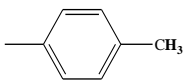
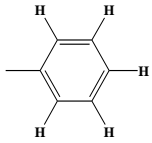
**Figure 6.3:** UV-Vis spectrum of **Au<sub>6</sub>Pd** and **Au<sub>6</sub>** in methanol solution

A resonance at *ca.* 626 nm was observed for the **Au<sub>6</sub>** and was clear indication of reduction of the Au-phosphine ions<sup>22</sup> in clusters. Both spectra show weak absorptions in the region from 500-800 nm that are assigned due to gold-gold interactions<sup>35</sup>. An interesting observation is the presence of an additional absorption at *ca.* 422 nm for **Au<sub>6</sub>Pd**. This feature arises due to gold-metal interactions as observed in related Au-Pt clusters<sup>36</sup>.

### 6.3.3 $^1\text{H}$ and $^{31}\text{P}$ Nuclear Magnetic Resonance (NMR) Spectroscopy

The  $^1\text{H}$  NMR resonance of the ligand was monitored throughout the synthetic procedure in order to confirm that no degradation occurred at any stage of cluster formation (Table 6.1). For the *p*-tol ligand, two types of  $^1\text{H}$  NMR resonance were observed, namely the aromatic protons and methyl group.

**Table 6.1:**  $^1\text{H}$ -NMR chemical shift

Type of $^1\text{H}$	Chemical shift, $\delta$ (ppm)				
	$\text{Ph}_2\text{P}(p\text{-tol})$	$(\text{Ph}_2\text{P}(p\text{-tol}))\text{AuCl}$	$(\text{Ph}_2\text{P}(p\text{-tol}))\text{Au}(\text{NO}_3)$	$\text{Au}_6\text{Pd}$	$\text{Au}_8\text{Sn}$
	2.38 (s)	2.43 (s)	2.44 (s)	2.17 (s)	2.45 (s)
	7.19-7.37 (m)	7.28-7.56 (m)	7.30-7.66 (m)	6.39-7.75 (m)	7.49-7.58 (m)

As can be seen (Table 6.1), the  $^1\text{H}$  NMR resonance for methyl group in  $\text{Au}_6\text{Pd}$  is shifted upfield ( $\delta$  2.17 ppm) as compared to the ligand and intermediate gold complexes. For  $\text{Au}_8\text{Sn}$ , the chemical shift of the same proton resonance is not distinguished further from the intermediate gold nitrate complexes. However, the protons of the aromatic groups appear downfield and in a smaller range as compared to the starting material. The use of phosphine ligands gives an advantage in cluster characterization as the  $^{31}\text{P}\{^1\text{H}\}$  NMR can be utilised. Indeed, this NMR gives a clearer information on cluster formation<sup>37-39</sup>. A full comparison of the  $^{31}\text{P}\{^1\text{H}\}$  NMR data is listed in Table 6.2 below.

**Table 6.2:**  $^{31}\text{P}\{^1\text{H}\}$  NMR chemical shift

Compound	$\delta$ (ppm)
(Ph <sub>2</sub> P( <i>p</i> -tol)) ligand	-6.4 (s)
(Ph <sub>2</sub> P( <i>p</i> -tol))AuCl	32.4 (s)
(Ph <sub>2</sub> P( <i>p</i> -tol))Au(NO <sub>3</sub> )	26.9 (s)
<b>Au<sub>6</sub>Pd</b>	49.2 (s) and 61.3 (m)
<b>Au<sub>8</sub>Sn</b>	33.1 (s)

For **Au<sub>8</sub>Sn** clusters values observed were in agreement with literature reports<sup>24, 40</sup>. According to literature<sup>31</sup>, peaks in the  $^{31}\text{P}\{^1\text{H}\}$  NMR spectrum of **Au<sub>6</sub>Pd** can be assigned to the presence of two types of phosphorus atoms; one linked to palladium and others linked to gold<sup>31</sup>. However, we observed that the signal at  $\delta$  49.2 ppm assigned to the phosphorus attached to gold bond is not a doublet as expected but is more like a singlet with a small shoulder (Figure 6.4). Likewise, the signal at  $\delta$  61.3 ppm assigned to the phosphorus at palladium was not a clean septet but more likely to appear as a multiplet. There were also extra signals at 44.6 ppm (m) and 32.4 ppm (m) which remain unassigned. Presumably, there was a mixture of **Au<sub>6</sub>Pd** and **Au<sub>8</sub>Pd** clusters. Pignolet *et. al.* also reported similar findings with diphosphine-ligated Pt-Au clusters, when mixture of clusters appeared resulting from skeletal rearrangement<sup>41</sup>. The observed singlet were caused by an (accidental) equal chemically equivalent chemical shift<sup>37</sup>.

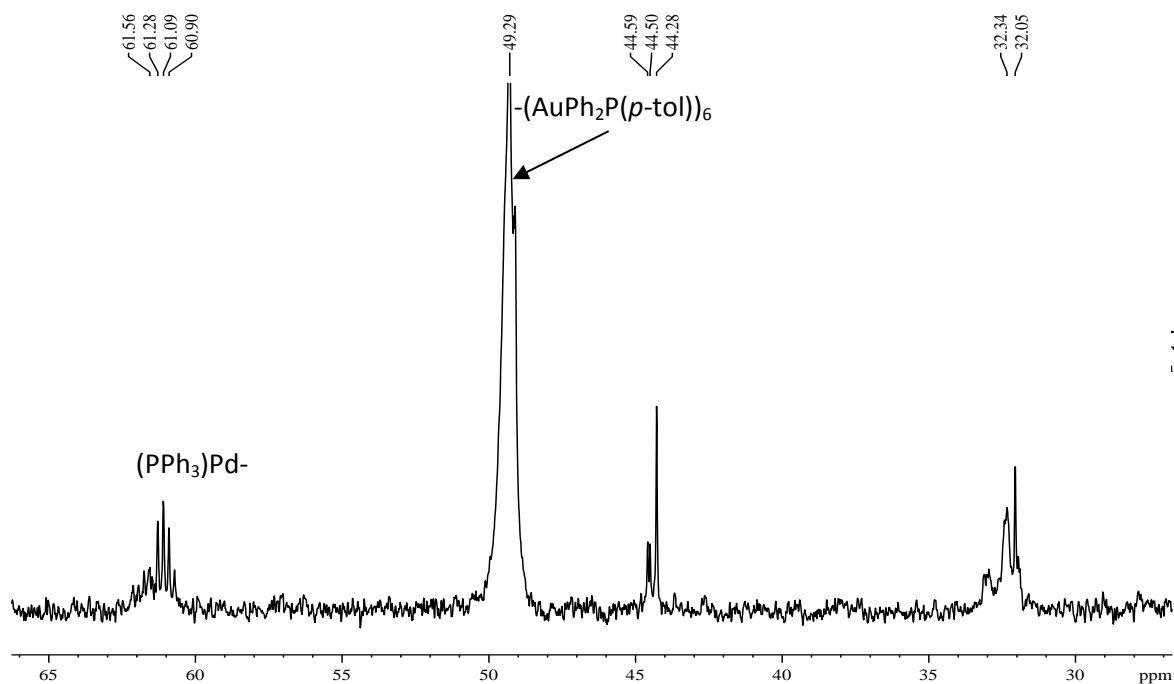


**Figure 6.4:**  $^{31}\text{P}\{^1\text{H}\}$  NMR spectrum of  $\text{Au}_6\text{Pd}$  clusters

#### 6.3.4 Thermogravimetric Analysis-Differential Scanning Calorimetry (TGA-DSC)

Thermogravimetric analysis of each sample was carried out in order to determine the temperature required for cluster decomposition in argon up to  $600^\circ\text{C}$  increasing by  $2^\circ\text{C}/\text{min}$ . Figure 6.5 shows the TGA-DSC curves for both clusters. TGA showed a relatively broad weight loss between  $250\text{--}350^\circ\text{C}$  of *ca.* 55% for  $\text{Au}_6\text{Pd}$  and  $300\text{--}360^\circ\text{C}$  of *ca.* 50% for  $\text{Au}_8\text{Sn}$ , coincident with a large exotherm in the DSC trace. This corresponds well to the calculated weight loss of 57.6% and 49.5% for each cluster respectively.

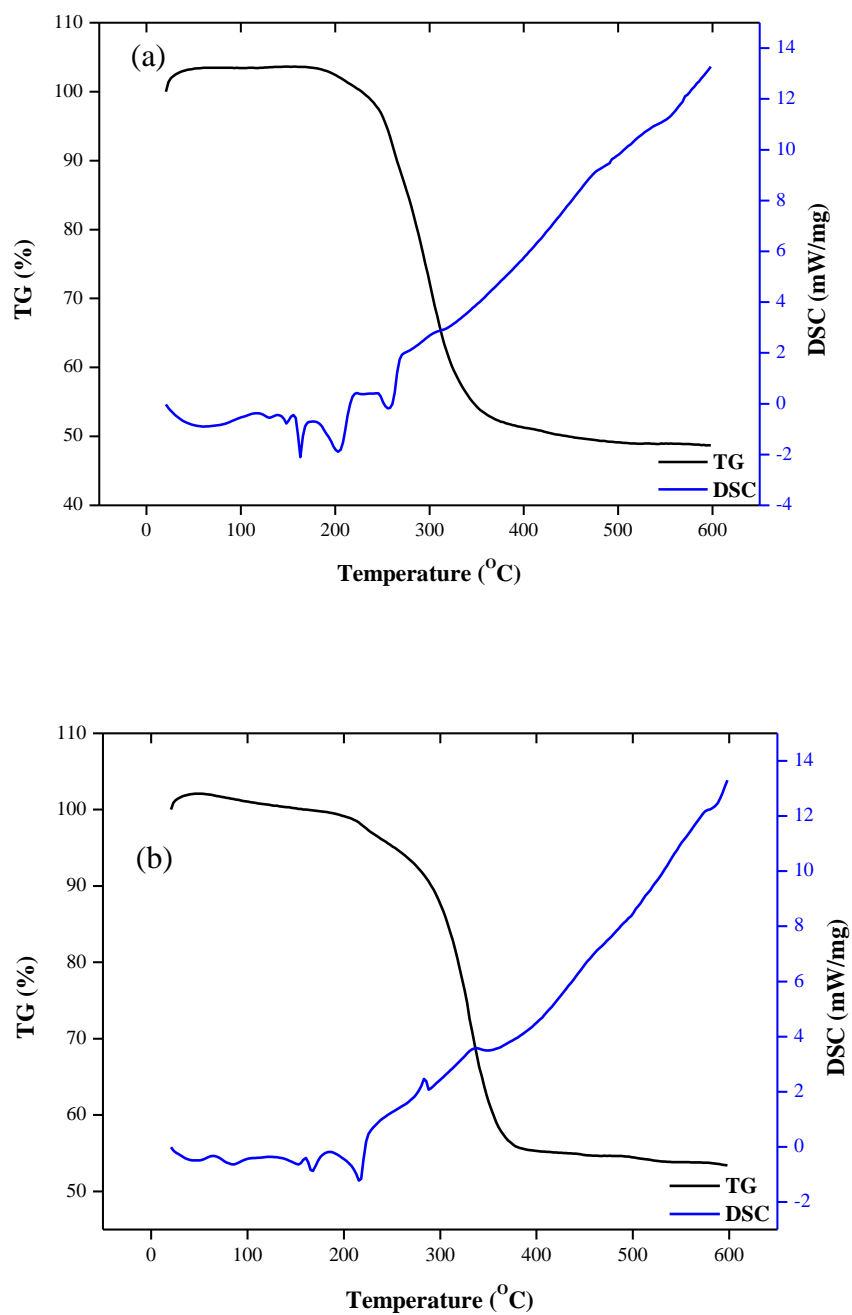


**Figure 6.5:** TGA-DSC curves for (a) Au<sub>6</sub>Pd clusters and (b) Au<sub>8</sub>Sn clusters

### 6.3.5 Electro spray Ionization-Mass Spectrometry (ESI-MS)

In order to determine the elemental composition of clusters synthesized, a mass spectrometric study using electro spray ionization (ESI) was carried out. Table 6.3 listed the expected  $m/z$  values for each clusters.

**Table 6.3:** Calculated  $m/z$  values of clusters

Clusters	Cation	$m/z$
<b>Au<sub>6</sub>Pd</b>	$[(\text{PPh}_3)\text{Pd}(\text{AuPh}_2\text{P}(p\text{-tol}))_6]^{2+}$	3100.2766
<b>Au<sub>8</sub>Sn</b>	$[\text{Au}_8(\text{Ph}_2\text{P}(p\text{-tol}))_7(\text{SnCl}_3)]^+$	3734.9807

Figure 6.6 shows the ESI-MS spectra for each cluster. Unfortunately, we were unable to identify any multiply charged clusters in the  $m/z$  range up to calculated mass value for each cluster. Clearly, the clusters are easily fragmented to other small clusters in gas-phase as so many peaks appeared at lower region than the clusters  $m/z$  region<sup>42</sup>. Other research groups have reported similar fragmentation patterns for small clusters as well as differences in sample composition in large clusters were observed and studied using ESI-MS<sup>42-47</sup>. Nevertheless, we did observe peaks in the expected  $m/z$  regions for each cluster.

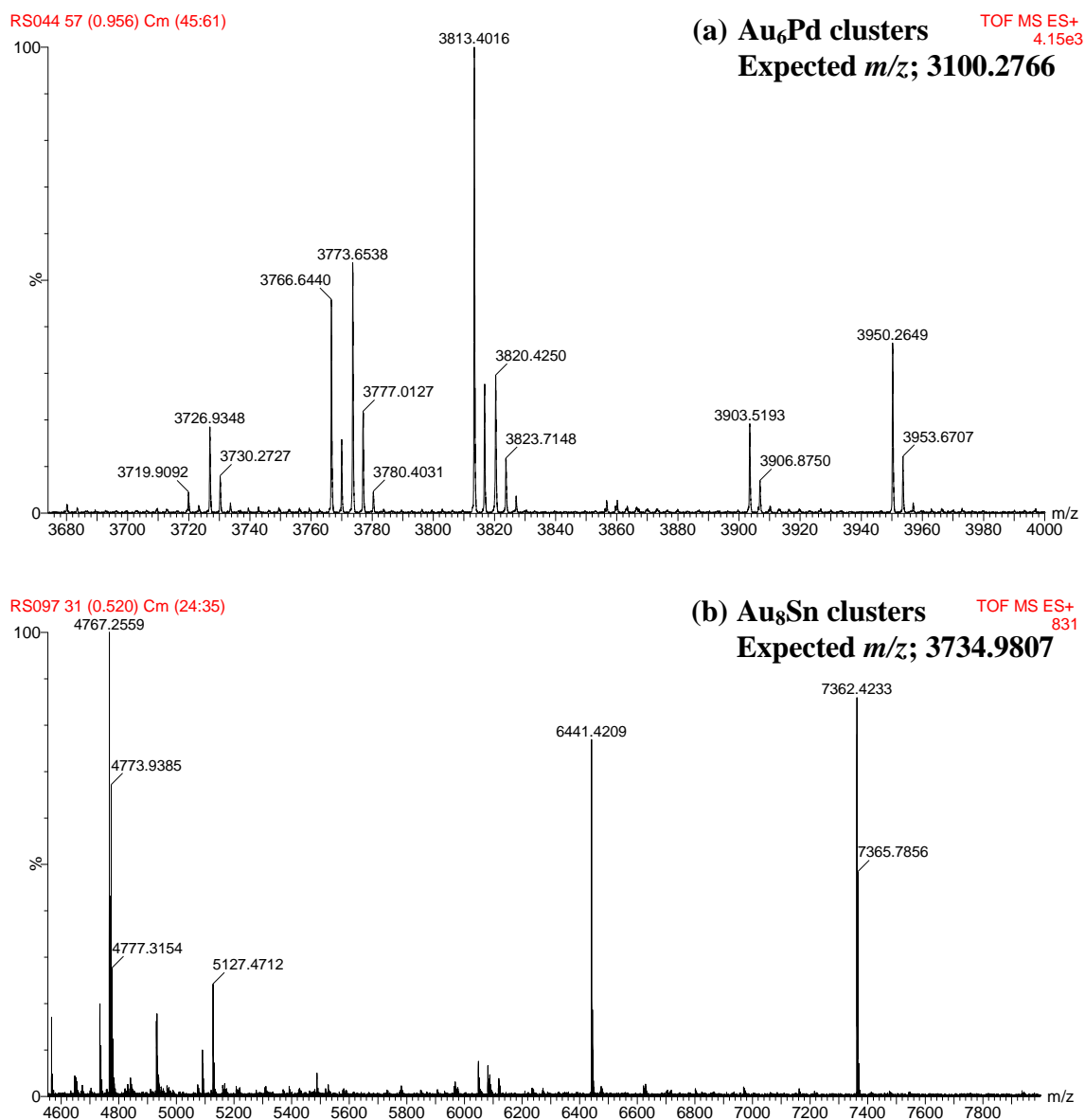


**Figure 6.6:** ESI-MS spectra of Au<sub>6</sub>Pd and Au<sub>8</sub>Sn clusters

### 6.3.6 X-ray Diffraction (XRD)

XRD patterns of mixed-metal catalysts together with that of Au<sub>9</sub> catalysts were shown in Figure 6.7. In all cases, crystallinity increased from uncalcined to calcined at 300°C and calcined at 500°C catalysts. The appearance of Au (111), (200), (220) and (311) peaks confirmed the transformation to gold nanoparticles.

However, no peaks corresponding Pd in  $\text{Au}_6\text{Pd}$  or Sn in  $\text{Au}_8\text{Sn}$  was observed possibly due to the extremely low concentration of both metals.

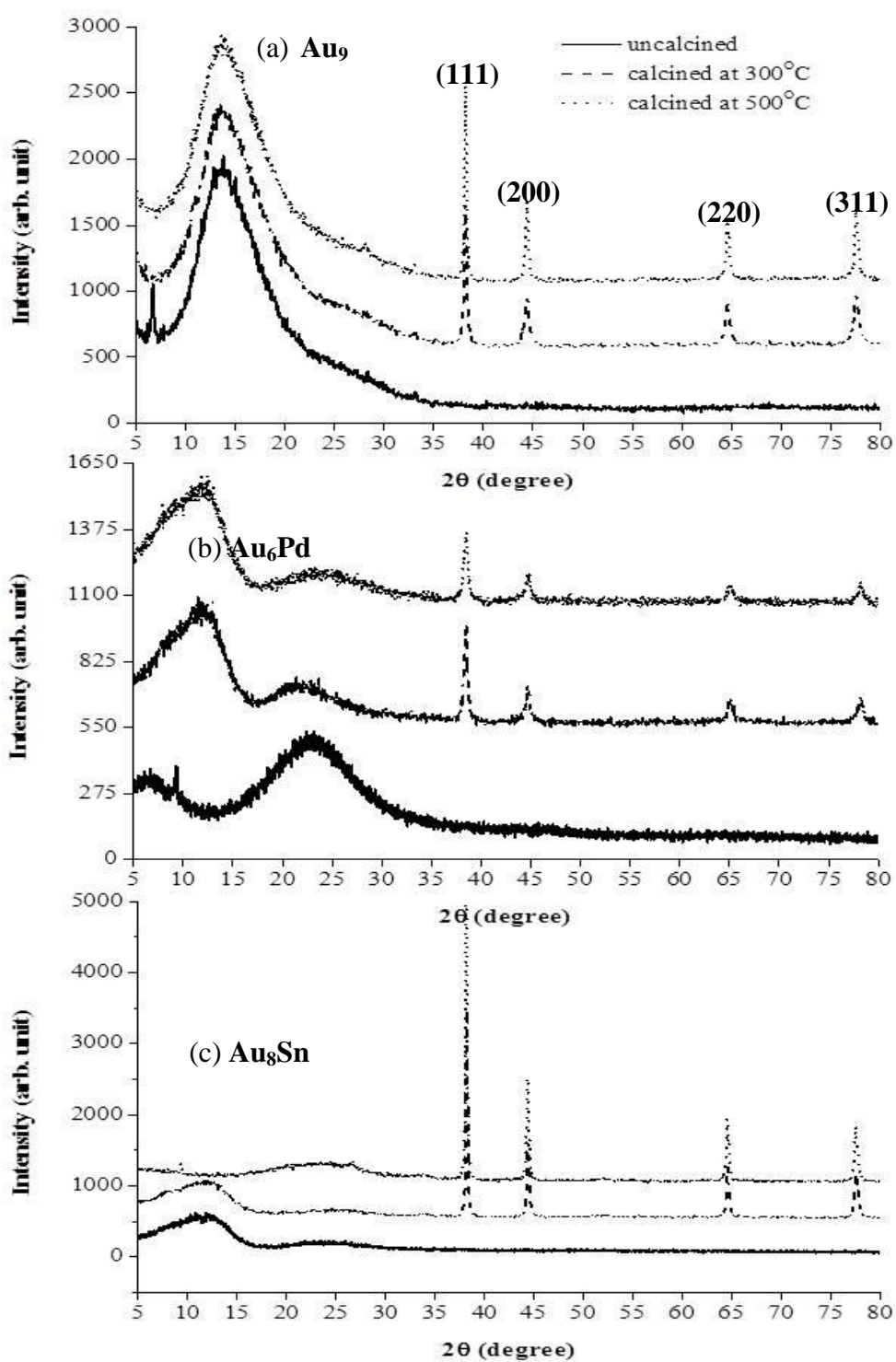


**Figure 6.7:** XRD patterns of uncalcined, calcined at 300°C and calcined at 500°C, (a)  $\text{Au}_9$ , (b)  $\text{Au}_6\text{Pd}$  and (c)  $\text{Au}_8\text{Sn}$  on  $\text{SiO}_2$  nanospheres

### 6.3.7 X-ray Absorption Near Edge Structure (XANES) and Extended X-ray Absorption Fine Structure (EXAFS)

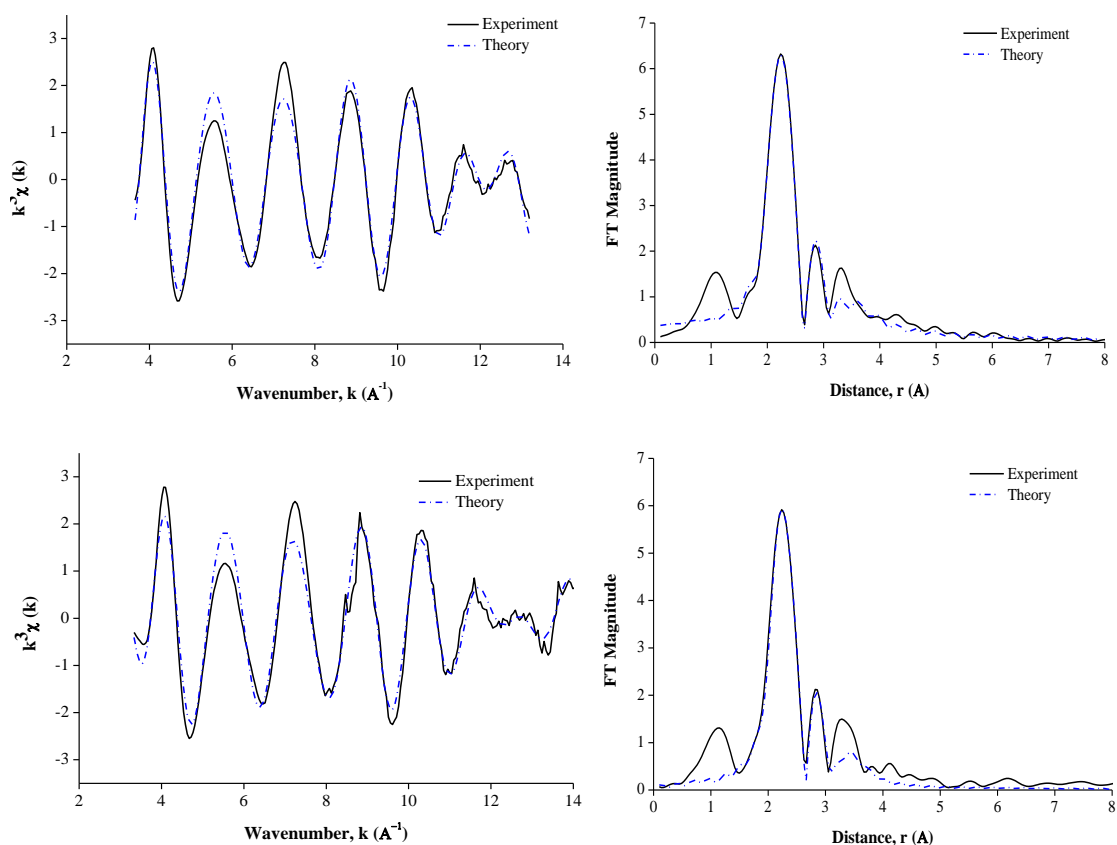


**Figure 6.8:** Best fit between experimental Au L<sub>III</sub> edge EXAFS and theory/calculated data for **Au<sub>6</sub>Pd**; clusters (top) and **Au<sub>8</sub>Pd** clusters (bottom). On the right corresponding Fourier transforms of the experimental and calculated data are shown.

XAS was employed as a method of structural characterisation with X-ray absorption measurements, carried out on the DUBBLE BM26A beamline of European Synchrotron Radiation Facility, Grenoble, France. Only precursor clusters were analyzed due to low loadings observed on supports that made it difficult to obtain sufficient edge jump for EXAFS data quality. The **Au<sub>6</sub>Pd** clusters was

pressed into a pellet with a thickness chosen to give a total absorbance ( $\mu x$ ) at the Au L<sub>III</sub> (11.918 keV) and Pd K edge (24.350 keV) edges of *ca.* 2.0 and an edge step ( $\Delta\mu x$ ) of *ca.* 0.5. Unfortunately, no data were collected for **Au<sub>3</sub>Sn** cluster due to the unstable nature of this cluster (it changed colour over time) and low concentration of Au and Sn on the supported catalyst.

**Table 6.4:** Structural parameters derived from the analysis of Au L<sub>III</sub> edge EXAFS data of **Au<sub>6</sub>Pd** clusters

Clusters	Atom pair	Au-P			Au-Au		
		<i>N</i>	<i>R</i> (Å)	$\sigma^2$ (Å <sup>2</sup> )	<i>N</i>	<i>R</i> (Å)	$\sigma^2$ (Å <sup>2</sup> )
	<b>Au<sub>6</sub>Pd</b>	1.04	2.30	0.007	0.28	2.53	0.007
	<b>Au<sub>3</sub>Pd</b>	1.08	2.31	0.008	0.49	2.53	0.008

Fit index **Au<sub>6</sub>Pd** = 20.36; **Au<sub>3</sub>Pd** = 29.02. *N* = coordination number; *R* = bond distance (Å);  $\sigma^2$  = standard deviation.

At the Au L<sub>III</sub> edge the **Au<sub>6</sub>Pd** clusters (Figure 6.8), gave Au-P and Au-Au characteristics similar to those in monometallic **Au<sub>9</sub>** clusters (Chapters 3 and 4). The bond distances in both clusters were less than that of Au foil (2.88 Å) which confirmed the non-bulky structures of the clusters. The Au-P coordination number (Table 6.4) for both clusters were closely similar (1.04 for **Au<sub>6</sub>Pd** and 1.08 for **Au<sub>3</sub>Pd** as well as Au-Au coordination number (0.28 for **Au<sub>6</sub>Pd** and 0.49 for **Au<sub>3</sub>Pd**). Observed bond distances were almost identical (*ca.* 2.3 Å for Au-P and *ca.* 2.5 Å for Au-Au). These results indicates that the structural surrounding of gold in both heterobimetallic Au-Pd clusters were almost identical with phosphines ligands attached to Au.

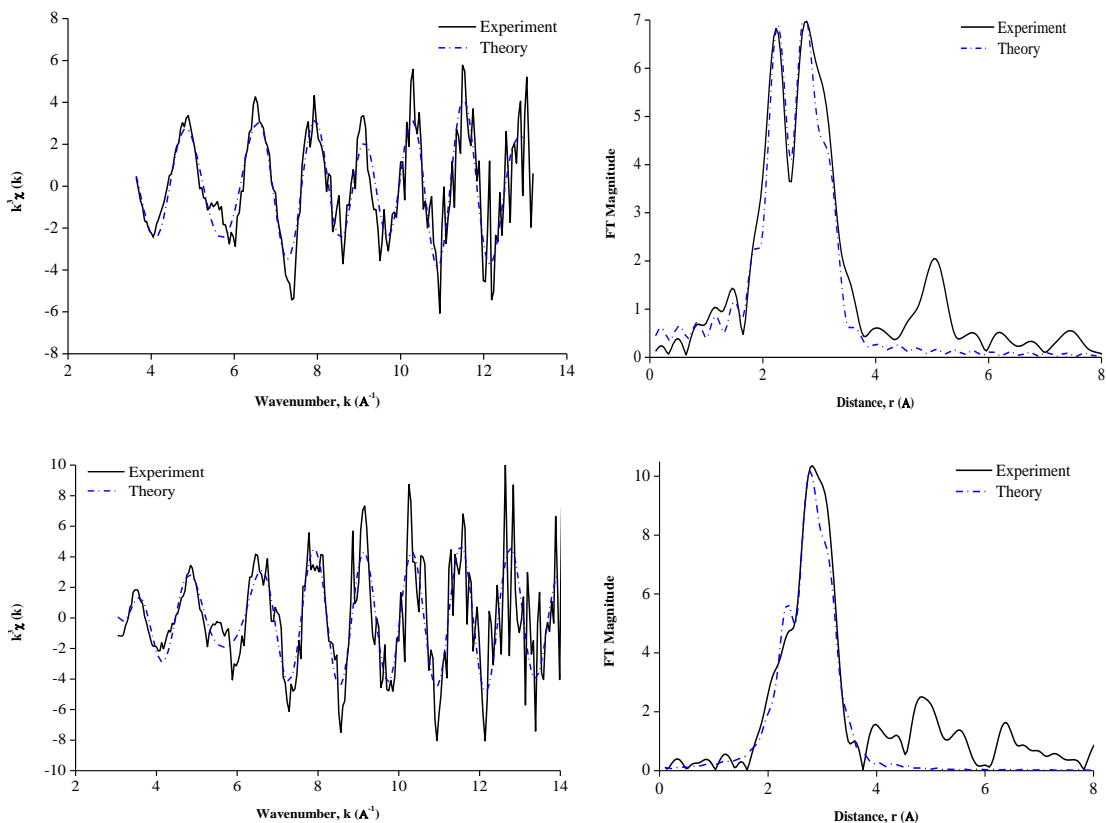


**Figure 6.9:** Best fit between experimental Pd K edge EXAFS and theory/calculated data for **Au<sub>6</sub>Pd** clusters (top) and **Au<sub>8</sub>Pd** clusters (bottom). On the right corresponding Fourier transforms of the experimental and calculated data are shown.

Table 6.5 shows the results of EXAFS fitting from the Pd K edge. Spectra for experimental and calculated fittings are shown in Figure 6.9. From these, it can be seen that the calculated structure model of the clusters obtained from analysis of EXAFS data perfectly match with experimental data. EXAFS of the Pd K edge showed significant metallic peaks between 2-3 Å. The EXAFS fit indicates that palladium has two coordination environments in **Au<sub>6</sub>Pd** clusters ( $N_{\text{Pd-P}} = 2.10$  at 2.36 Å and  $N_{\text{Pd-Au}} = 0.26$  at 2.63 Å) while one in **Au<sub>8</sub>Pd** clusters ( $N_{\text{Pd-Au}} = 3.40$  at 2.74 Å). Within the error of EXAFS measurements, the bond distances of Pd-Au of both clusters were identical, ca.  $\sim 2.70$  Å<sup>10</sup>.

**Table 6.5:** Structural parameters derived from the analysis of Pd K edge EXAFS data of **Au<sub>6</sub>Pd** clusters

Atom pair Clusters	Pd-P			Pd-Au		
	N	R (Å)	$\sigma^2$ (Å <sup>2</sup> )	N	R (Å)	$\sigma^2$ (Å <sup>2</sup> )
<b>Au<sub>6</sub>Pd</b>	2.10	2.36	0.013	0.26	2.63	0.011
<b>Au<sub>8</sub>Pd</b>	-	-	-	3.40	2.74	0.007

Fit index **Au<sub>6</sub>Pd** = 41.78; **Au<sub>8</sub>Pd** = 58.5. N = coordination number; R = bond distance (Å);  $\sigma^2$  = standard deviation.

Figure 6.10 gives a comparison between experimental EXAFS data for the two different species **Au<sub>6</sub>Pd** clusters together with Fourier transform and XANES spectra. Both XANES spectra were not identical to that of Pd foil (reference compound for Pd-Pd bond) indicating that the **Au<sub>6</sub>Pd** clusters were not in bulk. The XANES characteristic for both clusters also seems to be slightly different that determined the existence of Pd-P bond in **Au<sub>6</sub>Pd** clusters. The Fourier transforms of both clusters confirmed the prediction observed from XANES when there was no Pd-P characteristic observed for **Au<sub>8</sub>Pd** cluster.

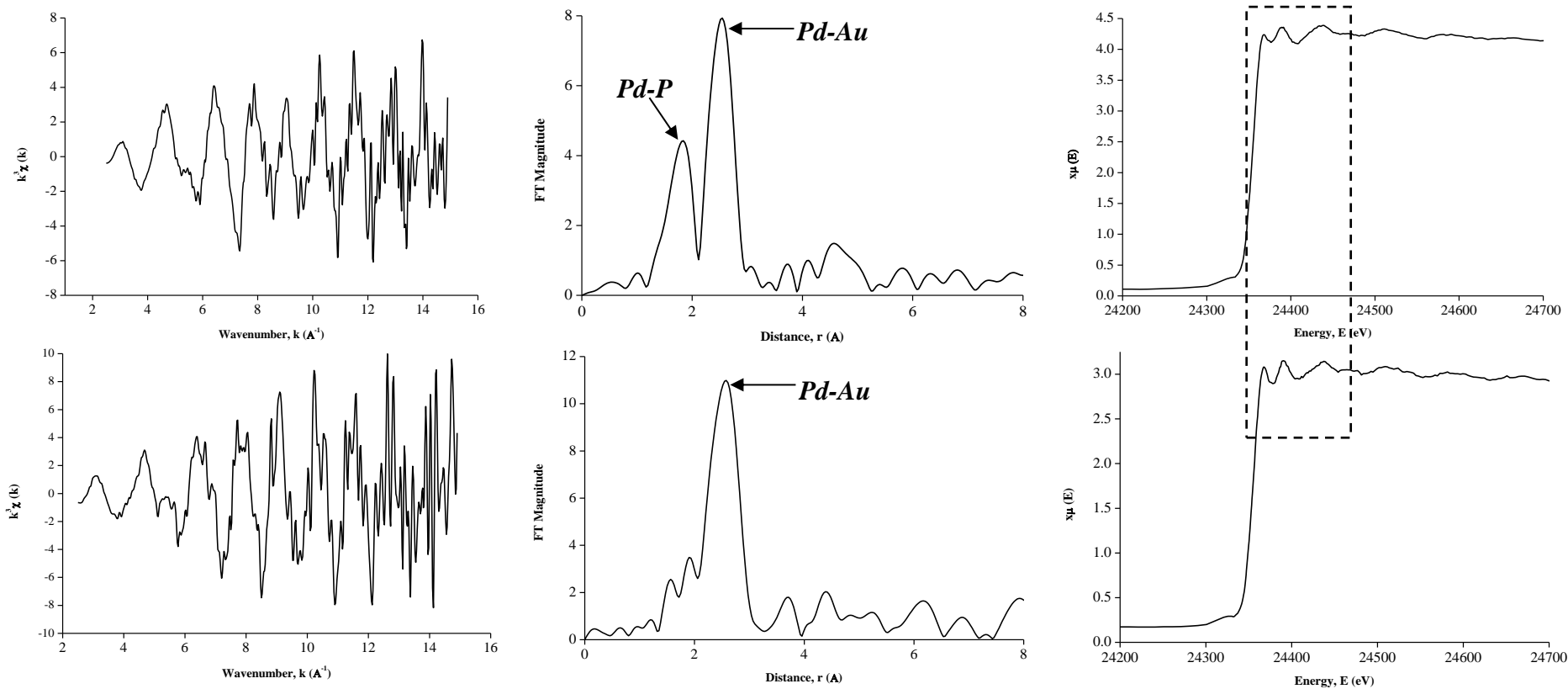


**Figure 6.10:** Comparison between experimental Pd K edge EXAFS data for **Au<sub>6</sub>Pd** clusters (top) and **Au<sub>8</sub>Pd** clusters (bottom). Corresponding Fourier transforms and XANES of the experimental data are shown.

---

## 6.4 Catalysis: Oxidation of Benzyl Alcohol

Our catalytic studies focused on the oxidation of benzyl alcohol. This was carried out using 0.20 g of catalyst, *tert*-butylhydroperoxide in decane (TBHP) as the oxidant (decane act as the GC internal standard) and *n*-heptane as solvent at 95 °C using the supported nanoparticle catalysts. Samples were taken every 30 minutes for the first hour of reaction then every hour for the remaining 4 hours of reaction. GC was used to determine the catalytic performance. The detailed procedure is described in Chapter 5.

Each catalyst was first submitted to thermal treatment at 300 °C and 500 °C for 1 hour. Uncalcined catalysts were also tested in order to observe the “*induction period*” found when using gold nanoparticle catalysts (Chapter 5). Figure 6.11 and 6.12 summarize the % conversion of benzyl alcohol using **Au<sub>6</sub>Pd** and **Au<sub>8</sub>Sn** as catalysts respectively. The analytical data show that the conversion of benzyl alcohol at higher percentage **Au<sub>6</sub>Pd** (>50% conversion) catalyst compared to **Au<sub>8</sub>Sn** catalyst (<50% conversion).

For both Au-Pd and Au-Sn, catalysts calcined at 300 °C gave higher conversion as compared those both uncalcined and calcined at 500 °C. Referring to the TGA-DSC data (section 6.3.4) the precursor clusters transform into nanoparticles upon removal of the capping ligands at *ca.* 300 °C. This explains the higher conversion achieved as the active sites were not blocked by surrounding ligands. Capping agents lower the accessibility to the active sites and may act as catalyst surface poison<sup>48</sup>. Higher temperature activation (500 °C) promotes gold-gold agglomeration, increasing particle size and limiting activity.

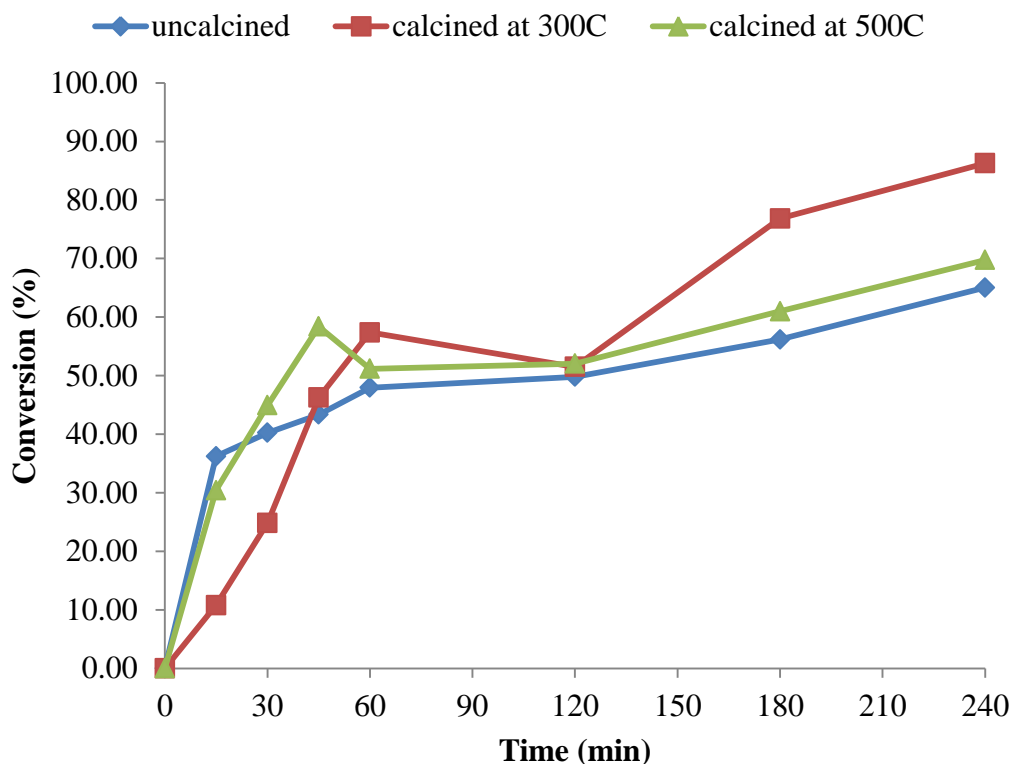


**Figure 6.11:** Comparison of % conversion of benzyl alcohol using 4.0 wt. % Au of  $\text{Au}_6\text{Pd}$  supported catalysts uncalcined, calcined at 300 °C and calcined at 500 °C

$\text{Au}_9$  clusters, used as a starting material for the synthesis of  $\text{Au}_6\text{Pd}$  and  $\text{Au}_8\text{Sn}$  clusters were also deposited onto  $\text{SiO}_2$  nanospheres by the wet impregnation method (see Chapter 3 and 5) and reported here are works with bimetallic system. The % conversion of benzyl alcohol achieved by  $\text{Au}_9$  on  $\text{SiO}_2$  nanospheres calcined at 300 °C after 4 hours was 38.2% with 97.8% benzaldehyde selectivity.  $\text{Au}_6\text{Pd}$  on  $\text{SiO}_2$  nanospheres calcined at 300 °C after 4 hours gave 86.3% conversion (Figure 6.9) with 88.0% benzaldehyde selectivity. In this manner, the key role of gold highlighted by a synergistic effect with palladium can be emphasized. Assuming the gold loading on  $\text{Au}_9$  and  $\text{Au}_6\text{Pd}$  catalysts are similar (*ca.* 4.0 wt. % Au), the most promising results are obtained with the mixed-metal Au-Pd catalyst, converting over 86.0% conversion of starting materials (more than twice as high as Au catalyst) and

with 88.0% benzaldehyde selectivity. Little induction period was observed for uncalcined  $\text{Au}_6\text{Pd}$  catalyst with the catalytic reaction starting as early as 15 minutes of reaction.

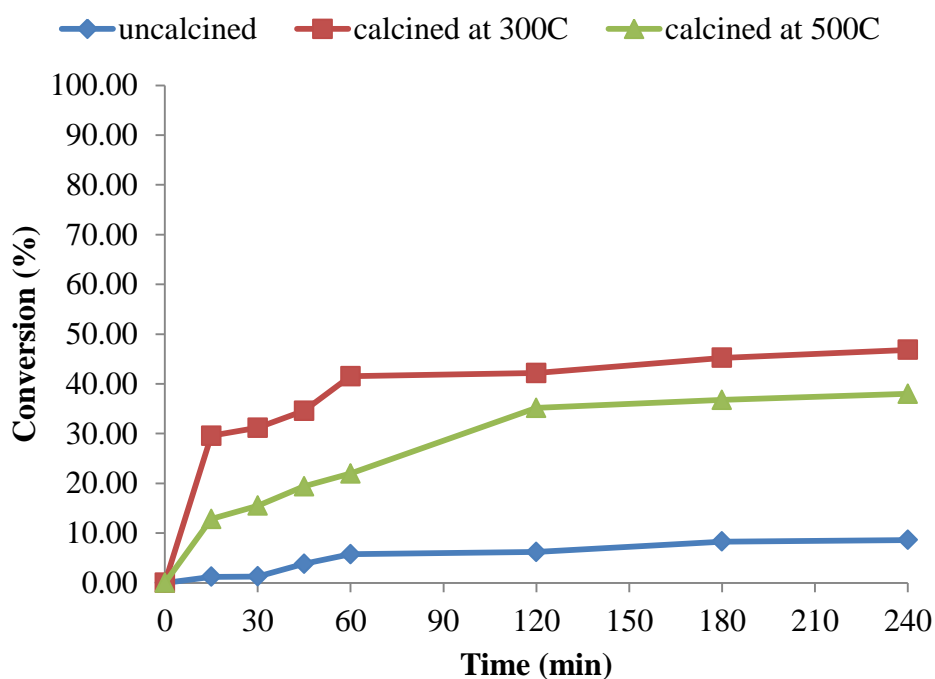


**Figure 6.12:** Comparison of % conversion of benzyl alcohol using 4.0 wt. % Au of  $\text{Au}_8\text{Sn}$  supported catalysts uncalcined, calcined at 300 °C and calcined at 500 °C.

However, the trend does not follow for the  $\text{Au}_8\text{Sn}$  catalyst which on  $\text{SiO}_2$  nanospheres calcined at 300 °C after 4 hours gave only 46.8% conversion (Figure 6.12) with 87.9% benzaldehyde selectivity (Figure 6.14). As compared to the  $\text{Au}_9$  catalyst, there was only a small, *ca.* 8.7% increase in benzyl alcohol conversion and 10% increase in benzaldehyde selectivity. Hence, the role of tin in boosting the catalytic performance together with gold is not seen here.

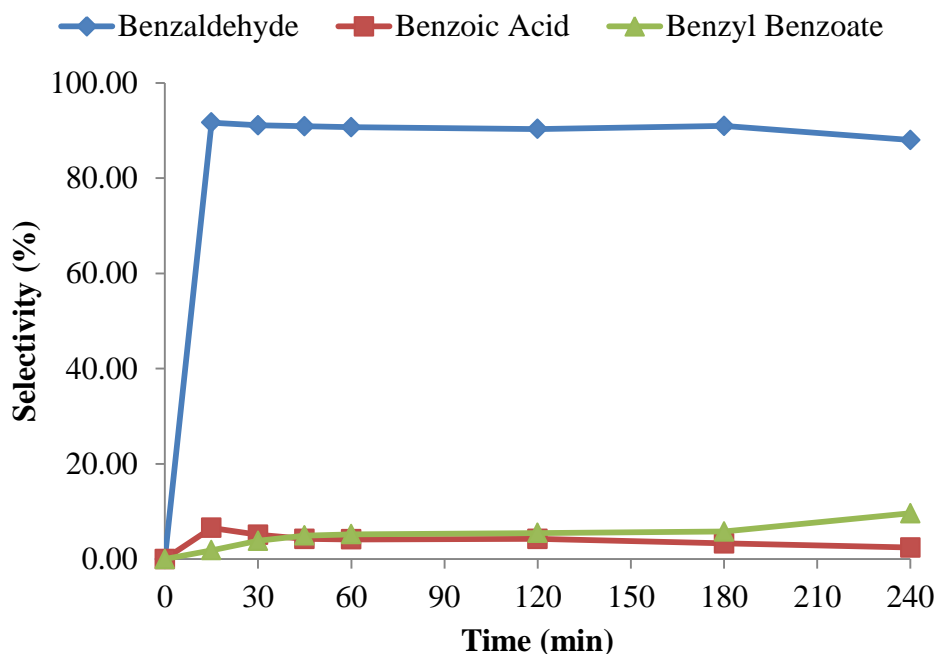


**Figure 6.13:** Selectivity of each product obtained by 4.0 wt. % Au of **Au<sub>6</sub>Pd** supported catalyst calcined at 300 °C

For the uncalcined catalysts, the reaction appears to begin after 45 minutes (Figure 6.12). This phenomenon was also observed with uncalcined **Au<sub>9</sub>** on SiO<sub>2</sub> nanospheres prepared by the wet impregnation method (Chapter 3 and 5). Presumably, the same effect occurs for **Au<sub>8</sub>Sn**. During the first 45 minutes removal of ligands occurs before transforming to Au-Sn nanoparticles and hence activating the catalyst.

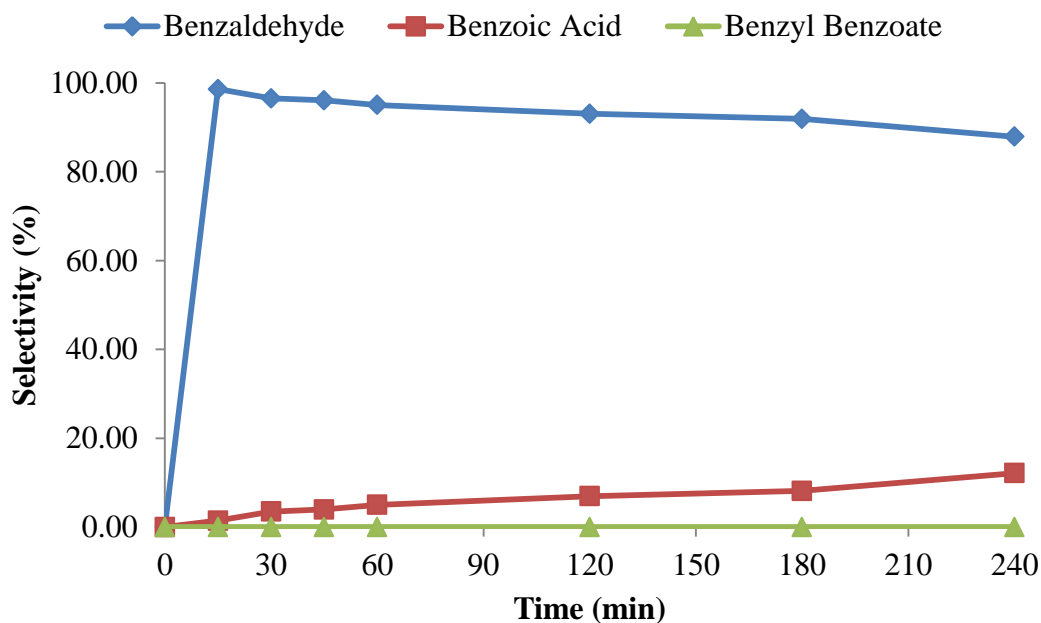


**Figure 6.14:** Selectivity of each product obtained by 4.0 wt. % Au of **Au<sub>8</sub>Sn** supported catalyst calcined at 300 °C

Figures **6.13** and **6.14** show the % selectivity of each product obtained from **Au<sub>6</sub>Pd** and **Au<sub>8</sub>Sn** catalysts respectively. For both, benzaldehyde is the main product with the selectivity being > 80%. However, traces of benzoic acid and benzyl benzoate appear especially after 2 hours of reaction. After 4 hours, **Au<sub>6</sub>Pd** gives 88.0% benzaldehyde, 2.4% benzoic acid and 9.6% benzyl benzoate, while 87.9% benzaldehyde and 12.1% benzoic acid but no benzyl benzoate is seen for **Au<sub>8</sub>Sn**.

## 6.5 Conclusion

Detailed structural studies especially single crystal X-ray diffraction and also computer simulation of the clusters needs to be investigated further in order to understand skeletal rearrangements, fragmentation and reversible transformations. **Au<sub>6</sub>Pd** was found to be active in catalyzing the oxidation of benzyl alcohol. The

---

**Au<sub>8</sub>Sn** cluster is somewhat difficult to characterize and determine the existence of Sn in the cluster. The only evidence that can come into our proposed of Sn metal presence is the slight increase in % conversion of benzyl alcohol in catalytic reaction compared to the corresponding monometallic Au cluster. Characterization of Pd and Sn metal need to be further investigated in order to understand the role played by both metal. Metal-support interactions, size particles effect and catalyst preparation method; those known to be affecting the catalytic performances were unclear to our findings and need more scientific evidence. Nonetheless, the results of this current study have advanced our knowledge of gold-metal clusters chemistry with respect to stability in and oxide support environment particularly SiO<sub>2</sub> nanospheres, methods of spectroscopic characterization in the solid state and oxidation catalysis mechanism in general on a support.

## 6.6 References

1. M. Boronat, A. Corma, F. Illas, J. Radilla, T. Rodenas and M. J. Sabater, *Journal of Catalysis*, 2011, **278**, 50-58.
2. A. Abad, C. Almela, A. Corma and H. Garca, *Tetrahedron*, 2006, **62**, 6666-6672.
3. C. González-Arellano, A. Corma, M. Iglesias and F. Sánchez, *European Journal of Inorganic Chemistry*, 2008, **2008**, 1107-1115.
4. A. Arnanz, C. Gonzalez-Arellano, A. Juan, G. Villaverde, A. Corma, M. Iglesias and F. Sanchez, *Chemical Communications*, 2010, **46**, 3001-3003.
5. P. D. Boyle, B. J. Johnson, A. Buehler and L. H. Pignolet, *Inorganic Chemistry*, 1986, **25**, 5-7.
6. D. I. Enache, D. W. Knight and G. J. Hutchings, *Catalysis Letters*, 2005, **103**, 43-52.
7. M. Conte, A. F. Carley, G. Attard, A. A. Herzing, C. J. Kiely and G. J. Hutchings, *Journal of Catalysis*, 2008, **257**, 190-198.

- 
8. S. Meenakshisundaram, E. Nowicka, P. J. Miedziak, G. L. Brett, R. L. Jenkins, N. Dimitratos, S. H. Taylor, D. W. Knight, D. Bethell and G. J. Hutchings, *Faraday Discussion, The Royal Society of Chemistry*, 2010, **145**, 341-356.
  9. E. Cao, M. Sankar, S. Firth, K. F. Lam, D. Bethell, D. K. Knight, G. J. Hutchings, P. F. McMillan and A. Gavriilidis, *Chemical Engineering Journal*, 2011, **167**, 734-743.
  10. Y.-L. Fang, J. T. Miller, N. Guo, K. N. Heck, P. J. J. Alvarez and M. S. Wong, *Catalysis Today*, 2011, **160**, 96-102.
  11. L. N. Ito, J. D. Sweet, A. M. Mueting, L. H. Pignolet, M. F. J. Schoondergang and J. J. Steggerda, *Inorganic Chemistry*, 1989, **28**, 3696-3701.
  12. L. N. Ito, A. M. P. Felicissimo and L. H. Pignolet, *Inorganic Chemistry*, 1991, **30**, 387-396.
  13. Y. M. Shulga, A. V. Bulatov, R. A. T. Gould, W. V. Konze and L. H. Pignolet, *Inorganic Chemistry*, 1992, **31**, 4704-4706.
  14. R. A. T. Gould and L. H. Pignolet, *Inorganic Chemistry*, 1994, **33**, 40-46.
  15. L. N. Ito, B. J. Johnson, A. M. Mueting and L. H. Pignolet, *Inorganic Chemistry*, 1989, **28**, 2026-2028.
  16. L. N. Ito, A. M. P. Felicissimo and L. H. Pignolet, *Inorganic Chemistry*, 1991, **30**, 988-994.
  17. P. D. Boyle, B. J. Johnson, B. D. Alexander, J. A. Casalnuovo, P. R. Gannon, S. M. Johnson, E. A. Larka, A. M. Mueting and L. H. Pignolet, *Inorganic Chemistry*, 1987, **26**, 1346-1350.
  18. P. D. Boyle, D. C. Boyd, A. M. Mueting and L. H. Pignolet, *Inorganic Chemistry*, 1988, **27**, 4424-4429.
  19. G. Pivoriunas, M. Richter and J. Strähle, *Inorganica Chimica Acta*, 2005, **358**, 4301-4306.
  20. O. Rossell, M. Seco, G. Segalés, M. A. Pellinghelli and A. Tiripicchio, *Journal of Organometallic Chemistry*, 1998, **571**, 123-128.
  21. S. Albonetti, R. Bonelli, J. Epoupa Mengou, C. Femoni, C. Tiozzo, S. Zacchini and F. Trifirò, *Catalysis Today*, 2008, **137**, 483-488.
  22. Y. Katsukawa, S. Onaka, Y. Yamada and M. Yamashita, *Inorganica Chimica Acta*, 1999, **294**, 255-265.

- 
23. S. Hagen, L. Wesemann and I. Pantenburg, *Chemical Communications*, 2005, 1013-1015.
  24. Z. Demidowicz, R. L. Johnston, J. C. Machell, D. M. P. Mingos and I. D. Williams, *Dalton Transactions*, 1988, 1751-1756.
  25. Y. Li and W.-T. Wong, *European Journal of Inorganic Chemistry*, 2003, 2651-2662.
  26. B. D. Alexander, M. P. Gomez-Sal, P. R. Gannon, C. A. Blaine, P. D. Boyle, A. M. Mueting and L. H. Pignolet, *Inorganic Chemistry*, 1988, **27**, 3301-3308.
  27. Z. Akhter, S. L. Ingham, J. Lewis and P. R. Raithby, *Journal of Organometallic Chemistry*, 1998, **550**, 131-139.
  28. T. G. M. M. Kappen, J. J. Bour, P. P. J. Schlebos, A. M. Roelofsen, J. G. M. Van der Linden, J. J. Steggerda, M. A. Aubart, D. A. Krogstad, M. F. J. Schoondergang and L. H. Pignolet, *Inorganic Chemistry*, 1993, **32**, 1074-1075.
  29. M. F. J. Schoondergang, J. J. Bour, P. P. J. Schlebos, A. W. P. Vermeer, W. P. Bosman, J. M. M. Smits, P. T. Beurskens and J. J. Steggerda, *Inorganic Chemistry*, 1991, **30**, 4704-4709.
  30. R. P. F. Kanters, P. P. J. Schlebos, J. J. Bour, W. P. Bosman, J. M. M. Smits, P. T. Beurskens and J. J. Steggerda, *Inorganic Chemistry*, 1990, **29**, 324-328.
  31. A. F. Sotelo, A. M. P. Felicissimo and P. G. Sal, *Inorganica Chimica Acta*, 2003, **348**, 63-68.
  32. R. J. H. Clark, L. Maresca and P. J. Smith, *Journal of Chemical Society (A) : Inorganic Physical Theory*, 1970, 2687-2690.
  33. J. Kilmartin, Thesis, University College London, 2010.
  34. J. Kilmartin, R. Sarip, R. Grau-Crespo, D. Di Tommaso, G. Hogarth, C. Prestipino and G. Sankar, *American Chemical Society - Catalysis*, 2012, **2**, 957-963.
  35. W. Haiss, N. T.H.Thanh, J. Aveyard and D. G. Fernig, *Analytical Chemistry*, 2007, **79**, 4215-4221.
  36. I. V. G. Graf, J. W. Bacon, M. B. Consugar, M. E. Curley, L. N. Ito and L. H. Pignolet, *Inorganic Chemistry*, 1996, **35**, 689-694.

- 
37. F. A. Vollenbroek, d. B. J. P. Van, d. V. J. W. A. Van and J. J. Bour, *Inorganic Chemistry*, 1980, **19**, 2685-2688.
38. D. V. J. W. A. Van, J. J. Bour, J. J. Steggerda, P. T. Beurskens, M. Roseboom and J. H. Noordik, *Inorganic Chemistry*, 1982, **21**, 4321-4324.
39. N. J. Clayden, C. M. Dobson, K. P. Hall, D. M. P. Mingos and D. J. Smith, *Journal of the Chemical Society, Dalton Transactions*, 1985, 1811-1814.
40. F. A. Vollenbroek, J. J. Bour, J. M. Trooster and J. W. A. V. D. Velden, *Journal of the Chemical Society, Chemical Communications*, 1978, 907-909.
41. D. A. Krogstad, V. G. Young and L. H. Pignolet, *Inorganica Chimica Acta*, 1997, **264**, 19-32.
42. J. S. Golithly, L. Gao, A. W. C. Jr., D. E. Bergeron, J. W. Hudgens, R. J. Magyar and C. A. Gonzalez, *The Journal of Physical Chemistry C*, 2007, **111**, 14625-14627.
43. C. J. McNeal, J. M. Hughes, L. H. Pignolet, L. T. J. Nelson, T. G. Gardner, J. P. Fackler, R. E. P. Winpenny, L. H. Irgens, G. Vigh and R. D. Macfarlane, *Inorganic Chemistry*, 1993, **32**, 5582-5590.
44. Y. Shichibu and K. Konishi, *Small*, 2010, **6**, 1216-1220.
45. P. Sevillano, O. Fuhr, O. Hampe, S. Lebedkin, E. Matern, D. Fenske and M. M. Kappes, *Inorganic Chemistry*, 2007, **46**, 7294-7298.
46. M. F. Bertino, Z.-M. Sun, R. Zhang and L.-S. Wang, *The Journal of Physical Chemistry B: Letters*, 2006, **110**, 21416-21418.
47. E. S. Andreiadis, M. R. Vitale, N. Mezailles, X. L. Goff, P. L. Floch, P. Y. Toullec and V. Michelet, *Dalton Transactions*, 2010, **39**, 10608-10616.
48. A. Quantanilla, V. C. L. Butselar-Orthlieb, C. Kwarkernaan, W. G. Sloof, M. T. Kreutzer and F. Kapteijn, *Journal of Catalysis*, 2010, **271**, 104-114.

---

## Chapter 7

### Conclusions and Future Works

#### 7.0 Conclusions

In this research, we have demonstrated the synthesis of **Au<sub>9</sub>** and **Au<sub>13</sub>** clusters (Figure 7.1) used as the molecular precursor towards generating controlled size of gold nanoparticles. Wet impregnation method was used to deposit the clusters onto support but along the investigation, we developed a new TBHP assisted deposition-precipitation method. Various characterisations techniques were used throughout the project. The clusters was first carefully characterised at molecular level before incorporating it onto solid support to produce supported heterogeneous catalyst. SiO<sub>2</sub> nanospheres and CATAPAL-A Boehmite alumina was employed as the solid support.

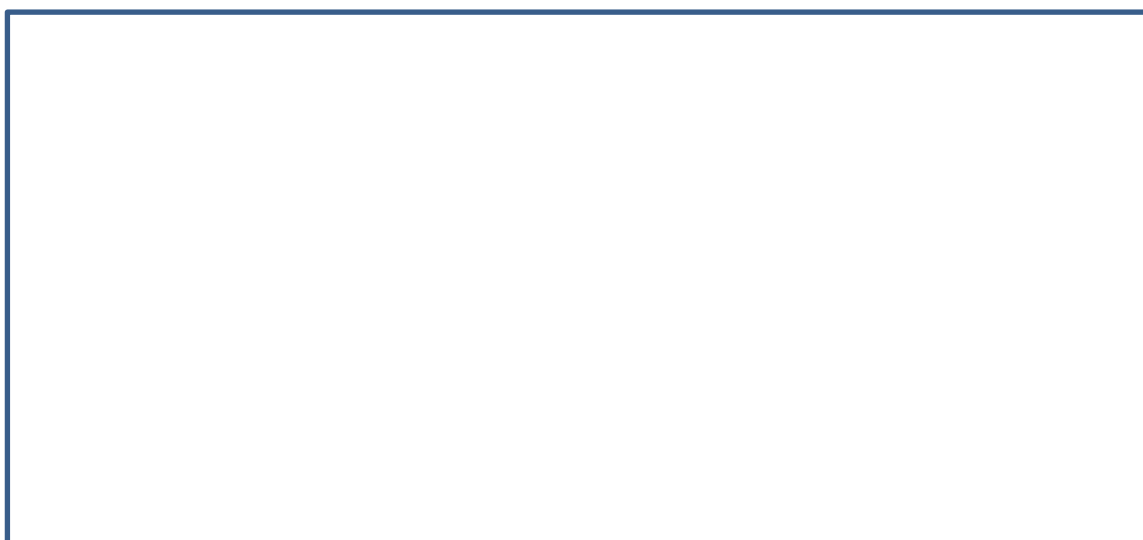


**Figure 7.1:** Crystal structure of (a) **Au<sub>9</sub>** and (b) **Au<sub>13</sub>** clusters from literature. Carbons and hydrogens were omitted for clarity

---

In Chapter 3 we discussed the wet impregnation method to produce gold nanoparticles through bottom-up approach utilising gold cluster compounds (Figure 7.2 (a)). Although this method of preparation involved activation at high temperature which tends to promote larger particles, no evidence was made in this study that particle sizes larger than 100 nm are produced. The existence of phosphine stabilized ligand as precursor that tailored the molecular clusters in the initial stage of particles formation also helps avoiding gold atoms to sinter further upon calcination. The results appeared to be in very good agreement with coordination number determined by EXAFS for both precursor complexes and clusters visualizing strong structural stability and limitation in mobility of gold on support surface.

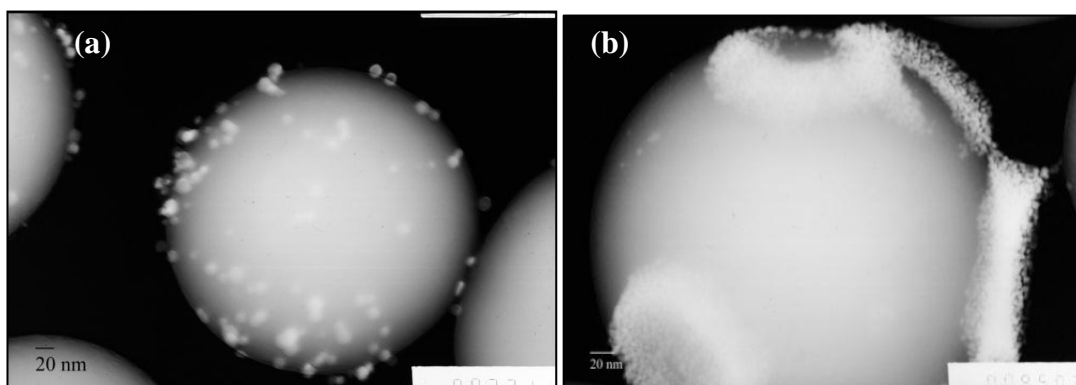


**Figure 7.2:** TEM images of (a)  $\text{Au}_{13}$  cluster on  $\text{SiO}_2$  (WI) nanospheres calcined at  $300^\circ\text{C}$  and (b)  $\text{Au}_{13}$  cluster on  $\text{SiO}_2$  (TBHP) nanospheres uncalcined

We believe that our approach of having control over particles size generation by using gold molecular cluster as precursor is relevant but the method used in preparing the catalyst has to be optimised, in particular a detailed study at a specific temperature close to the point at which the phosphine ligands are removed. There may be several advantages of this kind of approach for preparing fine size gold

---

nanoparticles catalysts, such as the likely of loss of Au in the preparation which is reported elsewhere. Having used gold molecular clusters as precursor added another advantage. Careful consideration on type of clusters to be used, method of preparation and appropriate solid support will leads to producing highly dispersed and small gold nanoparticles catalyst.

Chapter 4 is the highlight of our work, in which a new method of catalyst preparation, using TBHP as the medium to carry out deposition-precipitation for producing highly dispersed gold nanoparticles is reported. This is shown to be a very promising route in producing finely dispersed and relatively small gold nanoparticulate catalysts (Figure 7.2 (b)). The most widely applicable discovery of this work has been the development of a new chemical treatment method for ligand removal at low temperature (95°C) and a one-step procedure. This method may prove to be viable for the activation of a range of ligand-stabilised clusters catalysts that will minimise agglomeration of gold particles.

The most interesting finding was the self-assembled particles observed in  $\text{Au}_{13}$  supported on  $\text{SiO}_2$  support catalyst (Figure 7.3). The particles not only maintain the very small size (*ca.* 2 nm) but also promoted a crown-shaped formation on the edge of the  $\text{SiO}_2$  nanospheres. However, the explanation on what drives the particles to exist in that organization is still unknown to us. Further detailed investigation should be carried out in order to study the particle-support interactions between clusters and  $\text{SiO}_2$  nanospheres *via* this method that presumably promotes self-assembly nanoparticles as observed by high resolution TEM.

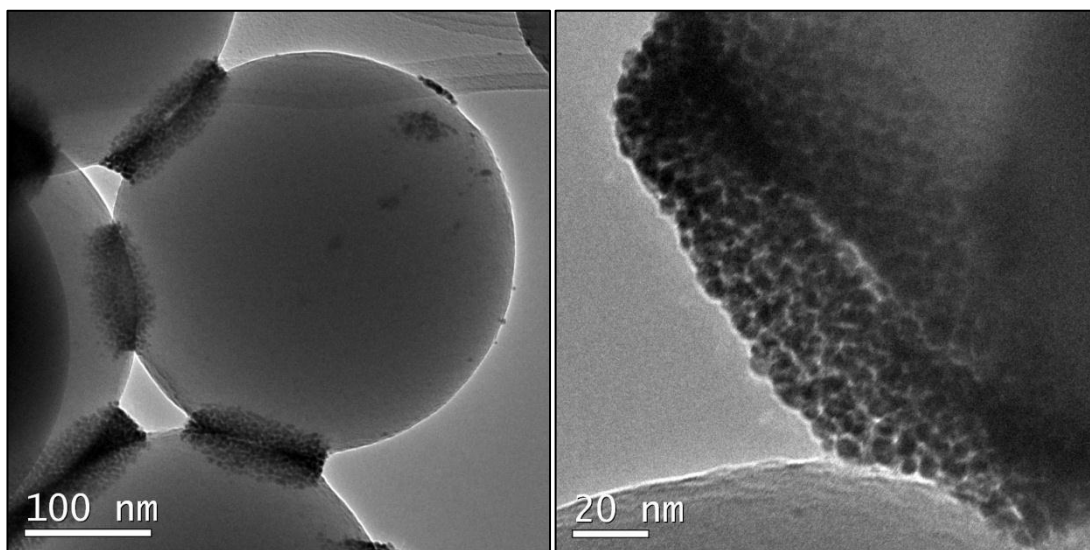


**Figure 7.3:** High resolution of TEM images of  $\text{Au}_{13}$  clusters catalyst deposited on  $\text{SiO}_2$  nanospheres *via* TBHP method uncalcined showing the self-assembled particles organization

Chapter 5 was focussed on the catalytic performances of all catalysts prepared either *via* WI or TBHP method. From the findings of our research work, the following main conclusions can be drawn:

1. Gold nanoparticle sizes ranging from 1 nm to 20 nm showed the excellent catalytic performance in terms of % substrate conversion. Nevertheless, gold nanoparticles sizes below 5 nm proved to be the best catalyst judging from the % substrate conversion, % product selectivity, TON, TOF and recyclability.
2. Regardless of differences in solid supports or gold molecular clusters as precursor to begin with, TBHP method prepared catalyst always gives better result in catalytic performance (Figure 7.4).

- 
3. Leaching of gold nanoparticles into reaction solution also seems to be minimised and catalyst can be recycled up to sixth usage with reasonable rate of catalytic inefficiency.
  4. The use of phosphine-stabilized gold molecular clusters can control the size of gold nanoparticles formation provided the activation of the catalyst step (i.e transformation process from ligand protected molecular clusters to naked nanoparticles) is carefully chosen for example by avoiding high temperature activation. This is one crucial stage in preparing gold nanoparticles catalyst and we achieved that with TBHP method where activation of catalyst can be done at 95°C.

In addition to two gold clusters, we also synthesized two bimetallic gold-metal clusters utilising palladium and tin. The synthesis, characterizations and catalytic testing of both bimetallic catalysts was discussed in Chapter 6. However, the work reported here is very minimal and the data obtained is considered to be preliminary. Nevertheless the study showed that bimetallic catalysts can be prepared by this route. From the findings, it is difficult to speculate further about the synergistic mechanism of catalytic behaviour reflecting the bimetallic properties since more data is needed to substantiate the findings. Detailed structural studies especially using X-ray single crystal as well as computer simulation of the clusters compounds need to be investigated in order to understand the skeletal rearrangements, fragmentation and reversible transformation that take place during the reaction. **Au<sub>6</sub>Pd** was found to be active in catalysing the oxidation of benzyl alcohol.

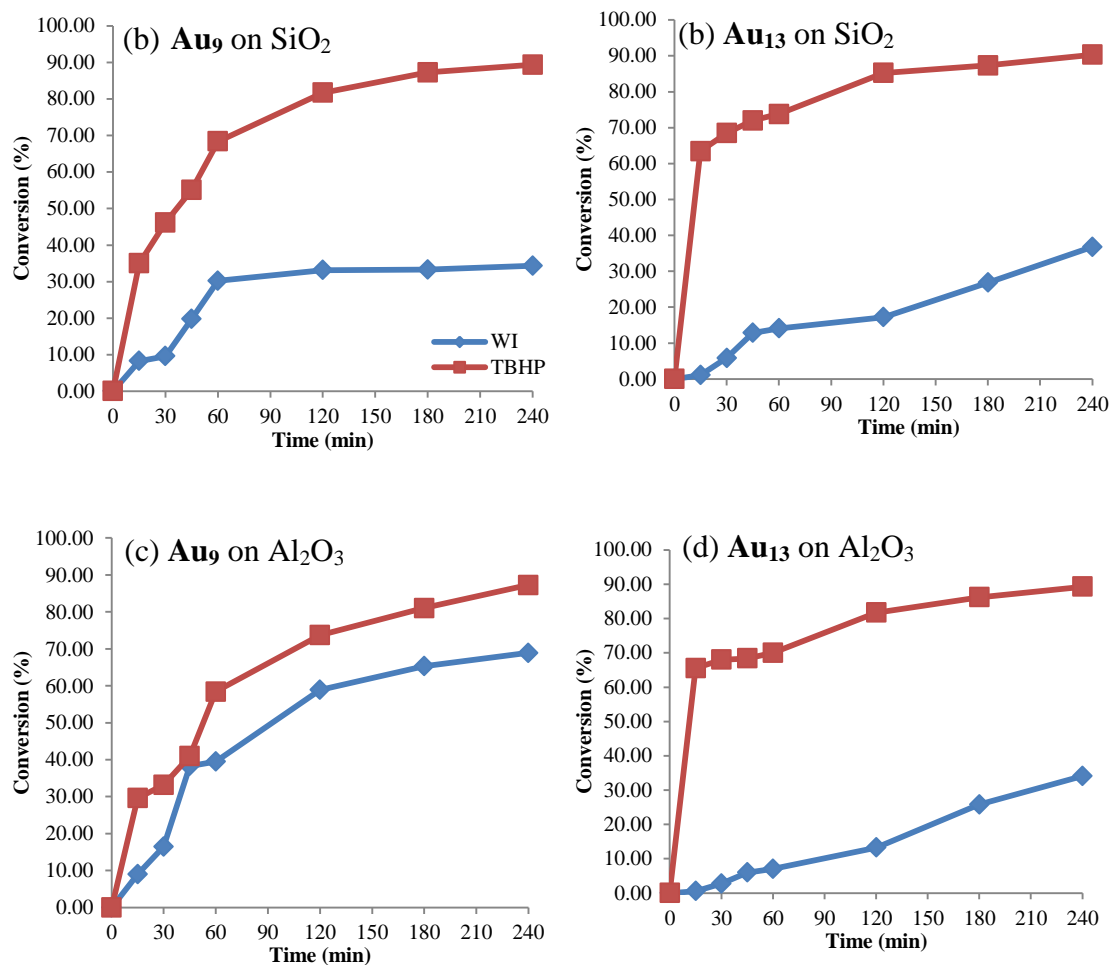


**Figure 7.4:** Kinetic comparison between uncalcined catalysts prepared using wet impregnation (WI) method and TBHP method over 4 hours of catalysis reaction. Experiment was done in 3 replicates and the average values were plotted.

With much issues in **Au<sub>8</sub>Sn** cluster synthesis as well as the compound being insoluble and unstable, it is hard to characterize and determined the existence of Sn in the cluster. The only evidence that can come into our prediction of Sn metal appearance is the slightly increasing % conversion of benzyl alcohol in catalytic reaction compared to the corresponding monometallic Au cluster. Characterizations on Pd and Sn part needs to be investigated further in order to understand the role played by both metal in addition to Au. Metal-support interactions, size particles

effect and catalysts preparation method are well known to affect the catalytic performances (Figure 7.5), but from our study it is unclear whether one or more of them contribute to the catalytic performance and need more scientific evidence to be able to draw conclusion. Nonetheless, the results of this current study have advanced, to our knowledge of gold-metal clusters chemistry with respect to stability in an oxide support environment particularly SiO<sub>2</sub> support supported by spectroscopic characterization in the solid state and oxidation catalysis.

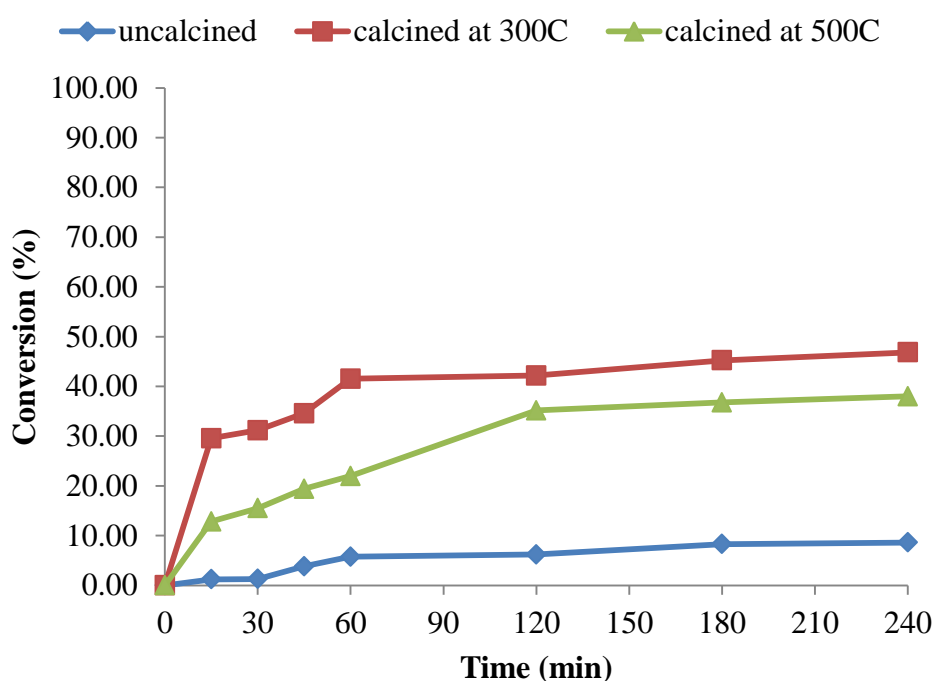


**Figure 7.5:** Comparison of % conversion of benzyl alcohol using 4.0 wt. % Au of Au<sub>8</sub>Sn supported catalysts uncalcined, calcined at 300°C and calcined at 500°C

In conclusion, this research employed two phosphine stabilized gold molecular clusters which are Au<sub>9</sub> and Au<sub>13</sub> (Figure 7.1). The TGA-DSC and concise study of *in-situ* EXAFS-XRD data on both clusters showed that Au<sub>13</sub> clusters transform to nanoparticles at slightly lower temperature (245°C) than the Au<sub>9</sub>

---

clusters (295°C). The information gathered and discussed in Chapter 3 and 4 also suggested that  $\text{Au}_{13}$ , owing to the icosahedral geometry was a more stable cluster than  $\text{Au}_9$ . Its shape helps to minimise particle aggregation and structural rearrangement which will also leads to sintering problem. Both clusters were deposited onto  $\text{SiO}_2$  nanospheres and  $\text{Al}_2\text{O}_3$  using WI and TBHP method. Catalyst activation was done for catalysts prepared by WI through the use of high temperature calcination (300°C and 500°C) while catalysts prepared using TBHP were activated *in-situ* during the impregnation process at 95°C. The higher temperature involved in WI method (*ca.* 300°C) promoted the sintering of the gold particles to larger nanoparticles in the range of 20-50 nm, whilst gold nanoparticles obtained by TBHP method dispersed on the support were about 1-15 nm diameter in size (Figure 7.2).

The results proved that we have two successful methods of controlling the size of gold nanoparticles generated which are (i) by using phosphine stabilized molecular clusters and (ii) by low temperature, chemical treatment during impregnation process offered by TBHP method. Hypothetically, from all the characterization data, TBHP method catalysts is better than WI method catalysts because of the smaller nanoparticles generated as well as better dispersion onto support. In Chapter 5 the performance of all catalysts prepared were discussed and confirming our hypothesis, the TBHP method catalysts always catalysed the reaction better than WI method catalysts.  $\text{SiO}_2$  and  $\text{Al}_2\text{O}_3$  supports did affect the catalytic activity in terms of the rate of reaction (Figure 7.4).  $\text{Al}_2\text{O}_3$  was observed to offer slower kinetics compared to  $\text{SiO}_2$  although at the end of reaction the % conversion obtained was comparable. In the end, we considered the uniform size of  $\text{SiO}_2$

---

nanospheres that responsible of such behaviour and also forcing the nanoparticles to self-assemble as observed in TBHP prepared catalysts (Figure 7.3). Heterobimetallic catalysts were an expanding area which caught our attention. From the catalysis data, **Au<sub>8</sub>Sn** did not offer synergistic effect compared to **Au<sub>6</sub>Pd**. Nevertheless, this research opens a wide area to be investigated further and several new possibilities that can be research in detail.

### 7.1 Future Works

Many aspects of the research reported here are still open for further studies.

To mention few of those:

1. Expanding the research to bigger gold clusters such as Au<sub>20</sub>, Au<sub>55</sub> and other ligand-stabilized gold molecular clusters.
2. The support effects should be investigated by varying the support using different oxides or zeolites and mesoporous silica.
3. The particle-support interaction can be studied by varying the parameters such as temperatures, solvent or pH during preparation.
4. The catalysts can be tested for their catalytic performances on other catalytic reactions such as gas phase oxidation reaction or hydrogenation.
5. The ability of TBHP method to be widely used as effective deposition method can be investigated further by employing the method towards preparation of other catalyst system.
6. The self-assembled particles that we observed can be characterised further to investigated the characteristics that drive the phenomenon to occur.
7. A complete study can be done on the heterobimetallic gold-metal catalysts topic.

---

## Publication

J. Kilmartin, R. Sarip, R. Grau-Crespo, D. Di Tommaso, G. Hogarth, C. Prestipino  
and G. Sankar, *ACS Catalysis*, 2012, **2**, 957-963.



AAS Data<sup>1</sup>

Support	Condition	Catalyst	Au detected (mg/l)
SiO <sub>2</sub>	Uncalcined	Au <sub>9</sub>	0.0369
		Au <sub>13</sub>	0.0600
	Calcined at 300°C	Au <sub>9</sub>	0.0410
		Au <sub>13</sub>	0.0738
Al <sub>2</sub> O <sub>3</sub>	Uncalcined	Au <sub>9</sub>	0.0340
		Au <sub>13</sub>	0.0405
	Calcined at 300°C	Au <sub>9</sub>	0.0955
		Au <sub>13</sub>	0.0350

*Catalysts prepared by TBHP method. Values are average from 3 replicates of analysis.*

<sup>1</sup> Collected and analysed by Siti Kamilah Che' Soh, Ph.D, Universiti Teknologi Malaysia (UTM), Skudai, Johor, Malaysia. In collaboration with Prof. Dr. Mustaffa Shamsuddin.